Institute of Bioorganic Chemistry
Polish Academy of Sciences in Poznan

Characterizing the roles of ETS-4 transcription factor in fat metabolism

mgr Aneta Agnieszka Dyczkowska

Integrative Biology Team
Supervisor: dr hab. Rafal Ciosk
Assistant supervisor: dr Agnieszka Chabowska-Kita

Poznan, 2022

This doctoral thesis was supported by the National Science Centre OPUS 10 grant (2015/19/B/NZ3/02412) "*Cytoplasmatic roadblocks in cell fate reprogramming: from players to molecular mechanisms*" and OPUS 18 grant (2019/35/B/NZ3/03503) "*REGE-1 and RLE-1 dependent mRNA decay: The "R2-co" model of messenger RNA silencing*".

ACKNOWLEDGMENTS

During my PhD, there were many people who supported me with a kind word. First, I would like to thank **Rafał Ciosk** for enabling me to work on this interesting and demanding project and for enabling me to participate in international conferences. I would like to thank **Agnieszka Chabowska-Kita** for cooperation in writing the publication and mentoring. I would also like to thank all the members of Ciosk lab who have been an essential part of my PhD experience. **Takashi Miki** from whom I learned the secrets of *C. elegans*, **Alicja Komur** and **Daria Sobańska**, who were an absolute support in the laboratory. **Edyta Kościańska, Jarosław Lewandowski** and **Bogna Juskowiak** who contributed to creating a nice atmosphere in the laboratory. I would also like to thank **Weronika Wendlandt-Stanek** for help with the 3D design of the MRP-1 structure and **Katarzyna Solka** for administrative help. I also extend a big bow to Laboratory of Animal Model Organisms, including **Agata Tyczewska**, **Karol Kołodziejczak** and **Natalia Barabasz** for preparing and delivering the necessary reagents and plates. Special thanks goes to my friends and family who have supported me throughout the years of this thesis. I would like to thank my husband, **Paweł Dyczkowski**, for being there for me whenever I needed it, for his great patience, understanding and playing together with science. I would also like to thank my father-in-law **Grzegorz Dyczkowski** for the bioinformatics support, without which the implementation of some experiments would not be possible.

TABLE OF CONTENTS

ABREVIATIONS

16:0	palmitic acid
2DG	2-deoxy-D-glucose
5-HT	5-hydroxytryptamine, serotonin
AAK	AMP activated kinase
ABC	ATP-binding cassette
ABCC1	ATP binding cassette subfamily C member 1
ACS	fatty acid CoA synthetase
ADP	adenosine diphosphate
AGE	phosphatidylinositol 3-kinase
AGR	anterior gradient
AKT	serine / threonine kinases
ALA	alanine
AMCA	amino-4-methylcoumarin-3-acetic acid
AMP	adenosine monophosphate
AMPK	AMP-activated protein kinase
APS	ammonium persulfate
ASAH	acylsphingosine amidohydrolase
ASM	acid sphingomyelinases
AT	adipose tissue
ATGL	adipose triglyceride lipase
ATP	adenosine triphosphate
BCAA	branched chain amino acids
BMI	body mass index
BSA	bovine serum albumin
C terminus	COOH terminus
C. elegans	*Caenorhabditis elegans*
CARS	Coherent anti-Stokes Raman scattering microscopy
cDNA	complementary DNA

CdTe QDs	cadmium telluride quantum dots
CE	cholesterol esters
C / EBPβ	CCAAT enhancer-binding protein beta
CEPT	choline / ethanolamine phosphotransferase
CFP	cyan fluorescent protein
CGC	Caenorhabditis Genetics Center
CHP	calcineurin homolog protein
CIP	alkaline phosphatase, calf intestine
CL	cytoplasmic loops
CoA	coenzyme A
CONTROL	wild-type animals fed with bacteria containing an empty vector
CPT	carnitine palmitoyl transferase
CRISPR	clustered regularly interspaced short palindromic repeats
DAE	DAF-16 associated element
DAF	abnormal dauer formation
DAG	diglyceride
DBE	DAF-16 binding element
ddH_2O	double-distilled water
DGAT	diacylglycerol O-acyltransferase
DHE	dihydroethidium
DHS	short-chain dehydrogenase
DIC	differential interference contrast
DMP	defecation motor program
DMSO	dimethyl sulfoxide
DNA	deoxyribonucleic acid
DR	dietary restriction
DRP	dynamin-related protein
dsRNA	double-stranded RNA
DTT	dithiothreitol
ECD	extracellular immunoglobulin-like domain
E. coli	*Escherichia coli*

EDTA	ethylenediaminetetraacetic acid
e.g.	for example
ELO	fatty acid elongase
EMS	ethane methyl sulfonate
ER	endoplasmic reticulum
ESI	electrospray ionization
EtOH	ethanol
FA	fatty acid
FASN	fatty acid synthase
FAT	fatty acid desaturase
FC	fold change
FFA	free fatty acid
FL	fluorescence
FLP	FMRF-like peptide
Fox	forkhead box
FOXO	forkhead box protein O
FZO	mitochondrial fusion protein
g	g force or relative centrifugal force (RCF)
GCNT	glucosaminyl (N-acetyl) transferase
GC/TOF MS	gas chromatography/time-of-flight mass spectrometry
GFP	green fluorescent protein
GSH	reduced glutathione
GSK	glycogen synthase kinase
GSSG	oxidized glutathione
GST	glutathione S-transferases
h	hour
HFD	high fat diet
HPL	HP1 like heterochromatin protein
H. sapiens	*Homo sapiens*
HYL	homolog of yeast longevity gene
IIS	insulin / insulin-like growth factor (IGF)-1 signaling

iNOS	inducible-nitric oxide synthase
INS	insulin like ligand
InsP3R	inositol 1,4,5-trisphosphate receptor
IPTG	isopropyl-D-thiogalactopyranoside
kDa	kilodalton
LB	Luria Broth
LC	liquid chromatography
LD	lipid droplet
LDL	low-density lipoproteins
ldrIs	transgene
LFD	low fat diet
LIPL	lipase like
LTA4H	leukotriene A4 hydrolase in mammals
LTAH	leukotriene A4 hydrolase in nematodes
LTC4	leukotriene C4
LYS	lysine
MAPK	p38 / mitogen-activated protein kinase
MBOA	membrane bound O-acyl transferase
MCPIP	monocyte chemotactic protein-induced protein
MDR	multidrug resistance
MFN	dynamamine-related GTPases mitofusin
MFS	major facilitator superfamily
min	minutes
MOCK	bacteria containing an empty vector (L4440)
MOD	serotonin-gated chloride channel
MosSCI	Mos1-mediated single-copy transgene insertions
mRNA	messenger RNA
MRP	multidrug resistance protein
MS / MS	tandem mass spectrometry
MSD	membrane spanning domain
mTOR	mechanistic target of rapamycin

MUFA	monounsaturated fatty acids
N2	wild-type
NAFLD	nonalcoholic fatty liver disease
NBD	nucleotide binding domain
NGM	normal growth medium
N terminus	NH_2 terminus
NHE	sodium–hydrogen exchanger
NHX	sodium–proton exchanger
NKX2-1	NK2 homeobox 1 (NKX2-1)
NPR	neuropeptide receptor
NRF	nuclear factor erythroid 2-related factor
NYN	Nedd4-binding protein 1
OA	octopamine
OCR	oxygen consumption rate
ORO	Oil red O
P	phosphate
PAR	abnormal embryonic partitioning of cytoplasm
PBEC	primary bronchial epithelial cells
PBO	PBOc defective (defecation)
PBS	phosphate-buffered saline
PC	phosphatidylcholine
PCR	polymerase chain reaction
PDB	protein data bank
PDK	3-phosphoinositide-dependent kinase 1
PE	phosphatidylethanolamine
PEPCK	phosphoenolpyruvate carboxykinase
PEPT	peptide transporter
PG	phosphatidylglycerol
Pi	inorganic phosphate
PIP-2	phosphatidylinositol (4,5)-bisphosphate
PIP-3	phosphatidylinositol (3,4,5)-trisphosphate

PL	phospholipids
PMSF	phenylmethyl sulfonyl fluoride
PNK	pantothenate kinase
POD	polarity and osmotic sensitivity defect
PPARγ	peroxisome proliferator-activated receptor gamma
PQM	paraquat (methylviologen) responsive
PS	phosphatidylserine
PUFA	polyunsaturated fatty acids
PVDF	polyvinylidene fluoride
PYC	pyruvate carboxylase
QTL	quantitative trait loci
RAF	strain number from Ciosk database
RAPTOR	regulatory associated protein of mTORC1
RNA	ribonucleic acid
RNAi	RNA interference
RNA-Seq	RNA sequencing
ROS	reactive oxygen species
rpm	revolutions per minute
RSK	ribosomal protein S6 kinase
RT	room temperature
RT-qPCR	quantitative reverse transcription PCR
S1P	sphingosine-1-phosphate
SDS	sodium dodecyl sulfate
sec	seconds
SER	serotonin / octopamine receptor
SERCA	sarco(endo)plasmic reticulum calcium ATPase
SFA	short fatty acids
SGK	serum and glucocorticoid inducible kinase homolog
SILAC	stable-isotope labeling with amino acids
SKN	skinhead
SM	sphingomyelin

SMS	sphingomyelin synthase
SOD	superoxide dismutase
SODH	sorbitol dehydrogenase
SPDEF	SAM-pointed domain-containing ETS transcription factor
SPHK	sphingosine kinase
SPT	serine palmitoyltransferase in mammals
SPTL	serine palmitoyltransferase in nematodes
T2D	type 2 diabetes
TAE	tris-acetate-EDTA
TAG	triglyceride
TALEN	transcription activator-like effector nucleases
TBS	tris buffered saline
TCA	tricarboxylic acid cycle
TEMED	tetramethylethylenediamine
TGF-β	transforming growth factor-β
t.j.	to jest
TLC	thin layer chromatography
TM	transmembrane
TOR	target of rapamycin
TORC	transducer of regulated CREB activity
TPH	tryptophan hydroxylase
UNC	uncoordinated
UTR	untranslated region
VHA	vacuolar H ATPase
WHO	World Health Organization
WT	wild-type animals
ZF	zinc finger
ZFN	zinc-finger nucleases

ABSTRACT

Obesity is a serious health problem affecting people all over the world, therefore it is crucial to understand the mechanisms that regulate fat metabolism. Previous research conducted on *C. elegans* allowed the discovery of the *rege-1*, whose inhibition activated the ETS-4, leading to a reduction in the body fat content. The aim of this thesis was to discover the regulatory axis through which the REGE-1 - ETS-4 influenced fat metabolism in nematodes.

The results from unbiased genetic screening and RNA-Seq data allowed for the selection of potential candidates that could regulate fat accumulation downstream of the REGE-1 - ETS-4 regulatory axis, such as MRP-1 or PEPT-1. However, silencing of genes related to their action, including *sphk-1*, *ltah-1.2*, *pbo-1* or *pbo-4*, resulted only in a partial recovery of the body fat levels in *rege-1* mutants, which may suggest that they regulated fat metabolism in parallel to the REGE -1 - ETS-4 regulatory axis. Moreover, expression of *skn-1* and activation of DAF-16 were enhanced in the *rege-1* mutants, however they were probably responsible for other aspects of physiology, such as oxidative stress response.

Characterization of changes that occured in response to *rege-1* depletion showed a change in the expression of genes associated with lipid metabolism, such as lipid catabolism (*lipl-1* and *lipl-2*), fatty acid desaturation (*fat-5*, *fat-7*) or sphingolipid metabolism (*sptl-1*, *sptl-2*, *hyl-1*, *hyl-2* or *sphk-1*). Simultaneous silencing of *sptl-1* and *sptl-2* in *rege-1* mutants resulted in complete fat recovery, suggesting regulation of fat accumulation via the REGE-1 - ETS-4 regulatory axis. In addition, the *rege-1* mutants were characterized by reduction in the oxygen consumption rate and an increase in the expression of genes related to the oxidative stress response (*sod-4* and *sod-5*). This might suggest disturbance of mitochondrial oxidative phosphorylation and that *rege-1* mutant animals use energy sources other than fatty acids for animal survival. The increase in the *sodh-1* mRNA levels could indicate that carbohydrate metabolism might be enhanced in the *rege-1* mutants.

In conclusion, the fat loss phenotype of the *rege-1* mutants depended on the interaction of multiple signaling pathways that worked in concert with the REGE-1 - ETS-4 regulatory axis, which seemed to modulate fat accumulation predominantly through changes

in the sphingolipid metabolism. Given the similarities between nematode REGE-1 and human Regnase-1, finding of potential downstream targets of the REGE-1 – ETS-4 regulatory axis might enable the discovery of potentially novel metabolic pathways that could find an application in the treatment of obesity.

STRESZCZENIE

Otyłość jest poważnym problemem zdrowotnym dotykającym ludzi na całym świecie, dlatego też bardzo ważne jest poznanie mechanizmów regulujących metabolizm tłuszczu. Wcześniejsze badania przeprowadzone na organizmie modelowym *C. elegans* pozwoliły na odkrycie genu *rege-1*, którego wyciszenie aktywowało ETS-4, prowadząc do zmniejszenia zawartości tłuszczu. Celem tego doktoratu było poznanie mechanizmu w jaki sposób szlak REGE-1 – ETS-4 regulował metabolizm tłuszczu u nicieni.

Wyniki analiz badań genetycznych pozwoliły na wyselekcjonowanie potencjalnych kandydatów, t.j. MRP-1 lub PEPT-1, którzy mogliby regulować akumulację tłuszczu w szlaku REGE-1 – ETS-4. Jednak wyciszenie genów związanych z ich pracą, jak *sphk-1, ltah-1.2, pbo-1* lub *pbo-4*, spowodowało jedynie częściowe zwiększenie poziomu tłuszczu u *rege-1* mutantów, co może sugerować, że regulują one metabolizm tłuszczów równolegle do szlaku REGE -1 - ETS-4. Co więcej, ekspresja *skn-1* i aktywność DAF-16 były zwiększone w mutantach *rege-1*, jednak prawdopodobnie są one odpowiedzialne za inne aspekty fizjologiczne, takie jak np. reakcja na stres oksydacyjny.

Charakterystyka zmian, które zaszły w odpowiedzi na wyciszenie transkyptu genu *rege-1* wykazała zmianę ekspresji wielu genów związanych z metabolizmem lipidów, t.j. odpowiedzialnych za katabolizm (*lipl-1*, *lipl-2*), desaturację kwasów tłuszczowych (*fat-5*, *fat-7*) lub metabolizm sfingolipidów (*sptl-1*, *sptl-2*, *hyl-1*, *hyl-2*, *sphk-1*). Jednoczesne wyciszenie mRNA *sptl-1* i *sptl-2* w mutantach *rege-1* spowodowało całkowite odzyskanie tłuszczu, co sugeruje, że regulują one akumulację tłuszczu poprzez szlak REGE-1 - ETS-4. Dodatkowo, u *rege-1* mutantów zaobserwowano zmniejszony poziom oddychania komórkowego i wzrost ekspresji genów związanych z odpowiedzią na stres oksydacyjny (*sod-4*, *sod-5*). Sugeruje to zaburzenia pracy mitochondriów oraz pozyskiwanie energii potrzebnej do życia z innych źródeł niż kwasy tłuszczowe. Wzrost poziomu *sodh-1* mRNA może sugerować, że metabolizm węglowodanów jest wzmocniony u *rege-1* mutantów.

Podsumowując, utrata tłuszczu u *rege-1* mutantów najprawdopodobniej zależy od interakcji wielu ścieżek sygnałowych, współdziałających ze szlakiem REGE-1 - ETS-4, która wydaje się modulować akumulację tłuszczu głównie poprzez zmiany w metabolizmie

sfingolipidów. Z uwagi na podobieństwo pomiędzy białkami REGE-1 u nicieni a Regnase-1 u ludzi, poznanie potencjalnie dalszych celów szlaku REGE-1 – ETS-4 może umożliwić odkrycie nowych ścieżek metabolicznych, które mogą znaleźć zastosowanie w leczeniu otyłości.

INTRODUCTION

1. Obesity as a global health problem

Obesity is a global health problem that affects people regardless of their age, socio-economic group and country development. Overweight and obesity are caused by abnormal or excessive accumulation of body fat, caused by a long-term imbalance between energy consumption and energy expenditure. The worldwide number of obese people has tripled since 1975 due to easy availability and consumption of high-energy food, lack of physical activity related to urbanization and sedentary lifestyle.

Energy homeostasis plays a very important role in maintaining a healthy body weight by coordinating the action of many signaling pathways that influence food perception, eating behavior, nutrient uptake, fat storage and energy expenditure (Pang et al., 2014a). Energy imbalance, due to disruption of any of these pathways, can lead to obesity and other metabolic diseases (Willett et al., 1999; World Health Organization (WHO), 1998). The rare monogenic forms of obesity in humans are caused by mutations in genes of the leptin-melanocortin pathway, resulting in abnormal nutritional behavior and endocrine disruption (Huvenne and Dubern, 2014). However, most common genetic forms of obesity (polygenic) are caused by the presence of various mutations in many genetic loci, as evidenced by the analysis of genome-wide scans showing more than 250 human obesity quantitative trait loci (QTL) (Rankinen et al., 2006). Obesity is influenced by the interaction of genetic and environmental factors, such as unhealthy food, sedentary lifestyle and use of medications (Poveda et al., 2016). In addition to excessive growth of adipose tissue (AT), obesity leads to the development of serious diseases such as high blood pressure, stroke, heart attack, gallbladder disease, type 2 diabetes (T2D) and various types of cancer (Kopelman, 2000). Therefore, it is very important to understand molecular mechanisms regulating fat metabolism and develop new experimental strategies that would be effective in prevention and / or treatment of obesity and its comorbidities.

2. *C. elegans* as a model organism to study fat metabolism

Obesity has been mostly studied using animal models, including rodents. However, to limit experiments on vertebrates, modern scientific research is often based on ethically more acceptable model organisms such as the nematode *Caenorhabditis elegans* (*C. elegans*).

C. elegans has been used in biomedical research for over 40 years, including in metabolism and obesity studies (Bolla, 1979). Nematodes are the first multicellular organisms to have a fully sequenced genome (The *C. elegans* Sequencing Consortium, 1998), as well as a mapped cell lineage of each cell type (Sulston and Schierenberg et al., 1983; Sulston and Horvitz, 1977). In addition, the *C. elegans* genome is similar to human, since more than 60% - 80% of the human genes associated with various diseases are conserved in nematodes (Lai et al., 2000; Sonnhammer and Durbin, 1997). Among the nematode genes that have orthologues in humans, there are genes regulating energy homeostasis and fat metabolism, such as genes responsible for the fatty acid (FA) synthesis, β-oxidation, desaturation and elongation, as well as pathways responsible for serotonergic, insulin / IGF-1 (IIS) and neuropeptide signaling (Mullaney and Ashrafi, 2009; Chiang and MacDougald, 2003). In addition to the genetic similarity between *C. elegans* and humans, the *C. elegans* model has been used widely in genetic analysis, including in forward and reverse genetic screens. It is also used to create transgenic animals. Ribonucleic acid (RNA), deoxyribonucleic acid (DNA) or nanoparticles can be delivered into the *C. elegans* gonads by microinjections. The genetic modifications induced by Cas9-mediated clustered regularly interspaced short palindromic repeats (CRISPR / Cas9), transcriptional activator-like nucleases (TALENs), Mos1-mediated single-copy transgene insertions (MosSCI) and zinc-finger nucleases (ZFNs), all enable the genetic engineering of nematodes (Kim and Colaiácovo, 2019; Iyer et al., 2018). Moreover, mRNA inhibition is possible through double-stranded RNA (dsRNA) interference (RNAi). Inhibition is accomplished by feeding the nematodes with bacteria bearing a plasmid expressing dsRNA matching the sequence of a target mRNA (Timmons and Fire, 1998). Moreover, techniques commonly used in nematodes, which allow measuring animal metabolites (von Reuss and Schroeder, 2015), such as lipidomic analysis (Witting and Schmitt-Kopplin, 2016), as well as the Seahorse technology, enables the measurement of glycolysis and oxygen consumption rate

(OCR) (Koopman et al., 2016). Consequently, *C. elegans* is considered an attractive model organism for studying the function of genes responsible for human diseases, including obesity caused by metabolic disorders, as it can help to identify new targets for therapeutic treatments.

2.1. The basic biology of *C. elegans*

As a model organism, *C. elegans* is easy to maintain and has many valuable experimental features such as a transparent body or large numbers of offspring. *C. elegans* are small-sized nematodes, about 1 mm long, which enables their observation with the use of contrast-interference microscopy (DIC). In the wild, this nematodes are found mainly on rotting vegetable matter (Felix and Braendle, 2010). In laboratory conditions, they are grown on agar plates with *Escherichia coli* (*E. coli*) bacteria as a food source (Brooks et al., 2009). The *C. elegans* is considered a powerful model organism for genetic studies, because it has a short life cycle of approximately 3 days at 20°C (Corsi, 2006), as shown in **Figure 1**. Development of *C. elegans* begins with oocyte fertilization by sperm and embryogenesis, which takes 16 h at 20°C. After hermaphrodite embryo hatches, it enters the first larval stage (L1). The L1 larvae begin to actively seek food that allows them to grow through the L2 - L4 larval stages, which are interrupted by sleep-like periods of inactivity, during which the old cuticle is replaced by a new one through molting (Turek and Bringmann, 2014). Without access to food, L2 larvae are able to enter an alternative larval stage, the dauer stage, where they arrest their development and break down accumulated fat, allowing them to survive for up to a month without feeding. When food reappears, *C. elegans* resumes its development by molting into the L4 larva and its life cycle continues as usual (Kaul et al., 2014). After the L4 stage, nematodes develop into young adult stage, which is characterized by fully developed gonads and vulva, but the absence of fertilized embryos in the uterus. In this dissertation, mostly young adults have been used, since oocytes contain a fat-rich yolk, which could have an impact on the overall fat measurements (Chen et al., 2016). The next development phase is the adult stage, which is distinguished by full maturity, when the nematodes are gravid and produce progeny for about 2 - 3 days while sperm is vailable.

After the breeding period is over, the nematode remains alive for a few more weeks, then undergoes senescence and dies.

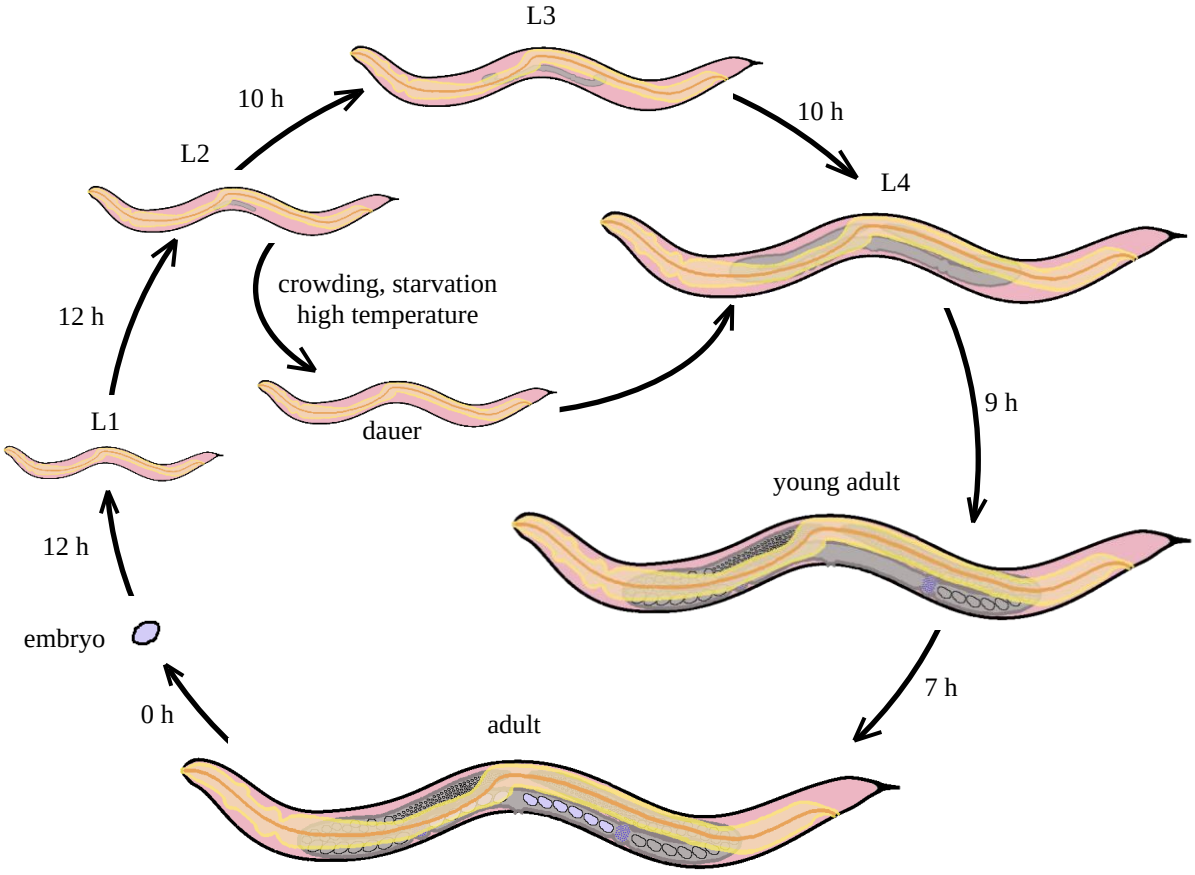

Figure 1. The life cycle of *C. elegans.* The life cycle of wild-type animals at 20°C, fed with OP50, where 0 h constitutes fertilization. Based on *Corsi, 2006*.

The body of *C. elegans* is composed of 3 parts: the head (containing the pharynx and the pharyngeal intestinal valve responsible for food intake; Albertson and Thomson, 1976), the main body (containing the intestine and gonads responsible for digestion and reproduction; McGhee, 2007; Green et al., 2008), and the tail, with a copulatory organ in males (Nguyen et al., 1999), as shown in **Figure 2** (**A**, **B**). From the outside, the body is surrounded by a cuticle, below which there are hypodermis with ganglia from the nervous system and muscle separated from the intestine and gonads by the pseudocoelom (Corsi et al., 2015), as seen in the cross-section of the adult hermaphrodite shown in **Figure 2 C**. Despite its simple structure, *C. elegans* is capable of performing complex functions enabling

it to navigate to food by sensing smell and taste, searching for a mating target, laying eggs, surviving in unfavorable conditions by creating a dauer larva and sensing touch and temperature (Rankin, 2002).

The *C. elegans* has two sexes, with hermaphrodites containing two X chromosomes and males, which result from a spontaneous X chromosome loss durning meiosis (Hodgkin et al., 1979). Hermaphrodites differ from males in appearance, as shown in the **Figure 2** (**A**, **B**). During hermaphrodite development, first sperm and then oocytes are produced (Bahrami and Zhang, 2013). As a result of self-fertilization, about 300 offspring are formed, of which only 0.2% - 0.5% are males (Hodgkin et al., 1979). In nature, male individuals are responsible for the exchange of genetic material, which contributes to increasing genetic diversity and adaptation to changing environmental conditions. In the laboratory, experiments are mainly conducted on hermaphrodites, because they self-fertilize and thus their offspring are clones of the parent nematode, facilitating the maintenance of *C. elegans* lines. Males are used in crosses to move mutations between various genetic backgrounds or get rid of unwanted mutations by outcrossing them against a wild-type (WT). The offspring of a male-fertilized hermaphrodite will contain up to 50% males and the brood size will rise from 300 up to 1400 due to higher amount of sperm delivered by the male (Chasnov, 2013). The nematodes are sensitive to the ambient temperature, therefore in laboratory conditions *C. elegans* are grown in the range of 15°C - 25°C. The application of higher temperature for a short time (4 - 6 hours at 30°C) causes a heat shock, which leads to an increase in the male population to about 2% - 5% in the F1 generation (Hodgkin, 1983). An additional important feature in *C. elegans* is the ability to synchronize them by treating gravid adults with bleach, that destroys everything except resistant embryos (Porta-de-la-Riva et al., 2012). Finally, *C. elegans* can be frozen and stored for a long time at -80°C in Trehalose-DMSO solution until reuse (McClanahan et al., 2020).

A

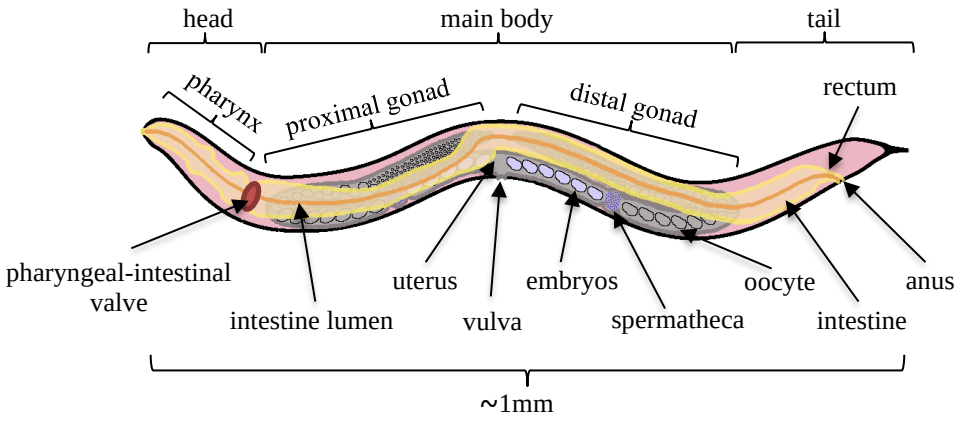

B

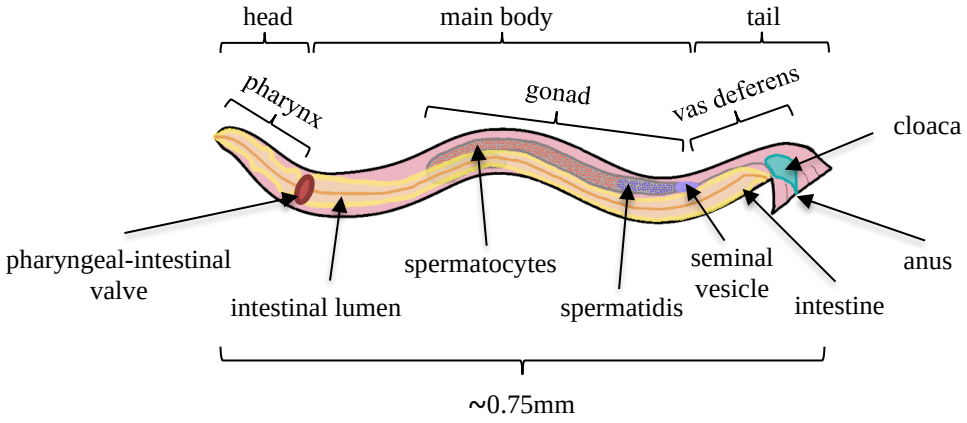

C

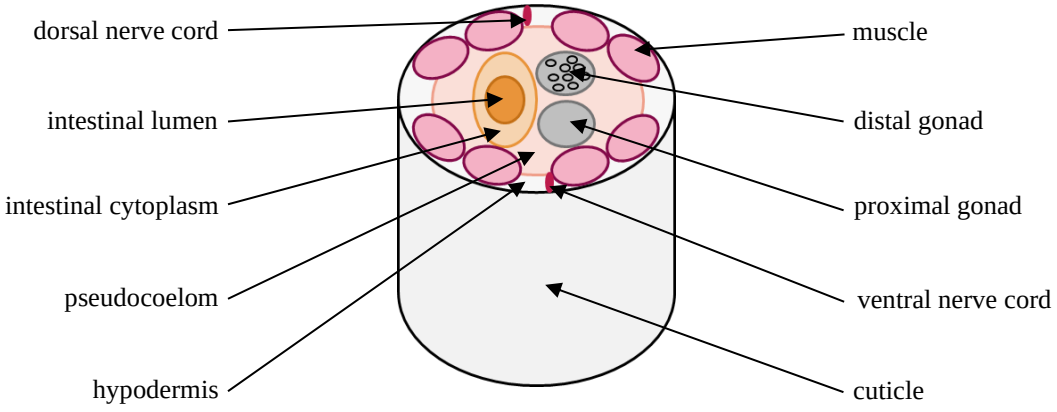

Figure 2. Scheme of the nematode's body plan. (**A**) The anatomy of an adult *C. elegans* hermaphrodite. Schematic drawing of anatomical structures, left lateral side. Based on *Corsi et al., 2015*. (**B**) The anatomy of an adult *C. elegans* male. Schematic drawing of anatomical structures, left lateral side. Based on *Corsi, 2015*. (**C**) Main body region of adult hermaphrodite. Based on *Corsi et al., 2015*.

2.2. Lipid accumulation

There is a strong similarity between molecular pathways regulating FAs metabolism in *C. elegans* and humans, e.g. FAs synthesis, elongation, desaturation as well as their degradation (Van Gilst et al., 2005; Yang et al., 2006; Watts and Browse, 2002). However, there are also some significant differences between *C. elegans* and humans. Instead of accumulating fat in AT, nematodes accumulate it in the intestine in the form of ubiquitous fat-storying lipid droplets (LDs) (O'Rourke et al., 2009). These organelles contain a lipid envelope composed of phosphatidylcholine (PC) and phosphatidylethanolamine (PE) (Tauchi-Sato et al., 2002). LDs range in size between 50 nm - 3000 nm (Zhang et al., 2012) and accumulate triglycerides (TAG) and cholesterol esters (CE) (Tauchi-Sato et al., 2002). Due to the fact that both the formation of TAG precursors and the conversion of diglycerides (DAG) to TAG by the diacylglycerol O-acyltransferase 2 (DGAT-2) take place on the surface of the endoplasmic reticulum (ER), LDs can be found in their close vicinity (Cao et al., 2019).

FAs are important for the proper functioning of all living organisms, because they serve as energy sources, build biological membranes and modulate cellular metabolism in response to extracellular signals (Calder, 2015). The composition of lipids also influences cell physiology. Because FAs differ in the number of double bonds, which affects the transition temperature of lipids, they impact the cell membrane fluidity and permeability (Choi et al., 2016).

In lipid biogenesis, humans use FAs derived from nutrients or provided by the intestinal microbiota (White, 2009; Jones et al., 2011). In contrast, *C. elegans* use FAs synthesized *de novo* from acetyl-CoA or provided via bacterial food (Perez and Van Gilst, 2008). The *de novo* synthesis of FAs in *C. elegans*, as shown in **Figure 3**, begins with acetyl-CoA, resulting from glycolysis or FA β-oxidation, which is converted into palmitic acid (16:0) by the carboxylation via *pod-2* enzyme (polarity and osmotic sensitivity defect enzyme) and *fasn-1* (fatty acid synthase) (Watts, 2009). The palmitic acid is further used for the synthesis of monounsaturated long-chain fatty acids (MUFAs) and polyunsaturated long-chain fatty acids (PUFAs). This happens with the help of numerous fatty acid desaturases (FATs) and elongases (ELOs) (Watts and Browse, 2002). The desaturases (FAT-3, FAT-4) and elongase (ELO-1) have their mammalian orthologs (Wallis et al., 2002). The main form of fat stored in *C. elegans* is TAG (Brock et al., 2006), consisting of an ester

of glycerol and three FAs (Srinivasan, 2015). In addition to TAGs, monoglycerides and DAGs are also accumulated in nematodes (Srinivasan, 2015). Their proportion depends on the temperature and the type of food (Tanaka et al., 1996; Brooks et al., 2009).

In the absence of food, nematodes are able to use energy obtained from the breakdown of fat (Jo et al., 2009). TAGs are hydrolyzed into FAs and glycerol by numerous lipases (Buis et al., 2019). The release of FAs cause *pod-2* inhibition, which leads to reduced levels of malonyl-CoA and the stimulation of carnitine palmitoyl transferase 1 (CPT-1) (Watts, 2009). FAs, after coenzyme A (CoA) attachment, are transported to the mitochondria by CPT-1, where they are β-oxidized (Watts, 2009). This leads to the shortening of the FA-CoA carbon chain and the formation of acetyl-CoA, needed for the adenosine triphosphate (ATP) synthesis in the tricarboxylic acid (TCA) cycle. An increase in carbohydrates and hence an increase in FAs is possible through the conversion of acetyl-CoA to glucose through glyoxylate shunt and gluconeogenesis, however it is more energetically beneficial to extract FAs directly from the diet (Watts, 2009).

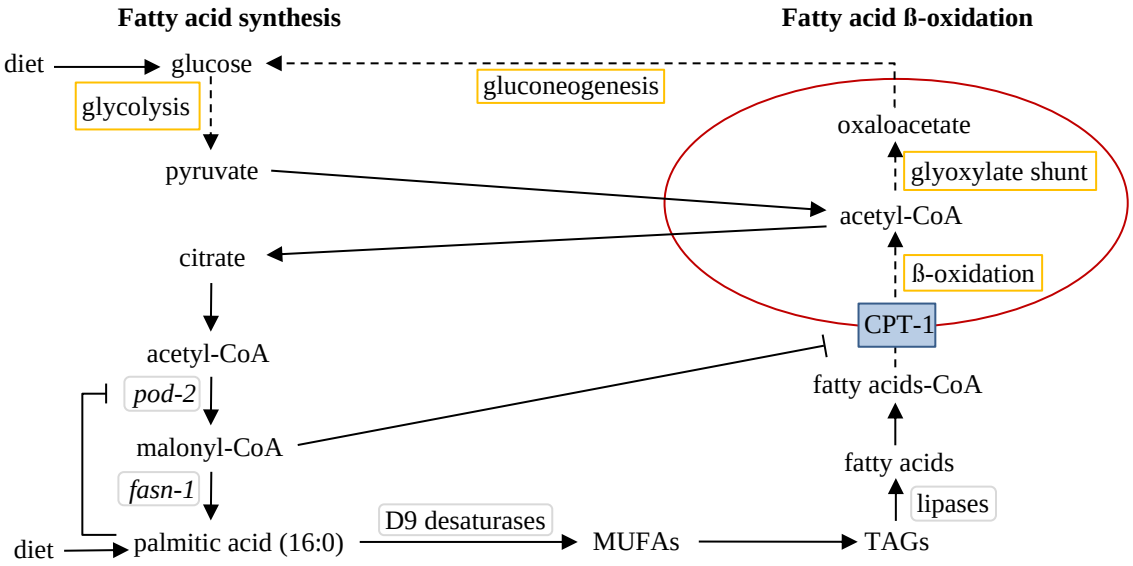

Figure 3. Scheme of the relationship between FA synthesis and FA oxidation in *C. elegans*. Glucose is converted to acetyl-CoA, which can be used to synthesize FAs that are stored as TAGs. Fat breakdown occurs through the mitochondrial ß-oxidation of FAs and the conversion of acetyl-CoA into glucose through the glyoxylate shunt and gluconeogenesis. Grey rectangle- lipid enzymes; orange rectangle- enzymatic steps; red oval- mitochondria. MUFAs- monounsaturated fatty acids; CPT- carnitine palmitoyl transferase; TAGs- triglycerides. Based on *Watts, 2009*.

2.3. Signaling pathways involved in lipid metabolism

Fat metabolism in *C. elegans* and humans is regulated via similar signaling pathways such as serotonin / 5-hydroxytryptamine (5-HT), transforming growth factor-β (TGF-β), insulin, AMP-activated protein kinase (AMPK) and target of rapamycin (TOR) (Soukas et al., 2009; Mihaylova and Shaw, 2012; Greer et at., 2008; Ashrafi, 2007; Srinivasan et al., 2008).

2.3.1. Serotonin signaling

5-HT is a conserved neuromodulator which, through serotonin signaling pathway, influences *C. elegans* feeding, reproductive life cycle, egg laying and fat storage in order to regulate energy balance (Noble et al., 2013; Sze et al., 2000). Due to the fact that food provides the energy necessary for the proper functioning of the body, its lack results in starvation and increased secretion of neuromodulators like 5-HT (Sze et al., 2000; Avery and Horvitz, 1990; Gray et al., 2005). Upon starvation, the energy needed to survive is obtained from the stored fat (Jo et al., 2009). During fasting, a large amount of 5-HT is synthesized in the ADF chemosensory neurons from tryptophan via the tryptophan hydroxylase 1 (TPH-1) (Noble et al., 2013), as shown in **Figure 4**. 5-HT, by binding to the serotonin-gated chloride channel 1 (MOD-1) on the URX neurons, induces release of the neuropeptide FMRF-like peptide 7 (FLP-7) from the ASI neuron (Palamiuc et al., 2017). FLP-7, by interacting with the neuropeptide receptor 22 (NPR-22) stimulates intestinal cells to break down lipids. This leads to an increase in the transcription of adipose triglyceride lipase 1 (*atgl-1*) and FAs β-oxidation, which results in the reduction of the body fat content (Noble et al., 2013; Palamiuc et al., 2017). Moreover, the activation of MOD-1 stimulates RIC neurons to release octopamine (OA), which, through the binding to the serotonin / octopamine receptor 6 (SER-6) present on AWB neurons, stimulates the expression of *tph-1* (Palamiuc et al., 2017). In contrast, deletion of the *tph-1* gene prevents 5-HT production, leading to animal growth arrest as dauers and increased fat accumulation (Sze et al., 2000).

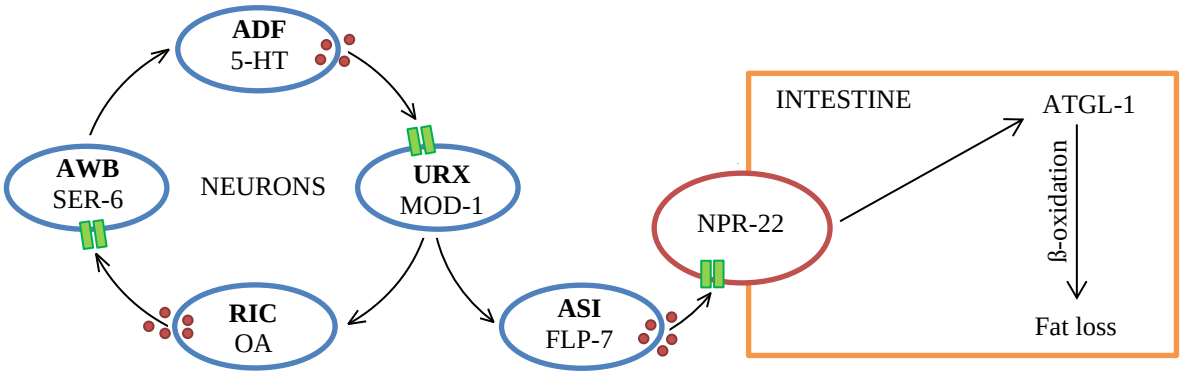

Figure 4. Serotonin signaling pathway. 5-HT produced in the ADF chemosensory neurons activates URX neurons via MOD-1. This induces the release of FLP-7 from the ASI neuron and stimulates the intestine to express ATGL-1 leading to a reduction in body fat. Bold- neurons; 5-HT- serotonin / 5-hydroxytryptamine; MOD- serotonin-gated chloride channel; OA- octopamine; SER- serotonin / octopamine receptor; FLP- FMRF-like peptide; NPR- neuropeptide receptor; ATGL- adipose triglyceride lipase. Based on *Noble et al., 2013* and *Palamiuc et al., 2017*.

2.3.2. TGF-ß signaling

In parallel to the 5-HT pathway, the TGF-β signaling pathway can regulate the *C. elegans* body fat, in addition to suppressing the entry into the dauer stage, as shown in **Figure 5** (Greer et al., 2008). The TGF-β ligand, produced in the ASI neurons, is encoded by the abnormal dauer formation 7 (*daf-7*), which upon the binding to the dauer formation 1 (DAF-1) and dauer formation 4 (DAF-4) receptors, activates the dauer formation 8 (DAF-8) and dauer formation 14 (DAF-14) signaling molecules (Dalfó et al., 2012; Lant and Storey, 2010). This inhibits transcription of the dauer-activating SMAD transcription factor (*daf-3*), which keeps the body fat at normal level, prevents larvae from passing into the dauer stage, stimulates growth and egg laying (Greer et al., 2008). Under unfavorable conditions, like high population density, high temperature, low food availability affecting early larval-stage animals or when the TGF-β signaling pathway is inactive due to *daf-7*, *daf-1* or *daf-4* mutations, DAF-3 is activated leading to increased body fat content by enhanced *de novo* fat synthesis and the transition of larvae into dauers (Greer et al., 2008).

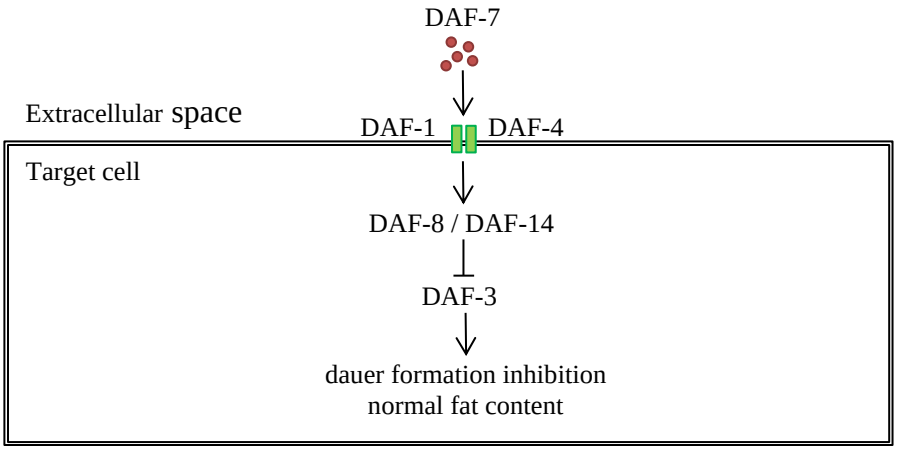

Figure 5. TGF-β signaling pathway. DAF-7, produced in the ASI chemosensory neurons, stimulates DAF-1 and DAF-4 receptors on target cells. This activates DAF-8 and DAF-14 and inhibits DAF-3, leading to normal fat accumulation and inhibition of dauer formation. Based on *Lant and Storey, 2010*.

2.3.3. Insulin signaling

Excessive food intake, which is one of the main causes of obesity in humans, is regulated by two hormones, insulin and leptin, secreted by pancreas and AT, respectively (Niswender and Schwartz, 2003). Since *C. elegans* does not have dedicated AT, it does not produce leptin and therefore insulin signaling pathway (IIS) is the main signaling pathway responsible for the regulation of body fat (Kimura et al., 1997).

In *C. elegans*, under favorable environmental conditions like optimal temperature, low population density and high food availability, the dauer formation 2 (DAF-2) receptor is activated by the insulin-like ligands, INS-1 through INS-39, which triggers a signaling cascade regulating target gene expression, as shown in **Figure 6** (Scerbak et al., 2014; Lant and Storey, 2010). Activated DAF-2, through auto-phosphorylation, stimulates AGE-1 (phosphatidylinositol 3-kinase), which leads to the conversion of PIP2 (phosphatidylinositol (4,5)-bisphosphate) to PIP3 (phosphatidylinositol (3,4,5)-trisphosphate), followed by the phosphorylation and activation of PDK-1 (3-phosphoinositide-dependent kinase 1) (Lant and Storey, 2010). PDK-1 is responsible for the phosphorylation and activation of the AKT-1 and AKT-2 (serine / threonine kinases 1 and 2) and the SGK-1 (serum and glucocorticoid inducible kinase 1), which then phosphorylate transcription factors such as DAF-16 (the dauer formation 16) and SKN-1 (skinhead 1), thus inhibiting their translocation

to the nucleus (Cohen and Dillin, 2008; Kimura et al., 1997). Environmental stress conditions such as overpopulation, temperature fluctuations, lack of food or mutations in the *daf-2* gene, leads to the activation of DAF-18 (dauer formation 18), which inhibits PIP-3 formation by AGE-1, negatively affects AKT-1 / -2 phosphorylation and dephosphorylates DAF-16 and SKN-1 (Ogg and Ruvkun, 1998; Tullet et al., 2008). These transcription factors translocate to the nucleus and stimulate expression of genes modulating life-span, growth, as well as glucose and lipid metabolism (McElwee et al., 2006; Murphy et al., 2003; Lee et al., 2003). Mutations within the *daf-2* gene cause lifespan extension and increase body fat content in adult animals, while in larvae it inhibits development by entering the dauer stage (Pierce et al., 2001). In mammals, the inactive IIS pathway leads to insulin resistance in muscle and liver, impairs glucose metabolism and hepatic lipid accumulation (Bugianesi et al., 2005).

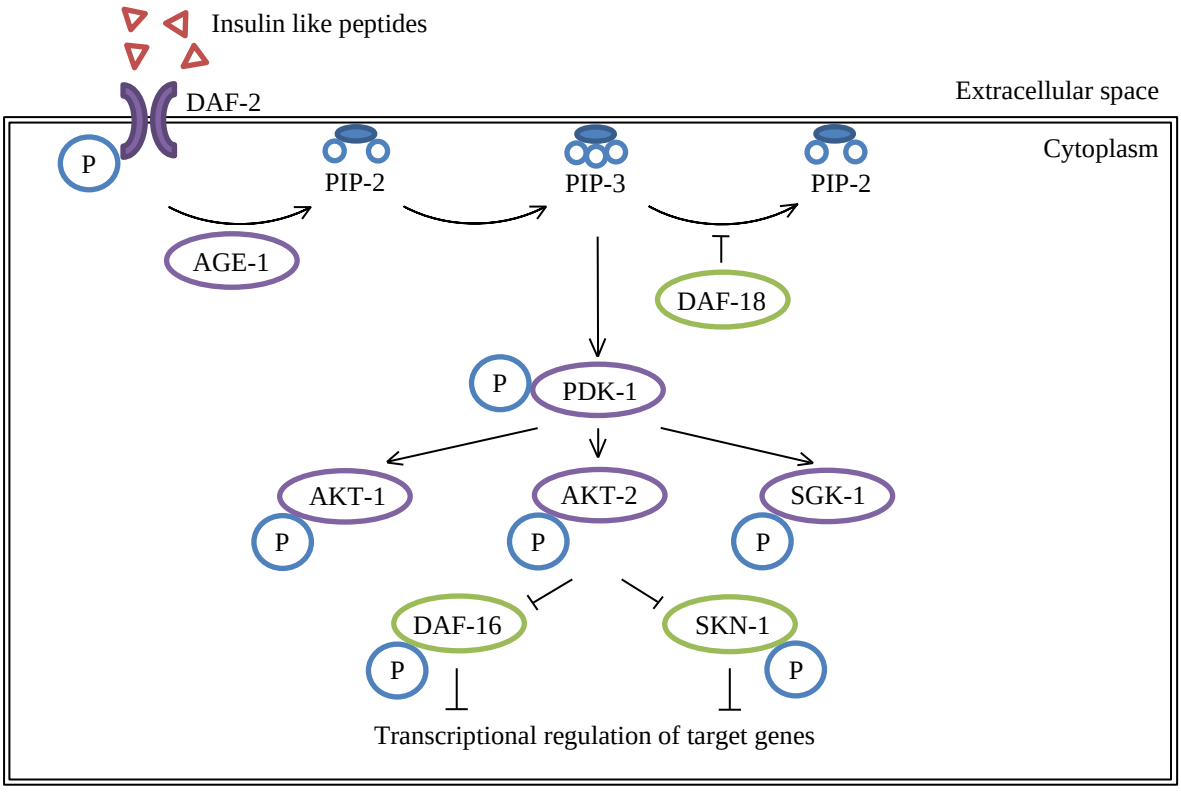

Figure 6. Insulin signaling pathway. Insulin-like peptides activate the DAF-2 receptor leading to the activation of the signaling cascade inactivating DAF-16 and SKN-1 through their phosphorylation. DAF- dauer formation; P- phosphate; AGE- phosphatidylinositol 3-kinase; PIP-2- phosphatidylinositol (4,5)-bisphosphate; PIP-3- phosphatidylinositol (3,4,5)-trisphosphate; PDK- 3-phosphoinositide-dependent kinase; AKT- serine / threonine kinase; SGK- glucocorticoid inducible kinase; SKN- skinhead. Based on *Ewald et al., 2017*.

2.3.4. Nutrient-sensing pathways: TOR and AMPK signaling

The body fat content of *C. elegans* can also be regulated by the evolutionarily conserved metabolic pathways TOR and AMP-activated protein kinase (AMPK), as shown in **Figure 7**. In *C. elegans*, TOR is activated by IIS and high level of amino acids provided with nutrients, whereas AMPK is activated in response to dietary restriction (DR) and low cellular energy reflected by the low AMP : ATP ratio (Wong and Roy, 2020; Gonzalez et al., 2020; Bar et al., 2016). The exact mechanism by which nutrients regulate TOR is not fully understood. There are two TOR complexes, the TORC1 and TORC2 (target of rapamycin complex 1 and 2), whereas AMPK is composed of two catalytic α subunits, the AAK-1 and AAK-2 (adenosine monophosphate (AMP) activated kinase 1 and 2). When food is available, AMPK remains inactive and TOR stimulates cell proliferation, lipid and protein synthesis, promoting growth and development (Jones et al., 2009; Bar et al., 2016). During nutrient deficiency in adult nematodes, AMPK is activated upon the binding of AMP and phosphorylation of its T-loop on Thr^{243} by the abnormal embryonic partitioning of cytoplasm 4 (PAR-4) (Wong and Roy, 2020). Active pAMPK inhibits TOR signaling pathway through its phosphorylation and promotes the expression of genes related to catabolism, including lipolysis by ATGL-1 and β-oxidation by the CoA fatty acid synthetase 2 (ACS-2) (Li et al., 2020). This leads to a reduction in the body fat content and an increase in the ATP level (Zaarur et al., 2019; Li et al., 2020). Nutrient deficiency in larvae leads to the transition of the nematodes into the dauer stage and fat accumulation. In order to survive unfavorable conditions and protect the energy fat stores, AMPK is activated, which, through the phosphorylation Ser^{303} of ATGL-1, inhibits lipid hydrolysis (Xie and Roy, 2015; Wong and Roy, 2020).

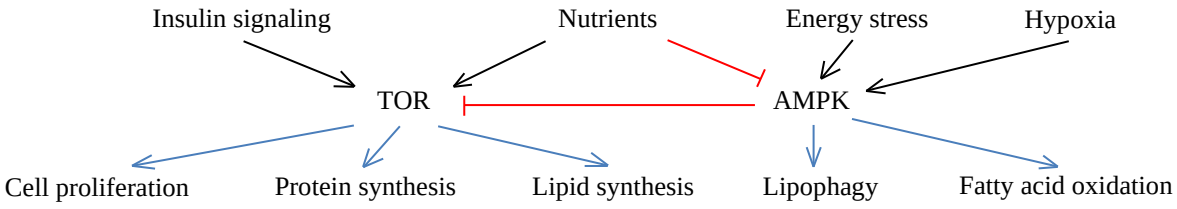

Figure 7. Regulation of metabolism by TOR and AMPK signaling pathway. Based on *Goncharova, 2013; Jones et al., 2009.*

2.4. Methods used to measure body fat levels in *C. elegans*

C. elegans is a promising model organism for obesity research, because there are many techniques available to measure and visualize its body fat content. The total body fat can be determined chemically by thin layer chromatography (TLC) (Aranaz et al., 2020) or by enzymatic reaction enabling the measurement of TAG content (Yen et al., 2010). LDs may contain different levels of unsaturated acyl chains depending on the presence or absence of double carbon bonds (Rinia et al., 2008). Since distinct bonds vibrate differently, the coherent anti-Stokes Raman scattering (CARS) microscopy may be used to measure the vibrations of C - C and C - H bonds in lipids (Rinia et al., 2008). Moreover, the transparent body of *C. elegans* enables easy observation of animals by Nomarski or DIC microscopy (Porta-de-la-Riva et al., 2012). At low magnification, the wild-type animals that contain high TAG content have a dark color. The visible dark appearance is caused by an increased refractivity of the fat storage granules (Vowels and Thomas, 1992). Therefore, animals with TAG-lowering mutations have a visible bright / pale appearance (McKay et al., 2003). The body fat can be easily visualized and measured by various techniques, such as staining with Nile Red or Oil Red O (ORO) dyes (Hellerer et al., 2007; Habacher et al., 2016). In addition to lipids, LDs also contain numerous proteins that are located on their surface, such as ATGL-1, short-chain dehydrogenases 3 (DHS-3), acyl-CoA synthetase 4 (ACS-4) and DGAT-2 (Vrablik et al., 2015; Zhang et al., 2012; Xu et al., 2012b; Liu et al., 2014). These proteins tagged with e.g. a green fluorescent protein (GFP) can be used for visualization and measurement of the amount of LDs, but also determination of their size, the increase of which reflects metabolic dysfunction and obesity phenotype (Trayhurn, 2007).

3. REGE-1 as a novel factor regulating fat metabolism in *C. elegans*

Previous studies on *C. elegans* aimed to understand the mechanisms responsible for hibernation, which allow morphological, physiological and behavioral adaptation to seasonal or daily temperature changes (Habacher et al., 2016). A genetic screening performed to find genes necessary for the survival of *C. elegans* at low temperatures, led to the discovery of the *rege-1* gene, the mutation of which increased the amount of the transcription factor

ETS-4, and at low temperatures caused nematodes' death. In addition, the *rege-1* mutation affected the body fat content of animals resulting in its significant decrease both at room and low ambient temperature (Habacher et al., 2016). Further studies demonstrated that REGE-1 is an endoribonuclease similar to mammalian monocyte chemotactic protein-induced protein MCPIP1 / Zc3h12a / Regnase-1 (Habacher et al., 2016; Xu et al., 2012a) and regulates *ets-4* expression through the messenger RNA (mRNA) cleavage on its 3' untranslated region (UTR) (Habacher and Ciosk, 2017). In *C. elegans* ETS-4 regulates the expression of genes related to catabolism and immunity (Habacher et al., 2016). Mammalian Regnase-1 exerts a similar function to nematode's REGE-1, as it regulates post-transcriptional gene expression influencing immune homeostasis as well as cellular adaptation in diseases such as autoimmune disorders and cancer (Mao et al., 2017; Habacher and Ciosk, 2017).

However, data regarding the effect of MCPIP1 / Zc3h12a / Regnase-1 on the regulation of AT are inconclusive. At first, the expression of *MCPIP1* was shown to be increased in obese people compared to individuals with lower body fat content (Lipert et al., 2014). However, more recent studies have shown that *MCPIP1* expression decreases with increased body mass index (BMI) (Losko et al., 2020). In addition, detailed analysis using the 3T3-L1 cell line also showed differences in the influence of *MCPIP1* expression on fat accumulation. Overexpression of MCPIP1 in 3T3-L1 cells stimulated adipogenesis, ER stress and autophagy by increasing the amount of iNOS (inducible-nitric oxide synthase) and reactive oxygen / nitrogen species (Younce and Kolattukudy, 2012). Moreover, MCPIP1 regulated C / EBPβ (CCAAT enhancer-binding protein beta) expression without affecting the level of the master adipogenic regulator PPARγ (peroxisome proliferator-activated receptor gamma) (Younce et al., 2009). Other studies on the 3T3-L1 cell line demonstrated that overexpression of MCPIP1 led to a decrease in the expression of genes related to adipocyte differentiation (*PPARG*, *CEBPA*), as well as lipid and FAs metabolism (*SCD1*, *LPL*, *ELOVL1*, *STAT5A*), TAG biosynthesis (*DGAT2*, *SREBF1*) and dicarboxylic acid transport (*SLC25A10*) (Losko et al., 2020). Moreover, MCPIP1 downregulated the expression of genes related to carbohydrate metabolism (*MGAT1*), insulin-stimulated glucose uptake (*SLC2A4* and *TBC1D4*) and inhibited the activity of IIS pathway (Losko et al., 2020).

Due to large discrepancies in the results of studies conducted both in humans and mammalian cell lines on the Regnase-1-mediated regulation of the body fat content and the similarity of mammalian Regnase-1 to *C. elegans* REGE-1, nematodes can be used as a model organism to expand the knowledge about Regnase-1 function and discover new metabolic pathways regulating fat accumulation in mammals. This can be helpful in the future for finding new treatments for obesity as well as reducing the incidence of obesity-related metabolic diseases.

THE AIM OF THE THESIS

It has previously been found that in *C. elegans* ribonuclease REGE-1 regulates the expression of genes involved in lipid metabolism and immunity by targeting the 3' UTR fragment of the *ets-4* mRNA (Habacher et al., 2016). Degradation of *ets-4* mRNA and inhibition of ETS-4 protein synthesis induces *rege-1* transcription, which creates an auto-regulatory module, as shown in **Figure 8**. Consequently, fat catabolism is repressed, which results in increased fat accumulation in *C. elegans*. Conversely, upon knock down of the *rege-1* gene, ETS-4 can activate lipid catabolism, leading to a reduction in the body fat content (Habacher et al., 2016).

The overall aim of the presented study was to uncover molecular mechanism/s downstream of the REGE-1 – ETS-4 regulatory axis that lead to inhibition of fat accumulation in *C. elegans*. Accordingly, the first aim of this work was to characterize phenotypic changes that occur in response to RNAi-mediated downregulation of the target *rege-1* mRNAs in nematodes. Changes in the amount of total body fat were visualized using the Oil red O staining. In addition to the relative triglyceride content, the sizes of the lipid droplets were determined. The second aim of this study was to identify and determine the function of potential ETS-4 target genes. Thus, the influence of candidate genes downstream from ETS-4 found in an unbiased genetic screening and through the RNA sequencing data analysis on fat accumulation in the *rege-1* mutants were examined. The third goal of this thesis was to test the effect of ETS-4 on cellular functions e.g. by checking the expression of genes influencing FA, sphingolipid metabolism, glycogen synthesis and by checking the effect of ETS-4 on cellular respiration.

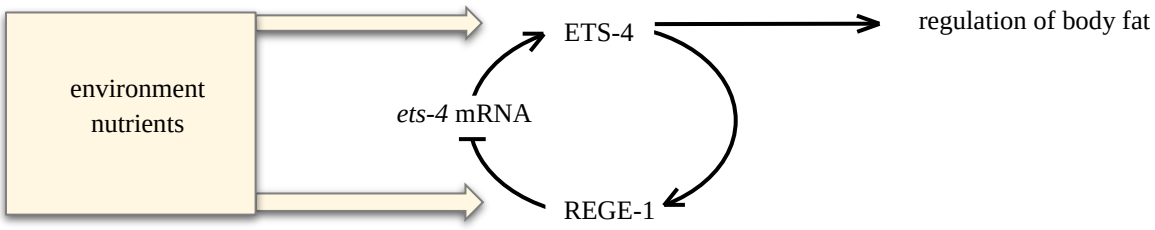

Figure 8. The REGE-1 – ETS-4 fat regulatory network. Based on *Habacher et al., 2016.*

RESULTS

1. Characterization of the *rege-1* mutant animals

Mutant nematodes carrying the deletion of the *rege-1* gene created via CRISPR-Cas9 are characterized by a large developmental delay compared to wild-type animals (Habacher et al., 2016). In order to investigate the functional relationship between the body fat levels and ETS-4, in this PhD thesis the experiments were carried out using animals in which the *rege-1* was silenced through RNAi by feeding animals with *E. coli* carrying dsRNA against the *rege-1* mRNA (see details in Materials and Methods). In RNAi-based mRNA targeting experiments, animals fed with bacteria carrying an empty vector were described as animals exposed to mock RNAi, while the wild-type exposed to mock RNAi were described as control. Feeding RNAi did not affect the body fat levels of nematodes, but allowed to slightly minimize the differences in development length between mutants.

1.1. *C. elegans* REGE-1 is an ortholog of human Regnase-1

To illustrate the protein sequence conservation, an alignment of *H. sapiens* Regnase-1 and *C. elegans* REGE-1 was performed, as shown in **Figure 9 A**. The analysis demonstrated that there is a 35.5% sequence similarity between the *C. elegans* REGE-1 and human Regnase-1.

Moreover, the similarity between *C. elegans* REGE-1 and human Regnase-1 can be observed in the protein structure proposed in **Figure 9** (**B**, **C**). Both proteins have four aspartic acids forming an active center with RNAse activity. Moreover, both proteins have CCCH-zinc finger domains, which are responsible for binding endoribonuclease to target RNA and increases the efficiency of its cleavage (Yokogawa et al., 2016). Since both sequences and protein structures of Regnase-1 and REGE-1 are similar, they might exert familiar biological functions.

A

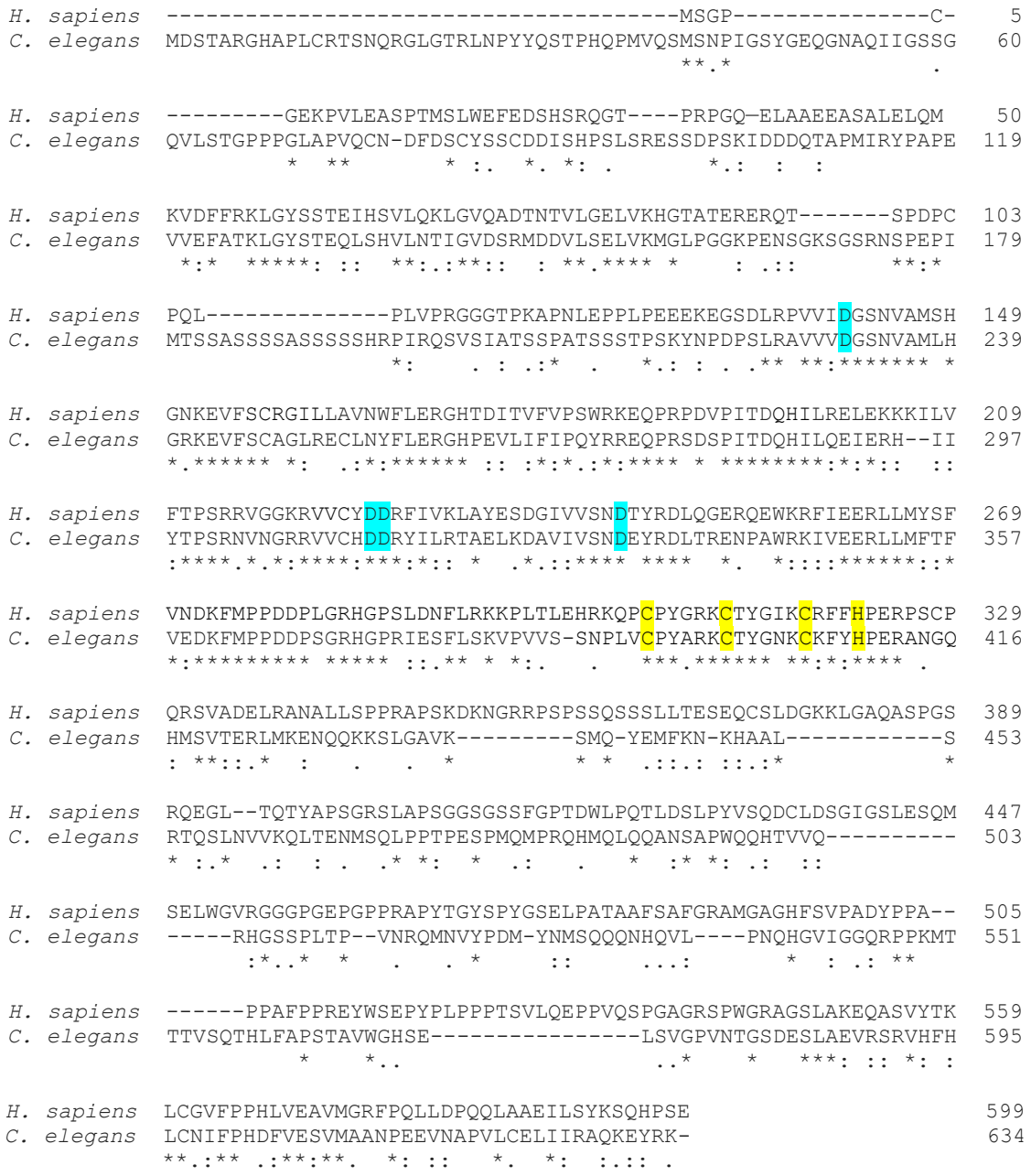
H. sapiens ----------MSGP----------C- 5
C. elegans MDSTARGHAPLCRTSNQRGLGTRLNPYYQSTPHQPMVQSMSNPIGSYGEQGNAQIIGSSG 60
H. sapiens ---------GEKPVLEASPTMSLWEFEDSHSRQGT----PRPGQ—ELAAEEASALELQM 50
C. elegans QVLSTGPPPGLAPVQCN-DFDSCYSSCDDISHPSLSRESSDPSKIDDDQTAPMIRYPAPE 119
H. sapiens KVDFFRKLGYSSTEIHSVLQKLGVQADTNTVLGELVKHGTATERERQT-------SPDPC 103
C. elegans VVEFATKLGYSTEQLSHVLNTIGVDSRMDDVLSELVKMGLPGGKPENSGKSGSRNSPEPI 179
H. sapiens PQL--------------PLVPRGGGTPKAPNLEPPLPEEEKEGSDLRPVVIDGSNVAMSH 149
C. elegans MTSSASSSSASSSSSHRPIRQSVSIATSSPATSSSTPSKYNPDPSLRAVVVDGSNVAMLH 239
H. sapiens GNKEVFSCRGILLAVNWFLERGHTDITVFVPSWRKEQPRPDVPITDQHILRELEKKKILV 209
C. elegans GRKEVFSCAGLRECLNYFLERGHPEVLIFIPQYRREQPRSDSPITDQHILQEIERH--II 297
H. sapiens FTPSRRVGGKRVVCYDDRFIVKLAYESDGIVVSNDTYRDLQGERQEWKRFIEERLLMYSF 269
C. elegans YTPSRNVNGRRVVCHDDRYILRTAELKDAVIVSNDEYRDLTRENPAWRKIVEERLLMFTF 357
H. sapiens VNDKFMPPDDPLGRHGPSLDNFLRKKPLTLEHRKQPCPYGRKCTYGIKCRFFHPERPSCP 329
C. elegans VEDKFMPPDDPSGRHGPRIESFLSKVPVVS-SNPLVCPYARKCTYGNKCKFYHPERANGQ 416
H. sapiens QRSVADELRANALLSPPRAPSKDKNGRRPSPSSQSSSLLTESEQCSLDGKKLGAQASPGS 389
C. elegans HMSVTERLMKENQQKKSLGAVK---------SMQ-YEMFKN-KHAAL----------S 453
H. sapiens RQEGL--TQTYAPSGRSLAPSGGSGSSFGPTDWLPQTLDSLPYVSQDCLDSGIGSLESQM 447
C. elegans RTQSLNVVKQLTENMSQLPPTPESPMQMPRQHMQLQQANSAPWQQHTVVQ---------- 503
H. sapiens SELWGVRGGGPGEPGPPRAPYTGYSPYGSELPATAAFSAFGRAMGAGHFSVPADYPPA-- 505
C. elegans -----RHGSSPLTP--VNRQMNVYPDM-YNMSQQQNHQVL----PNQHGVIGGQRPPKMT 551
H. sapiens ------PPAFPPREYWSEPYPLPPPTSVLQEPPVQSPGAGRSPWGRAGSLAKEQASVYTK 559
C. elegans TTVSQTHLFAPSTAVWGHSE----------------LSVGPVNTGSDESLAEVRSRVHFH 595
H. sapiens LCGVFPPHLVEAVMGRFPQLLDPQQLAAEILSYKSQHPSE 599
C. elegans LCNIFPHDFVESVMAANPEEVNAPVLCELIIRAQKEYRK- 634

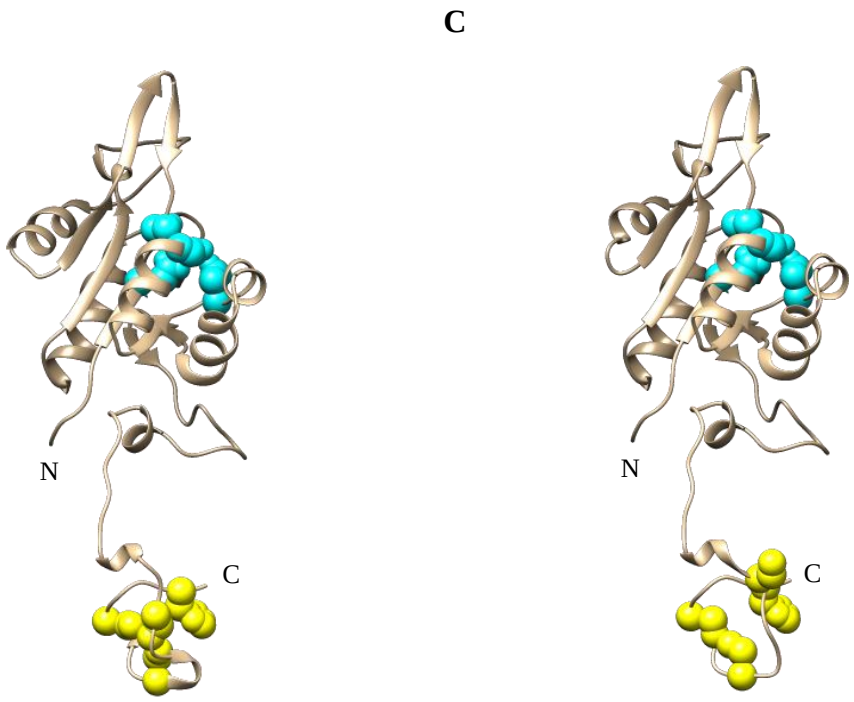

Figure 9. Comparison of the sequence and protein structure of human Regnase-1 and *C. elegans* REGE-1. (**A**) The alignment of *H. sapiens* Regnase-1 and *C. elegans* REGE-1 sequence. The alignment was performed using the multiple sequence alignment tool ClustalOmega. Marks indicate as follows: "*" perfect alignment; ":" strong similarity; "." weak similarity; cyan- four aspartic acids in the active center; yellow- CCCH-zinc finger domain. (**B**, **C**) Structure comparison of human Regnase-1 and *C. elegans* REGE-1. (**B**) Three-dimesional structure of human Regnase-1 made in the program Pyre 2 and colored in UCSF Chimera. Marks indicate as follows: N- NH_2 terminus; C- COOH terminus; cyan - four aspartic acids (D141, D225, D226, D244) in the active center; yellow– CCCH-zinc finger domain. (**C**) Three-dimesional structure of *C. elegans* REGE-1 made in the program Pyre 2 and colored in UCSF Chimera. Marks indicate as follows: N- NH_2 terminus; C- COOH terminus; cyan - four aspartic acids (D231, D313, D314, D332) in the active center; yellow– CCCH-zinc finger domain. Based on *Habacher et al., 2017*.

1.2. Mutation in *rege-1* increased *ets-4* mRNA levels

To confirm the effect of REGE-1 on ETS-4, reported by *Habacher et al. 2016*, *ets-4* mRNA expression was measured by quantitative reverse transcription PCR (RT-qPCR) in single *rege-1* and *ets-4; rege-1* double mutant animals exposed to mock RNAi. In further experiments, *ets-4; rege-1* double mutants were used as a negative control to exclude the regulation of gene expression by genes other than *rege-1* and *ets-4*. The *ets-4* mRNA levels in the mutant animals were compared to controls, as shown in **Figure 10**. To validate the RNAi plates, *rege-1* mRNA was targeted by RNAi in the wild-type animals. As expected, *ets-4* mRNA levels increased significantly in both the wild-type in which *rege-1* mRNA has

been targeted by RNAi and the *rege-1* mutants exposed to mock RNAi. In the *ets-4; rege-1* double mutants treated with mock RNAi, *ets-4* mRNA was significantly lower in comparison to controls. These results confirmed that functional REGE-1 significantly reduces *ets-4* mRNA levels in the wild-type animals.

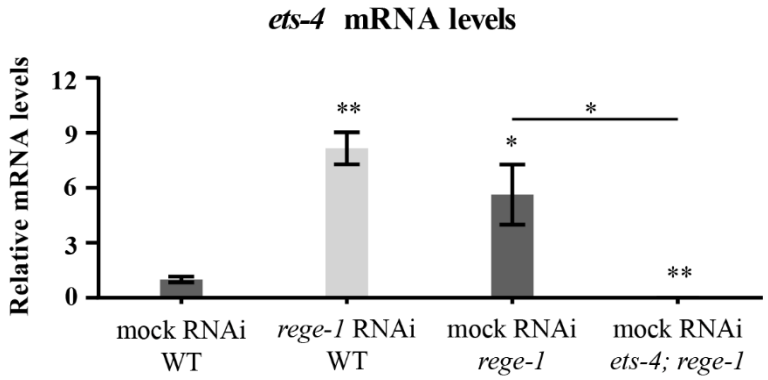

Figure 10. REGE-1 significantly reduced *ets-4* mRNA levels in the wild-type animals. The level of *ets-4* mRNAs was measured by RT-qPCR in the wild-type animals and in nematodes carrying either *rege-1* or *ets-4; rege-1* mutations exposed to mock or *rege-1* RNAi. *ets-4* mRNA levels were normalized to the levels mRNA of actin 1 and compared to wild-type animals subjected to mock RNAi. The P values were calculated using un-paired Student t-test (*n = 3*). Data are presented as mean; error bars represent SEM (* indicates $p < 0.05$; ** $p < 0.01$).

1.3. Depletion of *ets-4* rescued the fat loss phenotype of *rege-1* mutants

To confirm that the changes of ETS-4 levels affect body fat (Habacher et al., 2016), LDs were stained using the lipophilic dye ORO and the amount of TAG was determined biochemically.

The ORO staining showed that *ets-4* mutants exposed to mock RNAi had increased amount of body fat compared to controls, as presented in **Figure 11** (**A**, **B**). Both *rege-1* mutant animals exposed to mock RNAi and wild-type animals in which *rege-1* mRNA has been targeted by RNAi had reduced body fat content compared to controls. In contrast, fat accumulation in the *ets-4* mutant animals fed with bacteria targeting the *rege-1* mRNA, was significantly greater compared to controls and to the wild-type animals subjected to *rege-1* RNAi.

Similar results were obtained by the biochemical method measuring TAG content (**Figure 11 C**). The *ets-4* mutants had increased TAG levels compared to controls. Both *rege-1* mutants subjected to mock RNAi and wild-type animals fed with bacteria targeting *rege-1* mRNA had reduced TAG levels compared to controls. In contrast, targeting *rege-1* mRNA by RNAi significantly increased the amount of TAG in *ets-4* mutants compared to the wild-type animals fed with the same bacteria containing *rege-1* RNAi.

In summary, high levels of *ets-4* mRNA observed in *rege-1* mutant animals and *rege-1* RNAi wild-type animals cause a significant reduction in the amount of body fat as evidenced by the ORO staining and total TAG levels compared to controls. Moreover, targeting *rege-1* mRNA in the *ets-4* mutants is sufficient to rescue the fat loss phenotype of the *rege-1* mutants. These findings supported the previous observations by *Habacher et al., 2016.*

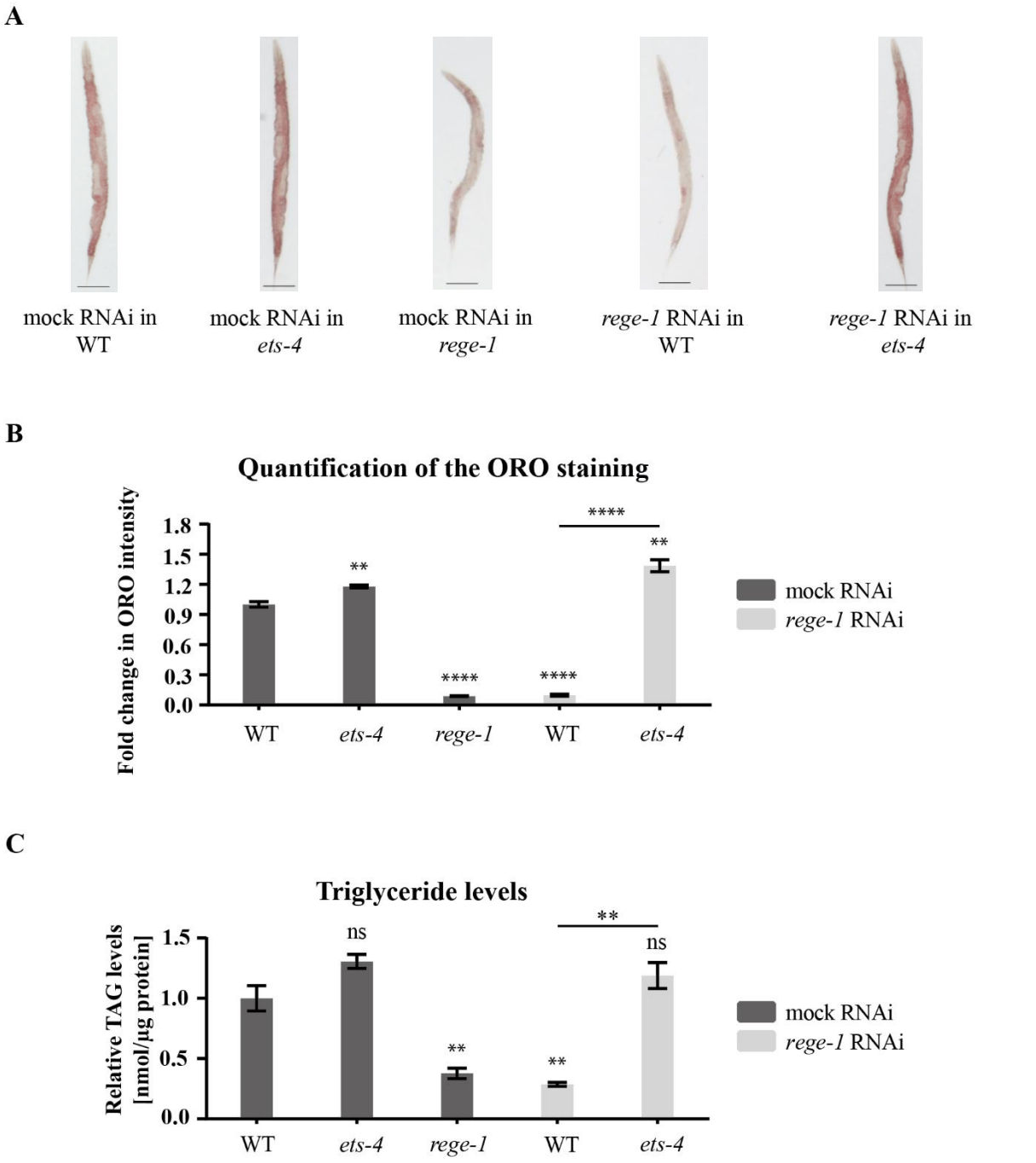

Figure 11. Depletion of *ets-4* mRNA rescued the fat loss phenotype of *rege-1* mutants. (**A**) Images of wild-type and animals carrying either *rege-1* or *ets-4* mutations exposed to mock RNAi or dsRNA targeting *rege-1* mRNA. The animals were stained with ORO to visualize body fat levels. Scale bar: 100 µm. (**B**) Quantification of relative changes in the ORO staining. 30 animals per condition were measured. Changes in body fat levels were determined in relation to wild-type animals subjected to mock RNAi. The P values were calculated using un-paired Student t-test (*n = 3*). Data are presented as mean; error bars represent SEM (** indicates $p < 0.01$; **** $p < 0.0001$). (**C**) Quantification of changes in TAG levels relative to the total protein content in wild-type or animals carrying either *rege-1* or *ets-4* mutations exposed to mock or *rege-1* RNAi. Changes in TAG levels were measured in relation to wild-type animals subjected to mock RNAi. The P values were calculated using un-paired Student t-test (*n = 3*). Data are presented as mean; error bars represent SEM (** indicates $p < 0.05$).

1.4. Deletion in one copy of *ets-4* partially rescued the fat loss phenotype of *rege-1* mutants

Silencing of *rege-1* mRNA or mutating the *rege-1* gene significantly increased the expression of the *ets-4* mRNA, which led to a reduction in total body fat and TAG levels. To find out what level of the *ets-4* mRNA is sufficient to regain fat in *rege-1* mutants, *rege-1* mutant animals were crossed with the *ets-4; rege-1* double mutant strain, as shown in **Figure 12**. In the F1 generation, heterozygotes for the *ets-4* gene on chromosome X and homozygous background for the *rege-1* on chromosome I was obtained.

ets-4(+/+)*X*; *rege-1*(-/-)*I* X *ets-4*(-/-)*X; rege-1*(-/-)*I* = *ets-4(+/-)X; rege-1*(-/-)*I*

Figure 12. Scheme demonstrating the procedure of genetic crosses. Generation of heterozygotes for the *ets-4* gene on chromosome X and the homozygous background for the *rege-1* gene on chromosome I. (+/+) gene expression on two alleles; (-/-) lack of gene expression; (+/-) gene expression on one allele.

100 hermaphrodites of similar developmental stage were manually selected for the RT-qPCR analysis. Examination of *ets-4* mRNA levels by RT-qPCR, presented in **Figure 13 A**, showed that the loss of one copy of the *ets-4* gene in heterozygotes does not affect the *ets-4* mRNA levels, which remain similar to that observed in the *rege-1* mutants. On the other hand, the measurement of the body fat content using the ORO staining, presented in **Figure 13** (**B**, **C**), demonstrated that the loss of one copy of the *ets-4* gene is sufficient to significantly increase the level of body fat in *ets-4*(+/-)*; rege-1*(-/-) mutants compared to the *rege-1* single mutant animals.

In summary, the loss of one copy of the *ets-4* gene did not lower *ets-4* mRNA levels, however is sufficient to partially rescue the fat loss in *rege-1* mutants. However, the lack of change in mRNA level does not rule out changes in protein level, which may be crucial for downstream stimulation of lipolytic genes.

A

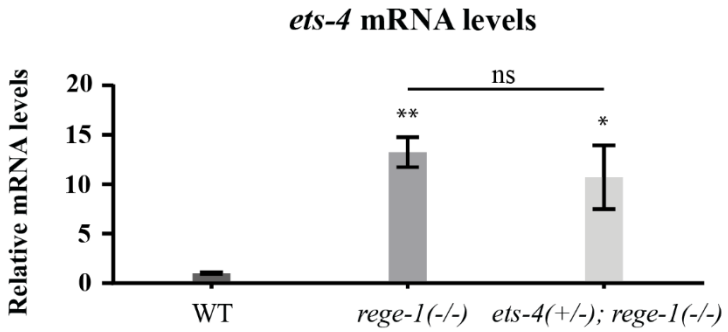

B

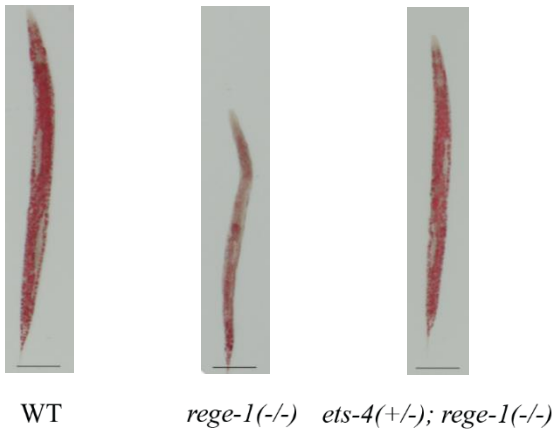

C

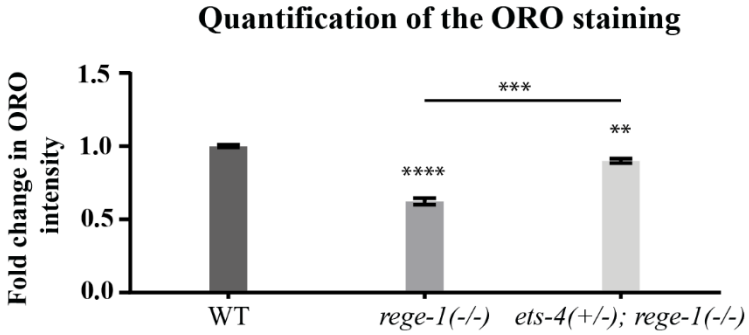

Figure 13. The loss of one copy of the *ets-4* gene was sufficient to partially rescue the fat loss phenotype of *rege-1* mutants. (**A**) *ets-4* mRNA levels in wild-type or animals carrying either *rege-1* or *ets-4(+/-); rege-1(-/-)* mutantions measured by RT-qPCR from 100 animals per condition. The mRNA levels were normalized to the levels mRNA of actin 1 and compared in relation to wild-type animals. The P values were calculated using un-paired Student t-test ($n = 3$). Data are presented as mean; error bars represent SEM (* indicates $p < 0.05$; ** $p < 0.01$). (**B**) Images of wild-type and animals carrying either *rege-1* or *ets-4(+/-); rege-1(-/-)* mutations. The animals were stained with the ORO to reveal fat level. Scale bar: 100 µm. (**C**) Quantification of changes in the ORO staining for at least 8 animals per condition were measured. Changes in the body fat levels were measured in relation to wild-type animals. The P values were calculated using un-paired Student t-test. Data are presented as mean; error bars represent SEM (** indicates $p < 0.01$; *** $p < 0.001$; **** $p < 0.0001$).

1.5. ETS-4 contributed to the regulation of lipolytic genes in *rege-1* mutants

To determine whether high levels of ETS-4 lead to a reduction in the body fat content through the expression of lipases, changes in the mRNA levels of *lipl-1* and *lipl-2* were measured in the *rege-1* mutants, as shown in **Figure 14**. The *lipl-1* and *lipl-2* mRNA levels were increased in both the wild-type animals with targeted *rege-1* mRNA and in *rege-1* mutants exposed to mock RNAi compared to controls. Whereas in *ets-4; rege-1* mutants (exposed to mock RNAi) mRNA levels of *lipl-1* and *lipl-2* lipases significantly decreased compared to *rege-1* mutants exposed to mock RNAi. These results indicated that ETS-4 stimulated the expression of lipoliytic genes in *rege-1* mutant animals.

A

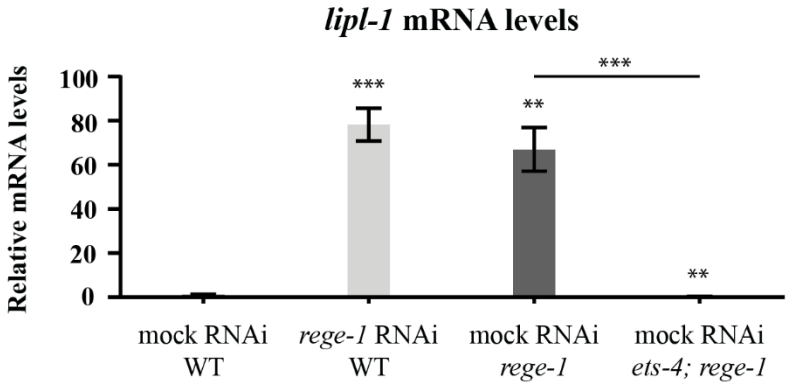

B

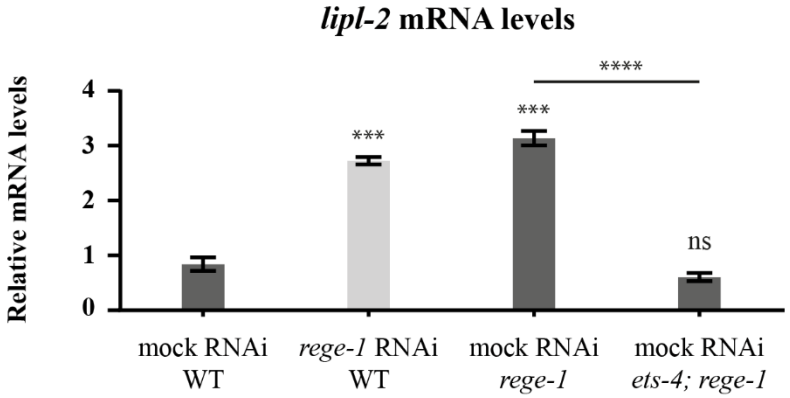

Figure 14. ETS-4 modulated the expression of lipolytic genes in the *rege-1* mutants. The levels of *lipl-1* (**A**) and *lipl-2* (**B**) mRNAs were measured by RT-qPCR in the wild-type animals and nematodes carrying either *rege-1* or *ets-4; rege-1* mutations exposed to mock or *rege-1* RNAi. The mRNA levels were normalized to the actin 1 mRNA levels and compared in relation to wild-type animals subjected to mock RNAi. The P values were calculated using un-paired Student t-test (*n = 3*). Data are presented as mean; error bars represent SEM (** indicates $p < 0.01$; *** $p < 0.001$; **** $p < 0.0001$).

2. Identification of ETS-4 target genes

In order to study the pathway regulating the level of the body fat through the REGE-1 - ETS-4 regulatory axis, the first step was to determine downstream ETS-4 target genes. This was carried out in two parallel ways, through a forward genetic screening and the analysis of available RNA sequencing data.

2.1. Candidate genes found in an unbiased genetic screening

In order to identify and characterize potential ETS-4 regulated genes responsible for the fat loss phenotype of the *rege-1* mutant animals, a forward genetic screening has previously been performed in Prof. Rafał Ciosk's laboratory in Basel, as shown in **Figure 15**. Forward genetic screen is a method that identifies genes responsible for a specific phenotype. Due to the fact that the *rege-1* mutants have reduced body fat content, through random mutagenesis using ethyl methanesulfonate (EMS), we searched for genes, whose mutation would change the fat loss phenotype and thus increase fat accumulation in *rege-1* mutants. EMS is an alkalic agent that, through chemical modification of guanine bases, leads to miss-pair with an arginine, resulting in mutations (Coulondre and Miller, 1977). Through EMS-mediated mutagenesis of the *rege-1* animals carrying two copies of the *ets-4* gene (one endogenous and one GFP-tagged allowing immediate evaluation of the ETS-4 level) multiple mutations in the multidrug resistance protein 1 (*mrp-1*) gene were identified (**Table 1**). The loss-of-function mutations, which increased the body fat content in *rege-1* deletion mutants were selected for further functional analysis.

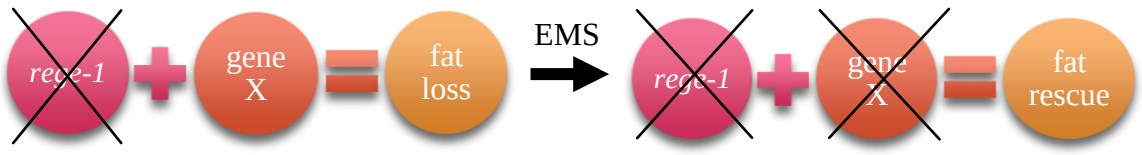

Figure 15. The scheme of mutagenesis screen designed to identify genes which can suppress "paleness" of *rege-1* mutants. Gene X- unknown gene; EMS- ethyl methanesulfonate.

Table 1. Genetic mutations revealed by the EMS screen. Mutations which increased fat accumulation in the *rege-1* mutants.

Gene	Mutation		Molecular consequences of mutation
mrp-1	chrX:587369	1452F6	splice site
	chrX:584039	Y491*	STOP
	chrX:579256	S1154F	MISSENSE
	chrX:586330	Q35*	STOP
	chrX:583762	P569S	MISSENSE
	chrX:583835	W544*	STOP
	chrX:583935	W526*	STOP
	chrX:578570	G1293R	MISSENSE
	chrX:584508	Q350*	STOP
	chrX:576778	D1456N	MISSENSE
	chrX:583104	A752T	MISSENSE
	chrX:584463	G365R	MISSENSE

2.1.1. *mrp-1* as a candidate target of ETS-4

The results of EMS mutagenesis showed that mutations in the *mrp-1* gene were the most common among other mutations, which increased fat accumulation in the *rege-1* mutants. This suggested that *mrp-1* could be a potential downstream target of the REGE-1 - ETS-4 regulatory axis that could influence the body fat content of nematodes. The aim of further experiments was to check the possible functional relationship between the MRP-1 transporter and the REGE-1 - ETS-4 regulatory axis.

2.1.1.1. The schematic representation of mammalian MRP1

Transporters from the ABC superfamily show high sequence homology between all living organisms (Saurin et al., 1999) including *C. elegans*, which shows 66% genomic sequence similarity and 47% identical protein sequence to human MRP1 (Broeks et al., 1996). This suggested that the structure and function of *C. elegans* MRP-1 might be similar to mammals MRPs, as shown in **Figure 16 A**. Both, mammalian and *C. elegans* MRP1 transporter are homodimers with an MSD1 – NBD1 – MSD2 – NBD2 domain structure (Yang et al., 2010; Sheps et al., 2004) in which membrane spanning

domains (MSDs) are connected with nucleotide binding domains (NBDs) through the cytoplasmic loops (CLs) (Iram and Cole, 2011). In this study, a three-dimensional prediction of the *C. elegans* MRP-1 structure was performed, which due to high protein sequence homology may correspond to the MRP1 structure in humans, as shown in **Figure 16** (**B**, **C**).

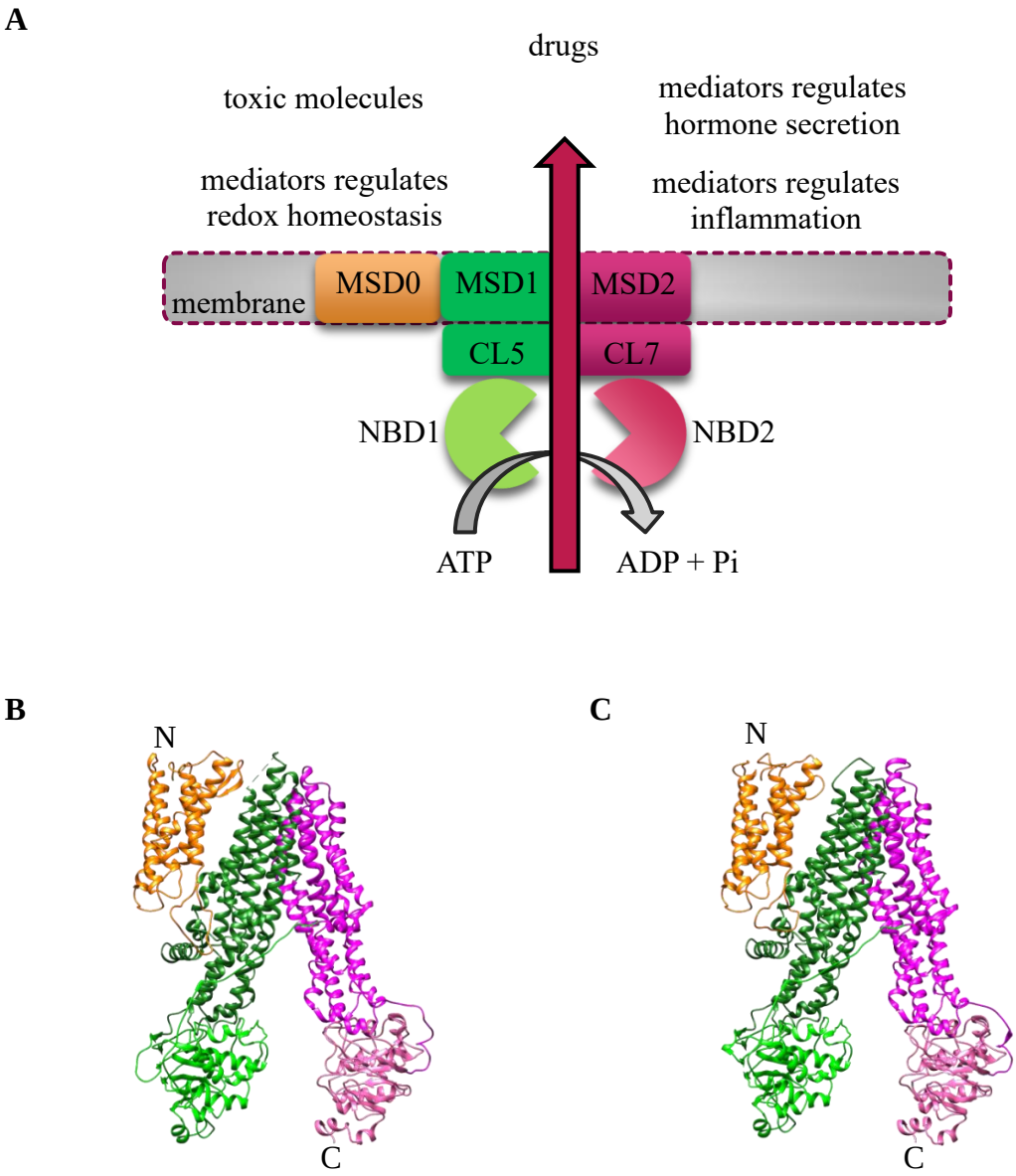

Figure 16. The structure of MRP1. (**A**) The schematic representation of mammalian MRP1 with putative type of substrates. MSD- membrane spanning domain; CL- cytoplasmic loop; NBD- nucleotide binding domain; ATP- adenosine triphosphate; ADP- adenosine diphosphate; Pi- inorganic phosphate. Based on *Cole, 2014*. (**B**) Three-dimesional structure of human MRP1. (**C**) Three-dimesional structure of *C. elegans* MRP-1 performed in the program Pyre 2 and colored in UCSF Chimera. Different colors correspond to distinct domains: orange- MSD0; forest green- MSD1 with CL5; green- NBD1; magenta- MSD2 with CL7; hot pink- NBD2. N- NH_2 terminus; C- COOH terminus.

2.1.1.2. Nematode MRP-1 was localized in epithelium and muscle

To determine the subcellular localization of MRP-1 protein in nematodes, endogenous MRP-1 was labeled with mCherry. The GFP filter and wild-type animals were used as a control for discrimination and correction of the autofluorescence of intestinal granules. Analysis based on the Worm Atlas indicates that the signal from the anterior part of the nematodes, as shown in **Figure 17 A**, was probably located in the epithelial cells of the pharynx, whereas the signal from the main body, as shown in **Figure 17 B**, corresponded to the epithelial cells of the vulva and spermathecae as well as the vulval muscles cells. Signal at the tail posteriorly to the intestine, near the rectum, as shown in **Figure 17 C**, presumably came from the stomatointestinal muscles and anal depressor muscle, which play an important role in defecation.

A

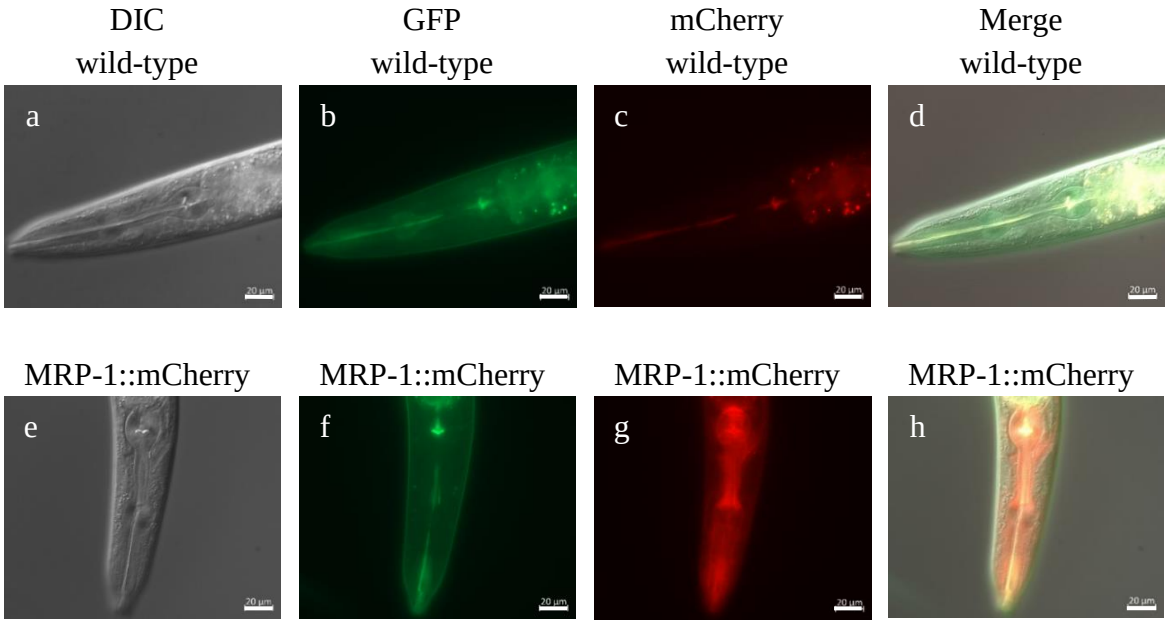

B

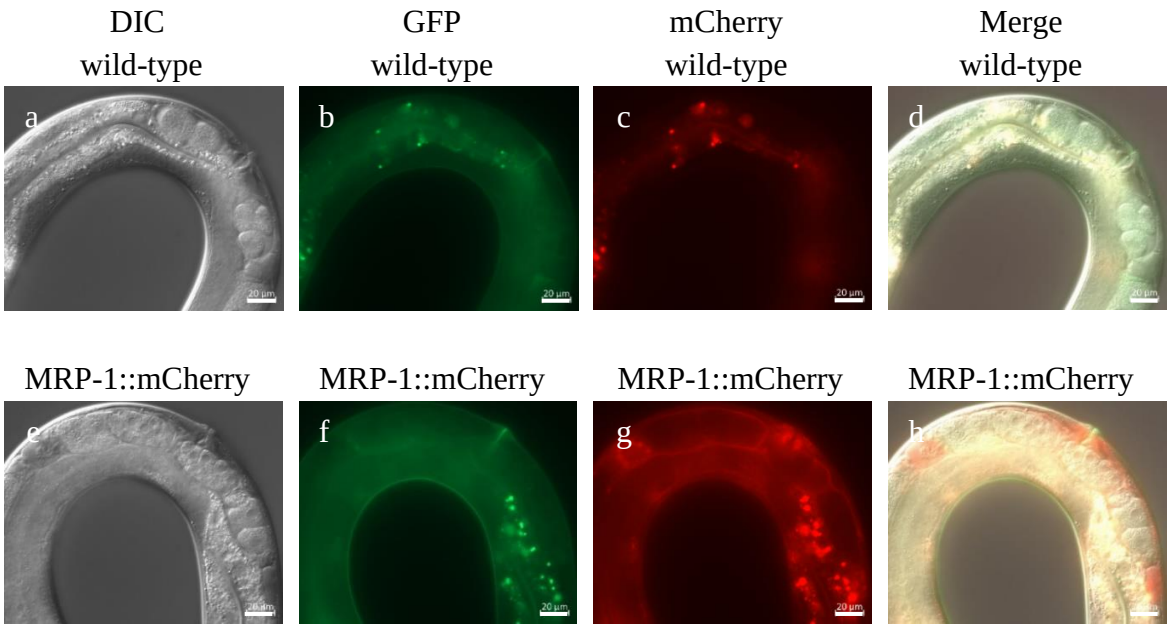

C

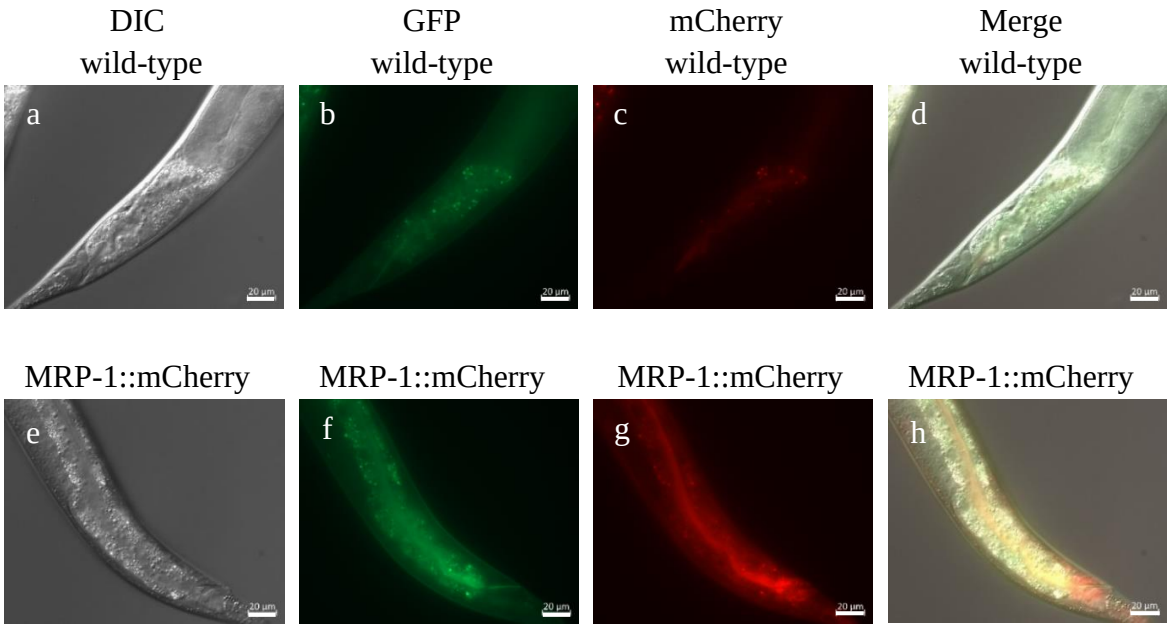

Figure 17. Localization of MRP-1::mCherry. DIC (a, e); GFP (b, f); m::Cherry (c, g) and Merged (d, h) images of wild-type (a, b, c, d) and MRP-1::mCherry (e, f, g, h) animals were shown. Wild-type strain and GFP filter were used as a control for discrimination and correction of the autofluorescence of intestinal granules. Scale bar: 20 µm. (**A**) Localization of MRP-1::mCherry in the pharynx. (**B**) Localization of MRP-1::mCherry in the vulva and spermathecae. (**C**) Localization of MRP-1::mCherry in the rectum.

2.1.1.3. The location of point mutations in mrp-1 revealed by the genetic screening

The results of EMS mutagenesis presented in **Table 1**, showed that among all which can increase fat accumulation in *rege-1* mutants, mutations in the *mrp-1* gene are the most common. To verify the location of the *mrp-1* mutations and their significance on MRP-1 function, an alignment of *C. elegans* MRP-1 and human MRP1 (ABCC1) was performed, with point mutations from the EMS screen marked, as shown in **Figure 18 A**. This analysis showed that all mutations were located in the region encoding conserved domains of the *mrp-1* gene, which can have significant influence on the proper functioning of MRP-1. Mutations within the MSDs may reduce the efficiency of substrate transport. Mutations located in the NBDs (**Figure 18 B**, **C**), within the conserved ATPase domain motif, prevent ATP hydrolysis, making the protein inactive and incapable of substrate transport.

A

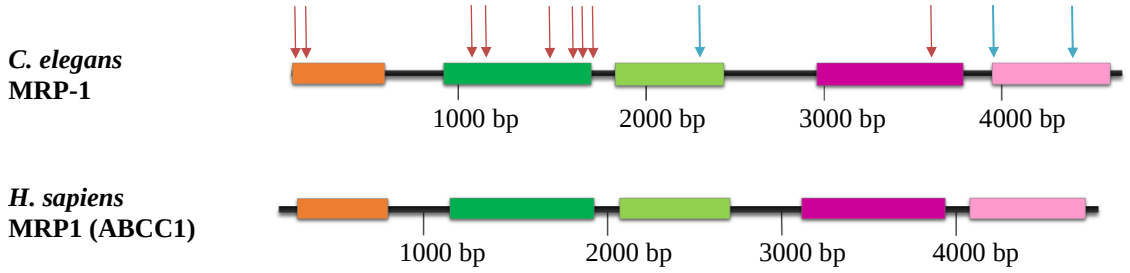

B

```
C. elegans                                                    IKMDGGSFAWGS     625
H. sapiens                                                    ITVRNATFTWAR     655
                                                              *.: ..:*:*.

                                        a
C. elegans     KEEDRKLHDITFNIKRGQLVAIVGRVGSGKSSLLHALLGEMNKLSGSVQVNGSVAYVPQL     685
H. sapiens     SD-PPTLNGITFSIPEGALVAVVGQVGCGKSSLLSALLAEMDKVEGHVAIKGSVAYVPQQ     714
               .:   .*:.***.* .* ***:**:**.****** ***.**:*:.* * ::********

                                                                        c
C. elegans     AWIQNLSLRNNILFNRPYDAKLYQNVIENCALVQDLESLPAEDRTEIGEKGINLSGGQKQ     745
H. sapiens     AWIQNDSLRENILFGCQLEEPYYRSVIQACALLPDLEILPSGDRTEIGEKGVNLSGGQKQ     774
               ***** ***:****.   :   *:.**: ***: *** **: *********:********

               c               b
C. elegans     RVSLARAVYQNAEIVLLDDPLSAVDSHVGKHIFENVISTATGCLGTKTRVLLTHGLTYLK     805
H. sapiens     RVSLARAVYSNADIYLFDDPLSAVDAHVGKHIFENVIGP-KGMLKNKTRILVTHSMSYLP     833
               *********.**:* *:********:***********.  .* * .***:*:**.::**

C. elegans     HCDQVIVLKD                                                     815
H. sapiens     QVDVIIVMSG                                                     843
               : * :**:..
```

C

```
                                                                        a
C. elegans                      GEISIKNFSVRYRPGLDLVLHGVTAHISPCEKIGIVGRTGAG    1334
H. sapiens                      GRVEFRNYCLRYREDLDFVLRHINVTINGGEKVGIVGRTGAG    1342
                                *.:.::*:.:*** .**:**: :.. *.  **:**********

               a
C. elegans     KSSLTLALFRIIEADGGCIEIDGTNIADLLLEQLRSRLTIVPQDPVLFSGTMRMNLDPFF    1394
H. sapiens     KSSLTLGLFRINESAEGEIIIDGINIAKIGLHDLRFKITIIPQDPVLFSGSLRMNLDPFS    1402
               ******.**** *:  * * *** ***.: *.:** ::**:*********::*******

                                                          c                b
C. elegans     AFSDDQIWEALRNAHLDSFVKSLQEGLHHHISEGGENLSVGQRQLICLARALLRKTKVLV    1454
H. sapiens     QYSDEEVWTSLELAHLKDFVSALPDKLDHECAEGGENLSVGQRQLVCLARALLRKTKILV    1462
                :**:::* :*. ***..**.:* : *.*. :*************:***********:**

               b
C. elegans     LDEAAAAVDVETDSLLQKTIREQFKDCTVLTIAHRLNTVMDSDRLLVLDKGCVAEFDTP    1513
H. sapiens     LDEATAAVDLETDDLIQSTIRTQFEDCTVLTIAHRLNTIMDYTRVIVLDKGEIQEYGAP    1521
               ****:****:***.*:*.*** **:**************:**  *::***** : *:.:*
```

Figure 18. The location of point mutations in the *mrp-1* revealed by the genetic screening. (**A**) The alignment of *C. elegans* and *H. sapiens* MRP-1 domains, with the location of point mutations indicated by arrows, revealed by the genetic screening. Red arrows- mutations within MSDs; cyan arrows- mutations within NBDs. The colors of domains correspond to: orange- MSD0; forest green- MSD1 with CL5; green- NBD1; magenta- MSD2 with CL7; hot pink- NBD2. bp- base pair. (**B**, **C**) Deduced amino acids sequence

of the MRP-1 NBDs. The alignment between *C. elegans* and *H. sapiens* was performed using the multiple sequence alignment tool ClustalOmega. Marks indicate as follows: "*" perfect alignment; ":" strong similarity; "." weak similarity. The Walker A and B motifs and the active transport family signature C motif are indicated by single lines and denoted as a, b, and c in bold. (**B**) The aligment of *C. elegans* and *H. sapiens* NBD1. A752T point mutation identified in the screen is located in a conserved ATPase domain motif in domain 1, marked as cyan. (**C**) The aligment of *C. elegans* and *H. sapiens* NBD2. G1293R point mutation identified in the screen, marked as cyan, is located in a conserved ATPase domain motif in domain 2. D1456N point mutation from the screen, marked as cyan, is placed in a conserved Walker B motif.

2.1.1.4. Depletion of mrp-1 slightly increased body fat content in rege-1 mutants

Forward genetic screening enabled the identification of potential ETS-4 targets, among which MRP-1 was found. To verify whether mutation in the *mrp-1* gene could recover the fat loss phenotype of *rege-1* mutants, *rege-1* mRNA was silenced via RNAi in the *mrp-1* mutants and the relative amount of body fat was measured by the staining with ORO and a biochemical measurement of TAG content.

Results from the ORO staining, presented in **Figure 19** (**A**, **B**), indicate that the *mrp-1* mutant animals had increased amount of body fat compared to controls. Wild-type animals fed with bacteria targeting *rege-1* mRNA had reduced body fat content compared to controls. On the other hand, the *mrp-1* mutants subjected to *rege-1* RNAi had significantly greater body fat mass compared to the wild-type animals exposed to *rege-1* RNAi. Results from biochemical measurement, presented in **Figure 19 C**, showed that *mrp-1* mutant animals had similar TAG levels compared to controls. Similar to the ORO staining, TAG levels were increased in *mrp-1* mutants exposed to *rege-1* RNAi compared to wild-type animals with targeted *rege-1* mRNA which had reduced TAG levels. However, inhibition of *mrp-1* in *rege-1* mutant animals led only to a partial recovery of the body fat.

Moreover, differences in the LDs size between mutants and wild-type animals were measured using the LD biomarker DHS-3 (short chain dehydrogenase) tagged with GFP, as shown in **Figure 20**. Wild-type animals were used as a control for discrimination and correction of the autofluorescence of intestinal granules. The *mrp-1* mutants expressing DHS-3::GFP had larger LDs compared to LDs found in the wild-type animals expressing DHS-3::GFP. The size of LDs in *rege-1* mutants determined using DHS-3::GFP was reduced as compared to wild-type animals expressing DHS-3::GFP. On the other hand, the size of

LDs in *mrp-1; rege-1* double mutant animals expressing DHS-3::GFP was greater than in single *rege-1* mutants. However, mean LDs size in *mrp-1; rege-1* double mutants was smaller compared to controls.

In summary, *mrp-1* mutants were characterized by greater fat accumulation, larger LDs size and similar amounts of TAG compared to controls. This may indicate that *mrp-1* mutants accumulate fat in a form other than TAG e.g. DAG, phospholipids or sphingolipids (Watts and Ristow, 2017). In contrast, nematodes with targeted *rege-1* mRNA via RNAi in *mrp-1* mutants or *mrp-1; rege-1* double mutants partially recovered the fat loss phenotype in *rege-1* mutant animals, increased TAG levels and LDs size. Altogether, these results suggest that MRP-1 might contribute to the fat loss phenotype of *rege-1* mutants.

A

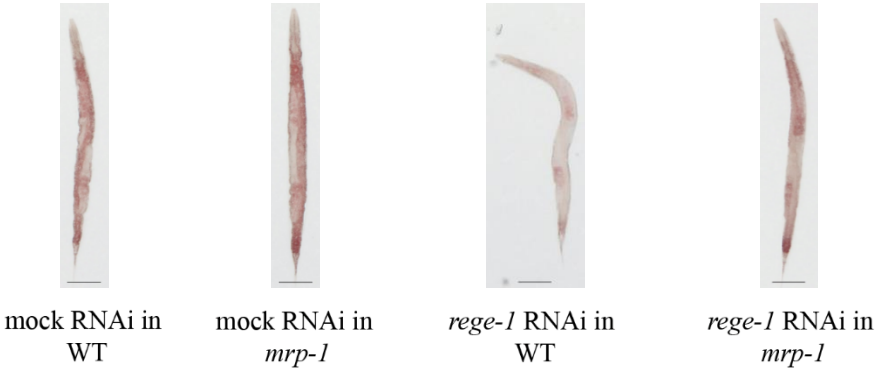

B

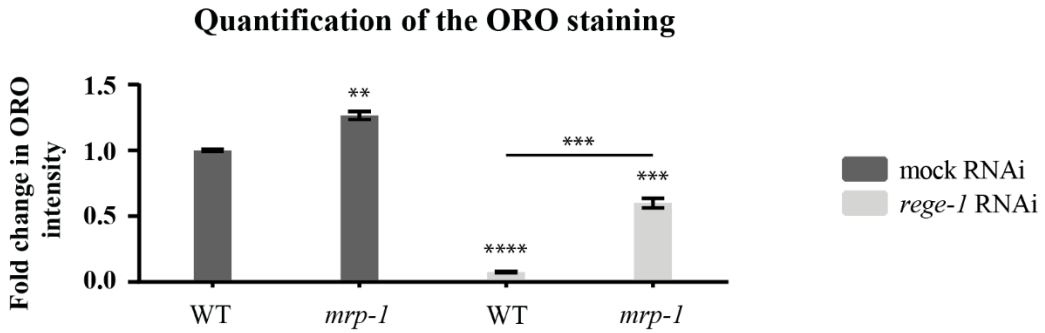

C

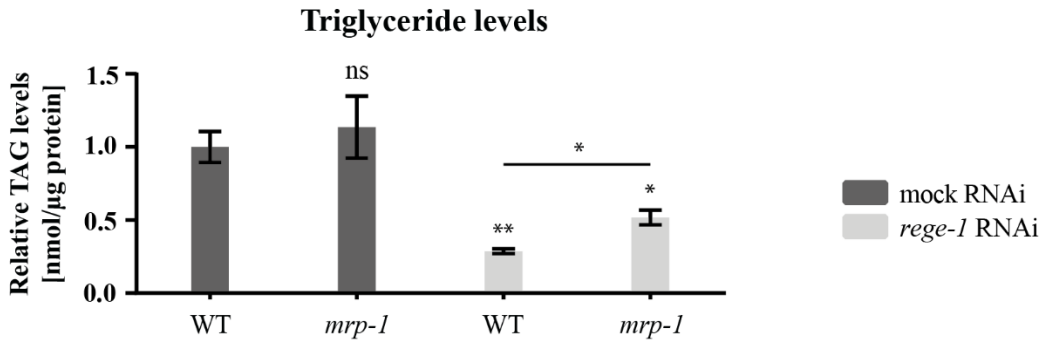

Figure 19. Depletion of *mrp-1* partially rescued the fat loss phenotype of *rege-1* mutants. (**A**) Images of wild-type and animals carrying *mrp-1* mutation exposed to mock or *rege-1* RNAi. The animals were stained with the ORO to visualize body fat levels. Scale bar: 100 µm. (**B**) Quantification of relative changes in the ORO staining. 30 animals per condition were measured. Changes in the body fat levels were determined in relation to wild-type animals subjected to mock RNAi. The P values were calculated using un-paired Student t-test (*n = 3*). Data are presented as mean; error bars represent SEM (** indicates $p < 0.01$; *** $p < 0.001$; **** $p < 0.0001$). (**C**) Quantification of changes in TAG levels relative to the total protein content in wild-type and *mrp-1* mutants exposed to mock or *rege-1* RNAi. Changes in TAG levels were measured in relation to wild-type animals subjected to mock RNAi. The P values were calculated using un-paired Student t-test (*n = 3*). Data are presented as mean; error bars represent SEM (* indicates $p < 0.05$; ** $p < 0.01$).

A

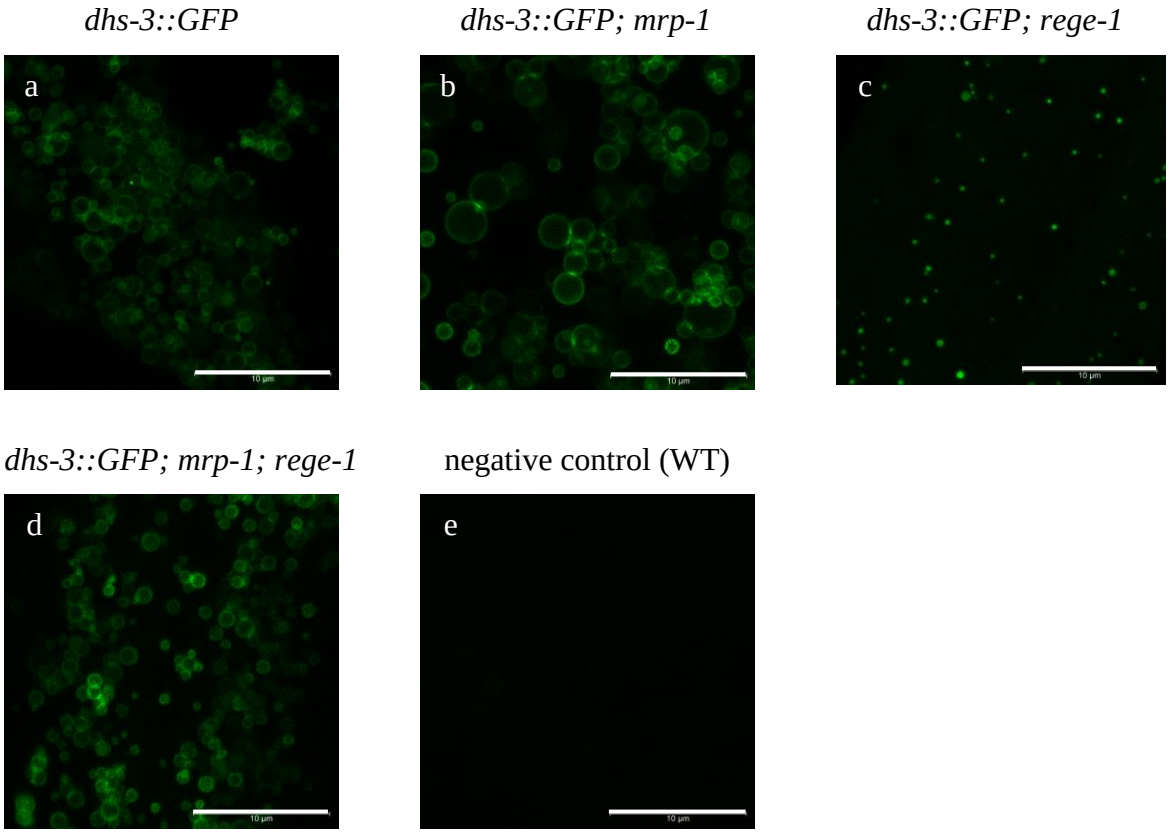

B

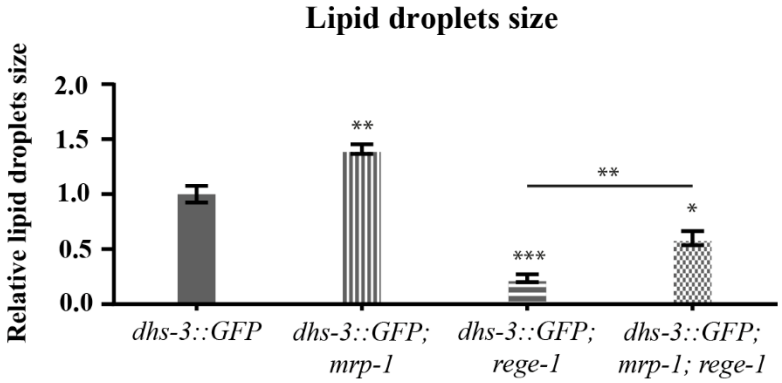

Figure 20. Mutation in *mrp-1* increased lipid droplets size in *rege-1* mutants. (**A**) The *dhs-3::GFP* strain (a) was crossed with either *mrp-1* (b), *rege-1* (c), or *mrp-1; rege-1* (d) mutants to observe the size of LDs by FL microscopy. The wild-type animals were used as a control for discrimination and correction of the autofluorescence of intestinal granules (e). Scale bar: 10 µm. (**B**) Quantification of LDs size. The diameter of LDs was measured as an average from 30 droplets per strain from 5 animals. Changes in LDs size were measured in relation to *dhs-3::GFP* strain. The P values were calculated using un-paired Student t-test (*n = 3*). Data are presented as mean; error bars represent SEM (* indicates $p < 0.05$; ** $p < 0.01$; *** $p < 0.001$).

2.1.1.5. The mrp-1 expression was independent of the presence of ets-4 mRNA in rege-1 mutants

The above results has shown that MRP-1 was necessary for the fat loss phenotype in *rege-1* mutants and mutation in the *mrp-1* gene led to a partial regain of the body fat. The next step to establish a possible functional relationship between the ETS-4 transcription factor and the MRP-1 transporter was to check whether ETS-4 affects *mrp-1* transcription. The results from the RT-qPCR analysis, presented in **Figure 21**, showed that wild-type animals subjected to *rege-1* RNAi and *rege-1* mutants exposed to mock RNAi had greater *mrp-1* mRNA levels compared to controls. Although mutations in the *mrp-1* gene increased body fat content in *rege-1* mutants, its expression does not apper to be regulated by ETS-4.

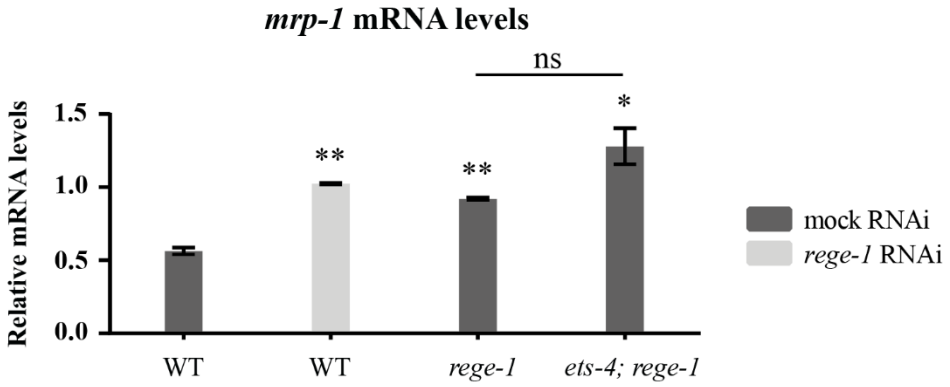

Figure 21. The *mrp-1* mRNA levels were not dependent on *ets-4* expression. The *mrp-1* mRNA levels were measured by RT-qPCR in wild-type or animals carrying either *rege-1* or *ets-4; rege-1* mutations exposed to mock or *rege-1* RNAi. The *mrp-1* mRNA levels were normalized to actin 1 mRNA levels and compared in relation to wild-type animals subjected to mock RNAi. The P values were calculated using un-paired Student t-test ($n = 3$). Data are presented as mean; error bars represent SEM (* indicates $p < 0.05$; ** $p < 0.01$).

2.1.1.6. High ets-4 mRNA levels contributed to an increase in sphk-1 mRNA level in rege-1 mutants

Due to the fact that the substrates for MRP-1 are not well characterized in *C. elegans*, it was checked whether the expression of genes responsible for the synthesis of ligands transported by the human MRP1, was changed in the *rege-1* mutant animals. At first, the expression of sphingosine kinase 1 (*sphk-1)* gene encoding the enzyme responsible for the synthesis of sphingosine-1-phosphate (S1P), was determined, as shown in **Figure 22**.

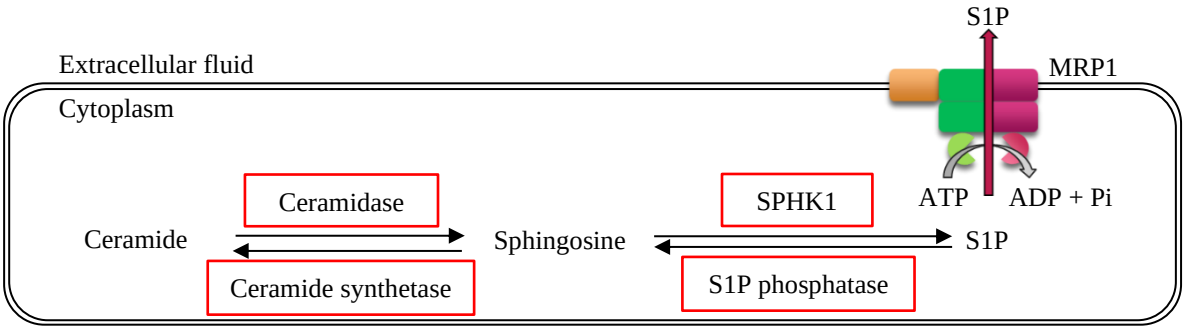

Figure 22. S1P synthesis pathway and transport through MRP1 in humans. S1P is synthesized by phosphorylation of sphingosine by sphingosine kinase 1 (SPHK1) and exported by MRP1 transporter. S1P can be dephosphorylated by S1P phosphatase to sphingosine and converted to ceramide through ceramide synthetase. ATP- adenosine triphosphate; ADP- adenosine diphosphate; Pi- inorganic phosphate; S1P- sphingosine-1-phosphate. Based on *Kwong et al., 2017*.

To determine whether ETS-4 had an effect on the S1P synthesis, *sphk-1* mRNA levels were measured in the wild-type and in animals carrying either *rege-1* or *ets-4; rege-1* mutations exposed to mock or *rege-1* RNAi, as shown in **Figure 23 A**. To validate the RNAi plates, *rege-1* mRNA was targeted with RNAi in the wild-type animals. The *sphk-1* mRNA levels were significantly increased in the wild-type animals subjected to *rege-1* RNAi and in the *rege-1* mutants exposed to mock RNAi in comparison to controls. The *sphk-1* mRNA levels in *ets-4; rege-1* double mutants exposed to mock RNAi did not differ from controls. These results suggested that ETS-4 significantly upregulated *sphk-1* mRNA levels and thus might increase S1P levels in the *rege-1* mutant animals.

Moreover, it was checked whether the RNAi-mediated silencing of *sphk-1* mRNA affected fat accumulation in *rege-1* mutant animals using the ORO staining. The wild-type nematodes exposed to *sphk-1* RNAi were characterized by a similar level of body fat

compared to controls (**Figure 23 B**, **C**). Fat accumulation in *rege-1* mutant animals exposed to *sphk-1* RNAi was slightly higher compared to *rege-1* mutants exposed to mock RNAi, however it did not lead to the regain of body fat compared to controls.

In summary, high levels of *sphk-1* mRNA observed in *rege-1* mutant animals and in *rege-1* RNAi wild-type animals contributed to a significant reduction in the amount of body fat as evidenced by RT-qPCR analysis and the ORO staining compared to controls. However, RNAi targeting *sphk-1* mRNA had little effect on fat accumulation in *rege-1* mutants. Thus, both *mrp-1* and *sphk-1* seem to regulate fat metabolism independently of the REGE-1 - ETS-4 regulatory axis.

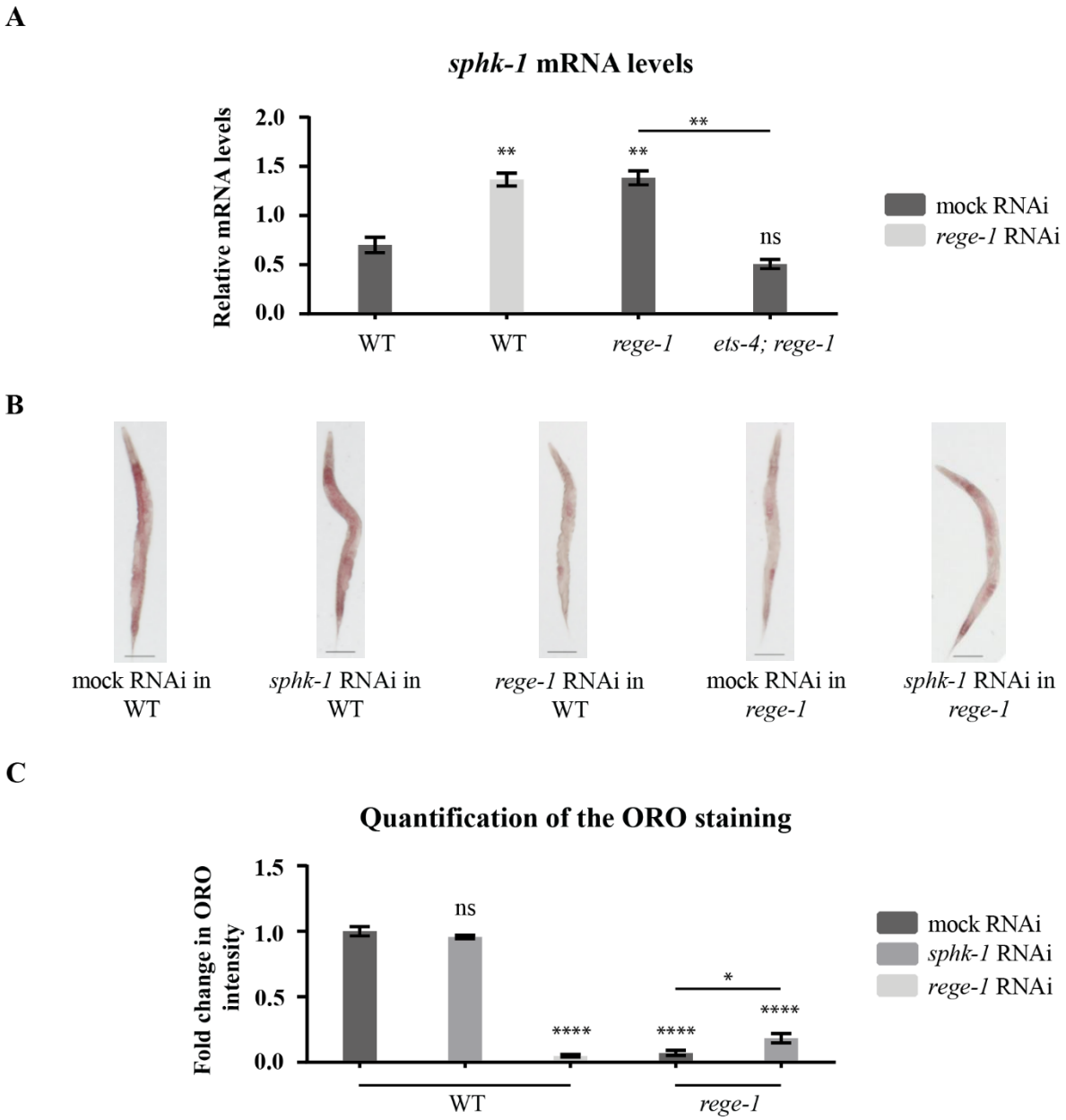

Figure 23. Inhibition of *sphk-1* mRNAs in *rege-1* mutants did not lead to the regain of body fat compared to controls. (**A**) The level of *sphk-1* mRNA was measured by RT-qPCR in the wild-type and in animals carrying either *rege-1* or *ets-4; rege-1* mutations exposed to mock or *rege-1* RNAi. The *sphk-1* mRNA levels were normalized to the levels mRNA of actin 1 and compared in relation to wild-type animals subjected to mock RNAi. The P values were calculated using un-paired Student t-test (*n = 3*). Data are presented as mean; error bars represent SEM (** indicates $p < 0.01$). (**B**) Images of wild-type and animals carrying *rege-1* mutation exposed to mock or dsRNA targeting either *rege-1* or *sphk-1* mRNA. The animals were stained with the ORO to visualize body fat levels. Scale bar: 100 μm. (**C**) Quantification of relative changes in the ORO staining. 30 animals per condition were measured. Changes in body fat levels were determined in relation to wild-type animals subjected to mock RNAi. The P values were calculated using un-paired Student t-test (*n = 3*). Data are presented as mean; error bars represent SEM (* indicates $p < 0.05$; **** $p < 0.0001$).

2.2. Candidate genes found through RNA sequencing data analysis

As another approach to find novel factors regulating fat metabolism in *C. elegans*, an analysis of RNA sequencing data (RNA-Seq) previously performed in the laboratory of Prof. Ciosk was made (Habacher et al., 2016). Changes in the mRNA levels between wild-type animals exposed to *rege-1* mRNA RNAi and the *rege-1* mutants exposed to RNAi targeting *ets-4* mRNA were compared and further analyzed. Among multiple transcripts increased in wild-type animals exposed to *rege-1* RNAi and decreased in *rege-1* mutants exposed to *ets-4* RNAi, respectively, *ets-4*, the peptide transporter (*pept-1*), the Na^+ / H^+ exchanger (*nhx-2*), paraquat (methylviologen) responsive transcription factor (*pqm-1*), fatty acids desaturases (*fat-5*) and genes involved in sphingolipid metabolism like serine palmitoyltransferase (*sptl-1*, *sptl-2*), were found, as shown in **Table 2**.

Table 2. Results from RNA-Seq data.

Gene name	Up upon *rege-1* RNAi in wild-type	Down upon *ets-4* RNAi in *rege-1* mutant
ets-4	4.43	0.21
pept-1	2.31	0.40
nhx-2	3.58	0.22
pqm-1	2.30	0.31
fat-5	6.43	0.15
sptl-1	2.08	0.37
sptl-2	5.04	0.18

2.2.1. *pept-1* as a candidate target for ETS-4

The analysis of RNA-Seq data, shown in **Table 2**, suggested that *pept-1* might be a potential target for the ETS-4 transcription factor, since *pept-1* mRNA levels were increased in the wild-type animals subjected to *rege-1* RNAi and decreased in *rege-1* mutants subjected to *ets-4* RNAi. The aim of further experiments was to determine whether REGE-1 – ETS-4 regulatory axis affected fat accumulation in nematodes via PEPT-1 and identify a potential mechanism of REGE-1 – ETS-4 – PEPT-1 - mediated fat regulation.

2.2.1.1. C. elegans PEPT-1 is an ortholog of human PEPT1 transporter

The *C. elegans* transporter PEPT-1 is an ortholog of human *PEPT1* and similar to humans is a low affinity high capacity transporter, which transports di- and tripeptides from the gut lumen to the intestine using electrochemical proton gradient as a driving force (Meissner et al., 2004). The proper function of PEPT-1 transporter depends on the interplay with a second transporter, NHX-2, which is an ortholog of humans sodium–hydrogen exchanger 3 (NHE3) (Nehrke, 2003), required to balance intracellular pH by exporting protons back into the intestinal lumen with simultaneous import of sodium ions (Spanier et al., 2009), as shown in **Figure 24**.

In order to confirm protein sequence conservation, an alignment of *C. elegans* PEPT-1 and *H. sapiens* PEPT1 was performed, as shown in **Figure 25 A**. This analysis showed that PEPT-1 in *C. elegans* has similar sequence homology to human PEPT1, as demonstrated by *Meissner et al., 2004*, which showed 36.9% sequence similarity (Meissner et al., 2004). Prediction models for the structure of the human PEPT1 protein and *C. elegans* PEPT-1 also show their similarity, as shown in **Figure 25** (**B**, **C**). The PEPT1 transporter is composed of 12 transmembrane helices (TMs) of the major facilitator superfamily (MFS), which form two six-helix bundles with the NH_2 and COOH ends facing the cytoplasm and the immunoglobulin-like extracellular domain (ECD) (Killer et al., 2021).

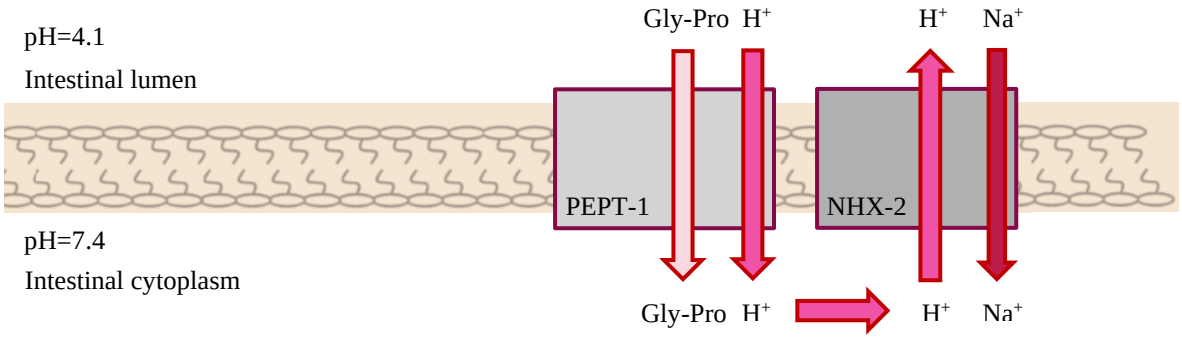

Figure 24. Scheme representing functional interplay between PEPT-1 and NHX-2 transporters. Based on *Nehrke, 2014*.

A

```
C. elegans    MEEKSLLQKLRSYPPAVFFMLGNEFCERFSFYGMKTILFIYLITEHEFSPSKATFIYHLF   60
H. sapiens    -MGMSKSHSFFGYPLSIFFIVVNEFCERFSYYGMRAILILYFTNFISWDDNLSTAIYHTF   59
                  *  :.: .** ::**:: ********:***::**::*: .  .:. . :* *** *

C. elegans    TCIAYLTPLIGSIMADSVFGRFKVILYGSSIYVVGHVLLSLGAVPF----------LSYP   110
H. sapiens    VALCYLTPILGALIADSWLGKFKTIVSLSIVYTIGQAVTSVSSINDLTDHNHDGTPDSLP   119
              ..:.****::*:::*** :*:**.*:  * :*.:*:.: *:.::             * *

C. elegans    IRSSLDFSGLFVIAFATGCIKPCVSAFAADQFTEDQKDLRSQFFSFFYFAINGGSLFAII   170
H. sapiens    VHVVLSLIGLALIALGTGGIKPCVSAFGGDQFEEGQEKQRNRFFSIFYLAINAGSLLSTI   179
              ::  *.: ** :**:.** ********..*** *.*:. *.:***:**:***.***:: *

C. elegans    ITPILRGRV-QCFGNAHCFPLAFGVPGVLMLLALILFLMGWSMYKKHPPSKENVGSKVVA   229
H. sapiens    ITPMLRVQQCGIHSKQACYPLAFGVPAALMAVALIVFVLGSGMYKKFKPQGNIMGKVAKC   239
              ***:** :    ..:  *:*******..** :***:*::* .****. *. : :*. . .

C. elegans    VIYTSLRKMVGGASRDKPVTHWLDHAAPEHSQKMIDSTRGLLNVAVIFCPLIFFWALFDQ   289
H. sapiens    IGFAIKNRFRHRSKAFPKREHWLDWAKEKYDERLISQIKMVTRVMFLYIPLPMFWALFDQ   299
              : ::  .::   :.      **** *  ::.:::*.. : : .* .:: ** :*******

C. elegans    QGSTWVLQARRLDGRVGHFSILPEQIHAINPVCVLILVPIFEGWVYPALRKIT-RVTPLR   348
H. sapiens    QGSRWTLQATTMSGKIGALEIQPDQMQTVNAILIVIMVPIFDAVLYPLIAKCGFNFTSLK   359
              *** *.***  :.*::* :.* *:*:::::* : ::*:****:. :** : *   ..* *:

C. elegans    KMAVGGLLTAFSFAIAGVLQLKVNETMEFPPSLGRIYLQ--RVGNESLISDFRYKSDGRL   406
H. sapiens    KMAVGMVLASMAFVVAAIVQVEIDKTLPVFPKGNEVQIKVLNIGNNTMNI----SLPGEM   415
              ***** :*::::*.:*.::*:::::*: . *. ..: ::  .:**:::      .  *.:

C. elegans    IGDGMLPKGRTELDAGIYTFNTGLKNESQEIDISTPNKGYVMAVFRLKD-----------   455
H. sapiens    VT-----LGPMSQTNAFMTFDV---NKLTRINISSPGSPVTAVTDDFKQGQRHTLLVWAP   467
              :       *  .   .: **:.   *:  .*:**:*..  . ..  :*:

C. elegans    -AVEVVK--FDYKVEKTDNGATRVFVVTAREDADTLVYAINKKGKILSSCELKSGSYVDV   512
H. sapiens    NHYQVVKDGLNQKPEKGENGIRFV---NTFNE----LITITMSGKVYANISSYNASTYQF   520
                 :***  :: * ** :**   *   .: ::    : :*. .**: :. .  ..*  :.

C. elegans    IPGIISDPNVRLYWGPKNSCSGVDC-PNTVTLNAQMGAVHVLH---IHPSTTEGDFNLLV   568
H. sapiens    FPSGIKGFTISS------TEIPPQCQPNFNTFYLEFGSAYTYIVQRKNDSCPEVKVFEDI   574
              :*. *.. .:        :    :* **  *:  ::*:.:.      : *  * ..   :

C. elegans    RPNSVSILWSLPQYIIITLGEVLLSVTGLEFAYSQAAPNMKSVLTAMWLLTVFAGNLIDM   628
H. sapiens    SANTVNMALQIPQYFLLTCGEVVFSVTGLEFSYSQAPSNMKSVLQAGWLLTVAVGNIIVL   634
                *:*.:  .:***:::* ***::*******:****  ****** * ***** .**:* :

C. elegans    MISGTRLIPHPALEFFFYSTLMVIVMGVFILLAMQYTYVEDNDDEITITESEKKDVIALT   688
H. sapiens    IVAGAGQFSKQWAEYILFAALLLVVCVIFAIMARFYTYINPAEIEAQFDEDEKKNRLEKS   694
              :::*:  : :   *::::::*:::*  :* ::*  ***::  : *  : *.***: :  :

C. elegans    EIESGTATSDKKE-                                                 701
H. sapiens    NPYFMSGANSQKQM                                                 708
              :    :.:..:*:
```

B

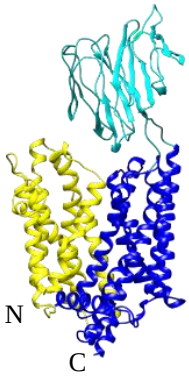

C

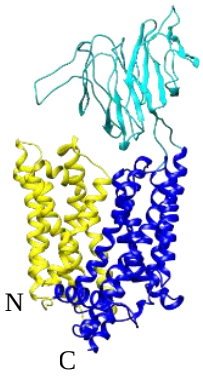

Figure 25. Structure and sequence comparison between human PEPT1 and *C. elegans* PEPT-1. (**A**) The alignment of *C. elegans* PEPT-1 and *H. sapiens* PEPT1 sequence. The alignment was performed using the multiple sequence alignment tool ClustalOmega. Marks indicate as follows: "*" perfect alignment; ":" strong similarity; "." weak similarity. (**B**) Three-dimesional structure of human PEPT1 made in the program Pyre 2 and colored in UCSF Chimera. (**C**) Three-dimesional structure of *C. elegans* PEPT-1 made in the program Pyre 2 and colored in UCSF Chimera. The colors of the domains correspond respectively: cyan- extracellular domain; yellow- transmembrane N-bundle; blue- transmembrane C-bundle. N- NH_2 terminus; C- COOH terminus. Based on *Killer et al., 2021*.

2.2.1.2. Nematode PEPT-1 was localized in the intestinal apical membrane

Visualisation of PEPT-1 in the wild-type animals was performed by tagging the endogenous protein with GFP on its COOH terminus, while its anatomical location was verified based on the Worm Atlas. Signal location analysis showed the presence in the intestinal apical membrane, as presented in **Figure 26**.

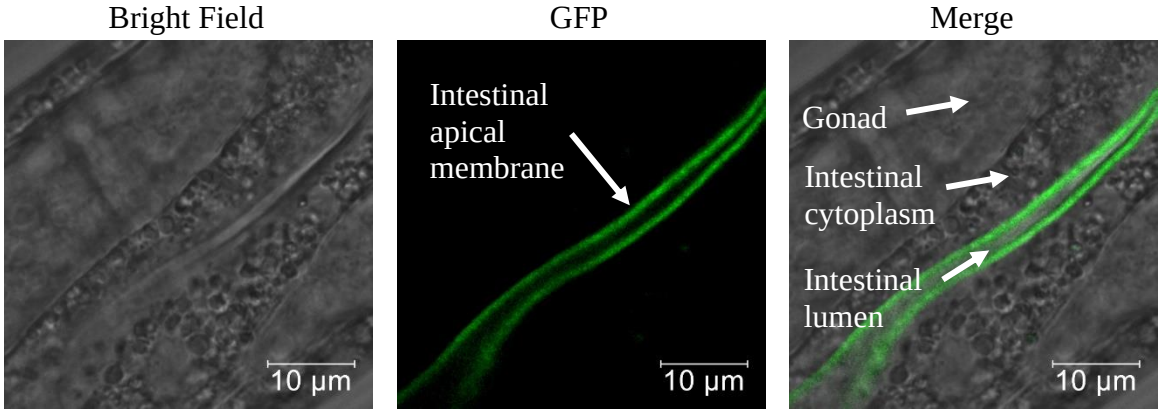

Figure 26. Localization of PEPT-1::GFP in the wild-type animals in the intestinal apical membrane. Scale bar: 10 µm.

2.2.1.3. The levels of pept-1 and nhx-2 mRNAs were increased in rege-1 mutants

The results from RNA-Seq analysis showed that both *pept-1* and the *nhx-2* mRNA levels increased in the wild-type exposed to *rege-1* RNAi and decreased in *rege-1* mutants exposed to *ets-4* RNAi (Habacher et al., 2016). To confirm these results, *pept-1* and *nhx-2* expression was measured by RT-qPCR in single *rege-1* and *ets-4; rege-1* double mutant animals subjected to mock RNAi, as shown in **Figure 27**. To validate RNAi plates,

rege-1 mRNA was targeted by RNAi in the wild-type animals. Both *pept-1* and *nhx-2* mRNA levels increased significantly in nematodes in which *rege-1* mRNA was targeted via RNAi and in *rege-1* mutants exposed to mock RNAi compared to controls. In the *ets-4; rege-1* double mutant animals fed with mock RNAi, *pept-1* and *nhx-2* mRNA levels were comparable to control. Altogether, these results showed that *pept-1* and *nhx-2* mRNA levels were significantly increased in animals with mutated or inhibited *rege-1*.

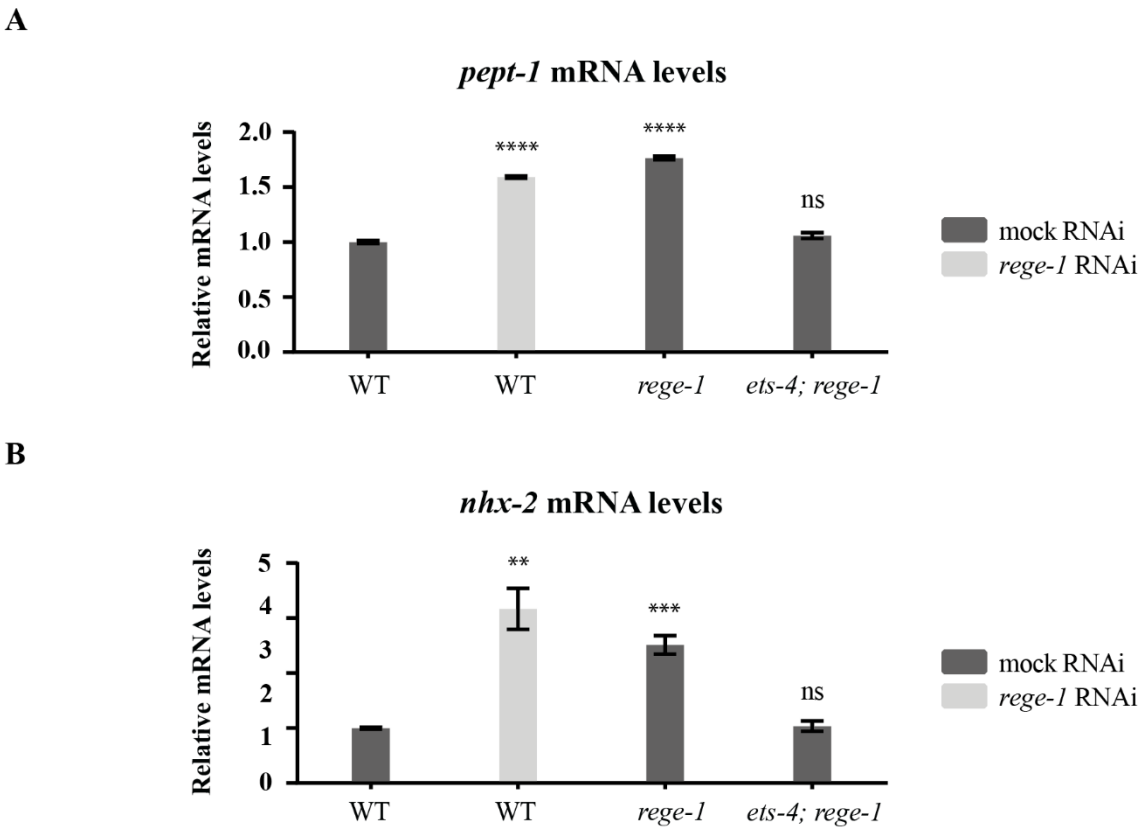

Figure 27. *pept-1* and *nhx-2* mRNA levels were increased upon inhibition / mutation of *rege-1*. The levels of *pept-1* (**A**) and *nhx-2* (**B**) mRNAs were measured by RT-qPCR in the wild-type and in animals carrying either *rege-1* or *ets-4; rege-1* mutations exposed to mock or dsRNA targeting *rege-1* mRNA. The *pept-1* and *nhx-2* mRNA levels were normalized to actin 1 mRNA levels and compared in relation to wild-type subjected to mock RNAi. The P values were calculated using un-paired Student t-test ($n = 3$). Data are presented as mean; error bars represent SEM (** indicates $p < 0.01$; *** $p < 0.001$; **** $p < 0.0001$).

2.2.1.4. Peptide transport activity was increased in rege-1 mutants

In order to investigate PEPT-1 function, the relative amount of endogenous PEPT-1 protein tagged with GFP (PEPT-1::GFP) and the transport activity of peptides through PEPT-1 in *rege-1* mutants were measured, as shown in **Figure 28**.

Western blot analysis showed that animals expressing PEPT-1::GFP and exposed to *rege-1* RNAi had similar amount of PEPT-1 protein compared to animals expressing PEPT-1::GFP and subjected to mock RNAi, as presented in **Figure 28** (**A**, **B**). However, the transport of a fluorescent dipeptides ß – Ala – Lys - AMCA, presented in **Figure 28 C**, were significantly increased in wild-type animals exposed to *rege-1* RNAi and *rege-1* mutants exposed to mock RNAi compared to controls. Both wild-type animals and *rege-1* mutants subjected to *pept-1* RNAi displayed no change in the transport activity of peptides compared to controls suggesting that AMCA was transported also by other transporters than PEPT-1.

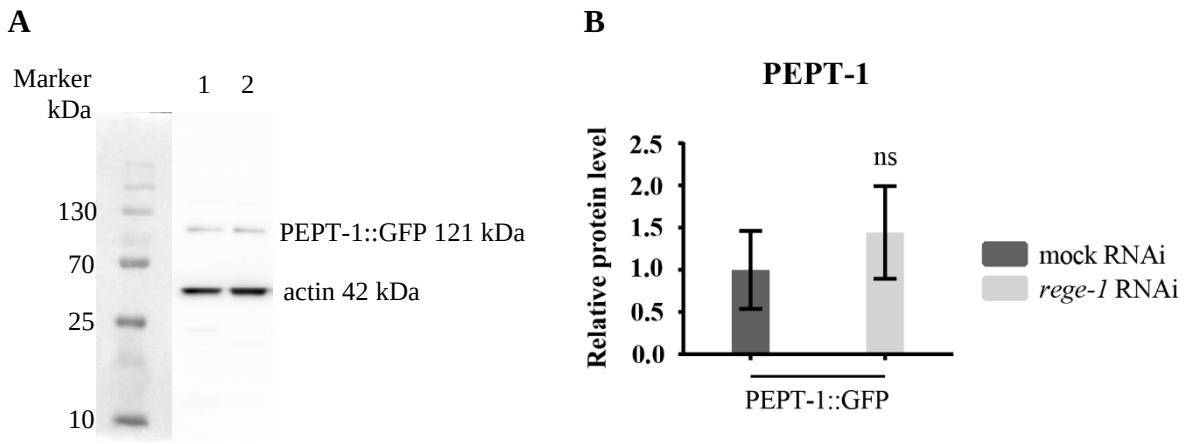

1- mock RNAi in the wild-type animals expressing PEPT-1::GFP
2- *rege-1* RNAi in the wild-type animals expressing PEPT-1::GFP

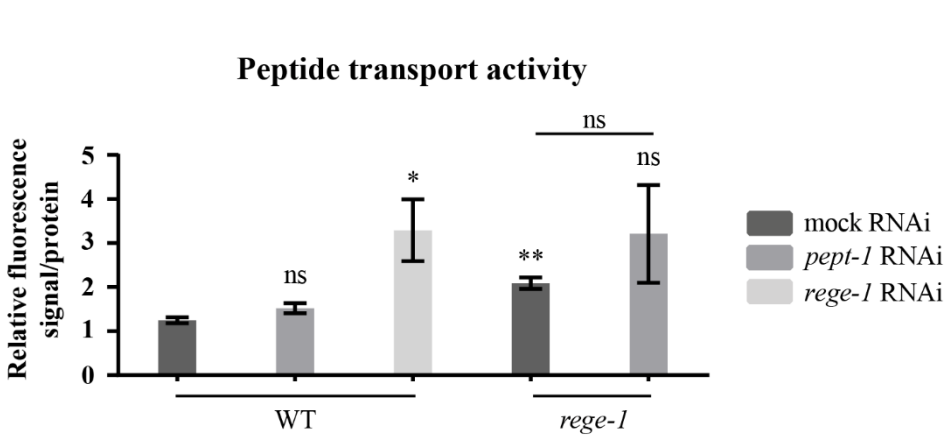

Figure 28. Peptide transport activity, but not the PEPT-1 protein level was increased in *rege-1* mutants. (**A**) The amount of PEPT-1::GFP protein was measured by Western blot in wild-type animals carrying PEPT-1 tag with GFP which were exposed to mock RNAi (1) or dsRNA targeting *rege-1* mRNA (2). 100 µg of protein lysate was loaded per lane on a 10% SDS-gel and α-Actin was used as a loading control. (**B**) Quantification of PEPT-1::GFP protein level relative to the total protein content. Changes in protein levels were determined in relation to the animals expressing PEPT-1::GFP and exposed to mock RNAi. The P values were calculated using un-paired Student t-test (*n = 3*). Data are presented as mean; error bars represent SEM ($p < 0.05$). (**C**) Quantification of the relative changes in ß – Ala – Lys - AMCA transport activity via PEPT-1 were measured in the wild-type and animals carrying *rege-1* mutation subjected to mock, *pept-1* or *rege-1* RNAi. Changes in transport activity relative to the total protein content were measured in relation to wild-type animals exposed to mock RNAi. The P values were calculated using un-paired Student t-test (*n = 4*). Data are presented as mean; error bars represent SEM (* indicates $p < 0.05$; ** $p < 0.01$).

2.2.1.5. PEPT-2 could exert compensatory role for PEPT-1 transporter

In addition to PEPT1 / PEPT-1, di- and tripeptides in humans and *C. elegans* are also transported via PEPT2 / PEPT-2 (Brandsch, 2013; Benner et al., 2011). Thus, changes in *pept-2* mRNA levels in the wild-type animals and *rege-1* mutants exposed to mock, *pept-1* or *rege-1* RNAi were measured by RT-qPCR, as shown in **Figure 29**. To validate RNAi plates, *rege-1* mRNA was targeted by RNAi in the wild-type animals. The *pept-2* mRNA levels did not change in wild-type animals subjected to *rege-1* RNAi or in *rege-1* mutants subjected to mock RNAi compared to controls. However, silencing of *pept-1* mRNA significantly increased *pept-2* mRNA levels in wild-type animals and *rege-1* mutants suggesting that PEPT-1 and PEPT-2 transporters might play similar roles and compensate for each other.

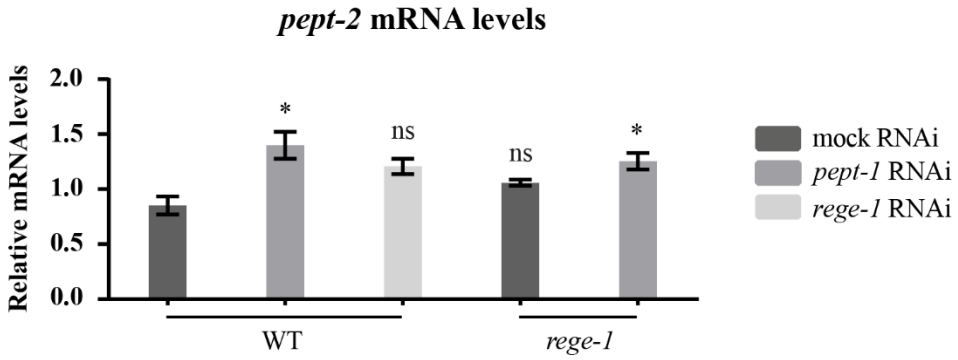

Figure 29. Inhibition of *pept-1* mRNA elevated the expression of *pept-2*. The *pept-2* mRNA levels were measured by RT-qPCR in the wild-type and in animals carrying *rege-1* mutation exposed to mock or dsRNA targeting either *pept-1* or *rege-1* mRNA. The *pept-2* mRNA levels were normalized to actin 1 mRNA levels and compared to controls. The P values were calculated using un-paired Student t-test ($n = 3$). Data are presented as mean; error bars represent SEM (* indicates $p < 0.05$).

2.2.1.6. Depletion of pept-1 increased body fat content in rege-1 mutants

The RNA-Seq data analysis demonstrated that RNAi-mediated silencing of *rege-1* mRNA increased *pept-1* mRNA levels in wild-type animals (**Table 2**). To determine whether inhibition of *pept-1* increased fat accumulation in *rege-1* mutants, the relative amount of body fat was measured by the ORO staining and TAG content was measured biochemically.

Results from the ORO staining, presented in **Figure 30** (**A**, **B**), showed that wild-type animals exposed to *pept-1* RNAi had an increased amount of body fat compared to controls. Fat accumulation was reduced in both, the wild-type animals subjected to *rege-1* RNAi and *rege-1* mutants subjected to mock RNAi compared to controls. Targeting *pept-1* mRNA via RNAi in *rege-1* mutants caused a significant developmental delay and a reduction in body size. However, when correcting for the animal volume, the ORO analysis showed a significant increase in the body fat content in *rege-1* mutants exposed to *pept-1* RNAi compared to *rege-1* mutants exposed to mock RNAi and recovery of fat at a similar level to controls.

Surprisingly, targeting *pept-1* mRNA by RNAi markedly decreased TAG levels in wild-type animals compared to their counterparts exposed to mock RNAi (**Figure 30 C**). Similar to the ORO staining, TAG levels were significantly lower in both the wild-type animals subjected to *rege-1* RNAi and *rege-1* mutants subjected to mock RNAi compared to controls. However, *rege-1* mutants exposed to *pept-1* RNAi did not have altered TAG levels compared to *rege-1* mutants exposed to mock RNAi.

In addition to measuring total body fat content and relative TAG levels, the LDs size was examined via the LD biomarker DHS-3 tagged with GFP, as shown in **Figure 30** (**D**, **E**). Wild-type animals exposed to mock RNAi were used as negative control for correction of the autofluorescence of gut granules. Targeting *pept-1* mRNA by RNAi increased LDs in animals expressing DHS-3::GFP compared to the corresponding strain subjected to mock RNAi. The size of LDs in *rege-1* mutants expressing DHS-3::GFP exposed to mock RNAi and in animals expressing DHS-3::GFP exposed to *rege-1* RNAi, were significantly reduced as compared to the animals expressing DHS-3::GFP subjected to mock RNAi. *rege-1* mutants expressing DHS-3::GFP and subjected to *pept-1* RNAi had an increased size of LDs compared to their counterparts exposed to mock RNAi, however LDs were smaller compared to animals expressing DHS-3::GFP exposed to mock RNAi.

In summary, inhibition of *pept-1* mRNA by RNAi in *rege-1* mutants caused an increase in the overall body fat content and LDs size, however did not change relative TAG levels. In addition, *pept-1* mRNA silencing in the wild-type animals significantly increased fat accumulation and LDs size while lowering relative TAG levels. These results suggest that inhibition of *pept-1* mRNA increased the body fat content through accumulation of lipid

species other than TAG. Thus, the functional PEPT-1 transporter might be essential for the fat loss phenotype of the *rege-1* mutants.

A

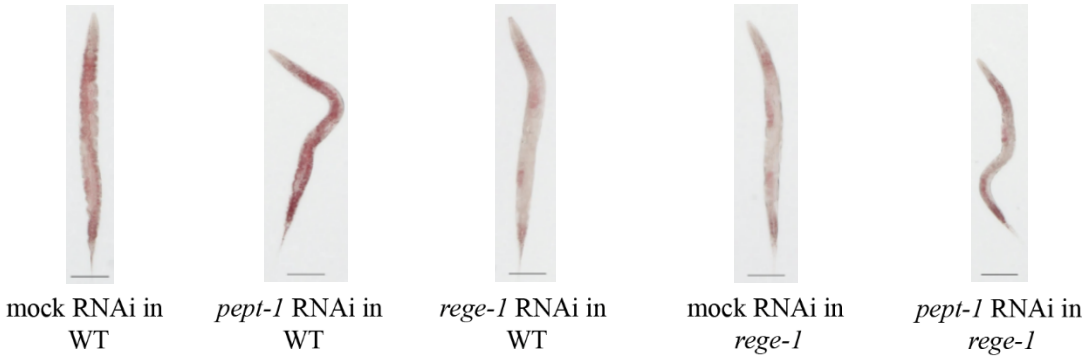

B

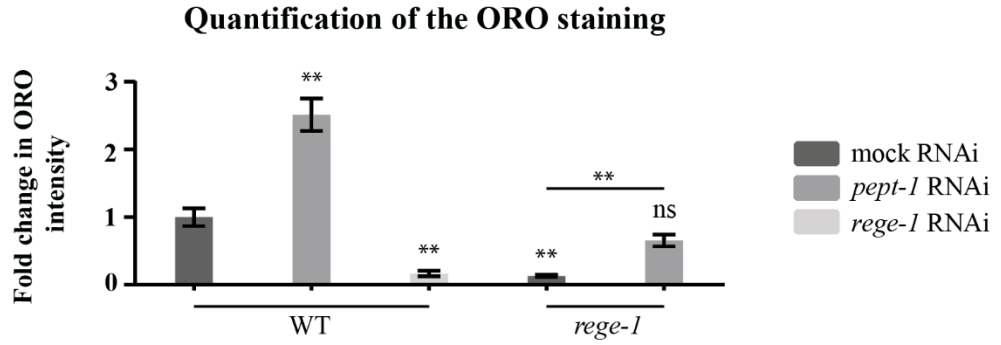

C

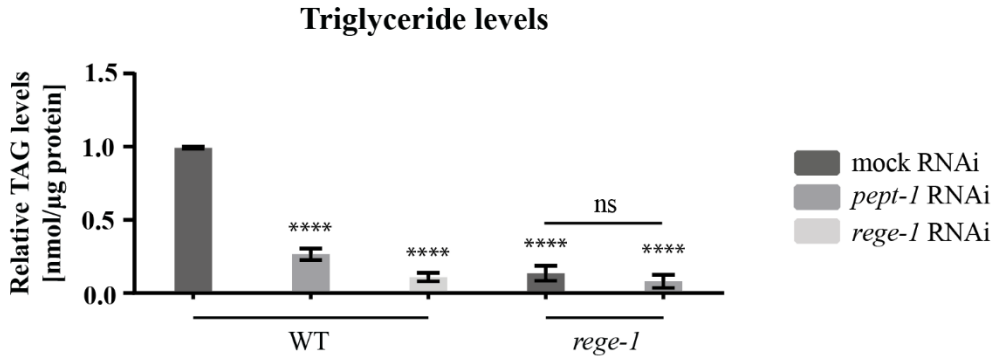

D

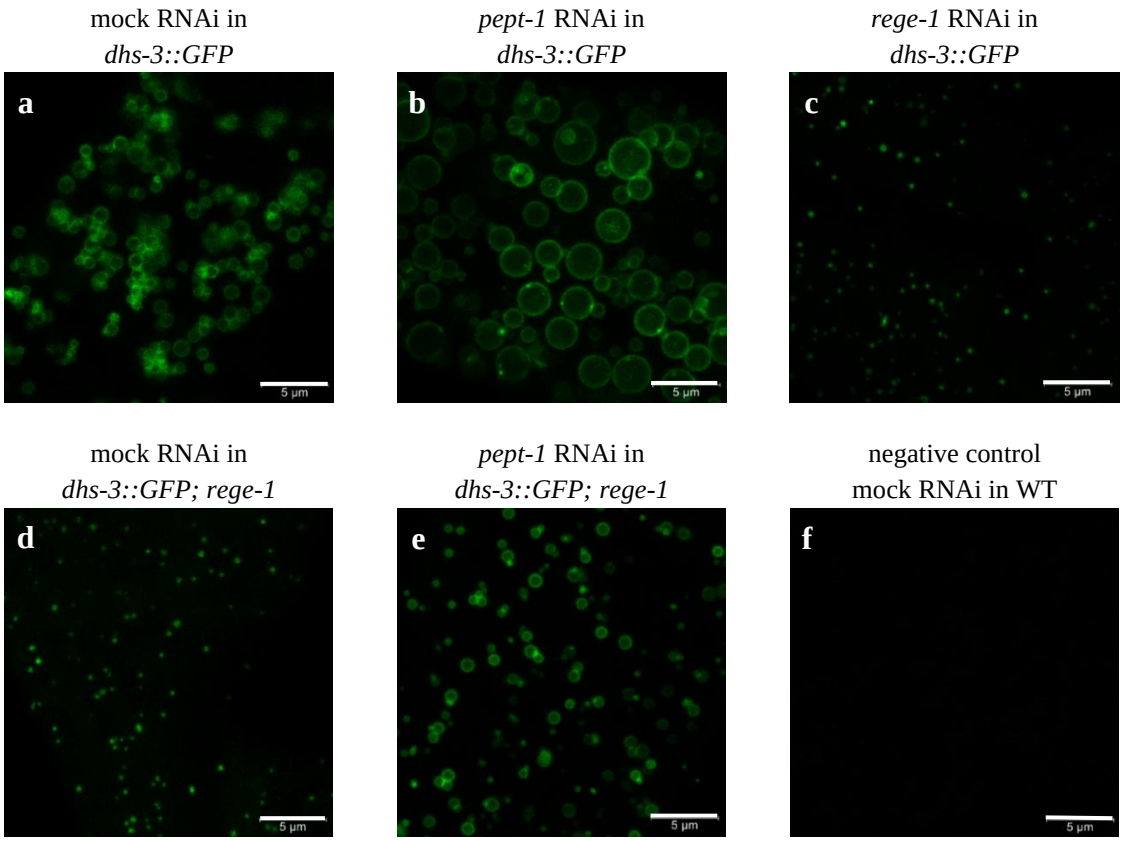

E

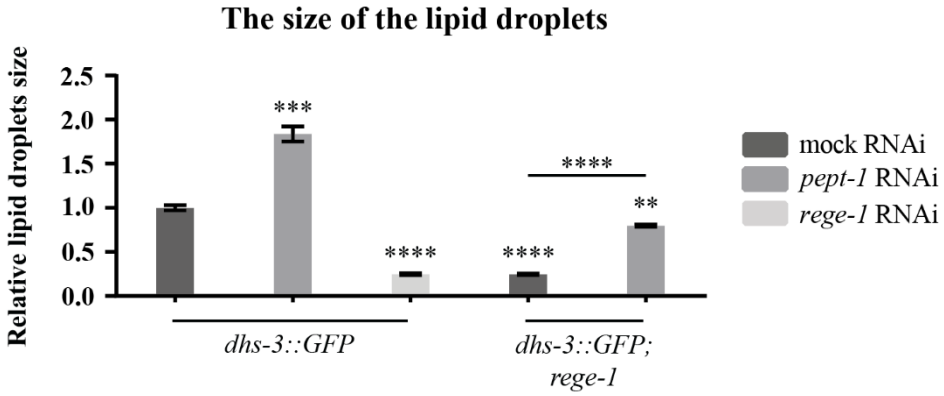

Figure 30. Inhibition of *pept-1* mRNA partially rescued the fat loss phenotype of *rege-1* mutants. (**A**) Images of wild-type and animals carrying *rege-1* mutation exposed to mock RNAi or dsRNA targeting either *pept-1* or *rege-1* mRNA. The animals were stained with the ORO to visualize body fat levels. Scale bar: 100 µm. (**B**) Quantification of relative changes in the ORO staining. 30 animals per condition were measured. Changes in body fat levels were determined in relation to wild-type animals subjected to mock RNAi. The P values were calculated using un-paired Student t-test (*n = 3*). Data are presented as mean; error bars represent SEM (** indicates $p < 0.01$). (**C**) Quantification of changes in TAG levels relative to the total protein content. Changes in TAG levels were measured in relation to wild-type animals exposed to mock RNAi. The P values were calculated using un-paired Student t-test (*n = 3*). Data are presented as mean;

error bars represent SEM (**** indicates p < 0.0001). (**D**) Determination of LDs size. The *dhs-3::GFP* strain was exposed to mock (a), *pept-1* (b) or *rege-1* (c) RNAi. The *dhs-3::GFP; rege-1* strain was exposed to mock (d) or *pept-1* (e) RNAi. Wild-type animals subjected to mock RNAi were used as a negative control for correction of the autofluorescence of gut granules (f). Scale bar: 5 µm. (**E**) Quantification of the LDs size. The diameter of the LDs were measured as an average from 30 droplets per strain from 5 animals. Changes in LDs size were measured in relation to *dhs-3::GFP* strain subjected to mock RNAi. The P values were calculated using un-paired Student t-test (*n = 3*). Data are presented as mean; error bars represent SEM (** indicates p < 0.01; *** p < 0.001; **** p < 0.0001).

2.2.1.7. Disturbance of dipeptide hydrolysis or proton transport across intestinal membrane slightly increased body fat content in rege-1 mutants

PEPT-1 transporter in *C. elegans* exerts dual function, as shown in **Figure 31**. In addition to transporting di- and tripeptides from the intestinal lumen into the intestinal cytoplasm, PEPT-1 works as a symporter, responsible for the influx of proton ions (Spanier et al., 2009).

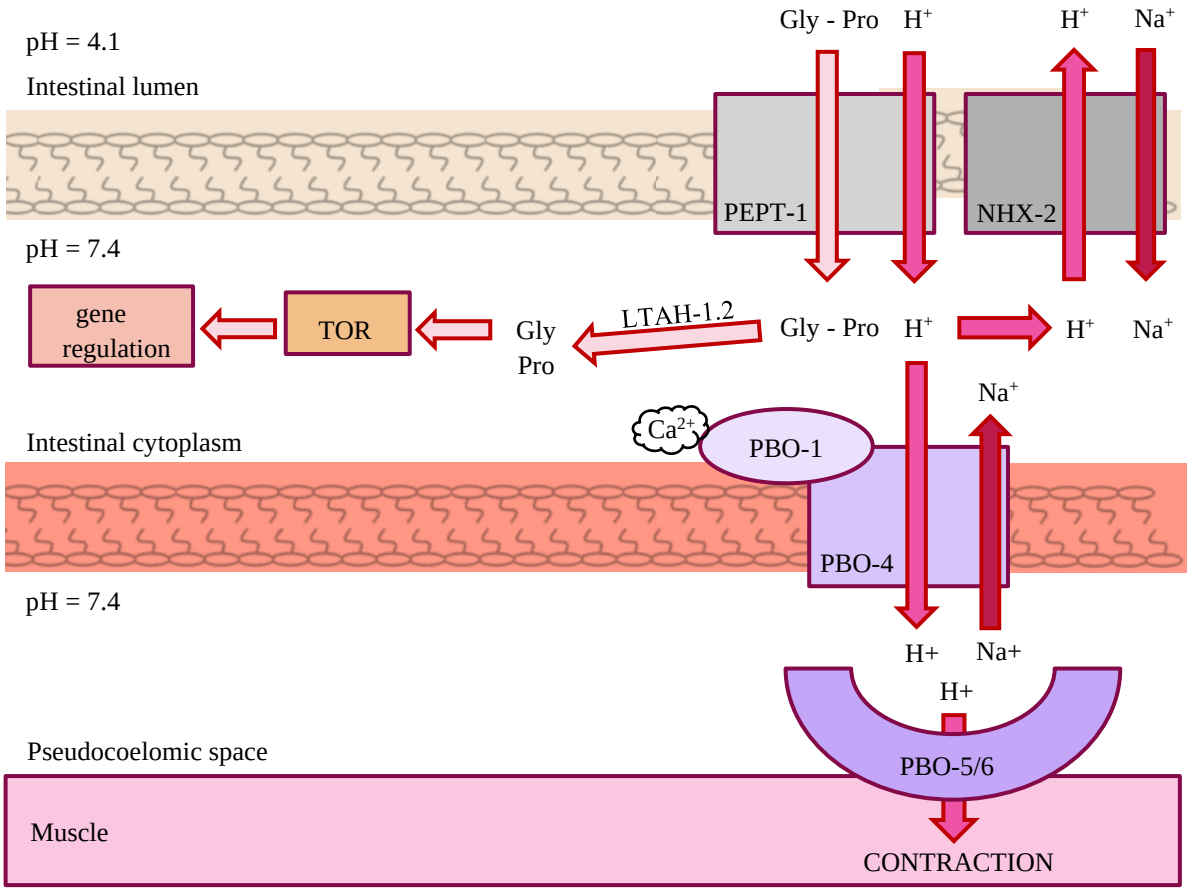

Figure 31. Model of the interactions between proton and peptides transport with muscle contraction and TOR signaling in *C. elegans*. Based on *Nehrke, 2014* and *Benner et al., 2011*.

2.2.1.7.1. Inhibition of aminopeptidase ltah-1.2 slightly increased body fat content in rege-1 mutants

In *C. elegans*, PEPT-1 transports di- and tripeptides from the intestinal lumen to the intestinal cytoplasm, where they are cut into individual peptides by aminopeptidase, leukotriene A4 hydrolase homolog (LTAH-1.2) (Baset et al., 1998), as shown in **Figure 31**. These peptides can stimulate the function of TOR, one of the major pathways, which can potentially regulate fat accumulation in nematodes (Meissner et al., 2004). To test whether the LTAH-1.2 function affected fat accumulation in *rege-1* mutants, the *ltah-1.2* mRNA was silenced by RNAi and the relative body fat content was measured by the ORO staining.

RNAi-mediated silencing of *ltah-1.2* mRNA did not influence the body fat levels in the wild-type animals compared to controls, as presented in **Figure 32**. However, *rege-1* mutants exposed to *ltah-1.2* RNAi had increased fat accumulation compared to their counterparts exposed to mock RNAi, but did not regain fat to a level observed in the control. Although, LTAH-1.2 aminopeptidase might modulate fat accumulation in *rege-1* mutants, the results indicate that the PEPT-1 - LTAH-1.2 may work in parallel to and is not exclusively dependent on the REGE-1- ETS-4 regulatory axis.

A

B

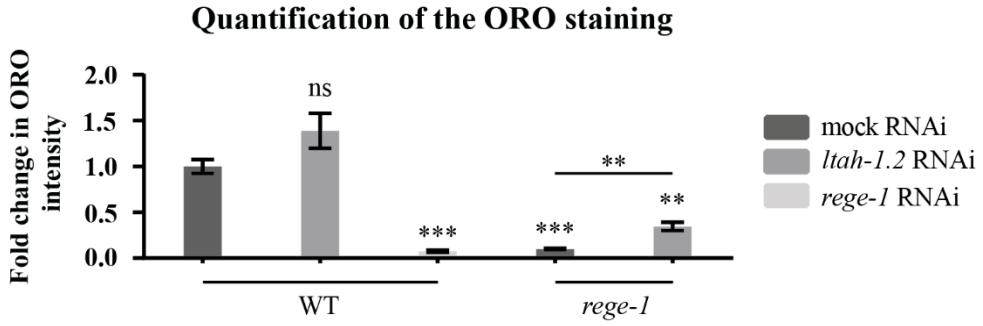

Figure 32. Inhibition of *ltah-1.2* partially rescued the fat loss phenotype of *rege-1* mutants. (**A**) Images of wild-type and animals carrying the *rege-1* mutation exposed to mock RNAi or dsRNA targeting either *rege-1* or *ltah-1.2* mRNA. The animals were stained with the ORO to visualize body fat levels. Scale bar: 100 µm. (**B**) Quantification of relative changes in the ORO staining. 30 animals per condition were measured. Changes in body fat levels were determined in relation to wild-type animals subjected to mock RNAi. The P values were calculated using un-paired Student t-test ($n = 3$). Data are presented as mean; error bars represent SEM (** indicates $p < 0.01$; *** $p < 0.001$).

2.2.1.7.2. Inhibition of pbo-1 or pbo-4 slightly increased body fat content in rege-1 mutants

In addition to peptide transport, PEPT-1 is responsible for translocation of protons from the intestinal lumen (pH 4.1) into the intestinal cytoplasm (pH 7.4), which cause cell acidification, as shown in **Figure 31** (Spanier et al., 2009; Pfeiffer et al., 2008). The change in pH activates PBO-1 and PBO-4, which affect proton transport from the basolateral part of the intestine into the pseudocoelomic space (Benomar et al., 2020; Beg et al., 2008; Nehrke, 2014) and control the dynamics of the posterior body muscle contraction and cyclic defecation (Dal Santo et al., 1999). In order to check whether genes controlling proton transport across biological membranes affect fat accumulation in *rege-1* mutants,

the *pbo-1* and *pbo-4* mRNAs were targeted by RNAi in *rege-1* mutants and the relative body fat content by the ORO staining and TAG levels were measured, as presented in **Figure 33** and **Figure 34**.

Targeting *pbo-1* or *pbo-4* mRNAs by RNAi in the wild-type animals did not change fat accumulation compared to controls. The *rege-1* mutants exposed to *pbo-1* or *pbo-4* RNAi had an increased total body fat content compared to *rege-1* mutants exposed to mock RNAi, as shown in **Figure 33** (**A**, **B**) and **Figure 34** (**A**, **B**). However, the increase in fat content did not reach the control levels. In addition, targeting *pbo-1* or *pbo-4* mRNA markedly increased TAG levels in wild-type animals relative to controls, as presented in **Figure 33 C** and **Figure 34 C**. Surprisingly, *rege-1* mutants subjected to *pbo-1* or *pbo-4* RNAi had similar levels of TAG compared to their counterparts exposed to mock RNAi.

These results suggest that PBO-1 and PBO-4 contribute to a reduction in total body fat content in *rege-1* mutants and in animals with RNAi-targeted *rege-1* mRNA. In contrast, inhibition of *pbo-1* or *pbo-4* mRNAs in *rege-1* mutants increased fat accumulation without a significant change in the relative TAG levels. Therefore, slight increases in fat accumulation in *rege-1* mutants with RNAi targeted either *pbo-1* or *pbo-4* might result from the accumulation of lipid species other than TAGs. Since the recovery of body fat in *rege-1* mutants exposed to *pbo-1* or *pbo-4* RNAi was partial and *pbo-1* / *pbo-4* mRNAs silencing increased TAG levels also in wild-type animals, the PEPT-1 - PBO-1 / PBO-4 pathway might regulate fat accumulation not exclusively via the REGE-1 - ETS-4 regulatory axis.

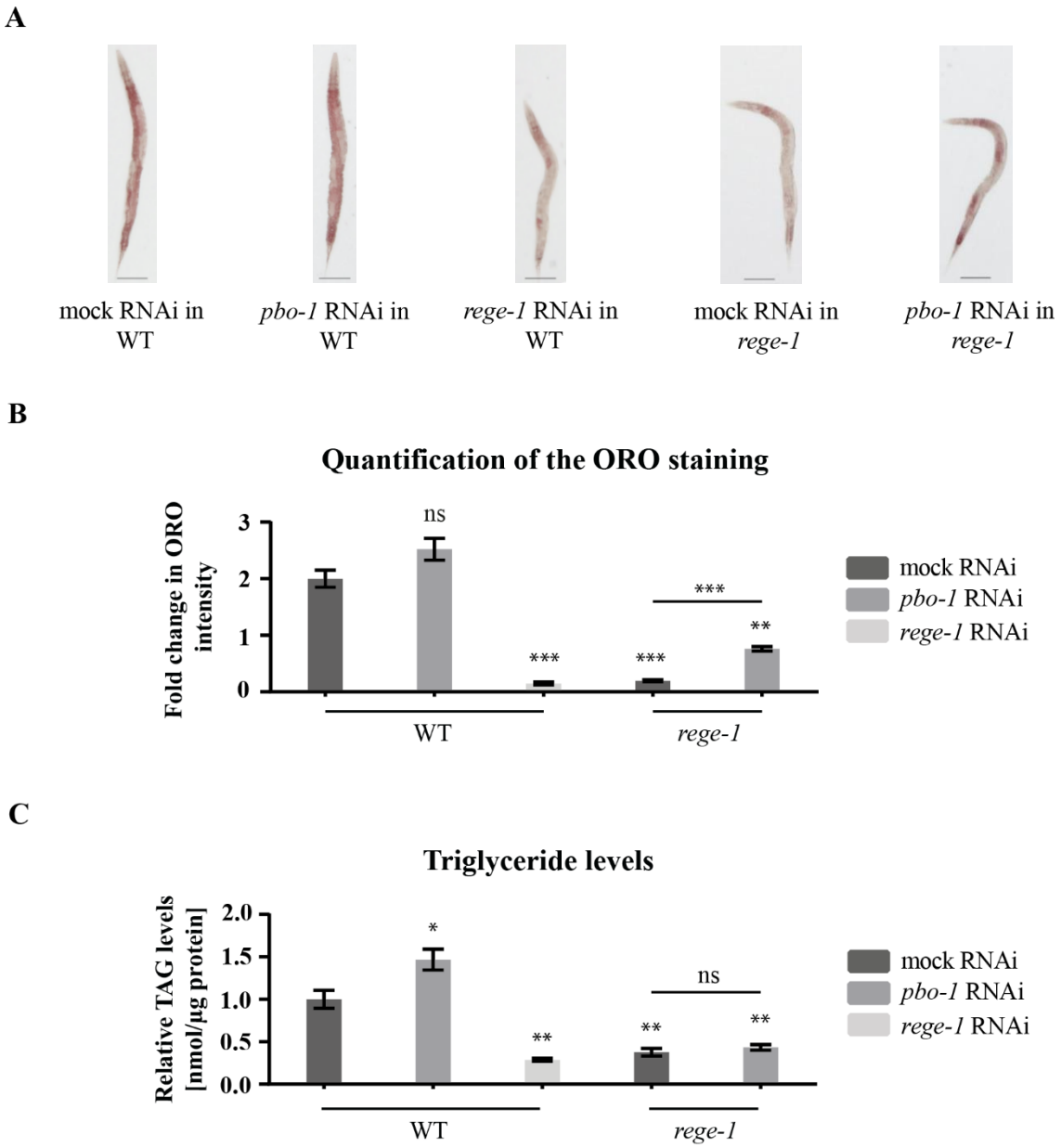

Figure 33. Inhibition of *pbo-1* mRNA partially rescued the fat loss phenotype in *rege-1* mutants. (**A**) Images of wild-type and animals carrying *rege-1* mutations exposed to mock RNAi or dsRNA targeting either *rege-1* or *pbo-1* mRNAs. The animals were stained with the ORO to visualize body fat levels. Scale bar: 100 µm. (**B**) Quantification of relative changes in the ORO staining. 30 animals per condition were measured. Changes in body fat levels were determined in relation to wild-type animals subjected to mock RNAi. The P values were calculated using un-paired Student t-test (*n = 3*). Data are presented as mean; error bars represent SEM (** indicates $p < 0.01$; *** $p < 0.001$). (**C**) Quantification of changes in TAG levels relative to the total protein content. Changes in TAG levels were measured in relation to wild-type animals exposed to mock RNAi. The P values were calculated using un-paired Student t-test (*n = 3*). Data are presented as mean; error bars represent SEM (* indicates $p < 0.05$; ** $p < 0.01$).

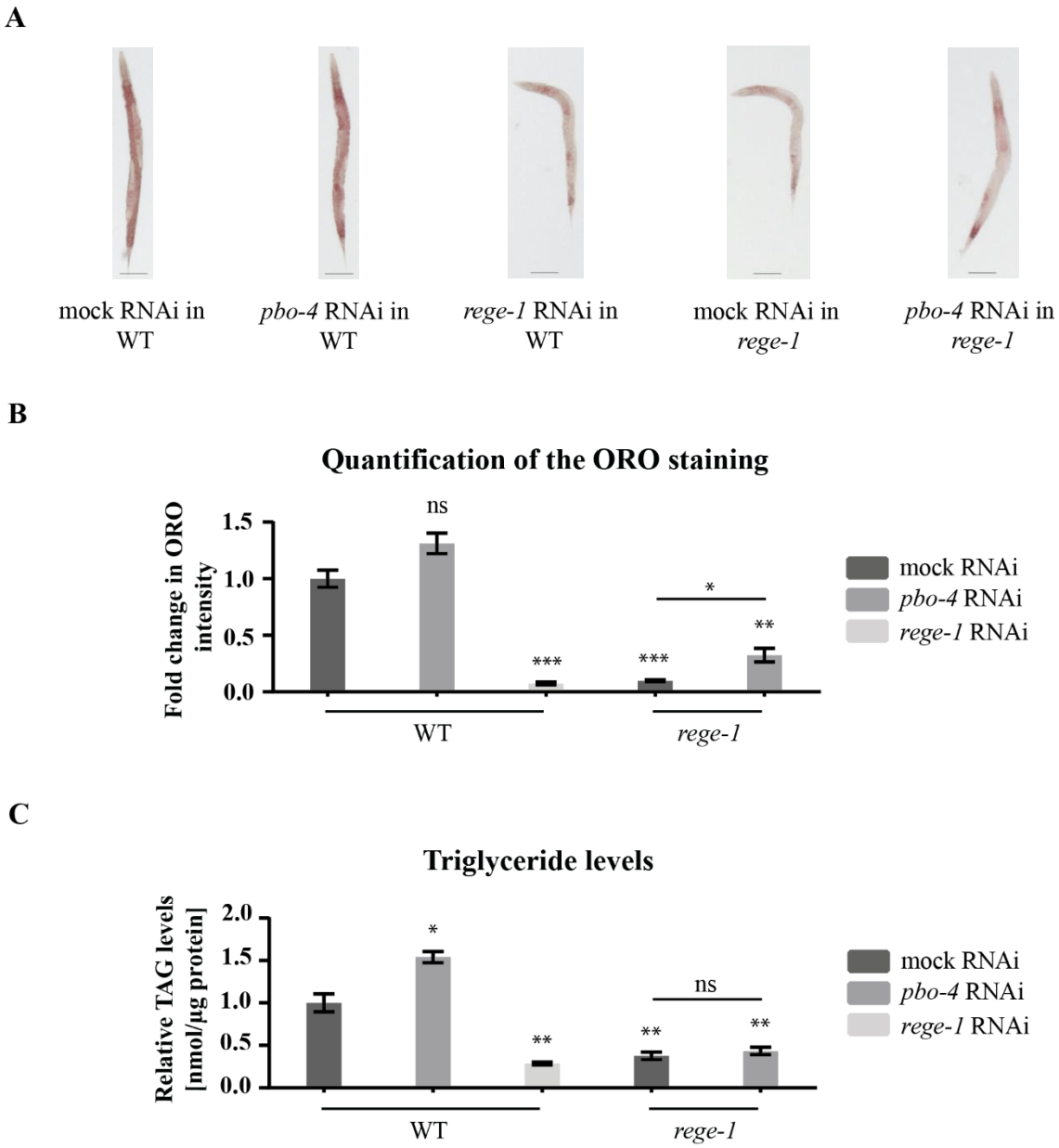

Figure 34. Inhibition of *pbo-4* mRNAs slightly increased fat accumulation in *rege-1* mutants. (**A**) Images of wild-type or *rege-1* mutant animals exposed to mock RNAi or dsRNA targeting either *rege-1* or *pbo-4* mRNAs. The animals were stained with the ORO to visualize body fat levels. Scale bar: 100 µm. (**B**) Quantification of relative changes in the ORO staining. 30 animals per condition were measured. Changes in body fat levels were determined in relation to wild-type animals subjected to mock RNAi. The P values were calculated using un-paired Student t-test (*n = 3*). Data are presented as mean; error bars represent SEM (* indicates $p < 0.05$; ** $p < 0.01$; *** $p < 0.001$). (**C**) Quantification of changes in TAG levels relative to the total protein content. Changes in TAG levels were measured in relation to wild-type animals exposed to mock RNAi. The P values were calculated using un-paired Student t-test (*n = 3*). Data are presented as mean; error bars represent SEM (* indicates $p < 0.05$; ** $p < 0.01$).

2.2.2. *daf-16* and *pqm-1* as candidate targets for ETS-4

As previously mentioned, ETS-4 might modulate transcription of the PQM-1 (Habacher et al., 2016), which is an antagonist of the DAF-16 (Sun et al., 2017). DAF-16 is regulated by a group of protein kinases which lead to inhibition or activation of DAF-16 function depending on the site of phosphorylation (Sun et al., 2017). The IIS pathway via serine / threonine kinases AKT leads to phosphorylation of DAF-16 which thus remains inactive in the cytoplasm (Sun et al., 2017), while dephosphorylated PQM-1 enters the nucleus where it activates transcription of developmental genes via DAF-16 associated element (DAE) sequence (TGATAAG) (Tepper et al., 2013), as shown in **Figure 35**. When the insulin pathway is inactive, PQM-1 is phosphorylated and enters the cytoplasm, while DAF-16 ceases to be dephosphorylated and moves to the nucleus where it activates the transcription of stress response genes via DAF-16 binding element (DBE) sequence (GTAAACA) (Tepper et al., 2013; Dowen et al., 2016). In further experiments, it was determined whether REGE-1 - ETS-4 regulatory axis regulate fat accumulation via PQM-1 and DAF-16.

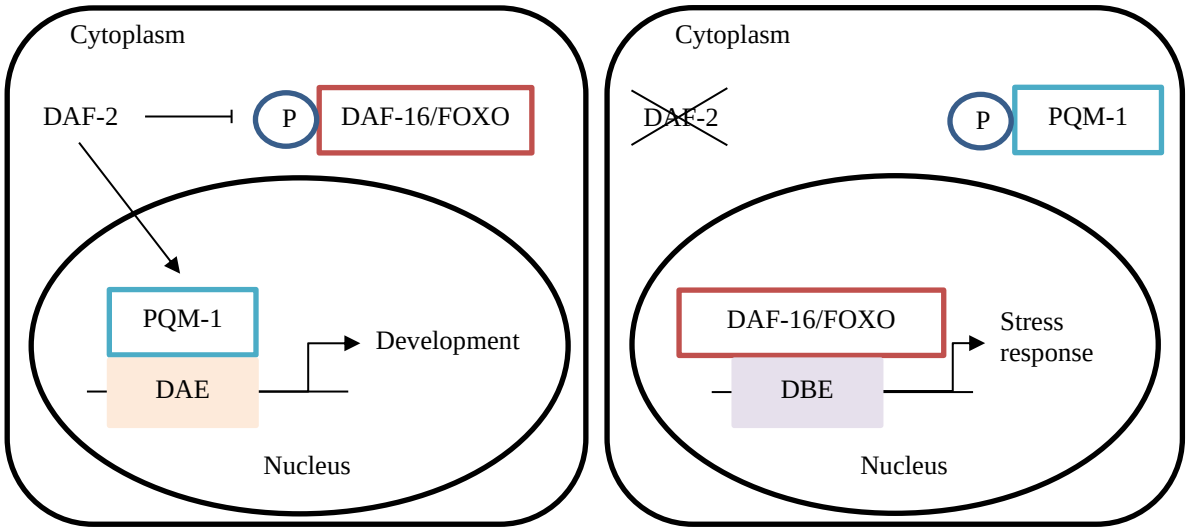

Figure 35. Insulin signaling pathway influence translocation of DAF-16 and PQM-1 between the cytoplasm and the nucleus. On the left, the active IIS pathway leads to inactivation of DAF-16 through its phosphorylation and activation of the transcription factor PQM-1 and its nuclear translocation. On the right, the inactive IIS pathway leads to inactivation of PQM-1 through its phosphorylation and activation of the transcription factor DAF-16 and its nuclear translocation. Based on *Dowen et al., 2016* and *Tepper et al., 2013*.

2.2.2.1. The levels of daf-16 and pqm-1 mRNAs were increased in rege-1 mutants

To determine whether ETS-4 regulates transcription of *daf-16* and *pqm-1*, *daf-16* and *pqm-1* mRNA levels were measured in wild-type animals and in animals carrying either *rege-1* or *ets-4; rege-1* mutations exposed to mock or *rege-1* RNAi, as shown in **Figure 36**. Both *daf-16* and *pqm-1* mRNA levels increased in wild-type animals subjected to *rege-1* RNAi and in *rege-1* mutants subjected to mock RNAi compared to controls. Furthermore, in *ets-4; rege-1* double mutants exposed to mock RNAi the levels of *daf-16* and *pqm-1* mRNAs were similar to controls. These results suggest that *ets-4* mRNAs contributed to increased transcription of *daf-16* and *pqm-1*. However, to determine if they are transcriptionally active, their subcellular location should be checked.

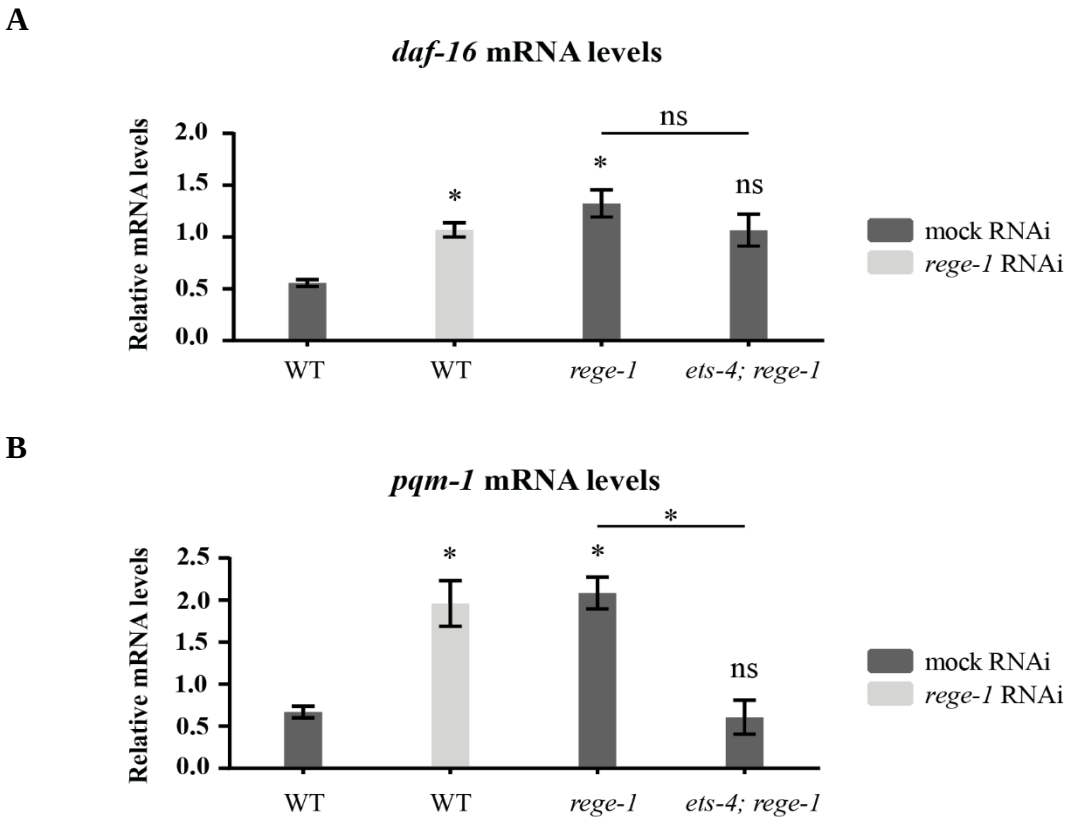

Figure 36. The levels of *daf-16* and *pqm-1* mRNAs were increased in *rege-1* mutants. The levels of *daf-16* (**A**) and *pqm-1* (**B**) mRNAs were measured by RT-qPCR in the wild-type and in animals carrying either *rege-1* or *ets-4; rege-1* mutations exposed to mock or *rege-1* RNAi. The mRNA levels were normalized to the actin 1 mRNA levels and compared in relation to wild-type animals subjected to mock RNAi. The P values were calculated using un-paired Student t-test ($n = 3$). Data are presented as mean; error bars represent SEM ($p < 0.05$).

2.2.2.2. Inhibition of rege-1 mRNA affected the nuclear location of DAF-16

Visualisation of DAF-16 was performed using endogenous DAF-16 protein tagged with GFP, while its anatomical location was verified based on the Worm Atlas. Signal location analysis showed the presence of DAF-16::GFP in the nuclei of intestinal cells in both, animals expressing DAF-16::GFP exposed to *rege-1* RNAi and in *rege-1* mutants expressing DAF-16::GFP exposed to mock RNAi, as presented in **Figure 37**. In contrast, in the animals expressing DAF-16::GFP subjected to mock RNAi, the signal was present in the cytoplasm of intestinal cells. Wild-type exposed to mock RNAi were used as a negative control for correction of the autofluorescence of gut granules. The presence of a signal from DAF-16::GFP in the nucleus in animals with inhibited *rege-1* may indicate its increased transcriptional activity.

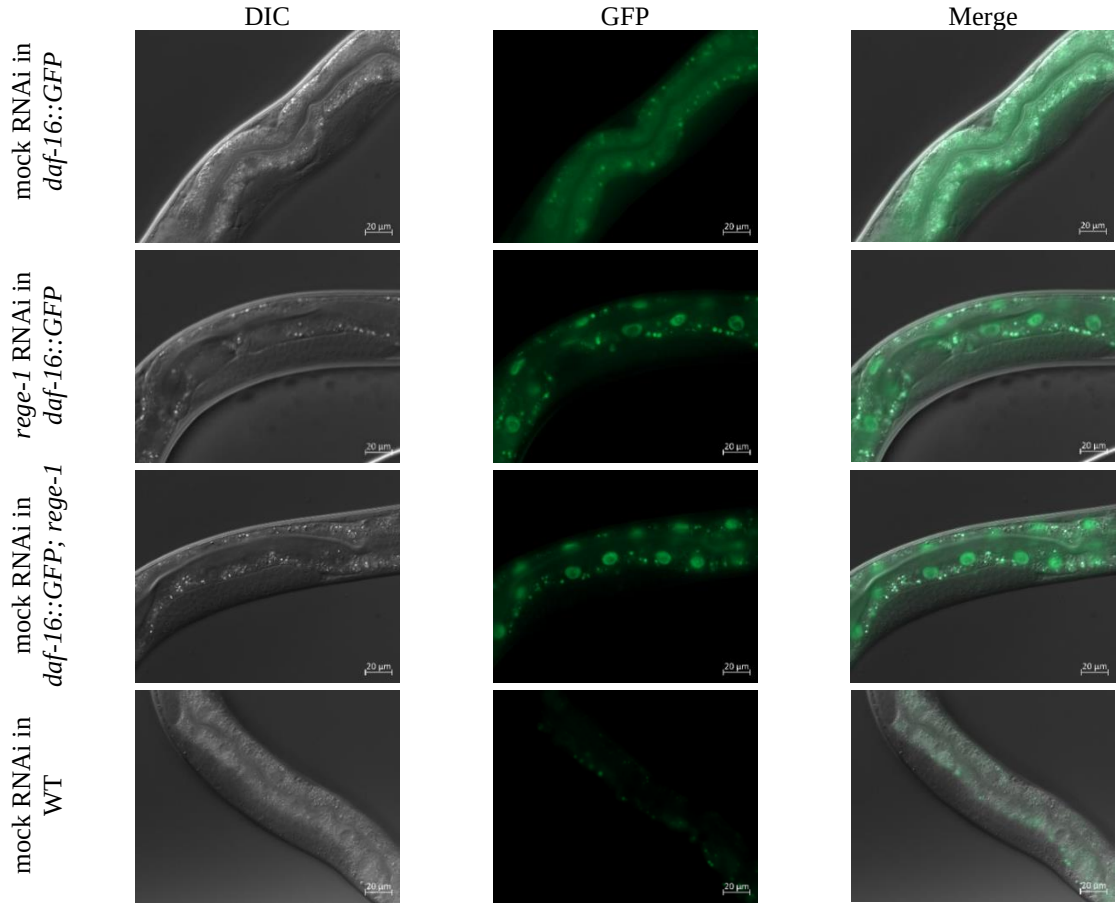

Figure 37. Localization of DAF-16::GFP in intestinal cells. The *daf-16::GFP* strain was exposed to mock or *rege-1* RNAi. The *daf-16::GFP*; *rege-1* strain was exposed to mock RNAi. Wild-type animals subjected to mock RNAi were used as a negative autofluorescence control. Scale bar: 20 µm.

2.2.2.3. DAF-16 and PQM-1 did not affect body fat levels in rege-1 mutants

Previous studies have shown a significant increase in the levels of *daf-16* and *pqm-1* mRNA (**Figure 36**) and an increase in nuclear translocalization of the DAF-16::GFP protein (**Figure 37**) in *rege-1* mutants. Therefore, it was checked whether the DAF-16 or PQM-1 are involved in the regulation of fat content through the REGE-1 - ETS-4 regulatory axis. For this purpose, *daf-16* or *pqm-1* mRNA were targeted by RNAi in *rege-1* mutants and stained by the ORO, as presented in **Figure 38**.

Targeting *daf-16* or *pqm-1* mRNAs by RNAi did not affect fat accumulation in the wild-type animals compared to controls. In addition, inhibition of *daf-16* or *pqm-1* mRNAs did not alter body fat levels in *rege-1* mutants compared to the corresponding strain exposed to mock RNAi. These results suggest that ETS-4 did not affect fat accumulation in the *rege-1* mutants through DAF-16 or PQM-1.

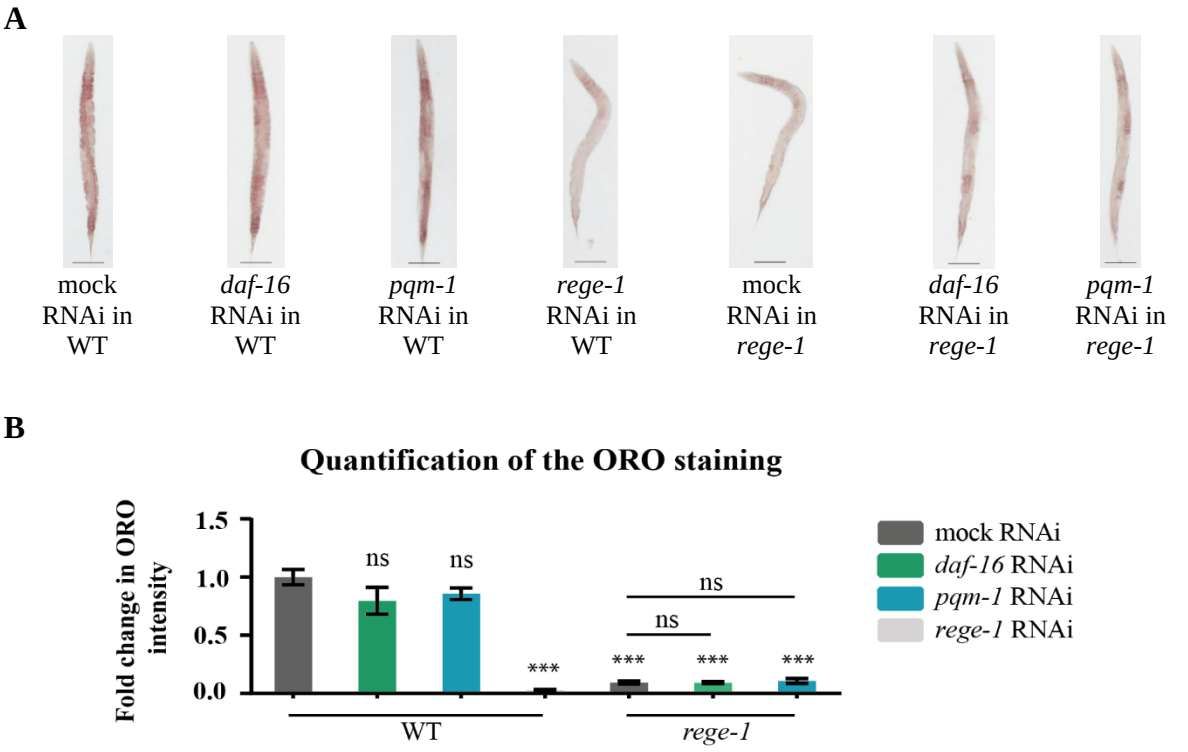

Figure 38. Inhibition of *daf-16* or *pqm-1* mRNAs did not affect body fat accumulation in *rege-1* mutants. (**A**) Images of wild-type and *rege-1* mutants exposed to mock or dsRNA targeting either *daf-16*, *pqm-1* or *rege-1* mRNAs. The animals were stained with the ORO to visualize body fat levels. Scale bar: 100 µm. (**B**) Quantification of relative changes in the ORO staining. 30 animals per condition were measured. Changes in body fat levels were determined in relation to wild-type animals subjected to mock RNAi. The P values were calculated using un-paired Student t-test (*n = 3*). Data are presented as mean; error bars represent SEM (*** indicates $p < 0.001$).

2.3. *skn-1* as a candidate target for ETS-4

Reports from human colon carcinoma cell line showed that nuclear factor erythroid 2-related factor 2 (NRF2), a counterpart of *C. elegans* SKN-1, increased the expression of *PEPT1* gene and PEPT1 protein level (Geillinger et al., 2014) as well as MRP1 in small cell lung cancer cell line (Ji et al., 2013). In addition, SKN-1 increased stress resistance and reduced body fat content in *C. elegans* (Steinbaugh et al., 2015). Since the research conducted here suggest the possible association of PEPT-1 and MRP-1 with body fat loss in *rege-1* mutants, it was investigated whether ETS-4 could indirectly influence their expression through another transcription factor SKN-1.

2.3.1. Depletion of *skn-1* mRNA slightly increased body fat content in *rege-1* mutants

In order to check whether the REGE-1 - ETS-4 regulatory axis influences the relative body fat content through SKN-1, its mRNA levels in the *rege-1* mutants and the relative body fat level by the ORO method in the *rege-1* mutants exposed to *skn-1* RNAi, were measured.

Quantitative analysis by RT-qPCR presented in **Figure 39 A**, showed that *skn-1* mRNA levels increased in both wild-type animals exposed to *rege-1* RNAi and *rege-1* mutants exposed to mock RNAi compared to controls. However, in *ets-4; rege-1* double mutants subjected to mock RNAi, *skn-1* mRNA levels were similar to controls.

The ORO staining, presented in **Figure 39** (**B**, **C**), showed a significant increase in the body fat content in the wild-type animals subjected to *skn-1* RNAi compared to controls. In contrast, targeting *skn-1* mRNAs by RNAi in the *rege-1* mutants increased fat accumulation compared to *rege-1* mutants exposed to mock RNAi, however, to a lower level than in controls.

In summary, *skn-1* mRNA levels were increased and thus SKN-1 could be partially responsible for the fat loss phenotype in *rege-1* mutants. However, since inhibition of *skn-1* did not fully recover the body fat content in *rege-1* mutants compared to controls and increased fat accumulation also in wild-type animals, SKN-1 may regulate fat metabolism via signaling independent of the REGE-1 - ETS-4 regulatory axis.

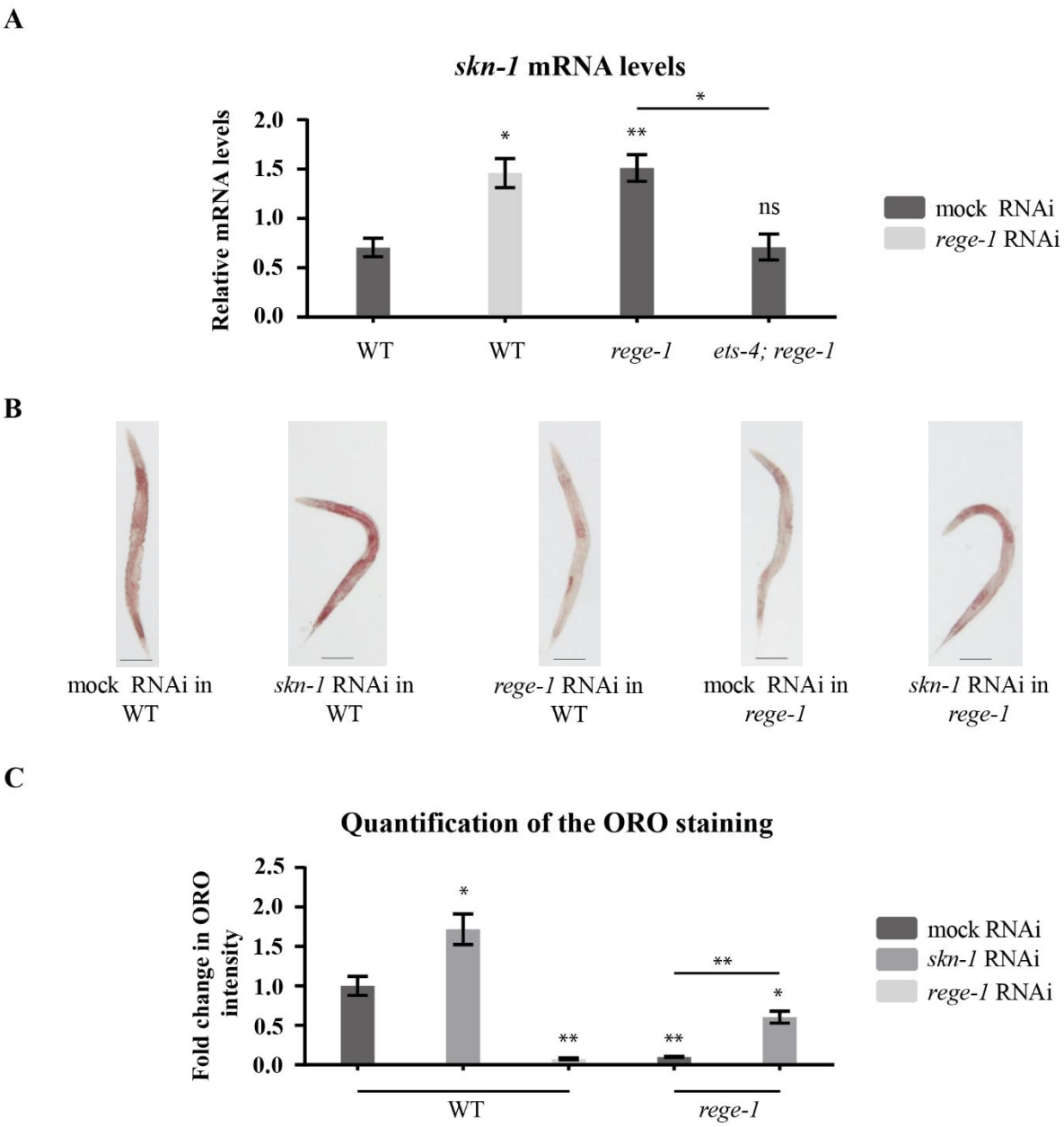

Figure 39. Inhibition of *skn-1* mRNA partially rescued the fat loss phenotype of *rege-1* mutants. (**A**) The level of *skn-1* mRNAs were measured by RT-qPCR in wild-type and animals carrying either *rege-1* or *ets-4; rege-1* mutations exposed to mock or *rege-1* RNAi. The *skn-1* mRNA levels were normalized to actin 1 mRNA levels of and compared in relation to wild-type animals subjected to mock RNAi. The P values were calculated using un-paired Student t-test (*n = 3*). Data are presented as mean; error bars represent SEM (* indicates $p < 0.05$; ** $p < 0.01$). (**B**) Images of wild-type and animals carrying *rege-1* mutation exposed to mock RNAi or dsRNA targeting either *skn-1* or *rege-1* mRNAs. The animals were stained with the ORO to visualize body fat levels. Scale bar: 100 μm. (**C**) Quantification of relative changes in the ORO staining. 30 animals per condition were measured. Changes in body fat levels were determined in relation to wild-type animals subjected to mock RNAi. The P values were calculated using un-paired Student t-test (*n = 3*). Data are presented as mean; error bars represent SEM (* indicates $p < 0.05$; ** $p < 0.01$).

2.3.2. The expression of oxidative stress response genes was increased in *rege-1* mutants

Previous studies demonstrated that high levels of the transcription factor ETS-4 in *rege-1* mutants stimulated the expression of genes responsible for catabolism and immunity in *C. elegans* (Habacher et al., 2016). Due to the fact that both catabolism and immune response can cause reactive oxygen species (ROS) formation (Chavez et al., 2007), and that SKN-1 was activated in response to ROS and oxidative stress, it was checked whether ETS-4 influenced transcription of the oxidative stress response genes.

Analysis of *sod-4* and *sod-5* mRNA levels by RT-qPCR showed a significant increase in both wild-type animals exposed to *rege-1* RNAi and in *rege-1* mutants exposed to mock RNAi compared to controls, as shown in **Figure 40**. However, in the case of *ets-4; rege-1* double mutants *sod-4* and *sod-5* mRNA levels were similar to controls. Moreover, the expression of SOD-5::GFP was located in neurons in the pharynx of *rege-1* mutant animals compared to their counterparts subjected to mock RNAi (**Figure 41**). These results demonstrated high expression of genes related to oxidative response in *rege-1* mutants.

A

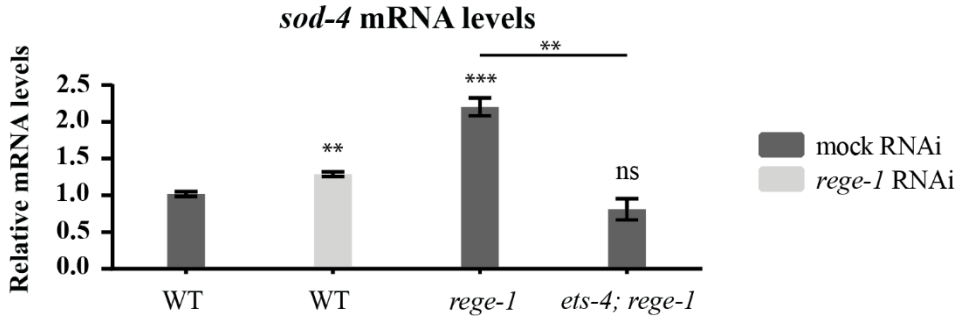

B

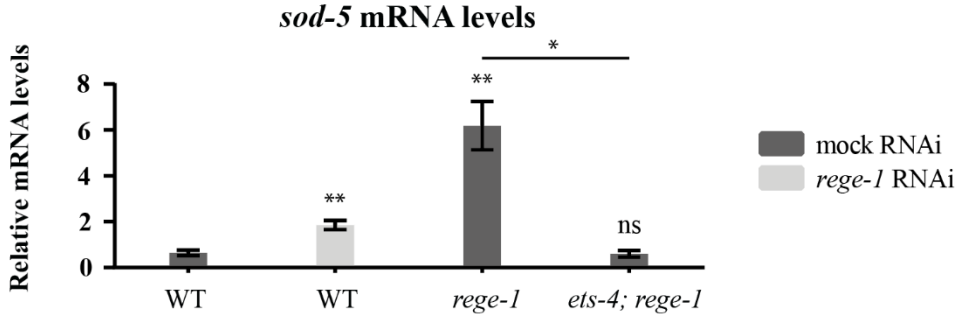

Figure 40. The expression of oxidative stress response genes was increased in *rege-1* mutant animals. The *sod-4* (**A**) and *sod-5* (**B**) mRNAs levels were measured by RT-qPCR in the wild-type and animals carrying either *rege-1* or *ets-4; rege-1* mutations exposed to mock or *rege-1* RNAi. The mRNA levels were normalized to the actin 1 mRNA levels and compared in relation to wild-type animals subjected to mock RNAi. The P values were calculated using un-paired Student t-test (*n = 3*). Data are presented as mean; error bars represent SEM (* indicates $p < 0.05$; ** $p < 0.01$; *** $p < 0.001$).

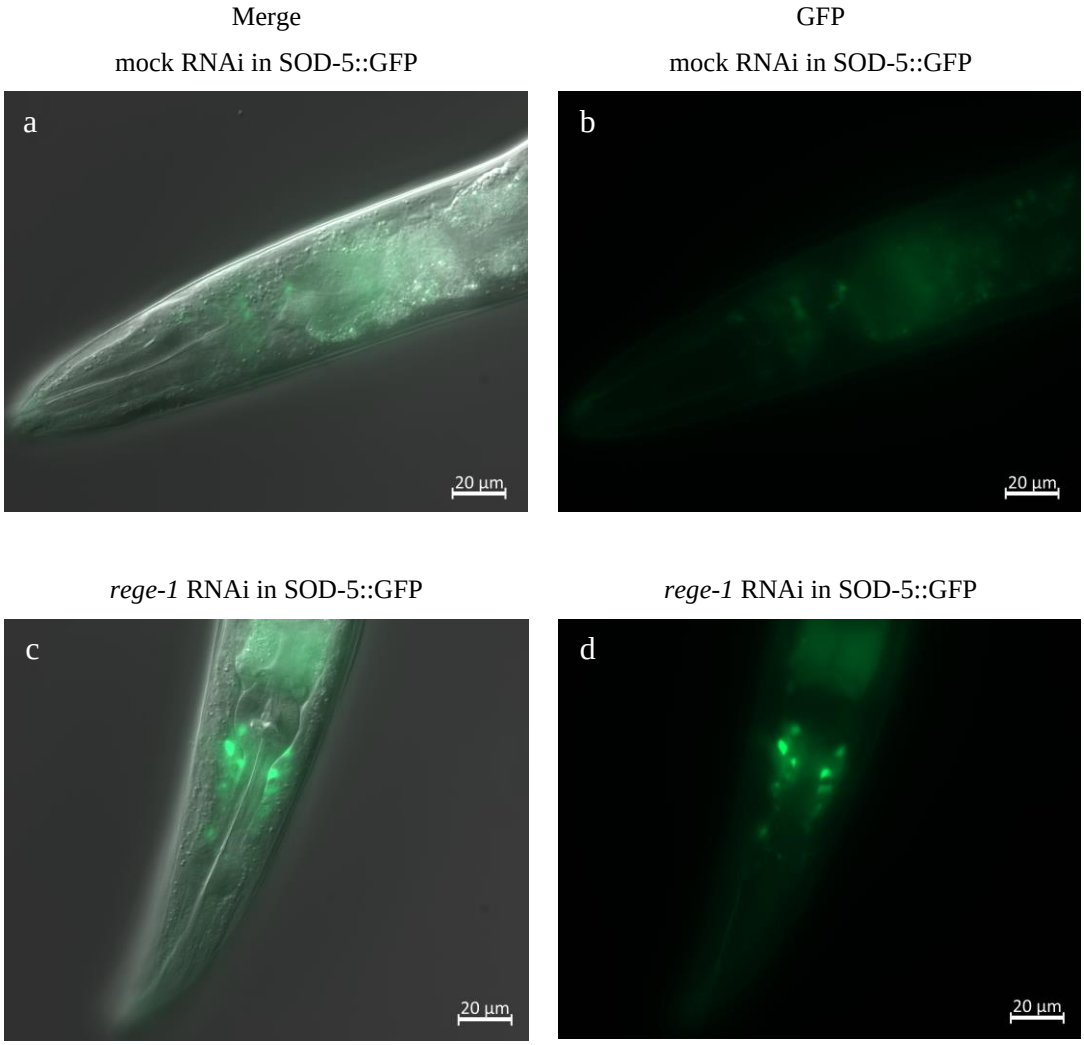

Figure 41. Localization of SOD5::GFP in neurons. GFP (b, d) and megre (a, c) images of animals expressing SOD-5::GFP exposed to mock RNAi (a, b) or dsRNA targeting *rege-1* mRNA (c, d). Scale bar: 20 µm.

3. Metabolic changes caused by ETS-4

In order to find out how ETS-4 reduces fat accumulation, the expression of genes affecting lipid composition, as well as changes in cellular respiration and glycogen synthesis in the *rege-1* mutants were determined.

3.1. The effect of ETS-4 on lipid metabolism in *rege-1* mutants

High levels of *ets-4* mRNA in *rege-1* mutants lead to a reduction in the body fat content (**Figure 10** and **Figure 11**). This chapter describes the effects of ETS-4 on the expression of genes influencing FA and sphingolipid metabolism.

3.1.1. The expression of genes involved in FA metabolism was changed in *rege-1* mutant animals

Fatty acids are the main components of lipids and the lipid composition is regulated by the activity of Δ9 desaturases such as *fat-5*, *fat-6* and *fat-7*, as shown in **Figure 42** (Brock et al., 2007). Disruption of FAT-6 or FAT-7 activity led to an enhancement of the activity of FAT-5, which changed lipid composition in *C. elegans* (Brock et al., 2007). The potential influence of ETS-4 on chages in the lipid composition was checked by measuring the mRNA levels of *fat-5*, *fat-6* and *fat-7*, as shown in **Figure 43**.

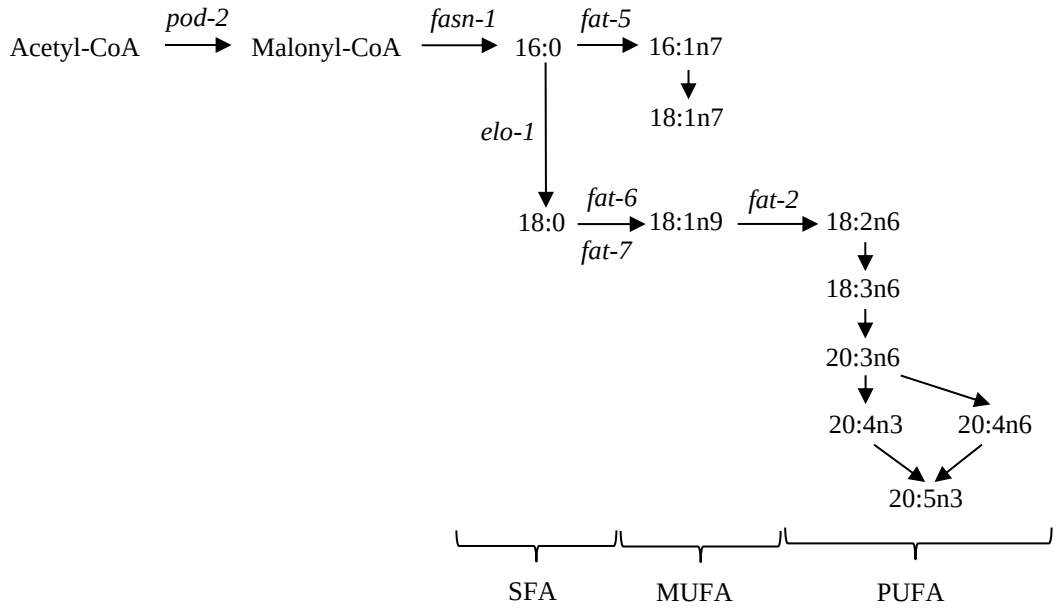

Figure 42. Scheme of FAs synthesis pathways. Palmitic acid (16:0); palmitoleic acid (16:1n7); vaccenic acid (18:1n7); stearic acid (18:0); oleic acid (18:1n9); linoleic acid (18:2n6); gamma linolenic acid (18:3n6); dihomogamma-linolenic acid (20:3n6); eicosatetraenoic acid (20:4n-3); arachidonic acid (20:4n6); eicosapentaenoic acid (20:5n-3); short fatty acids (SFA); mono-unsaturated fatty acids (MUFA); poly-unsaturated fatty acids (PUFA). Based on *Mejia-Martinez et al.,* 2017 and *Brock et al., 2007*.

RT-qPCR analysis showed a significant increase in *fat-5* mRNA levels in the wild-type animals exposed to *rege-1* RNAi and in *rege-1* mutants exposed to mock RNAi compared to controls. In contrast, *ets-4; rege-1* double mutants exposed to mock RNAi had similar levels of *fat-5* mRNA compared to controls. The expression of *fat-6* mRNAs did not change in *rege-1* and *ets-4; rege-1* double mutants compared to controls. The expression of *fat-7* mRNA was significantly decreased in both wild-type animals subjected to *rege-1* RNAi and in *rege-1* mutants subjected to mock RNAi compared to controls. In the case of *ets-4; rege-1* double mutants, *fat-7* mRNA levels were significantly lower compared to controls.

These results suggested that lipid composition in *rege-1* mutants might be affected by an upregulation of *fat-5* mRNA and a reduction in *fat-7* mRNA levels presumably via ETS-4. Upon FAT-7 deficiency, FAT-6 may play a compensating role (Brock ry al., 2006). In contrast, the expression of *fat-6* mRNA remained unchanged. Given that *fat-5* mRNA levels were significantly decreased in *ets-4; rege-1* double mutants it seems that FAT-5 contributes to the regulation of lipid composition in *rege-1* mutants, possibly through the REGE-1 – ETS-4 regulatory axis.

A

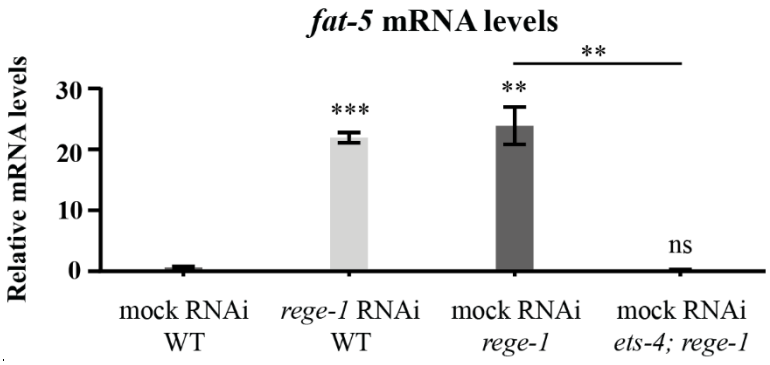

B

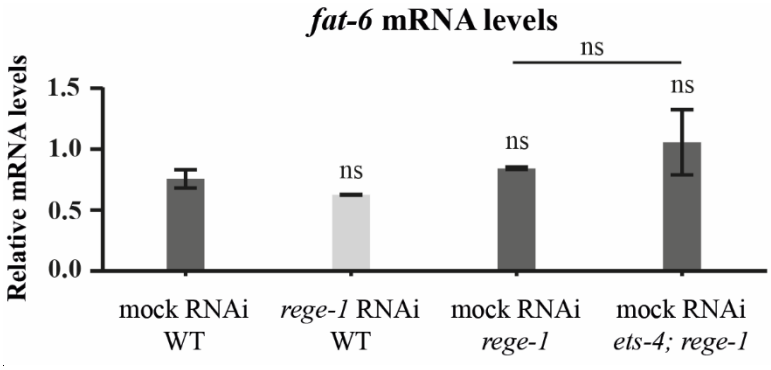

C

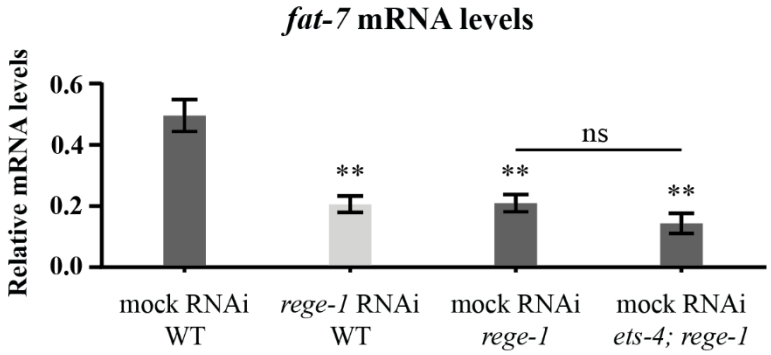

Figure 43. The expression of genes responsible for FA metabolism was changed in *rege-1* mutants. The levels of *fat-5* (**A**), *fat-6* (**B**) and *fat-7* (**C**) mRNAs were measured by RT-qPCR in the wild-type animals exposed to *rege-1* RNAi or dsRNA targeting *rege-1* mRNA. The mRNA levels were normalized to the actin 1 mRNA levels and compared in relation to wild-type animals subjected to mock RNAi. The P values were calculated using un-paired Student t-test (*n = 3*). Data are presented as mean; error bars represent SEM (** indicates $p < 0.01$; *** $p < 0.001$).

3.1.2. The expression of genes responsible for sphingolipid metabolism was influenced by inhibition of *rege-1*

Analysis of the RNA-Seq data showed that *sptl-1* and *sptl-2* mRNA levels were increased upon inhibition of *rege-1* mRNAs by RNAi and decreased in the *rege-1* mutants in with *ets-4* mRNAs was silenced (**Table 2**) (Habacher et al., 2016). Due to the fact that sphingolipids might influence lipid composition (Hänel et al., 2019), it was examined whether the REGE-1 - ETS-4 regulatory axis affected fat accumulation in nematodes by influencing genes involved in sphingolipid metabolism, as shown in **Figure 44**.

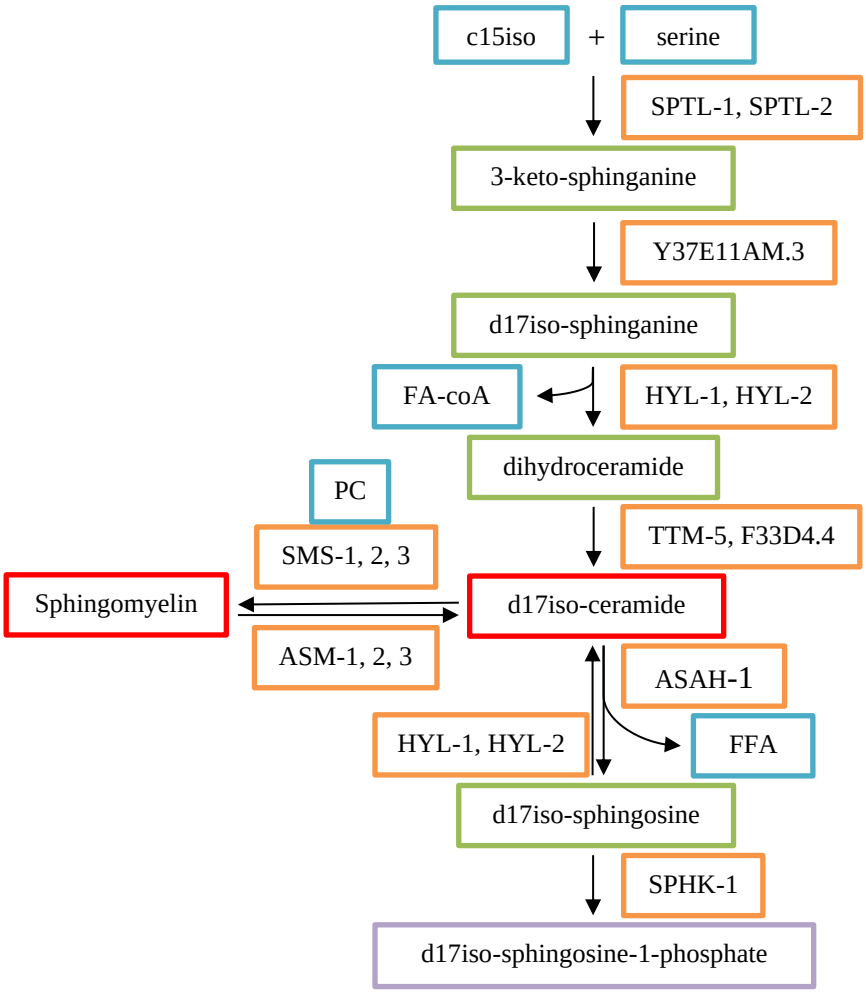

Figure 44. Sphingolipid synthesis pathway. Blue rectangle- substrates; green rectangle- minor lipids and intermediates; red rectangle- major lipid products; purple rectangle- signaling lipids; orange rectangle- enzymes. C15iso- 13-methyltetradecanoic acid; FA-coA- fatty acyl coenzyme A; HYL- homolog of yeast longevity gene; ASAH- acylsphingosine amidohydrolase; FFA- free fatty acid; ASM- acid sphingomyelinase; SMS- sphingomyelin synthase; PC- phosphatidylcholine; SPHK- sphingosine kinases. Based on *Watts and Ristow, 2017*.

3.1.2.1. High ets-4 mRNA levels in rege-1 mutants increased expression of genes responsible for sphingolipid metabolism

To confirm the RNA-Seq results, mRNA levels of *sptl-1* and *sptl-2* were measured by RT-qPCR in wild-type or *rege-1* mutant animals exposed to mock or *rege-1* RNAi, as shown in **Figure 45** (**A**, **B**). Both *sptl-1* and *sptl-2* mRNA levels increased in the wild-type animals subjected to *rege-1* RNAi and in *rege-1* mutants subjected to mock RNAi in comparison to controls. The *sptl-1* mRNA levels were lower in *ets-4; rege-1* double mutants exposed to mock RNAi, while the *sptl-2* mRNAs were similar to controls.

In addition to *sptl-1* and *sptl-2* mRNA levels, the expression of other genes involved in sphingolipid metabolism, *hyl-1* and *hyl-2* (homologs of yeast longevity genes), were checked, as shown in **Figure 45** (**C**, **D**). The *hyl-1* and *hyl-2* mRNA levels were significantly increased in wild-type animals exposed to *rege-1* RNAi and *rege-1* mutants exposed to mock RNAi compared to controls. In contrast, *hyl-1* and *hyl-2* mRNA levels in *ets-4; rege-1* double mutants were similar to controls.

In summary, these results indicated that sphingolipid metabolism might be enhanced in *rege-1* mutants as evident by increased expression of *sptl-1*, *sptl-2*, *hyl-1* and *hyl-2* possibly through the REGE-1 – ETS-4 regulatory axis.

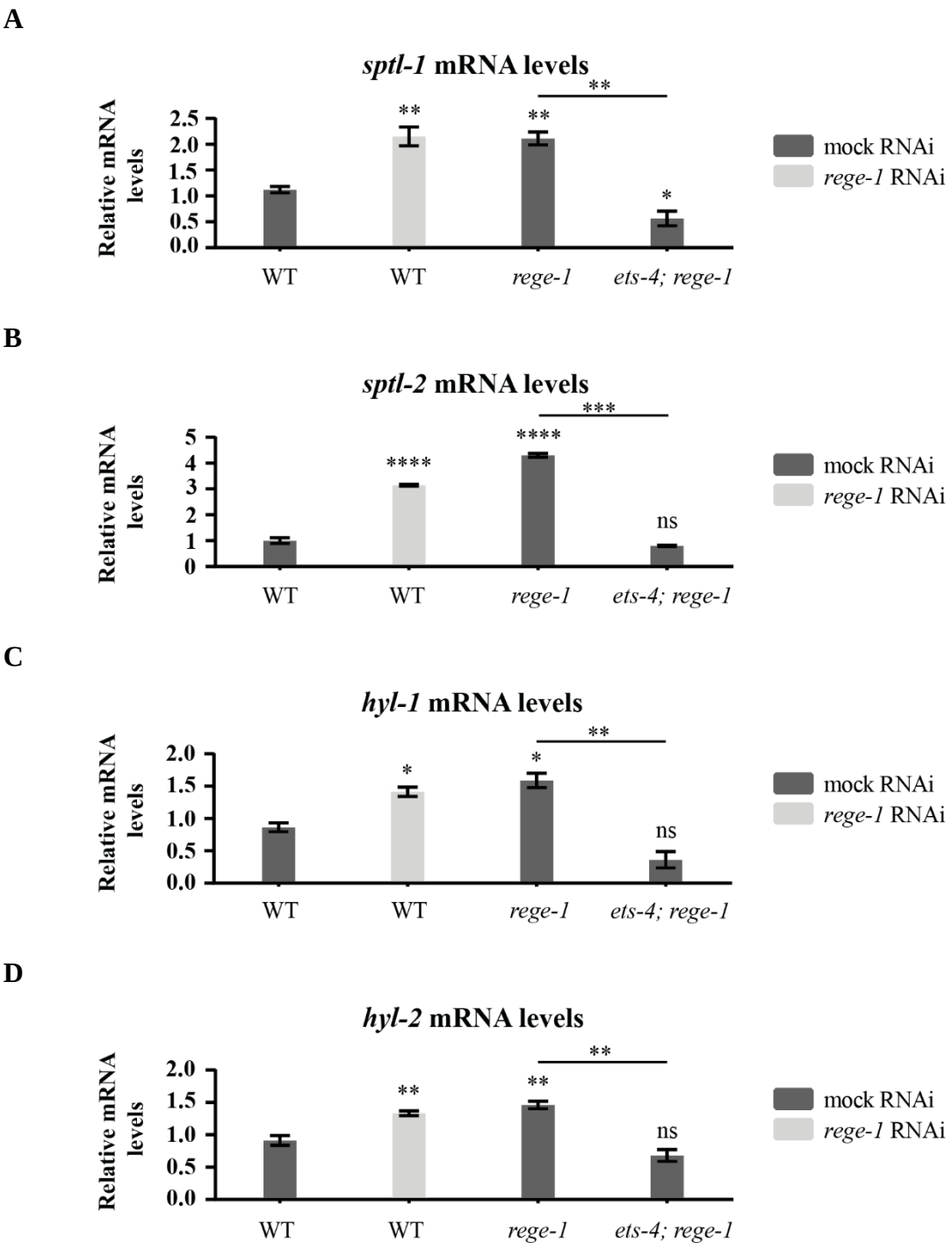

Figure 45. High *ets-4* mRNA levels increased in *sptl-1*, *sptl-2*, *hyl-1* and *hyl-2* mRNA levels in *rege-1* mutants. The levels of *sptl-1* (**A**), *sptl-2* (**B**), *hyl-1* (**C**) and *hyl-2* (**D**) mRNAs were measured by RT-qPCR in the wild-type and in animals carrying either *rege-1* or *ets-4; rege-1* mutations exposed to mock RNAi or dsRNA targeting *rege-1* mRNAs. The mRNA levels were normalized to the actin 1 mRNA levels and compared in relation to wild-type animals subjected to mock RNAi. The P values were calculated using un-paired Student t-test ($n = 3$). Data are presented as mean; error bars represent SEM (* indicates $p < 0.05$; ** $p < 0.01$; *** $p < 0.001$; **** $p < 0.0001$).

3.1.2.2. Inhibition of enzymes regulating sphingolipid metabolism rescued the fat loss phenotype of rege-1 mutants

Given that ETS-4 stimulates the expression of genes related to sphingolipid metabolism, it was checked whether genes such as *sptl-1* and *sptl-2* contribute to the fat loss phenotype in *rege-1* mutants by using ORO staining.

Depletion of *sptl-1* mRNA by RNAi significantly reduced the body fat content and the body size in the wild-type animals compared to controls, as presented in **Figure 46**. Silencing of *sptl-1* mRNA in *rege-1* mutants caused an increase in body size compared to wild-type animals exposed to *sptl-1* RNAi. Moreover, RNAi-mediated inhibition of *sptl-1* in the *rege-1* mutants increased the body fat levels compared to *rege-1* mutants exposed to mock RNAi.

The wild-type nematodes exposed to RNAi targeting mRNA of another enzyme regulating sphingolipid metabolism, *sptl-2*, were characterized by a similar lavel of body fat content compared to controls, as shown in **Figure 47**. In contrast, targeting *sptl-2* mRNA via RNAi in *rege-1* mutants, resulted in a significant increase in the body fat content compared to *rege-1* mutants subjected to mock RNAi. However, the recovery of body fat was partial compared to controls.

Wild-type animals exposed to RNAi targeting *sptl-1* and *sptl-2* mRNAs had similar body fat levels as their counterparts exposed to mock RNAi, as shown in **Figure 48**. Simultaneous silencing of *sptl-1* and *sptl-2* in *rege-1* mutants resulted in a significant increase in fat accumulation compared to *rege-1* mutants subjected to mock RNAi. Blocking the pathway of sphingolipid metabolism allowed for complete fat recovery in *rege-1* mutants to the level comparable to controls.

In summary, increased *sptl-1* and *sptl-2* mRNA levels could lead to accumulation of sphingolipids and thus be partially responsible for the fat loss phenotype in *rege-1* mutants. Since silencing of *sptl-1* mRNA in *rege-1* mutants led to a significant increase in body size and fat content compared to wild-type animals exposed to corresponding RNAi, sphingolipids may potentially regulate fat metabolism via the REGE-1 - ETS-4 regulatory axis. Since silencing of *sptl-1* or *sptl-2* by RNAi allowed for partial fat recovery in *rege-1* mutants, while their simultaneous silencing led to a complete fat recovery compared to

control, sphingolipids may potentially regulate fat metabolism via the REGE -1 - ETS-4 regulatory axis.

A

B

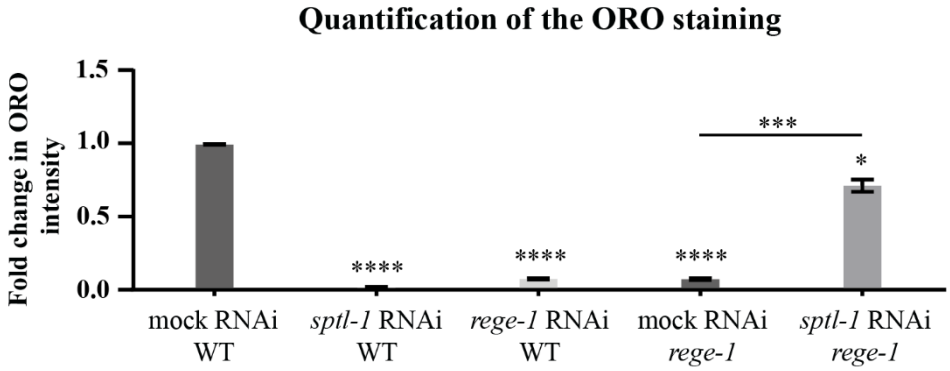

Figure 46. Inhibition of *sptl-1* largely rescued the fat loss phenotype of *rege-1* mutants. (**A**) Images of wild-type and animals carrying *rege-1* mutation exposed to mock RNAi or dsRNA targeting either *rege-1* or *sptl-1* mRNAs. The animals were stained with the ORO to visualize body fat levels. Scale bar: 100 µm. (**B**) Quantification of relative changes in the ORO staining. 30 animals per condition were measured. Changes in body fat levels were determined in relation to wild-type animals subjected to mock RNAi. The P values were calculated using un-paired Student t-test (*n = 3*). Data are presented as mean; error bars represent SEM (* indicates $p < 0.05$; *** $p < 0.001$; **** $p < 0.0001$).

A

mock RNAi in WT | *sptl-2* RNAi in WT | *rege-1* RNAi in WT | mock RNAi in *rege-1* | *sptl-2* RNAi in *rege-1*

B

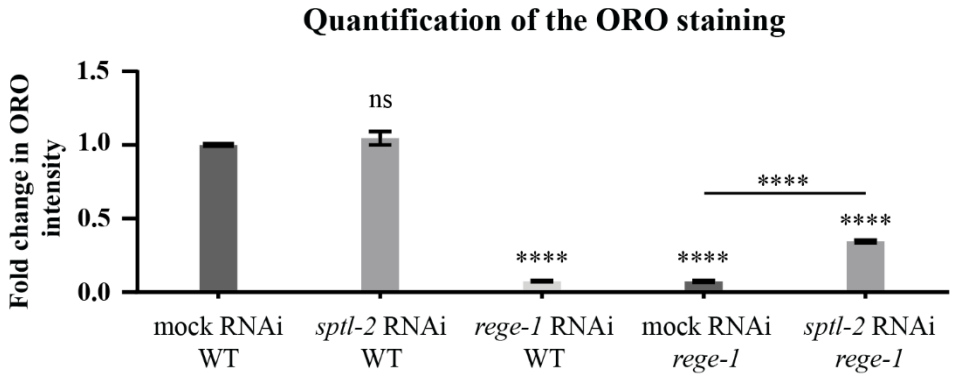

Figure 47. Inhibition of *sptl-2* partially rescued the fat loss phenotype of *rege-1* mutants. (**A**) Images of wild-type and animals carrying *rege-1* mutations exposed to mock RNAi or dsRNA targeting either *rege-1* or *sptl-2* mRNAs. The animals were stained with the ORO to visualize body fat levels. Scale bar: 100 μm. (**B**) Quantification of relative changes in the ORO staining. 30 animals per condition were measured. Changes in body fat levels were determined in relation to wild-type animals subjected to mock RNAi. The P values were calculated using un-paired Student t-test (*n = 3*). Data are presented as mean; error bars represent SEM (**** indicates $p < 0.0001$).

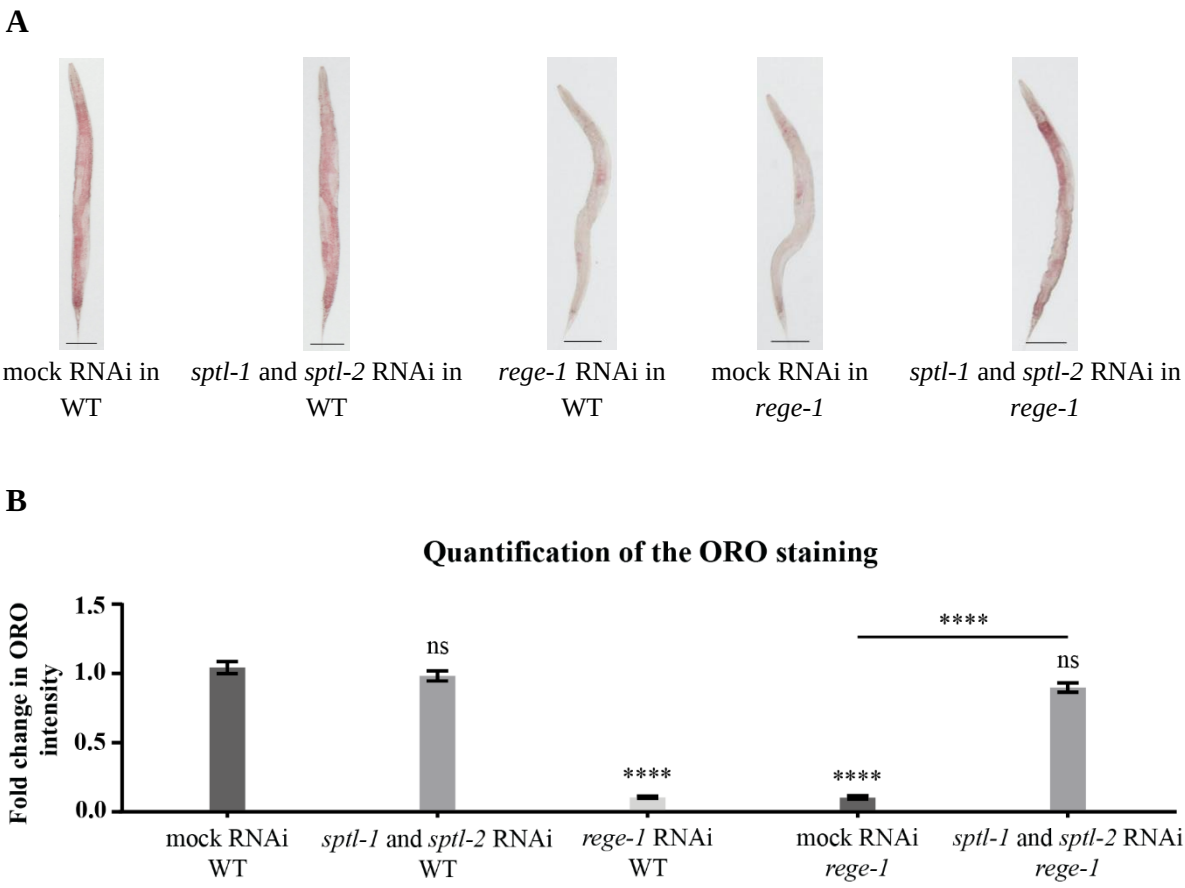

Figure 48. Simultaneous inhibition of *sptl-1* and *sptl-2* mRNAs by RNAi completely rescued the fat loss phenotype of *rege-1* mutants. (**A**) Images of wild-type and animals carrying *rege-1* mutations exposed to mock RNAi or dsRNA targeting either *rege-1* or *sptl-1 / sptl-2* mRNAs. The animals were stained with the ORO to visualize body fat levels. Scale bar: 100 μm. (**B**) Quantification of relative changes in the ORO staining. 30 animals per condition were measured. Changes in body fat levels were determined in relation to wild-type animals subjected to mock RNAi. The P values were calculated using un-paired Student t-test (*n = 3*). Data are presented as mean; error bars represent SEM (**** indicates $p < 0.0001$).

3.2. The effect of *rege-1* depletion on energy metabolism

Reduced body fat levels in the *rege-1* mutants might result from an increased β-oxidation which requires a high energy input and contributes to an increase in ROS production as byproducts (Yu et al., 2019). This chapter examines whether decreased fat accumulation in the *rege-1* mutants was a consequence of changes in energy metabolism.

3.2.1. The oxygen consumption rate was reduced upon depletion of *rege-1*

The energy needed for life is mainly obtained through mitochondrial oxidative phosphorylation, which takes place on the mitochondrial membrane. Therefore, changes in the energy metabolism of the cell may be associated with disturbances in cellular respiration (Wilson, 2017). Oxygen consumption rate (OCR) reflects mitochondrial function as well as metabolic activity of the cell under normal and stressful conditions with high ROS production (Palikaras et al., 2015). The change in OCR may indicate a switch from oxidative phosphorylation to aerobic glycolysis (Luz et al., 2016). Thus, it was checked whether inhibition of *rege-1* influenced mitochondrial function by changing OCR, as presented in **Figure 49**. As a positive control for the mitochondrial dysfunction, wild-type animals exposed to mock RNAi were used, which were fasted for 4 hours directly before the experiment.

OCR were significantly lower in both wild-type animals exposed to *rege-1* RNAi and *rege-1* mutants exposed to mock RNAi compared to controls. Moreover, no differences in OCR were observed between the wild-type animals subjected to *rege-1* RNAi and wild-type animals subjected to mock RNAi and deprived of food for 4h (stress control). These results showed that OCR was significantly reduced in animals with depleted *rege-1*.

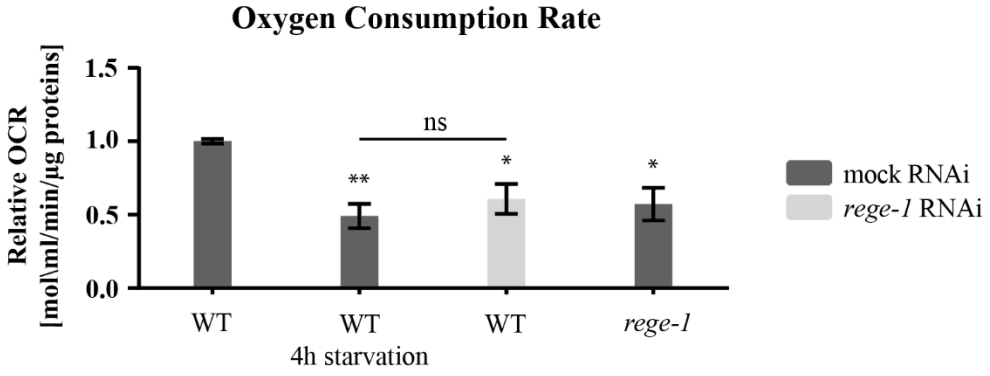

Figure 49. Depletion of *rege-1* contributed to reduction in OCR. Quantification of relative changes in the OCR in the wild-type and the *rege-1* mutants exposed to mock RNAi or dsRNA targeting *rege-1* mRNA. Wild-type animals subjected to mock RNAi and starved for 4h were used as a control for reduced OCR. Changes in OCR relative to the total protein content were measured in relation to wild-type animals exposed to mock RNAi. The P values were calculated using un-paired Student t-test ($n = 3$). Data are presented as mean; error bars represent SEM (* indicates $p < 0.05$; ** $p < 0.01$).

3.2.2. Sorbitol dehydrogenase transcription was increased in *rege-1* mutants

Due to reduction in the OCR and the body fat content in animals with depleted *rege-1*, it was indirectly checked whether the energy utilized for functioning came from carbohydrate metabolism. An inverse relationship between the body fat loss and an increase in the glycogen levels in the intestine, hypodermis and muscle under hypoxic conditions in the wild-type animals was previously demonstrated (Zecić et al., 2019; Heimbucher et al., 2020). Sorbitol dehydrogenase-1 (*sodh-1*) transforms sorbitol into fructose which then undergoes further conversions to glycogen (El-Kabbani et al., 2004). Therefore, it was checked whether the expression of the *sodh-1* was changed in *rege-1* mutants, as shown in **Figure 50**.

RT-qPCR analysis showed that *sodh-1* mRNA levels were significantly increased in both wild-type animals exposed to *rege-1* RNAi and *rege-1* mutants exposed to mock RNAi compared to controls. In contrast, in double mutants *ets-4; rege-1* exposed to mock RNAi *sodh-1* mRNA levels dropped significantly compared to *rege-1* mutants exposed to mock RNAi. These results suggested that high *ets-4* mRNA levels in *rege-1* mutants might have contributed to an increase *sodh-1* mRNA levels.

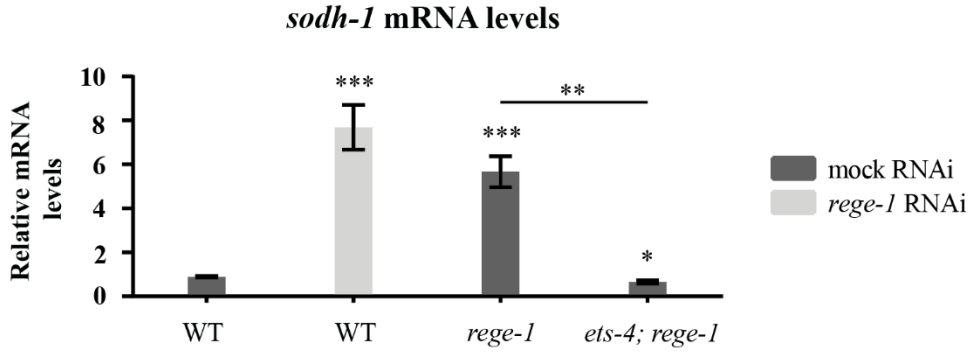

Figure 50. High *ets-4* mRNA levels contributed to increasd expression of *sodh-1* upon *rege-1* depletion. The levels of *sodh-1* mRNA were measured by RT-qPCR in the wild-type and animals carrying either *rege-1* or *ets-4; rege-1* mutations exposed to mock RNAi or dsRNA targeting the *rege-1* mRNAs. The mRNA levels were normalized to the actin 1 mRNA levels and compared to the wild-type animals subjected to mock RNAi. The P values were calculated using un-paired Student t-test ($n = 3$). Data are presented as mean; error bars represent SEM (* indicates $p < 0.05$; ** $p < 0.01$; *** $p < 0.001$).

DISCUSSION

1. The role of REGE-1 - ETS-4 axis in fat accumulation

1.1. *C. elegans* REGE-1 is as ortholog of human Regnase-1

Obesity is a serious medical problem associated with numerous comorbidities and reduced quality of life. Given the complexity of human fat metabolism regulation, biomedical research using a simple model organism such as *C. elegans* might lead to the identification of new molecules and signaling pathways that could also function in humans. The discovery of an endoribonuclease REGE-1 in *C. elegans*, which is an ortholog of human Regnase-1, and its role in the regulation of the body fat content, gives opportunities to unravel the novel function of Regnase-1. Previous findings on the regulation of the body fat via Regnase-1 in mammals have not been conclusive (Younce and Kolattukudy, 2012; Younce et al., 2009; Losko et al., 2020), therefore uncovering the pathway regulating fat accumulation in nematodes through REGE-1 may help in understanding the metabolic function of Regnase-1.

To confirm the similarity of *C. elegans* REGE-1 to human Regnase-1, their amino acid sequences were compared as well as the prediction of their protein structures was performed, as shown in **Figure 9**. This analysis showed 35.5% sequence similarity between REGE-1 and Regnase-1. Both REGE-1 and Regnase-1, as ribonucleases, contain NYN domains (Nedd4-binding protein 1), with catalytic center rich in four aspartic acids, which enabled them to function as RNAses (Anantharaman and Aravind, 2006). The first three aspartic acids are responsible for the chelation of magnesium ions, leading to the nucleophilic attack of water on the phosphodiester bond of the target mRNA, while the fourth aspartic acid, in addition to chelating magnesium ions, is also responsible for catalyzing the reaction through the interaction of magnesium ions with water (Anantharaman and Aravind, 2006). Substitution of these amino acids in Regnase-1 led to the loss of the catalytic activity of RNAse in HEK293 cell line (Matsushita et al., 2009). The second very important domain for endoribonucleases, which is present in both REGE-1

and Regnase-1, is the CCCH-type zinc finger (ZF) domain, with a **C**$_1$X$_5$**C**$_2$X$_5$**C**$_3$X$_3$**H** motif, containing three cysteines and a histidine, responsible for target binding and the efficiency of RNA cleavage (Yokogawa et al., 2016). Comparative analysis of the amino acid sequence between *C. elegans* and humans revealed a sequence difference in the ZF domain. *C. elegans* had **C**PYARK**C**TYGNK**C**KFY**H**, whereas *H. sapiens* had **C**PYGRK**C**TYGIK**C**RFF**H** sequence, respectively. These differences in the ZF domain suggest its divergent evolution from a common ancestor (Garg et al., 2021). Studies performed on human embryonic kidney (HEK293T) cells regarding the effect of *C. elegans* REGE-1 on the mammalian Regnase-1 mRNA targets, as well as the effect of human Regnase-1 on *C. elegans* REGE-1 mRNA targets showed that both, REGE-1 and Regnase-1 were capable of cleavage and degradation of the same mRNAs (Sobańska et al., 2021).

Due to the similarities in the amino acid sequence and the protein structure of REGE-1 and Regnase-1, as well as recent reports indicating that REGE-1 and Regnase-1 regulate the same mRNA targets, one might presume that these RNAses perform similar functions. Thus, research on *C. elegans* REGE-1 could be used to improve understanding of Regnase-1 function in humans.

1.2. Depletion of *ets-4* rescued the pale phenotype of *rege-1* mutants

Previous studies demonstrated that the major target mRNA degraded by REGE-1 in *C. elegans* was the transcription factor *ets-4* localized in the intestine and responsible for the regulation of expression of genes involved in lipid catabolism, immunity and longevity (Habacher et al., 2017; Thyagarajan et al., 2010). In humans, the orthologue of ETS-4, SAM-pointed domain-containing ETS transcription factor (SPDEF) was located in epithelial cells of the gastrointestinal tract, salivary and mammary glands, endometrial and ovarian epithelia, prostate, trachea and lungs (Korfhagen et al., 2012; Horst et al., 2010), while in mice it was present in epithelial cells in the stomach, caecum, small intestine, colon, coagulating gland, oviduct, prostate, seminal vesicles, trachea, bronchi and lungs (Park et al., 2007). Thus, SPDEF was expressed in tissues that required special protection against pathogens or where an appropriate microbiome had to be maintained.

The SPDEF regulated the expression of genes associated with the differentiation of goblet cells that secrete mucus like anterior gradient 2 (*Agr2*), forkhead box A3 (*Foxa3*) and glucosaminyl (N-acetyl) transferase 3 (*Gcnt3*) (Horst et al., 2010; Korfhagen et al., 2012; Chen et al., 2009). Mucus in the lungs serves as the initial barrier to protect the body from various inhaled toxins, allergens and bacterial colonization. Overexpression of SPDEF observed in humans with cystic fibrosis, chronic obstructive pulmonary disease or asthma increased the number of mucus-secreting cells as well as the amount of mucus in the lungs leading to airway obstruction and increased susceptibility to viral and bacterial infections (Korfhagen et al., 2012). On the other hand, SPDEF deficiency in mammals led to colitis (Ray, 2021), but also to breast, ovarian and prostate cancer (Horst et al., 2010; Moussa et al., 2009). However, so far there are no reports of a direct effect of SPDEF on the regulation of the body fat content in mammals.

Knowing that ETS-4 affects the expression of genes stimulating lipid catabolism in *C. elegans* (Habacher et al., 2016), this thesis attempted to find potential pathways modulating fat accumulation through the REGE-1 - ETS-4 module. Results from RT-qPCR analysis, presented in **Figure 10**, showed that both, animals with targeted *rege-1* mRNA and single *rege-1* mutants fed with mock RNAi were characterized by an increase in *ets-4* mRNA levels relative to colntrols. In contrast, *ets-4* mRNA was significantly lower in *ets-4; rege-1* double mutants confirming the dependence of the level of *ets-4* mRNA on the presence of REGE-1 ribonuclease.

Further analyses showed that increased *ets-4* mRNA levels significantly reduced total body fat content as well as TAG levels in both the *rege-1* mutants and in the *rege-1* silenced animals, as presented in **Figure 11**. Research designed to determine whether decrease in *ets-4* gene expression can prevent fat loss in *rege-1* mutants, showed that heterozygotes *ets-4(+/-); rege-1(-/-)*, with one *ets-4* allele, did not affect *ets-4* mRNA levels, however was sufficient for partial regain of fat (**Figure 13**). Due to the fact that the offspring in the F1 generation were unsynchronized and a large part of them were males, 100 heterozygotes at a similar stage were selected manually for the analysis. This study should be carried out on a much larger number of animals, which could give much more accurate measurements and reduce variations in the results. Gene expression can be modulated at many stages, not only at the level of transcription, but is also controlled by

translation efficiency and protein activity through posttranslational modifications. In further studies, it is worth checking whether the level of ETS-4 protein changes in heterozygotes, because it is possible that a slight reduction in the ETS-4 level results in increased fat accumulation. The reduction of total body fat content as well as TAGs in *rege-1* mutants may result from enhanced expression of *lipl-1* and *lipl-2* lipases, as shown in **Figure 14**, which are responsible for TAGs breakdown to free fatty acid (FFA) and glycerol. In *C. elegans*, the expression of lipases such as *lipl-1* and *lipl-2* varied according to nutritional status and was activated by DR (O'Rourke and Ruvkun, 2013). Since the regulation of *ets-4* mRNA by REGE-1 depends on the environmental conditions, including food availability, it is also possible that ETS-4 regulates fat accumulation by modulating the expression of lipolytic genes. Unpublished data from *C. Habacher's* thesis showed that ETS-4 did not affect feeding behavior, as shown by measuring pharyngeal pumping rate in *rege-1* mutants (unpublished data from Habacher, 2018). Therefore, a different mechanism regulating the body fat content through ETS-4 was sought.

In summary, increased expression of *ets-4* mRNA leads to activation of the expression of lipases, which stimulate catabolism and reduce the overall body fat content in *rege-1* mutants. In further research, RT-qPCR analysis might be used to determine whether the expression of lipases was stimulated by ETS-4 in response to the increased energy requirements during the molting period (Cyr et al., 2008; Li et al., 2022). FAs influence the cuticle formation, thus the body fat loss via changing the lipid composition can cause a molting defect (Antebi, 2015). During molting the old cuticle is renewed, which allows the nematode to enter the next developmental stage (Turek and Bringmann, 2014). If ETS-4 was temporarily active in the molting process to provide energy from the breakdown of fat, its continued activity could lead to a lean phenotype in the *rege-1* mutants. Moreover, in addition to having a reduced body fat content, the *rege-1* mutants have smaller size and are developmentally delayed, which may indicate a disturbed molting process (Mullaney et al., 2010).

Further analyzes should be performed to investigate whether heterozygotes *ets-4 (+/-); rege-1(-/-),* despite the high level of *ets-4* mRNA, regain body fat content by changing the amount or transcriptional activity of the ETS-4 protein, e.g. by tagging ETS-4 with GFP and observing its subcellular location. In addition to the regulation of gene

transcription, ETS-4 can affect protein-protein interactions with other transcription factors (Gamsjaeger et al., 2007). Therefore, through protein interaction assays (Shimokawa, 2005) it could be checked whether ETS-4 in combination with another transcription factor, such as SKN-1, regulated transcription in the *rege-1* mutants.

2. MRP-1 regulated fat content possibly in parallel to REGE-1 – ETS-4 pathway

Previous research through forward genetic screening has identified *mrp-1* as potential target for the REGE-1 - ETS-4 regulatory axis, which mutation can increase fat content in *rege-1* mutants, as shown in **Table 1**. However, the analysis conducted in this thesis showed that MRP-1 may work in parallel to the REGE-1 - ETS-4 regulatory axis. The ORO study showed that MRP-1 modulates fat accumulation also in wild-type animals (**Figure 19** and **Figure 20**). RT-qPCR analysis showed that the expression of *mrp-1* was independent of ETS-4 (**Figure 21**), and moreover RNA-Seq data did not identify *mrp-1* as a potential target for ETS-4 (**Table 2**).

2.1. MRP-1 is a transporter conserved between nematodes and mammals

ATP-binding cassette (ABC) transporters are the largest transport superfamily present in both prokaryotes and eukaryotes (Dean, 1995). Through binding of ATP, ABC transporters obtain the energy needed to transport various molecules through the plasma membrane (Thiebaut et al., 1987) or the intracellular membranes of organelles such as ER, mitochondria and peroxisomes, as shown in **Figure 16 A** (Dean, 1995). ABC transporters transfer various substrates important for animal physiology like organic anions, including oxidized and reduced glutathione (GSSG and GSH), as well as anionic conjugates of GSH, glucuronide and sulfate, which protect cells from toxins, oxidative stress, regulate hormone secretion and inflammation (Loe et al., 1996a; Loe et al., 1996b; Leier et al., 1996; Jedlitschky et al., 1996, Lucia et al., 2005). Some ABC transporters like ABCA and ABCG carry lipids such as cholesterol, phospholipids (PL) and other sterols, which can be further transported to the bile or to the cellular membrane and regulate its

composition (Aye et al., 2009; Van Helvoort et al., 1996). In mammals, MRP1 is one of the best known ABC transporters in the subfamily C1 (ABCC1). MRP1 is capable of transporting various chemotherapeutic drugs like Vincristine, Vinblastine or Methotrexate, and is referred to as multidrug resistance (MDR) (Massey et al., 2013). Its ability to transport drugs causes "pharmacologic" resistance to chemotherapy in human cancer patients, as confirmed by research conducted on leukemia (Flens et al., 1994), lung (Flens et al., 1994; Cole et al., 1992), breast (Morrow et al., 1998), neuroblastoma (Manohar et al., 2004) and prostate (Zalcberg et al., 2000) tumor cell lines, that could result from higher expression of the MRP1 transporters and decreased drug absorption (Massey et al., 2013). Moreover, MRP1 was found to regulate inflammation through transport of lipid mediators such as leukotriene C4 (LTC4), a potent chemotactic factor controlling dendritic cell migration from peripheral tissues to lymph nodes (Robbiani et al., 2000) and sphingolipids like S1P (Mitra et al., 2006). The potential involvement of ABCC1 transporter in the regulation of fat metabolism has also been demonstrated. *Abcc1* mRNA and protein levels were significantly reduced in the livers of diet-induced obese mice compared to lean mice (More and Slitt, 2011). On the other hand, another group showed that ABCC1 was expressed in human AT and was responsible for the export of corticosterone, and its expression was up-regulated in obese individuals (Nixon et al., 2016). Therefore, *C. elegans* might be used as a simple model organism to investigate molecular mechanism/s through which MRP1 might influence fat metabolism.

The *C. elegans* MRP-1 is an ortholog of human MRP1, which shows 66% genomic sequence similarity and 47% identical protein sequence (Broeks et al., 1996). The spatial structures of MRP1 and MRP-1 proteins are very similar, because they are both homodimers and have MSD0 - MSD1 - NBD1 - MSD2 - NBD2 domain structure, as shown in the **Figure 16** (**B**, **C**) (Yang et al., 2010; Sheps et al., 2004). In *C. elegans*, MRP-1 is involved in transport of vitamin B_{12}, which is an essential nutrient that functions as a cofactor (McDonald et al., 2017), but also MRP-1 allows animals to survive in environments rich in heavy metals like cadmium and arsenite (Broeks et al., 1996). However, the function of MRP-1 in the regulation of nematode's fat metabolism has not been demonstrated yet.

2.2. MRP-1 is localized in the membranes of various types of cells

Examination of the localization of endogenous MRP-1 in *C. elegans* using MRP-1 tagged with mCherry on the COOH terminus, showed the presence of MRP-1 in epithelial cells of the pharynx and vulva, but also in spermathecae, rectum in stomatointestinal and anal depressor muscles, as shown in **Figure 17**. Other studies on *C. elegans*, where MRP-1 was tagged with GFP, showed its localization in the intestine, pharynx, vulva and neurons (Zhao et al., 2004; Yabe et al., 2005; Broeks et al., 1996). Studies conducted on the human HEK293 cell line, where MRP1 was fused at the COOH terminus with cyan fluorescent protein (CFP), showed its location on the plasma membrane and in the post-Golgi compartment (Westlake et al., 2005), whereas immunostaining of MRP1 showed a basolateral localization in the rabbit conjunctival epithelial cells (Yang et al., 2007). Due to the fact that ABC transporters transport a variety of compounds that help to maintain organism homeostasis, they are present on the membranes of various types of cells. However, their highest abundance can be seen on the surface of cancer cells. By pumping drugs out of the cell, ABC transporters protect cell from harmful substances, often preventing effective chemotherapy (Depeille et al., 2005).

2.3. Loss-of-function mutations in the conserved domains of MRP-1 increased fat accumulation in *rege-1* mutants

MRP1 is built of two MSDs domains each with six TM α-helices that form the TM channel, which are characteristic for ABC transporters (Iram and Cole, 2011), as shown in **Figure 16 A.** Additional MSD domain (MSD0), with five TM α-helices is probably necessary for MRP1 retention or recycling to the plasma membrane (Iram and Cole, 2011; Westlake et al., 2005). In addition to MSDs, the MRP1 transporter has two nucleotide-binding domains (NBD), which contains two short ATP binding motifs like Walker A and Walker B motif (Zhao et al., 2004; Hyde et al., 1990) and a unique C motif, which is also known as signature motif, because it can be found in all ABC subunits, but usually not in other ATPases (Nikaido, 2002; Schneider, 1998). Walker A motif (**G** – X – X – **G** – X – **G** – **K** – **S**) is built with glycine-rich loop and uncapped K-helix and is responsible for the orienting the triphosphate chain of MgATP to a proper conformation

required for catalysis (Schneider et al., 1994; Jones and George, 1999). Walker B motif (h – h – h – h – **D**) has many hydrophobic residues (h) and aspartate that is involved in the coordination of the catalytic Mg^{2+} ion (Walker et al., 1982; Jones and George, 1999). C motif (**L** – **S** – X – **G** – **Q** – X – **Q** – X) is rich in glutamine and glycine residues and is involved in energy transfer from ATP hydrolysis to conformational changes in the MSD required for translocation of the substrate (Ames and Lecar, 1992; Hyde et al., 1990). The two NBDs of human MRP1 differs in their functions, because NBD1 is responsible for ATP binding, while NBD2 is responsible for ATP hydrolysis and ADP binding (Gao et al., 2000).

The results from EMS mutagenesis, presented in **Table 1** and **Figure 18 A**, showed that presence of point mutations in each of the conserved domains of the *mrp-1* gene influenced the fat content of the *rege-1* mutants. This suggests that all these mutations affected the function of MPR-1. Mutations located in MSDs may affect the efficiency of substrate transport, whereas mutations within NBDs, shown in **Figure 18** (**B**, **C**), may prevent ATP hydrolysis, making the protein inactive due to lack of energy for substrate transport. A752T point mutation was located in a conserved ATPase domain motif in NBD1, G1293R point mutation was present in a conserved ATPase domain motif in NBD2, whereas D1456N point mutation was placed in a conserved Walker B motif in NBD2. Mutational analyzes of ABC transporters have shown that the substitutions within the Walker A and Walker B motifs, in particular substitutions in conserved lysine and aspartate, that are responsible for ATP hydrolysis, cause inhibition of substrate transport (Urbatsch et al., 1998, Jones and George, 1999). Two NBDs cannot function independently as catalytic sites, because their cooperative interaction is required for ATP hydrolysis. Therefore, mutations in the NBDs domains result in the loss of the transport activity.

An unbiased genetic screening found mutations within the *mrp-1* gene which increased fat content in *rege-1* mutants (**Table 1**). Thus, here a new function of MRP-1 in the regulation of fat accumulation evidenced by measurement of total fat content by ORO staining and TAG levels (**Figure 19**), was discovered. In addition, *mrp-1; rege-1* double mutants expressing DHS-3::GFP had a partial recovery of mean LDs size compared to controls, as shown in **Figure 20**. However, the RT-qPCR analysis (**Figure 21**) showed that *mrp-1* mRNA levels increased in both wild-type animals exposed to *rege-1* RNAi

and *rege-1* mutants exposed to mock RNAi, as well as in *ets-4; rege-1* double mutants in comparison to controls. Moreover, RNA-Seq data did not identify *mrp-1* as a potential target for ETS-4 (**Table 2**). Therefore these results suggest that MRP-1 may work parallely to the REGE-1 - ETS-4 regulatory axis. However, in order to confirm whether MRP-1 regulates fat metabolism independently of ETS-4 additional analyzes using *rege-1* and *ets-4; rege-1* double mutants should be performed, e.g. analysis of the MRP-1 activity using the EFLUXX-ID Green Multidrug Resistance Assay Kit (Prasad et al., 2021) and the measurement of the MRP-1 protein level e.g. using fluorescently tagged MRP-1, MRP-1::GFP, via western blot analysis. Taking into account reports that sphingolipids transported by MRP1 might regulate lipid metabolism, the role of sphingolipids in regulating body fat content in *rege-1* mutants was analyzed (**Figure 23**).

2.4. ABC transporters are involved in transport of bioactive signaling molecules

One of the substrates transported by MRP1 in humans is sphingosine 1-phosphate (S1P), a sphingolipid which is derived from the transformation of d17iso-sphingosine by sphingosine kinases (SphKs), as shown in **Figure 22** (Cartwright et al., 2013). S1P is a bioactive signaling molecule that, in mammals, activates signaling pathways responsible for growth, cell survival, angiogenesis and transport of immune cells (Kwong et al., 2017). Moreover, sphingolipids regulate cellular processes such as proliferation, differentiation, migration and lipid metabolism (Kwong et al., 2017). In addition, sphingolipids are known for their impact on the development of multiple human diseases such as atherosclerosis, osteoporosis, pulmonary arterial hypertension, diabetes and nonalcoholic fatty liver disease (NAFLD) (Maceyka et al., 2012). Furthermore, S1P through the regulation of cancer-fibroblast microenvironment niche can influence the development of cancer metastasis in melanoma, breast, prostate and lung cancer (Pyne et al., 2018). In *C. elegans* S1P was associated with immune response to bacterial pathogens, while mutations in the *sphk-1* gene decreased nematode survival after infection, reduced lifespan, increased susceptibility to oxidative stress and caused a reduction in body size and brood size (Lee et al., 2020; Chan et al., 2017).

Due to the fact that sphingolipids are active biomolecules, which activate various metabolic pathways, it was checked whether MRP-1 via sphingolipids influences fat accumulation in the *rege-1* mutants, as shown in **Figure 23**. The study showed that ETS-4 significantly increased *sphk-1* mRNA levels in *rege-1* mutants and in animals with targeted *rege-1* mRNA by RNAi, resulting in the body fat loss compared to controls as evidenced by the ORO staining. However, silencing of *sphk-1* mRNA slightly increased body fat content in *rege-1* mutants compared to *rege-1* mutants exposed to mock RNAi.

The role of sphingolipids in the regulation of glucose and lipid metabolism in mammals may be different depending on the type of tissue. In the liver of diabetic mice, SphK stimulated IIS and glucose uptake and reduced TAG, cholesterol and low-density lipoproteins levels (LDL) (Ma et al., 2007). Moreover, mice overexpressing SphK1 in the liver had decreased levels of TAG when fed with a low fat diet (LFD), while mice fed with high fat diet (HFD) did not have altered TAG levels (Kowalski et al., 2015). In addition, studies conducted in *SphK1* knock-out mice fed with HFD showed an increase in plasma cholesterol and TAG levels (Qi et al., 2013). Moreover, studies on the effect of SphK1 in AT showed its rise in ob / ob mice compared to the wild-type mice (Hashimoto et al., 2009), as well as in HFD-fed mice compared to LFD-fed animals (Wang et al., 2014). Furthermore, obese patients showed an increase in S1P levels in AT compared to lean people (Blachnio-Zabielska et al., 2012). The differences in the regulation of the body fat levels by sphingolipids may be explained by the fact that S1P is a ligand, which when transported to the intercellular space can bind to various receptors and perform an autocrine as well as a paracrine function in different tissue (Maceyka et al., 2012).

Results presented in this thesis showed a significant influence of sphingolipids and the MRP-1 transporter on the regulation of fat accumulation in nematodes. Although both MRP-1 and SPHK-1 seem to have contributed to the reduction of fat accumulation in *rege-1* mutants, silencing of their mRNAs allowed for the recovery of the fat content to a small extent. Thus, and the fact that they modulate fat accumulation in wild-type animals indicate that they might function in parallel to the REGE-1 - ETS-4 regulatory axis. However, it would be very interesting to check whether SPHK-1 in *rege-1* mutants, like in mammals, could stimulate IIS pathway, for example by checking the expression of genes from the IIS pathway such as *daf-2*, *age-1*, *akt-1*, *akt-2*, *sgk-1*. Due to the fact that

sphk-1 mRNA level was increased in the *rege-1* mutants, as presented in the **Figure 23 A**, and SphK could stimulate glucose uptake in mice (Ma et al., 2007), it might be interesting to check whether the *rege-1* mutants had increased glucose uptake using 2-deoxy-D-glucose (2DG) containing 3H-2DG (Kitaoka et al., 2016). In addition, liquid chromatography-electrospray ionization-tandem mass spectrometry (LC - ESI - MS / MS) (Yamada et al., 2018) could be used to determine whether the transport of S1P via MRP-1 was increased in *rege-1* mutants.

3. PEPT-1 regulated fat content possibly in parallel to REGE-1 – ETS-4 pathway

Data analysis from RNA-Seq previously performed in the laboratory of Prof. Ciosk revealed that the PEPT-1 transporter is another potential factor enabling body fat regulation downstream of REGE-1 - ETS-4 regulatory axis, as shown in **Table 2**. Due to the fact that in forward genetic screening the selection of genes that increased the body fat content in the *rege-1* mutants was carried out by visual selection of animals with a dark appearance, which indicated greater amount of fat (**Table 1**), some genes potentially important for the regulation of fat accumulation through the REGE-1 - ETS-4 regulatory axis could have been omitted. For example, *pept-1* mutants had a clear appearance, which might have indicated low body fat content, however, the ORO and TAG analyzes carried out in this PhD thesis showed that they had 2.5 times more fat than the wild-type, while the TAG levels were very low (**Figure 30**). This proves that the dark appearance does not reflect the amount of body fat. Thus, it may be assumed that the *pept-1* gene could also be found via forward genetic screening, when a more accurate method to asses body fat levels, such as CARS analysis, would have been used. The following section describes the effect of PEPT-1 on the regulation of fat accumulation in *C. elegans* and a possible downstream signaling pathway.

3.1. PEPT-1 is a transporter conserved between nematodes and mammals

Nutrients provided with the food are needed to supply energy for the survival of all living organisms, therefore animals possess specialized membrane proteins responsible for

the transport of various substances (Daniel et al., 2006). Short amino acids can be transported from the intestinal lumen via transmembrane transporters in free or protein-bound form (Meissner et al., 2004). Human PEPT1 and PEPT2 are transmembrane transporters which, in addition to transporting di- and tripeptides from food, could transport peptide-mimicking drugs into the intestine (Brandsch, 2013; Ganapathy et al., 1995). *C. elegans* transporter PEPT-1 is an ortholog of human PEPT1, which via electrochemical proton gradient could also transport di- and tripeptides from the gut lumen to the intestine (Meissner et al., 2004; Ganapathy and Leibach, 1983), as shown in **Figure 24**. Moreover, PEPT-1 stimulated development and growth of nematodes, whereas its mutation caused delayed post-embryonic development and reduction in the amount of progeny and body size (Meissner et al., 2004).

To confirm the relatedness between *C. elegans* PEPT-1 and human PEPT1, an amino acid sequence comparison was performed, as shown in **Figure 25 A**. These results confirm the conservative amino acids sequence of this transporter, which was also shown by *Meissner et al., 2004* indicating 36.9% sequence similarity between them (Meissner et al., 2004). Moreover, the spatial visualization of PEPT1 and PEPT-1 showed high similarity between their structures, as shown in **Figure 25** (**B**, **C**). Both transporters are constructed of 12 MSD domains, which form two six-helix bundles and the ECD domain (Killer et al., 2021), while their amino and carboxyl ends are located in the cytosol (Daniel et al., 2006).

Moreover, the similarity between *C. elegans* PEPT-1 and human PEPT1 is demonstrated by anatomical location of these transporters. Visualization of PEPT-1 in *C. elegans* by tagging the endogenous protein with GFP on its COOH terminus, showed its presence in the intestinal apical membrane, as presented in **Figure 26**. Other research conducted on *C. elegans* revealed that PEPT-1 was located in intestinal epithelial cells, suggesting it played a role in absorption of peptides from the gut lumen (Meissner et al., 2004). Similar, studies on mammals have shown the presence of PEPT1 in the apical membrane of epithelial cells in the small intestine and kidney, while PEPT2 was present only in the epithelial cells in the kidney (Wolf et al., 2010; Ganapathy et al., 1995). Despite some similarities, further research is needed to determine whether remaining differences in the sequence and structure of these proteins significantly affect their function, which might be distinct in nematodes and mammals.

3.2. Depletion of *rege-1* increased *pept-1* mRNA level and peptide transport activity

The RNA-Seq results showed that wild-type animals with *rege-1* RNAi had elevated *pept-1* mRNA levels, (**Table 2**). The activity of the PEPT-1 transporter depends on the membrane potential and extracellular pH, which enables the transport of peptides together with protons and leads to an intracellular acidification (Ganapathy and Leibach, 1983; Spanier et al., 2009). Therefore, for its proper function PEPT-1 needs a second NHX-2 transporter, which is responsible for restoring intracellular pH by proton export into the intestinal lumen with simultaneous import of sodium ions (Spanier et al., 2009), as shown in **Figure 24**. Interestingly, RNA-Seq results indicated that wild-type animals exposed to *rege-1* RNAi also increased the expression of *nhx-2* (**Table 2**), which is a human NHE3 counterpart (Nehrke, 2003). In this thesis, the RT-qPCR analysis showed that high *ets-4* expression increased mRNA levels of *pept-1* and *nhx-2* transporters, in both wild-type animals exposed to *rege-1* RNAi and *rege-1* mutants exposed to mock RNAi, as shown in **Figure 27**.

Next, it was checked whether ETS-4 affected PEPT-1 protein levels or its transport activity, as shown in **Figure 28**. Western blot analysis showed no increase in PEPT-1 protein levels in animals expressing PEPT-1::GFP and subjected to *rege-1* RNAi in comparison to the same strain but exposed to mock RNAi. The measurements of PEPT-1 transport activity using a fluorescent dipeptide ß – Ala – Lys - AMCA showed an increase in both wild-type animals subjected to *rege-1* RNAi and *rege-1* mutants subjected to mock RNAi. The transport activity of peptides did not change in the wild-type animals or *rege-1* mutants in which the *pept-1* mRNA was targeted via RNAi. Large standard deviations in these experiments could have been caused by the presence of an intracellular pool of aminopeptidases, like LTA4H. LTA4H could hydrolyze intracellular di- and tripeptides (Benner et al., 2011), which could have an impact on stability of the fluorescent dipeptide and thus reduce the intensity of its intracellular signal.

Due to the fact that peptide transport was not changed in animals exposed to *pept-1* RNAi, it was checked whether depletion of *pept-1* mRNA influenced the expression of another peptide transporter, *pept-2*. RT-qPCR analysis presented in **Figure 29**, showed that silencing of *pept-1* mRNA enhanced the expression of *pept-2*. In addition to the fact that the

amino acid sequence of mammalian *PEPT1* is approximately 50% homologous to *PEPT2* (Shen et al., 2003), it has been shown that PEPT2 could also transport di- and tripeptides in rats (Alghamdi et al., 2017). Thus, in *C. elegans* PEPT-2 might play a compensatory role when PEPT-1 transporter is inactive, to maintain proper protein absorption.

According to data, the high levels of *ets-4* mRNA have contributed to an increase in *pept-1* mRNA levels, whereas *pept-1* mRNA silencing increased the expression of *pept-2*, and that both PEPT-1 and PEPT-2 can transport di- and tripeptides, it should be further investigated whether the lack of functional PEPT-1 enhanced PEPT-2 mediated peptide transport. It could be checked whether the PEPT-2 protein levels were changed in the *pept-1* mutants by western blot analysis. Moreover, it could be determined whether targeting *pept-2* mRNA by RNAi in *rege-1* mutants would affect the transport activity of PEPT-1. In addition, through the LC - MS / MS analysis (Spanier et al., 2018), amino acid profiles in *rege-1* mutants could be examined.

3.3. PEPT-1 affected the body fat content in *C. elegans*

The experiments presented above demonstrated a possible involvement of PEPT-1 transporter in the maintenance of intestinal homeostasis in *C. elegans*. Studies using human intestinal epithelial cell line, Caco-2, showed involvement of PEPT1 in fat metabolism, where both, the amount of PEPT1 and its transport activity were stimulated by leptin and insulin hormones (Thamotharan et al., 1999; Buyse et al., 2001; Hindlet el al., 2009). Moreover, studies on mammals demonstrated that Pept1 reduced postprandial blood glucose levels, whereas intake of peptides during high-protein diet treatment improved glycemic control in the upper small intestine (Dranse et al., 2018). On the other hand *Pept1* knock-out mice were characterized by a reduced fat content and disturbed intestinal homeostasis through shortened intestinal microvilli (Kolodziejczak et al., 2013; Zhang et al., 2016). At first, studies on *C. elegans* showed that *pept-1* mutants had a reduced fat content (Ashrafi et al., 2003; Nehrke, 2003). However, few years later other studies on *C. elegans* indicated that a mutation in the *pept-1* gene increased fat accumulation, possibly through enhanced transport of FFAs across the intestinal membrane by a flip-flop diffusion (Spanier et al., 2009; Benner et al., 2011; Brooks et al., 2009). Altogether, these findings

indicate that PEPT-1 might influence the body fat content by affecting intestinal homeostasis through enhanced nutrient absorption from bacterial food. However, the exact mechanism by which PEPT-1 could regulate fat accumulation remains unknown.

The *rege-1* mutants exposed to *pept-1* RNAi had increased fat accumulation, evidenced by the ORO staining presented in **Figure 30** (**A**, **B**), with a corresponding increased size of LDs, as shown in **Figure 30** (**D**, **E**). However, the relative TAG levels in the *rege-1* mutants subjected to *pept-1* RNAi remained unchanged compared to the *rege-1* mutants exposed to mock RNAi, as presented in **Figure 30 C**. Similarly, targeting the *pept-1* mRNA by RNAi in the wild-type animals significantly increased fat accumulation and LD size, while the relative TAG levels were lower in comparison to controls. Thus, RNAi-mediated *pept-1* mRNA silencing might increase the body fat content through accumulation of lipid species other than TAG. These results are surprising, since microscopic analysis indicate that *rege-1* mutants exposed to mock or *pept-1* RNAi as well as a wild-type animals subjected to *pept-1* RNAi were transparent, which could indicate that they had a low amount of fat compared to the wild-type, that has dark appearance and high levels of fat. The overall increase in the body fat levels observed by the ORO with reduced relative TAG content in wild-type animals or *rege-1* mutants exposed to *pept-1* RNAi might also be explained by the fact that the ORO is not a specific fat-soluble dye, while it stains all lipid types and other structures, such as lysosome-related organelles (Escorcia et al., 2018; Yen et al., 2010). The analysis of fat measurement using the ORO method should be supported by other methods such as CARS microscopy, which is sensitive to molecular vibration of CH_2 groups and thus enables visualization of lipid-rich organelles (Yen et al., 2010). However, a similar example of a mutant that is transparent, but contains fat is HP1 like heterochromatin protein 2 (*hpl-2*) mutant (Meister et al., 2011). Although the ORO staining showed no differences in fat accumulation compared to controls, *hpl-2* mutants were transparent, suggesting reduced body fat content (Meister et al., 2011). In these mutants quantitative lipid analysis showed changes in the composition of PL and sphingolipids which are the components of cellular membranes (Meister et al., 2011). Thus, further lipidomic analyzes should be performed to determine whether ETS-4, presumably via PEPT-1, affects the overall lipid composition and how it might influence the body fat levels and LDs size in *rege-1* mutants. Due to the fact that the *pept-1* mutants had increased body fat content

through enhanced transport of FFAs via the flip-flop mechanism (Spanier et al., 2009), it would be very interesting to check whether FFAs transport across the intestinal membrane was reduced in the *rege-1* mutants using the fluorescent dye C1- BODIPY 500 / 510 C12 (Sheng et al., 2015; Spanier et al., 2009; Benner et al., 2011; Brooks et al., 2009).

3.4. PEPT-1 might regulate the body fat levels in *rege-1* mutants by increasing the intracellular pool of amino acids

PEPT-1 might regulate fat accumulation in *C. elegans* via two potential mechanisms, either by altering the content of intracellular peptides or by changing the intracellular pH, as shown in **Figure 31**. The first mechanism assumes that di- and tripeptides, transported by PEPT-1, are hydrolyzed to individual peptides by the aminopeptidase LTAH-1.2, which then stimulates the function of TOR, one of the major pathways which might regulate fat metabolism by affecting transcription, protein translation and degradation (Benner et al., 2011; Meissner et al., 2004). In this thesis, it was demonstrated that *ltah-1.2* mRNA silencing in the *rege-1* mutants led to an increase in body fat levels compared to *rege-1* mutant exposed to mock RNAi, as shown in **Figure 32**. This indicated that the level of intracellular peptides might influence the body fat content in the *rege-1* mutants. Due to the fact, that TOR work as an intracellular amino acid sensor (Goberdhan et al., 2009), reduced pool of intracellular amino acids in *C. elegans pept-1* mutants inhibited TOR function, resulting in increased fat content (Meissner et al., 2004). Studies in human HepG2 cell lines treated with ethanol showed that supplementation with branched chain amino acids (BCAA) activated mTOR signaling, which led to improved fat oxidation and mitochondrial function, reduction of the body fat levels, as well as increased expression of genes related to anti-reactive oxygen species compared to untreated cells (Tedesco et al., 2018). In humans supplementation with leucine, which is one of the BCAAs activating the mTOR signaling pathway in mammals, inhibited food intake and fat mass gain and stimulated glucose metabolism and leptin secretion, thereby contributing to satiety (Li et al., 2011). In addition, unpublished data from *Johansen and Færgeman* thesis showed that glutamine, serine and asparagine levels were increased in *rege-1* mutants in comparison to the wild-type animals (unpublished data from Johansen and Færgeman, 2018).

Due to the fact that *pept-1* mRNA (**Figure 27**) and possibly the PEPT-1-mediated peptide transport were increased in the *rege-1* mutants (**Figure 28 C**), peptides and TOR signaling pathway might at least in part influenced the lean phenotype of the *rege-1* mutants. However, since the *rege-1* mutants exposed to *ltah-1.2* RNAi did not lead to a full recover fat content compared to controls, it is possible that the PEPT-1 - LTAH-1.2 - TOR pathway regulates the fat metabolism in parallel to the REGE-1 - ETS-4 regulatory axis. To verify this hypothesis, further analyzes should be performed. It could be checked whether the level of metabolites related to lipid oxidation and TOR signaling pathway were changed in the *rege-1* mutants subjected to mock, *pept-1* or *ltah-1.2* RNAi via gas chromatography / time-of-flight mass spectrometry (GC / TOF MS) (Yun et al., 2017).

3.5. PEPT-1 might regulate fat accumulation in *rege-1* mutants via changes in intracellular pH

Another possible pathway of PEPT-1-mediated regulation of the body fat content is its plausible effect on cell acidification in the intestine, as shown in **Figure 31** (Spanier et al., 2009; Pfeiffer et al., 2008). In *C. elegans* changes in the intestinal pH might regulate the calcium ions (Ca^{2+}) wave and rhythmic defecation behavior (Allman et al., 2009; White et al., 1991; Pfeiffer et al., 2008). Ca^{2+} ions, transported from the ER to the intestinal cytoplasm via the inositol 1,4,5-trisphosphate receptor (InsP3R receptor), control the dynamics of the posterior body muscle contraction and cause cyclic defecation every 45 - 50 seconds (Dal Santo et al., 1999). Ca^{2+} ions bind to PBO-1, which is an ortholog of human calcineurin homolog protein 1 (CHP1), and stimulate sodium-proton exchanger PBO-4 to secrete protons from the basolateral part of the intestine into the pseudocoelomic space (Benomar et al., 2020; Beg et al., 2008; Nehrke, 2014). Protons by binding to the muscle cell receptors PBO-5 and PBO-6, cause depolarization of the membrane, muscle contraction and consequently, defecation (Beg et al., 2008). The return of Ca^{2+} ions to the initial level by transport through the sarco(endo)plasmic reticulum calcium ATPase SCA-1 receptor (SERCA) to the ER and the equalization of the intestinal cytoplasm pH level by Na^{+} / H^{+} antiport through NHX-2, are essential steps in the re-transport of peptides and protons through the PEPT-1 transporter (Allman et al., 2009).

Targeting *pbo-1* and *pbo-4* mRNAs by RNAi in the *rege-1* mutants resulted in partial recovery of the body fat content, as shown in **Figure 33** and **Figure 34**. Considering that *pbo-1* and *pbo-4* belong to the defecation motor program (DMP) and that their action depend on the proton transport, these results indicated that changes in the intestinal pH could have a significant effect on the body fat reduction in *rege-1* mutants. However, there were no apparent changes in the relative TAG content in the *rege-1* mutants upon *pbo-1* or *pbo-4* RNAi, respectively. This might result from the accumulation of lipid species other than TAGs. Although reports from studies conducted on *C. elegans* indicate a significant effect of the pH changes in the cytoplasm of intestinal cells on the DMP (Pfeiffer et al., 2008) and the body fat content (Nehrke, 2003), molecular mechanisms leading to these phenotypic changes remain unknown. Silencing of *nhx-2* mRNA led to acidification of the intestinal cytoplasm, inhibition of dipeptide transport and reduction of body fat content in *C. elegans* (Nehrke, 2003). Moreover, the reduction of the activity of another proton transporter, VHA-6 (vacuolar H ATPase 6), led to impeded intracellular pH recovery after defecation, inhibition of dipeptide transport and reduction of fat levels (Allman et al., 2009). On the other hand, mutations in the InsP3R receptor reduced the level of cytoplasmic Ca^{2+} in the intestine and slowed down defecation, while its overexpression accelerated defecation (Dal Santo et al., 1999). Moreover, high calcium intake increased insoluble Ca^{2+} in the intestinal lumen, thereby binding to bile acids, enhancing fecal excretion and stimulating weight loss in calves (Xu et al., 1998; Bendsen et al., 2008).

These findings indicate that acidification of intestinal cells by enhanced proton transport might promote weight loss by Ca^{2+} stimulation of defecation. Considering that both *pept-1* and *nhx-2* mRNA levels are elevated in the *rege-1* mutants (**Figure 27**), the intense transport of protons together with peptides may lead to over-stimulation of DMP. Given that silencing of *pbo-1* or *pbo-4* mRNAs did not result in complete recovery of body fat in *rege-1* mutants, the PEPT-1 - PBO-1 / PBO-4 signaling may influence fat accumulation in parallel to the REGE-1 - ETS-4 regulatory axis. Thus, further research is needed to establish the relationship between PEPT-1 and REGE-1 - ETS-4 in fat regulation, and to investigate how PBO-1 / PBO-4 contributes to fat loss in *rege-1* mutants. Thus, potential changes in the intestinal pH levels in *rege-1* mutants could be determined using the pH-sensitive fluorescent dye (KR35) (Benomar et al., 2020).

Moreover, *pbo-1* mutants were shown to have altered pH and thus failed to protect the host from pathogens, while treatment with pH-buffering bicarbonates regained this ability (Benomar et al., 2020). Thus, it could be checked whether treatment of *rege-1* mutants with the bicarbonate resulted in the recovery of body fat content. Exposure of nematodes to cadmium telluride quantum dots (CdTe QDs) prolonged defecation cycle length and caused an increase in the body fat content (Wu et al., 2016), whereas Ca^{2+} waves stimulated the defecation cycle (Dal Santo et al., 1999). Moreover, silencing of *elo-2* mRNA, which is responsible for FA elongation, led to reduction in the body fat levels and shorter defecation cycle (Horikawa and Sakamoto, 2010; Kniazeva et al., 2003). Thus, it could be checked whether *rege-1* mutants had an accelerated intercellular Ca^{2+} wave by measuring Ca^{2+} oscillation period (Espelt et al., 2005) and whether the defecation cycle length was shortened in *rege-1* mutants (Sheng et al., 2015).

4. ETS-4 regulated fat accumulation irrespective of DAF-16 and PQM-1

The PQM-1 transcription factor was another potential factor regulating the body fat content in *C. elegans* downstream of the REGE-1 - ETS-4 regulatory axis, as shown in **Table 2**. The mechanism of transcriptional regulation through PQM-1 along with its antagonist DAF-16 was presented in **Figure 35**. PQM-1 is a transcription factor, which controls transcription of genes responsible for development, growth and reproduction (Heimbucher et al., 2020; Tepper et al., 2013). In contrast, DAF-16, integrates the response from various signaling pathways, such as IIS, AMPK, TOR, germline signaling and JNK signaling pathways, which influence aging, longevity, stress resistance and fat metabolism (Sun et al., 2017; Hansen et al., 2013). DAF-16 can activate or inhibit gene transcription depending on the stimulation of upstream signaling pathway (Sun et al., 2017). The IIS pathway inhibits transcriptional activity of DAF-16, while inactivation of IIS leads to dephosphorylation of DAF-16 and its nuclear translocation where it activates transcription of genes such as pantothenate kinase (*pnk-1*) involved in coenzyme A biosynthesis (Lee et al., 2003), gluconeogenic genes e.g. pyruvate carboxylase (*pyc-1*) and phosphoenolpyruvate carboxykinase PEPCK (R11A5.4, W05G11.6) (McElwee et al., 2006) and *fat-7* involved in unsaturated FAs synthesis (Murphy et al., 2003), leading to an increase

in the body fat accumulation (Shi et al., 2013). On the other hand, the AMPK signaling pathway through phosphorylation of DAF-16 causes its activation and translocation to the nucleus and stimulation of oxidative metabolism (Greer et al., 2007). Increased oxygen consumption, lipid mobilization by lipolysis and FA β-oxidation as well as decreased synthesis of PUFAs led to a reduction in body fat content (Moreno-Arriola et al., 2016).

Since PQM-1 and DAF-16 regulate transcription of genes involved in many of the major metabolic pathways in *C. elegans*, their effect on the regulation of the body fat content in *rege-1* mutants were investigated. RT-qPCR analysis confirmed the results from RNA-Seq (**Table 2**) and demonstrated an increase in *pqm-1* mRNA levels in both wild-type animals exposed to *rege-1* RNAi and *rege-1* mutants exposed to mock RNAi (**Figure 36 B**). Although DAF-16 usually acts as an antagonist of PQM-1 (Sun et al., 2017), its expression increased in animals with depleted *rege-1*, as shown in **Figure 36 A**. The analysis of subcellular localization of DAF-16::GFP, presented in **Figure 37**, showed its presence in the nuclei in the *rege-1* mutants and in animals with targeted *rege-1* mRNA, whereas in the wild-type animals expressing DAF-16::GFP and exposed to mock RNAi, the signal was stronger in the cytoplasm. The nuclear localization of DAF-16 suggested its enhanced transcriptional activity. However, silencing of *daf-16* or *pqm-1* mRNAs in *rege-1* mutants did not change their body fat levels compared to *rege-1* mutants exposed to mock RNAi (**Figure 38**). This results suggest that although DAF-16 was activated, as observed by its enhanced nuclear translocation, its function might not be related to the regulation of the body fat content in the *rege-1* mutants. Similarly, despite an increase in *pqm-1* mRNA level in *rege-1* mutants, it did not regulate fat accumulation. Thus, a lot of open questions, such as which metabolic pathways affect DAF-16 activation, what function DAF-16 plays and whether the location of PQM-1 changes in the *rege-1* mutants, still remain to be answered. DAF-16 may regulate other aspects of physiology in *rege-1* mutants related to the oxidative stress. Therefore, additional experiments are required for deeper understanding of metabolic changes occurring in *rege-1* mutants. It would be interesting to check whether the active DAF-16 signaling pathway in *rege-1* mutants was responsible for stimulation of the oxidative stress response by measuring ROS production through Amplex Red assay for H_2O_2 measurements (Chavez et al., 2007) or by ROS-sensitive dye dihydroethidium (DHE)

(Senchuk et al., 2018). Moreover, PQM-1 tagged with GFP could be used to determine the subcellular localization and thus the activity of PQM-1 in *rege-1* mutants.

5. SKN-1 regulated fat content possibly in parallel to REGE-1 – ETS-4 pathway

SKN-1 is a transcription factor, which enhanced the activity of the *pept-1* promoter and increased its mRNA and protein levels (unpublished data from Geillinger, 2012). Moreover, research carried on PAM212 mouse keratinocytes showed that a mammalian orthologue of *C. elegans* SKN-1, NRF2, increased *Mrp1* mRNA levels, as well as the amount and activity of MRP1 protein (Udasin et al., 2016). However, it is not known whether SKN-1 can be the molecular link between PEPT-1 and MRP-1 or whether they work independently. Glutathione (GSH) is a tripeptide γ – Glu – Cys - Gly responsible for antioxidant defense and detoxification (Lu, 2009). Many substances are exported from the cell in the form of GS-conjugated anions via MRP1 (Cole, 2014). Therefore further research is required to investigate whether the function of the PEPT-1 transporter is necessary for the transport of di- and tripeptides needed for GSH synthesis.

In this thesis, it was checked whether REGE-1 - ETS-4 regulatory axis could indirectly regulate the body fat content by influencing another transcription factor, SKN-1. Although *skn-1* was not found through forward genetic screening (**Table 1**) and RNA-Seq analysis (**Table 2**), due to its functional connection to the regulation of PEPT-1 and MRP-1 expression, it was decided to determine its possible relationship with REGE-1 and ETS-4. The RT-qPCR study, presented in **Figure 39 A**, showed a significant increase in *skn-1* mRNA levels in both wild-type animals exposed to *rege-1* RNAi and *rege-1* mutants exposed to mock RNAi compared to controls. In addition, targeting *skn-1* mRNA by RNAi increased fat accumulation in *rege-1* mutants. However, the recovery of body fat was partial compared to controls (**Figure 39 B** and **Figure 39 C**). Research conducted on both *C. elegans* and mice has shown that constitutive activation of *skn-1* / *Nrf-2* causes starvation-like phenotype (Pang et al., 2014b; Paek et al., 2012). People suffering from anorexia have a high level of antioxidant markers compared to healthy individuals, however whether oxidative stress

caused a reduction of the body fat or lower fat levels increased oxidative stress remained unknown (Solmi et al., 2015).

The activity of SKN-1 is tightly regulated by phosphorylation (Li et al., 2017). Phosphorylation at specific serine and threonine sites via the p38 / mitogen-activated protein kinase (MAPK) signaling pathway activated SKN-1, while phosphorylation through glycogen synthase kinase-3 (GSK-3) and IIS signaling pathways resulted in its inactivation (Li et al., 2017). Oxidative stress activates SKN-1 through its phosphorylation (An and Blackwell, 2003). Given the possible effect of the oxidative stress on the body fat loss, it was plausible that SKN-1 by influencing oxidative stress response genes could have influenced some phenotypic changes observed in the *rege-1* mutants.

Oxidative stress is caused by increased ROS production through transformation of oxygen to superoxide anion or into hydrogen peroxide, while its neutralization is based on the reduction of superoxide anion to hydrogen peroxide through superoxide dismutase (SOD), and then transformation of hydrogen peroxide to harmless water and oxygen by catalase (Chavez et al., 2007; Clifford and Repine, 1982). ROS production usually occurs on cellular membranes or organelle membranes due to the solubility of molecular oxygen, leading to peroxidation of lipids, which promotes apoptosis and autophagy (Su et al., 2019). Bacteria produce ROS to kill its host by modifying DNA, proteins and lipids (Bolm et al., 2004; McCallum and Garsin, 2016). Moreover, ROS can be produced by *C. elegans* to increase the expression of antioxidants and ingest bacterial pathogens (Chavez et al., 2007), as well as wound repair (Zou et al., 2013).

The RT-qPCR analysis presented in **Figure 40** showed in both wild-type animals exposed to *rege-1* RNAi and *rege-1* mutants exposed to mock RNAi significant increase in the expression of genes involved in the response to oxidative stress like *sod-4* and *sod-5* mRNAs. Moreover, targeting *rege-1* mRNA by RNAi increased the expression of SOD-5::GFP in neurons in the pharynx, as shown in **Figure 41**. Previous studies on *C. elegans* showed that high levels of ETS-4 stimulated the transcription of genes responsible for catabolism and immunity in *rege-1* mutants (Habacher et al., 2016). One of the reasons why oxidative stress might be increased in the *rege-1* mutants is the fact that the catabolic processes occurring in the intestine can lead to its acidification, which directly or indirectly affect cell function (Johnson and Nehrke, 2010). Active PEPT-1 transporter,

through enhanced proton transport, could influence intracellular pH in the intestine and also cause its acidification (Nehrke, 2014). Moreover, intestinal acidification protected nematodes from pathogenic bacteria by regulation of the immune response (Benomar et al., 2020) associated with ROS formation and oxidative stress signaling (Chavez et al., 2007; Johnson and Nehrke, 2010). Therefore, an increase in the expression of oxidative stress response genes might result from enhanced transport of di- and tripeptides and protons via PEPT-1 that leads to intracellular acidification, which could, at least in part, be responsible for the metabolic phenotype of the *rege-1* mutants.

Studies presents in this thesis indicate that SKN-1 might play a possible role in the regulation of the body fat content via the REGE-1 - ETS-4 regulatory axis. Next, it could be determined whether dsRNA targeted *skn-1* mRNA in the *rege-1* mutants reduced *pept-1* mRNA levels. Moreover, it would be interesting to check whether, RNAi-mediated silencing of *pept-1* mRNA in the *rege-1* mutant, by reducing intracellular acidification, inhibited the expression of genes related to the oxidative stress response. Moreover, by using stable-isotope labeling with amino acids (SILAC) (Larance et al., 2011) it could be examined whether PEPT-1 transported peptides, needed for GSH synthesis, can be further transported by MRP-1.

6. The effect of *rege-1* depletion on lipid metabolism

Lipid composition determines the function and fluidity of cellular membranes (Ntambi, 1999). Moreover, lipids mediate signal transduction (Kahn-Kirby et al., 2004) and are the components of TAG and CE (Ntambi, 1999). Lipids are responsible for the transmission of extracellular signals to the interior of the cell, they affect cell polarity and membrane structural stability (Choi et al., 2016). Alterations in lipid composition of the mitochondrial cell membrane can disrupt mitochondrial energy metabolism (Calzada et al., 2016), cause development of human diseases such as Alzheimer's and atherosclerosis, but can also contribute to obesity through hyperlipidemia (Casares et al., 2019; Kao et al., 2020; Engelmann et al., 1992; Muller et al., 1990; Gillies and Robinson, 1988). Since the compositions of membrane lipids and their functions

were often studied *in vitro* (Casares et al., 2019; Harrison and Vickers, 1990), the genetic mechanisms regulating this process *in vivo* are not fully understood.

The research carried out in this thesis showed a significant effect of ETS-4 on the expression of genes influencing FA and sphingolipid metabolism. These factors, possibly through their influence on lipid composition, could also be responsible for the lean phenotype of *rege-1* mutants.

6.1. Depletion of *rege-1* influenced fatty acid metabolism

In *C. elegans* MUFA, which are transformed through D9 desaturases from saturated FAs to unsaturated FAs (Brock et al., 2007), as shown in **Figure 42**, can be accumulated as TAG or form biological membranes as components of cholesterol and PL (Brock et al., 2007). Reports have shown that changing the expression of genes affecting FA compositions causes changes in the overall body fat content and survival of nematodes. Single *fat-5*, *fat-6* or *fat-7* mutants show a small effect on lipid composition (Brock et al., 2006). Due to the fact that FAT-6 and FAT-7 play a compensatory role to each other, the effect of limiting one of them is reduced (Brock et al., 2006). In contrast, *fat-6; fat-7* double mutants were characterized by reduced fertility, slow growth, increased expression of genes responsible for FA ß-oxidation, as well as decreased level of body fat and LD size, increased level of saturated FA and reduced amount of PUFA (Brock et al., 2006; Brock et al., 2007; Shi et al., 2013). In addition *fat-5; fat-6; fat-7* triple mutants were lethal unless additional oleic acid supplementation was provided (Brock et al., 2006).

In this thesis, RT-qPCR analysis was performed to check the expression levels of D9 desaturases, as shown in **Figure 43**. This analysis showed significant increase in the level of *fat-5* mRNA and a decrease in the level of *fat-7* mRNAs in both wild-type animals exposed to *rege-1* RNAi and *rege-1* mutants exposed to mock RNAi compared to controls. In contrast, the expression of *fat-6* remained unaffected. Similar observations, i.e. decrease in the body fat content with a simultaneous reduction in *fat-7* mRNA levels were reported in studies conducted on wild-type animals treated with chemical hypoxia (Heimbucher et al., 2020). FAT-7 requires oxygen as an electron acceptor to function

properly (Heimbucher et al., 2020). Upon chemical hypoxia, *fat-7* mRNA levels decreased, which led to a decline in the body fat levels (Heimbucher et al., 2020). The *fat-2* mutants had slower growth and reduced fertility, albeit the body fat content was unchanged, which further suggested that among other desaturases functional FAT-7, which acts upstream of FAT-2, was crucial for proper fat accumulation in nematodes (Brock et al., 2007). Since FAT-6 and FAT-7 play a compensatory role to each other (Brock et al., 2006), PUFA synthesis in *rege-1* mutants could be slightly changed or remain similar to the control. Given an increased expression of *fat-5*, MUFA synthesis could be increased in the *rege-1* mutants and thus alter lipid composition.

LDs contain TAGs surrounded by a phospholipid monolayer, composed of PC and PE (Vrablik et al., 2015). D9 desaturases, by modulating the ratio of PC to PE, regulate the size of LDs and the correct membrane lipid composition (Shi et al., 2013). In mutant animals characterized by excessive fat accumulation like *aak-1*, ribosomal protein S6 kinase (*rsks-1*) and *daf-2*, a higher PC : PE ratio compared to the wild-type animals was observed (Shi et al., 2013). In contrast, *fat-6; fat-7* double mutants had a lower PC : PE ratio compared to the wild-type nematodes (Shi et al., 2013). Preliminary unpublished data from *Johansen and Færgeman* thesis, showed that *rege-1* mutants had decreased levels of phosphatidylserine (PS) 40:4 and 40:1 along with increased levels of PS 38:1 (unpublished data from Johansen and Færgeman, 2018). Moreover, *rege-1* mutants contained higher phosphatidylglycerol (PG) 38:6 and PE 36:2 and lower PE 40:6 levels compared to the wild-type animals. Furthermore, *rege-1* mutants were characterized by a rise in PC 35:3 levels with a concurrent decrease in PC 38:4 and sphingomyelin (SM) 38:2;1 and an increase in 39:2;2 and 40:2;2 ceramides. In addition, DAGs' levels were altered in the *rege-1* mutants with a noticed increase in 33:1 and a simultaneous decrease in 34:2 and 36:2 (unpublished data from Johansen and Færgeman, 2018).

These studies indicated that a specified lipid composition was important for the body fat accumulation. The expression of genes influencing lipid composition was altered in *rege-1* mutants and some PL were increased while other decreased. Thus, further research should be carried out in order to discover whether the amount of specific PL was responsible for obtaining the lean phenotype of *rege-1* mutants for example by increasing the amount of detectable lipids in lipidomic analysis or by using stable isotope profiling.

6.2. Depletion of *rege-1* influenced sphingolipid metabolism

Sphingolipids influence the function of cellular membranes through the formation of lipid rafts (Hänel et al., 2019). Moreover, sphingolipids as bioactive molecules regulate a wide range of cellular functions and their excessive production in mammals was stimulated by stress such as oxidative stress, pro-inflammatory cytokines and starvation (Nikolova-Karakashian and Rozenova, 2010). In mammals, sphinganine is the precursor of sphingolipids formed from the junction of l-serine and palmitoyl-CoA via serine palmitoyltransferase (SPT) (Deevska and Nikolova-Karakashian, 2017). Sphinganine is then converted to dihydroceramide and later to ceramides. Next, the phosphocholine group from PC is attached to the ceramides via sphingomyelin synthase (SMS), resulting in the formation of SM, the major mammalian sphingolipid.

The pathway of sphingolipid formation in *C. elegans* depicted in **Figure 44** is very similar to that of mammals. Interestingly, the expression of many genes encoding enzymes involved in sphingolipid metabolism turned out to be increased in *rege-1* mutants. In addition to the rise in *sphk-1* mRNA levels, which RNAi-mediated inhibition increased the body fat in *rege-1* mutants, as presented in **Figure 23**, ETS-4 had a significant effect on the mRNA levels of other enzymes related to the ceramide synthesis such as *sptl-1*, *sptl-2*, *hyl-1* and *hyl-2*, as presented in **Figure 45**. Moreover, inhibition of *sptl-1* or *sptl-2* mRNAs by RNAi resulted in partial body fat recovery in *rege-1* mutants (**Figure 46** and **Figure 47**), while their simultaneous inhibition caused a complete fat recovery compared to controls (**Figure 48**). The observed large phenotypic similarity between *rege-1* mutants exposed to *sptl-1* / *sptl-2* RNAi and controls, suggested that sphingolipid metabolism could be responsible for the regulation of fat accumulation via the REGE-1 - ETS-4 regulatory axis.

The observed phenotypic changes can be explained by the interplay between sphingolipids and TAG metabolism (Deevska et al., 2017). In humans excess dietary calories promoted an ectopic accumulation of TAG and sphingolipids within the skeletal muscle, which led to the development of insulin resistance and obesity (Kelley and Goodpaster, 2001; Meikle and Summers, 2016; Choi and Snider, 2015). However, high levels of sphingolipids like SM, could lower TAG levels in the HepG2 cells lines with overexpressed SMS1 (Deevska et al., 2017). Consuming large amounts of fatty foods increased the blood level of palmitic acid, which was responsible for the development of ER stress and increased ROS

production. In turn, this led to recruitment of macrophages to the pancreas, liver and AT causing an inflammation (Korbecki and Bajdak-Rusinek, 2019). Under conditions of elevated levels of palmitic acid, the activity of SPT increased, which led to an enhancement of sphingolipids' production like ceramides (Deevska et al., 2009). In the HepG2 cell line with overexpressed SMS1, SMS1 increased *de novo* PC synthesis, which together with ceramides formed SM (Deevska et al., 2017). PC is produced by adding phosphorus to DAG via the enzyme choline / ethanolamine phosphotransferase 1 (CEPT1). Acylation of DAG leads to TAG synthesis via the enzyme diacylglycerol acyltransferase 1 (DGAT1). Thus, the activities of DGAT1 and CEPT1 determine whether DAG is used for TAG and / or PC synthesis (Deevska et al., 2017). Therefore, overexpression of genes involved in the sphingolipid synthesis pathway like *SMS1* divert DAG away from DGAT and increase PC synthesis relative to TAG (Deevska and Nikolova-Karakashian, 2017). Consuming large amounts of fatty foods increased the level of palmitic acid, which favored the increased production of SM in relation to TAG (Deevska et al., 2017).

Body fat accumulation is not only regulated by the balance between the amount of sphingolipids and TAGs, but also by the relative levels of SM and ceramides. In *C. elegans*, a mutation in the acid sphingomyelinase 3 (*asm-3*) gene, responsible for the transformation of SM into d17iso-ceramide, caused an increase in the amount of SM compared to the amount of ceramides and an increase in the size of LDs (Schmokel et al., 2016). Moreover, mice with the *Sms2* knock out, which had lower levels of SM than ceramides, had reduced body weight (Yano et al., 2011) and LDs' size (Mitsutake and Igarashi, 2013). Furthermore, *Sms1*-null mice, in addition to enhanced ceramide production, were characterized by increased levels of ROS, mitochondrial dysfunction and impaired insulin secretion in response to high glucose levels (Yano et al., 2011).

Results presented in this thesis suggested that, most likely, REGE-1 – ETS-4 regulatory axis reduced fat accumulation in *rege-1* mutants through changes in sphingolipid metabolism. In order to determine whether in *C. elegans*, similarly to mammals, a physiological competition between the TAG and sphingolipid formation pathway exists, it would be necessary to check the expression of *Dgat1* and *Cept1* orthologs in nematodes, membrane bound O-acyl transferase (*mboa-2*) and *cept-1*, respectively. In addition, it could be determined whether inhibition of the sphingolipid metabolism by simultaneous

silencing of *sptl-1* and *sptl-2* mRNAs increased the amount of TAG in the *rege-1* mutants. Moreover, sphingolipidomic profiling analysis using liquid chromatography – mass spectrometry coupled with multiple reaction monitoring mode (LC – MS - MRM) could be performed (Cheng et al., 2019) in order to discover the composition of sphingolipids, in particular whether the SM levels were changed in *rege-1* mutants.

7. Depletion of *rege-1* affects energy metabolism

FAs play an important biological role. They act as energy source and can be stored in the form of TAG in AT. Moreover, they are structural components of the membranes and affect the fluidity of cell membrane and membranes of other organelles, such as mitochondria (Rustan and Drevon, 2005). PUFAs are responsible for the formation of the PL that form the mitochondrial membranes, such as PC and PE, as well as cardiolipins, which are crucial for the optimal mitochondrial function (Stanley et al., 2012). Moreover, FAs are substrates for mitochondrial ß-oxidation (Stanley et al., 2012) and as ligands of nuclear receptors might regulate the expression of mitochondrial proteins (Noy, 2007). The transport of electrons through the electron transport chain to the inner mitochondrial membrane causes polarization of the mitochondrial membrane and generation of an electron potential, which is used for the synthesis of ATP from ADP by oxidative phosphorylation (Li and Graham, 2012). As a result of oxidative phosphorylation, oxygen is consumed and reduced by protons to form water (Li and Graham, 2012).

In *C. elegans* mitochondrial dysfunction, caused by a reduction in mitochondrial function (Ng and Gruber, 2019) or a reduction in the number of mitochondria (Hibshman et al., 2018) can be measured by OCR (Li and Graham, 2012). In both *C. elegans* and humans proper function, shape and mitochondrial number are maintained through mitochondrial fission and fusion (Luz et al., 2015), the disturbance of which negatively affects OCR (Son et al., 2017). In *C. elegans*, mitochondrial fission is regulated by dynamin-related protein 1 (DRP-1), which is an ortholog of human DRP1, whereas mitochondrial fusion is regulated by Fzo mitochondrial fusion protein 1 (FZO-1), which is an ortholog of human dynamin-related GTPases mitofusin-2 (MFN2) (Son et al., 2017; Luz et al., 2015).

Since in *C. elegans* mitochondrial disfunction increased ROS production and induced oxidative stress response (Palikaras et al., 2015), which also increased in animals with depleted *rege-1* (**Figure 40** and **Figure 41**), it was checked whether mitochondrial function was also altered by measuring OCR. Animals with depleted *rege-1* had significantly lower OCR levels compared to controls, as presented in **Figure 49**, which may suggest abnormal mitochondrial function. In murine 3T3-L1 preadipocytes mitochondrial uncoupling inhibited FA synthesis and stimulated lipolysis, which in turn decreased TAG content (Tejerina et al., 2009; De Pauw et al., 2012). In contrast, mitochondrial dysfunction also contributed to the excessive fat accumulation in the skeletal muscle in rats (Gumucio et al., 2019). However, the potential relationship between mitochondrial function and body fat loss in the *rege-1* mutants need to be further tested.

Alterations in lipid composition of the mitochondrial cell membrane had an effect on the disturbance of mitochondrial energy metabolism (Calzada et al., 2016). Given that in *rege-1* mutants the expression of genes affecting lipid composition were altered (**Figure 43**), this could have influenced mitochondria and result in lowering OCR (**Figure 48**) compared to controls. Thus, in *rege-1* mutants energy might be obtained from processes other than FA ß-oxidation. Carbohydrates and FAs are the main source of energy. Altough FA ß-oxidation provides more ATP it requires more oxygen per mole for ATP synthesis compared to glycolysis (Leverve et al., 2007; Heimbucher et al., 2020). Under conditions of oxygen deficiency, anaerobic glycolysis is activated to save oxygen, but at the cost of lower ATP production compared to mitochondrial lipid catabolism (Leverve et al., 2007). Among carbohydrates, glucose and glycogen supply the energy for *C. elegans* maintained in axenic medium (i.e. bacteria-free) (Zecić et al., 2019) and under anoxic conditions (Heimbucher et al., 2020). Both humans and *C. elegans* can store glucose in the form of glycogen in the skeletal muscle and liver, while *C. elegans* in the intestine, muscle and hypodermis (Zecić et al., 2019). Under conditions of limited access to oxygen, in *C. elegans* an inverse relationship between the body fat loss and an increase in the glycogen levels was observed (Zecić et al., 2019; Heimbucher et al., 2020). In *C. elegans* the enzyme responsible for conversion of sorbitol into fructose, which is then further converted into glycogen, is *sodh-1* (El-Kabbani et al., 2004). Therefore, it was checked whether the level of *sodh-1* mRNA was changed in *rege-1* depleted animals, as shown in **Figure 50**. The *sodh-1* mRNA

levels significantly increases in wild-type animals exposed to *rege-1* RNAi and in *rege-1* mutants exposed to mock RNAi compared to controls, indicating possible contribution of carbohydrate metabolism to energy supply upon limited lipid availability. Prior studies indicated that PQM-1 could control OCR, as well as reduce glycogen levels by inhibiting *sodh-1* transcription (Heimbucher et al., 2020). RNA-Seq data analysis performed in this thesis indicated that *pqm-1* mRNA levels were increased in the *rege-1* mutants in comparison to controls (**Table 2** and **Figure 37 B**). Given increased *pqm-1* expression, the activity of its protein should be determined. Since reduced PQM-1 transcriptional activity can lead to reduction of fat accumulation in nematodes (Heimbucher et al., 2020), the analysis of subcellular localization of PQM-1::GFP would enable determination of its activity in *rege-1* mutants.

The results presented in this thesis showed that mutations within the *rege-1* gene had far-reaching consequences. Changing the lipid composition in *rege-1* mutants might cause structural changes in the mitochondrial membrane, which could influence their ability to produce energy. However, to verify these assumptions, additional lipidomic analyzes should be performed to determine the exact composition of lipids in the mitochondrial membrane, including cardiolipin. It would be interesting to check mitochondrial activity by determining the mitochondrial membrane potential ($\Delta\Psi m$) using rhodamine 123, the activity of respiratory chain complexes in isolated mitochondria via Clark-type electrode and mitochondrial integrity via transmission electron microscopy (Dilberger et al., 2019). Moreover it might be worth to check whether the reduced OCR in *rege-1* mutant was caused by a change in the membrane structure or as a result of a reduction in the mitochondrial content by measuring the expression of genes responsible for fusion and fission (Son et al., 2017; Luz et al., 2015). Studies in mice showed that glycogen accumulation was regulated via AMPK signaling pathway and glycogen was utilized for the survival during hyperosmotic stress or under conditions of low ATP levels (Possik et al., 2015). Due to the fact that low ATP level affects the AMPK signaling (Apfeld et al., 2004), it could be checked whether the AMP / ATP ratio was altered in the *rege-1* mutants. Since the expression of *sodh-1* was increased in the *rege-1* mutants, glycogen levels, e.g. via the Glycogen Assay Kit (Gusarov et al., 2017), could be determined.

CONCLUSIONS

Obesity is a serious global problem affecting people all over the world. Prior research revealed that *rege-1* inhibition increased the expression of the transcription factor ETS-4 and led to the body fat loss in *C. elegans* (Habacher et al., 2016). The aim of this PhD thesis was to discover downstream metabolic pathway/s which regulated the body fat in the *rege-1* mutants through the REGE-1 – ETS-4 axis. Since depletion of *ets-4* led to the recovery of body fat levels in *rege-1* mutants, a search for targets downstream of ETS-4, which inhibition in *rege-1* mutants would allow recovery of body fat to the levels comparable to controls, was performed.

Numerous studies have shown that *rege-1* mutants undergo various metabolic changes that lead to fat loss. Unbiased genetic screening allowed the discovery of the *mrp-1* gene, whose numerous mutations increased fat accumulation in *rege-1* mutants. RNA-Seq data analysis of changes in *rege-1* mutants compared to control animals, showed an increase in the expression of *sphk-1*, responsible for the synthesis of ligands transported by the MRP-1. Preliminary results indicate that the activity of PEPT-1 transporter was enhanced in *rege-1* mutants. PEPT-1 could modulate fat accumulation in several ways, either by altering the content of intracellular peptides which stimulate the function of TOR or by changing the intracellular pH, which might regulate the calcium ions wave and rhythmic defecation behavior in nematodes. However, silencing potential ETS-4 targets, including *mrp-1*, *sphk-1*, *ltah-1.2*, *pbo-1* or *pbo-4*, resulted only in a partial recovery of the body fat levels in *rege-1* mutants, which may suggest that they regulate fat metabolism in parallel to REGE -1 - ETS-4 regulators axis. Another possible scenario assumes ETS-4 as a master metabolic regulator affecting multiple down-stream targets which simultaneously modulate fat metabolism and thus all together exert an additive effect on the fat loss phenotype in *rege-1* mutants.

Another ETS-4 candidate gene found through RNA sequencing data analysis was *pqm-1*, which was considered to work together with its antagonist *daf-16*. The expression of *pqm-1* and *daf-16* increased in *rege-1* mutants. Moreover, enhanced DAF-16::GFP signal in the nuclei was observed, indicating that its transcriptional activity was increased upon

rege-1 deletion. However, RNAi-mediated silencing of *pqm-1* and *daf-16* mRNAs did not cause any changes in the amount of body fat in *rege-1* mutants suggesting that the REGE-1 - ETS-4 regulatory axis did not regulate fat metabolism through DAF-16 and PQM-1 transcription factors. Yet, DAF-16 can regulate other aspects of physiology in *rege-1* mutant animals, such as oxidative stress response.

The last candidate downstream target of ETS-4 considered in the study was the transcription factor SKN-1, which could influence the expression of *mrp-1* or *pept-1* genes. However, silencing of *skn-1* mRNA in *rege-1* mutants enabled only partial recovery of body fat. Therefore, SKN-1 may contribute to the fat loss or exert a different function in *rege-1* mutants e.g. SKN-1, similarly to DAF-16, could increase the expression of genes associated with the oxidative stress response e.g. *sod-4* and *sod-5*.

In animals with depleted *rege-1*, in addition to the reduced level of body fat, an increased response to ROS was observed. Enhanced formation of ROS could be associated with acidification of the intestine via increased proton transport by the PEPT-1 transporter. Catabolic processes related to the stimulation of lipases (*lipl-1*, *lipl-2*) or the change in the expression of genes responsible for the lipid composition (*fat-5*, *fat-7*), may indirectly affect mitochondrial function and cause oxidative stress. Inhibition of genes modulating sphingolipid metabolism like *sptl-1, sptl-2* or *sphk-1,* led to partial body fat recovery, whereas simultaneous inhibition of *sptl-1* and *sptl-2* resulted in total body fat recovery in *rege-1* mutants compared to controls. This may suggest that changes in sphingolipid metabolism might contribute to the fat loss in *rege-1* mutants through inhibition of TAG production. Moreover, mitochondrial function indicated by decreased OCR levels, may be impaired in *rege-1* mutants. Mitochondrial uncoupling can inhibit FA synthesis and stimulate lipolysis leading to a reduction in fat accumulation. In addition, reduced OCR, TAG and the body fat content suggested that *rege-1* mutants obtain energy from a source other than high-energy fats, such as carbohydrates, e.g. glucose and glycogen. An increase in *sodh-1* mRNA levels further indicated that lipid availability could be limited in the *rege-1* mutants and the energy could be obtained from carbohydrate metabolism.

In conclusion, results presented in this thesis demonstrate the complexity of the regulation of body fat content through the REGE-1 - ETS-4 regulatory axis. Simultaneous activation of different metabolic pathways and their action lead to a reduction of fat

accumulation in *rege-1* mutants. Although inhibition of chosen signaling pathways through silencing of individual mRNAs increased fat accumulation in *rege-1* mutants it did not lead to full recovery of the body fat levels. Concomitant silencing of *sptl-1* and *sptl-2* mRNAs resulted in the greatest phenotypic change, indicating that changes in sphingolipid metabolism may exert the strongest effect on fat accumulation in *rege-1* mutants. Thus, the pathway of sphingolipid metabolism most likely regulates fat accumulation downstream of the REGE-1 - ETS-4 regulatory axis, as shown in **Figure 51**.

In addition, this work showed a great advantage of using *C. elegans* as a model organism in metabolic research as each signaling pathway examined had their functional counterpart in humans. This suggests that similar mechanisms may regulate fat accumulation in *C. elegans* and humans. Thus, the discovery of molecular mechanism/s regulating the body fat content in nematodes in the future may lead to the discovery of new treatments for obesity and reduce the incidence of obesity-related metabolic diseases.

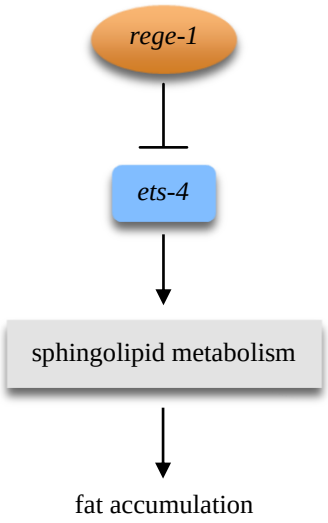

Figure 51. Possible mechanism of the REGE-1 - ETS-4 fat regulatory network in *C. elegans*.

EXPERIMENTAL PROCEDURES

1. Materials

1.1. *C. elegans* strains

C. elegans strains used in this study are listed in **Table 3**. The strains were ordered from the Caenorhabditis Genetics Center (CGC), obtained from the Ciosk Laboratory collection or were created in this study. Nematode strains from the Ciosk Laboratory collection were marked as 'RAF'. The mCherry tagged *mrp-1b(syb2461)X* strain and GFP::FLAG tagged *pept-1(syb3497)X* and *daf-16(syb707)I* strains were made by SunyBiotech via a CRISPR / Cas9 genome editing method. The animals expressing DHS-3::GFP *ldrIs1[dhs-3p::dhs-3::GFP + unc-76(+)]* was a kind gift from Anne Spang (Zhang et al., 2012). The animals expressing SOD-5::GFP *wuIs57[pPD95.77 sod-5::GFP; rol-6(su1006)]* was a kind gift from David Gems (Doonan et al., 2008). The genetic sequence of each strain was confirmed using PCR-based genotyping or DNA sequencing using Sanger method performed at the Laboratory of Molecular Biology Techniques at the University of Adam Mickiewicz in Poznan. Files in ab.1 format with Sanger-type sequencing results were visualized in Chromas program. Obtained sequence in FASTA format was entered into the USCS Genome Browser Gateway Blast Search Genome program, where the sequence consistency was checked.

Table 3. The list of *C. elegans* stains used in this study.

Genotype	**CGC** / RAF
wild-type	**N2** / 5044
daf-16(syb707)I	5010
daf-16(syb707)I; rege-1(rrr13)I	5123
ets-4(rrr16)X	1729
ets-4(rrr16)X; rege-1(rrr13)I	1759
ldrIs1[dhs-3p::dhs-3::GFP + unc-76(+)]	1964
ldrIs1[dhs-3p::dhs-3::GFP + unc-76(+)]; rege-1(rrr13)I	1972
ldrIs1[dhs-3p::dhs-3::GFP + unc-76(+)]; mrp-1(pk89)X	5092
ldrIs1[dhs-3p::dhs-3::GFP + unc-76(+)]; mrp-1(pk89)X; rege-1(rrr13)I	5095
mrp-1(pk89)X	**NL147** / 2096
mrp-1b(syb2461)X	5117
pept-1(syb3497)X	5151
rege-1(rrr13)I	1657
rrrSi400[Pets-4::ets-4-GFP::ets-4 3'UTR; unc-119(+)]II; unc-119(ed3)III; ets-4(rrr16)X; rege-1(rrr13)I	1769
wuIs57[pPD95.77 sod-5::GFP; rol-6(su1006)]	5106

1.2. Bacterial strains and plasmid

OP50 strain used in this study come from the CGC, whereas DH5α strain and L4440 plasmid are a gift from Friedrich Miescher Institute for Biomedical Research in Basel (Switzerland), listed in **Table 4**. Bacterial strains used as *C. elegans* feeding bacteria for RNA interference, listed in **Table 5**, came from Ahringer or Vidal libraries, respectively, and possessed HT115 bacteria resistant to ampicillin and tetracycline.

Table 4. Bacteria and plasmid used for cloning in this study.

Name	**Description**
OP50	Bacteria *Escherichia coli*
DH5α	Bacteria *Escherichia coli* used for RNAi
L4440	Plasmid used for RNAi, resistant for ampicillin

Table 5. Bacterial strains used as *C. elegans* feeding bacteria for RNA interference.

Gene	Source
empty vector	
daf-16	Ahringer library
ltah-1.2	Vidal library
pbo-1	Vidal library
pbo-4	Ahringer library
pept-1	Created in this study
pqm-1	Vidal library
rege-1	Ahringer library
skn-1	Ahringer library
sphk-1	Ahringer library
sptl-1	Ahringer library
sptl-2	Ahringer library

1.3. Instruments and kits

Table 6. List of instruments and materials used in this study.

Instrument	Company
0.22 μm pore syringe filter	Bionovo, cat. 6-0044
0.45 x 25mm hypodermic needles	Henke-ject
1.5 ml protein LoBind tubes	Eppendorf, cat. 0301081160
1.5 ml Semi-Micro Disposable Cuvettes	Plastic Group, cat. 7590 15
10 ml syringe	BD Discardit II
96 x 0.1 ml Well Plate	Bioplastics, cat. B17489
96 Well Polystyrene Cell Culture Microplates	Greiner bio-one, cat. 655086, black
Azure Biosystem c600	Bioanalytical Imaging System
Centrifuge 5424R	Eppendorf
Centrifuge 5804R	Eppendorf
Cigarette paper	Commercial
Confocal Microscopy DMI 4000B	Leica Microsystems, Germany
Cover Glass 24 x 50 mm	VWR, cat. 631-0146P
Digital incubators IL10	Incu-Line
Disposable Glass Pasteur Pipettes 230 mm	VWR, cat. 612-1702
Exella E24 Incubator Shaker	New Brunswick Scientific
Extended Length Tip	Gantour

Filter papers	Watman Benchkote surface protector, cat. WHA2300917
Five Easy F20 pH meter	Mettler Toledo
Horizontal bench-top autoclave DB-65	Systec
Horizontal electrophoresis	BTLab Systems
Hotplate	VWR
HTL pippetes	HTL Lab Solution
Incubator Hett Cube 600R	Hettich
KS 130 Basic	IKA
LH-930 Aspirator	Lab Helper
Light Cycler 480 II	Roche
LSE Mini microcentrifuge	Corning
Magnetic stirrer MS11HS	Wigo
Mediajet and Mediaclave 10	Integra
Microscope Imager Z2 with Axiocam 506 mono camera	Zeiss
Microscope slides	VWR, cat. 631-1551P
Mini Protean 15-well, 1.5 mm Comb	Bio-Rad
Mini Protean glass plates and short plates	Bio-Rad
Mini Protean Tetra Cell tank	Bio-Rad
Nalgene Rapid-Flow Sterile Single Use Vacuum Filter Units	Thermo Fisher Scientific, cat. 564-0020
NanoDrop One C	Therno Fisher Scientific
Neptune barrier tips	Gentaur
Opti-Seal Optical Sealing Sheet	Bioplastics, cat. 157300
Oxygraph+	Hansatech, serial number: 19035
Picoruptor with Minichiller 300	Diagenode, Huber
Pioner PA512CM/1	Ohaus
Polytetrafluorethylene (PTFE) membrane	Hansatech
ProFlex PCR System	Applied Biosystems by Life Technology
PVDF membrane	BioRad, cat. 1704156
Resin Mixer MX-T6-S	Dlab
SimpliAmp Thermal Cycler	Thermo Fisher Scientific
Microscope SMZ25, DeltaPix colour camera	Nikon
Stereo Zoom Microscope SMZ745	Nikon
Swiftped Pro Pippetor	HTL Lab Solution
Technical 10	Hydrolab
Thermomixer F1.5	Eppendorf
Trans-Blot Turbo Transfer System	Bio-Rad

Victor Nivo Multiple Plate Reader	PerkinElmer
Vortex-Genie 2	Scientific Industries

Table 7. Free software online tools used in this study.

Name	**Web-adress**	**Purpose**
Add Gene	http://addgene.org/1654/	Map of L4440
Clustal Omega	https://www.ebi.ac.uk/Tools/msa/clustalo/	Sequence alignment
Genemania	http://genemania.org	Networks analysis
KEGG	https://www.genome.jp/kegg/mapper/	Pathway analysis
Oligo Calculator	http://biotools.nubic.northwestern.edu/OligoCalc.html	Calculation of Tm
Primer 3.0 software	http://bioinfo.ut.ee/primer3	Primer design
UCSC Genome Browser Gateway	http://genome.ucsc.edu	Genomic sequence, blast
Worm Base	http://wormbase.org	General information
Worm Atlas	http://wormatlas.org	General information

Table 8. Software packages employed during this work.

Software	**Purpose**
ApE	Primer design
Chromas	Visualization of sequencing results
DeltaPix InSight	Analysis of ORO pictures
Fiji / imageJ	Quantification ORO staining
Gimp 2.10.22	Creating figures
Graph Pad / Prism 8	Statistical analysis
Image Studio Lite Version 5.2.5	Western blot analysis
LAS X SP8ax	Analysis of confocal microscope pictures
Microsoft Excel	Data analysis
Microsoft Word	Generation of text files
Microsoft Power Point	Design of overviews
OxyTrace+ Recording 1.0.48	Analysis of oxygen consumption rate
Pyre 2	3D protein structure
UCSF Chimera	Analysis of protein structure
Zen 2.6 and 3.3 blue edition	Analysis of microscope pictures

Table 9. Commercially available kits used during this work.

Kit	Company
Direct-zol RNA MicroPrep	Zymo Research, cat. R2062
Electrode Maintenance Kit	Hansatech
High-Capacity cDNA Reverse Transcription Kit	Thermo Fisher Scientific, cat. 4368814
Monarch PCR and DNA Cleanup Kit	New England BioLabs, cat. T1030S
Plasmid Mini Kit	A&A Biotechnology, cat. 020250
Phusion High-Fidelity PCR Kit	New England BioLabs, cat. E0553L
QIAqiuck PCR Purification Kit	Qiagen, cat. 28104
Triglyceride Quantification Colorimetric / Fluorometric Kit	Biovision, cat. K622-100

1.4. Oligonucleotides

Table 10. The list of primers used for PCR-based genotyping.

Primer name	Direction	5' Sequence
daf-16::GFP	Forward	GTAAATCGACACATGGCGCT
	Reverse	CCAGACAACCATTACCTGT
ets-4 outside deletion	Forward	GCTCAGTCGGTCACAGATGG
	Reverse	GGAGGCAGGAATTTGTACACC
ets-4 inside deletion	Forward	GCTCAGTCGGTCACAGATGG
	Reverse	GCATATCCATCGGATGTGG
L4440 vector	Forward	AACCTGGCTTATCGAAATTAATAC
mrp-1 outside deletion	Forward	AATTACTTTCGTGGCTTTGGC
	Reverse	GGAGTCGGTAGTCGATGACG
mrp-1 inside deletion	Forward	AATCATTCGCAACGGACTTC
	Reverse	CCGCTTCTTTTTCAATGAGC
mrp-1::mCherry	Forward	GCAGTTCAAAGATTGTACTG
	Reverse	CCATACATGAACTGTGGAG
pept-1 clone	Forward	GACCCGGGCTATACCACACCACTTCT
	Reverse	CTCCCGGGATCATAGATCCTGCGTT
pept-1::GFP	Forward	AGCTCTGGTACAAGCCCTCT
	Reverse	TTCACCCTCTCCACTGACAGA
rege-1	Forward	ACAGAGCAACTAAGTCAC
	Reverse	TCTGTGGTCACTTAGTTA

Table 11. The list of primers used for gene expression analysis by RT-qPCR.

Gene name	Direction	5' Sequence
actin 1	Forward	GTTGCCCAGAGGCTATGTTC
	Reverse	CAAGAGCGGTGATTTCCTTC
daf-16	Forward	CGACTACAAAGGCTCAACTCG
	Reverse	CGTGAGAAATCGTTTGAATCG
ets-4	Forward	ACATGCAGTCAAAAACTAATTGGCTAG
	Reverse	ACATGTTTGGATACCCTCCGTTTC
fat-5	Forward	GGACGGATACTGATGCTGAC
	Reverse	GGATCCTCGTACAAATCGCT
fat-6	Forward	CCATCACACATTCCCACAAG
	Reverse	TTCCGGTCGTAGACAAGTCC
fat-7	Forward	CCCATCGTCTCTGGTCTCAT
	Reverse	ACGGGTGGTGTTATGTGGAT
hyl-1	Forward	AGTCGGAACCTTGATTCTTC
	Reverse	CCCAAAGTATGTAATCTGGC
hyl-2	Forward	CTTTCTCAGCCGCAAAAATC
	Reverse	ACAAGGTACAACCCGCAGAC
lipl-1	Forward	CGGTTTGCGCTGGACTTA
	Reverse	GAACACGAGTTGCGTTAA
lipl-2	Forward	TGGATGCAGATGGTTCGC
	Reverse	GCCCTTGATGGCTCCGAA
mrp-1	Forward	GCATACGGAGGAACAGACTCTG
	Reverse	CAAGTTGACCACGCTTGATG
nhx-2	Forward	GCCGTGTTCGGAGAATCTCTA
	Reverse	CCACCAAATGCAACAACCA
pept-1	Forward	ACTATGGAATGAGAACGGT
	Reverse	CTTGTCCGATTGCGTAT
pept-2	Forward	AGCGTTAGCTCGAAAGGCAA
	Reverse	CGCAGAATTCGTTGGACACG
pqm-1	Forward	CCTCCAATCAAATGCAACG
	Reverse	CGAGAACCTTGGTCGATACTCTC
skn-1	Forward	CTGGCATCCTCTACCACCAC
	Reverse	TTGGTGATGATGGCCGTGTT
sodh-1	Forward	CTGGATGGCAACTTGGAGAC
	Reverse	AATTCGCAGTTGAGGCAGTT
sod-4	Forward	AATCATTGGCCGAAGTGTGG
	Reverse	AAGTCGGCTTCCAGCATTTC

sod-5	Forward	ATTGCCAATGCCGTTCTTCC
	Reverse	AGCCAAACAGTTCCGAAGAC
sodh-1	Forward	CTGGATGGCAACTTGGAGAC
	Reverse	AATTCGCAGTTGAGGCAGTT
sphk-1	Forward	AAAGCCGACCTTGGAAAGTT
	Reverse	GAACAATTCCGATTGGGAGA
sptl-1	Forward	TCGGCCAAGCATTCGAGTAA
	Reverse	AACAGAAAAATTTGGCACGAGA
sptl-2	Forward	TCTGGCACATATGACAGTCCG
	Reverse	TGGCGAATTTCGTTTCGCTAC

1.5. Antibodies

Table 12. List of antibodies used in Western blot.

Raised against	Source	Dilution	Company
Anti-actin, clone C4	Mouse	2:4000	Merck / Milipore, cat. MAB1501
Anti-mouse	Horse	1:5000	Cell Signaling, cat. 7076S
Anti-rabbit	Goat	2:5000	Cell Signaling, cat. 7074S
GFP	Rabbit	3:4000	Cell Signaling, cat. 2555S

1.6. Chemicals and reagents

Table 13. Chemicals and reagents used in this study.

Substance	Company
1 kb Plus DNA Ladder	New England BioLabs, cat. N3200L
35 - 38% hydrochloric acid	Chempur, cat. 115752837
99.5% chloroform	POCH, cat. 234430111
99.7% 2-propanol	POCH, cat. 750006411
99.8% ethanol	POCH, cat. 396420113
Agarose	Bioshop, cat. AGA001.1
Ampicillin	Bioshop, cat. AMP201
AmplifyMe SG Universal Mix	Blirt, cat. AM02-020

ß – Ala – Lys - AMCA	BioTrend, cat. NB-48-0188-5 mg
Bovine Serum Albumine	Sigma Life Technology, cat. A1470
Bradford reagent	Sigma, cat. B6916
Cell Lysis Solution	Qiagen, cat. 158906
CIP	New England BioLabs, cat. M0290S
Cut Smart Buffer	New England BioLabs, cat. B7204S
Femtogram HRP substrate	Azure Biosystem Radiance Plus, cat. AC2103
GoTaq G2 Green Master Mix 2x	Promega, cat. M7823
Levamisole hydrochloride	Abcam, cat. ab141217
Methanol pure	Chempur, cat. 116219904
Oil red O	Sigma Aldrich, cat. O0625-25G
Page Ruler Plus Prestained Protein Ladder	Thermo Fisher Scientific, cat. 26619
Proteinase K	Promega, cat. V3021
Protein Precipitation Solution	Qiagen, cat. 158910
RNase A	Bioshop, cat. RNA675.50
SimplySafe	EURx, cat. E4600-01
Skim Milk Powder	Bioshop, cat. SKI400.500
Sodium chloride	Bioshop, cat. SOD001
T4 DNA ligase buffer 10x	New England BioLabs, cat. B0202S
T4 DNA ligase	New England BioLabs, cat. M0202S
TAE buffer	Bioshop, cat. TAE222.4
Tetracycline	Bioshop, cat. TET701
Tri Reagent	Thermo Fisher Scientific, cat. AM9738
XmaI restriction enzyme	BioLabs

1.7. Buffers and solutions

All buffers and solutions were prepared in ddH_2O unless otherwise noted.

Table 14. List of buffers and solutions used in this study.

Buffer for hypochloride treatment (1 l)	
1.5%	Sodium hypochlorite, 5% (VWR, cat. CHMP528066500.1000)
0.75 mM	Potassium hydroxide (POCH, cat. P5958)
	filter through Nalgene Rapid-Flow Sterile Single Use Vacuum Filter Units (Thermo Fisher Scientific, cat. 564-0020)
	store at 4°C

LB buffer (1 l)

20%	LB Broth Lennox (Bioshop, cat. LBL405)
	autoclave

M9 10x buffer (1 l)

0.22 M	Potassium phosphate monobasic (Bioshop, cat. PPM302)
0.485 M	Sodium phosphate dibasic (Bioshop, cat. SPD307.500)
0.85 M	Sodium chloride (Bioshop, cat. SOD001)
2 mM	Magnesium sulphate (Bioshop, cat. MAG513)
	autoclave

PBS 1x (1 l)

137 mM	Sodium chloride (Bioshop, cat. SOD001)
2.7 mM	Potassium chloride (Bioshop, cat. POC888.500)
10 mM	Sodium phosphate dibasic (Bioshop, cat. SPD307.500)
10 mM	Potassium phosphate monobasic (Bioshop, cat. PPM302)
	adjust pH to 7.4 with concentrated Hydrochloric acid (Chempur, cat. 363-115752837)

PBS-T 1x (1 l)

137 mM	Sodium chloride (Bioshop, cat. SOD001)
2.7 mM	Potassium chloride (Bioshop, cat. POC888.500)
10 mM	Sodium phosphate dibasic (Bioshop, cat. SPD307.500)
10 mM	Potassium phosphate monobasic (Bioshop, cat. PPM302)
	adjust pH to 7.4 with concentrated Hydrochloric acid (Chempur, cat. 363-115752837)
0.05%	Tween20 (Bioshop, cat. TWN510.100)

S-basal buffer (1 l)

98.6 mM	Sodium chloride (Bioshop, cat. SOD001)
50 mM	sterile Potassium phosphate, pH 6.0
	(132 mM Potassium phosphate dibasic (Bioshop, cat. PPD303.500)
	868 mM Potassium phosphate monobasic (Bioshop, cat. PPM302))
	adjust pH of 1 M Potassium phosphate to 6.0 with 1 M Potassium hydroxide (POCH, cat. P5958))
5 µg/ml	sterile Cholesterol (Bioshop, cat. CHL500) (in EtOH from POCH, cat. 396420113)
	autoclave

Trehalose-DMSO nematode freezing solution (1 l)

80 mM	D-(+)-Trehalose dihydrate (Bioshop, cat. TRE222)
3.5%	DMSO (Bioshop, cat. DMS666)
fill to 1 l	1x M9 buffer
	filter through Nalgene Rapid-Flow Sterile Single Use Vacuum Filter Units (Thermo Fisher Scientific, cat. 564-0020)

Tris-buffered saline (TBS) 1x (1 l)

50 mM	Tris Base (Bioshop, cat. TRS003)
150 mM	Sodium chloride (Bioshop, cat. SOD001)
	adjust pH to 7.5 with 1 M Hydrochloric acid (Chempur, cat. 363-115752837)
	filter through Nalgene Rapid-Flow Sterile Single Use Vacuum Filter Units (Thermo Fisher Scientific, cat. 564-0020)

Tris-buffered saline (TBS) 1x + protease inhibitors (5 ml)

1:7	cOmplete EDTA-free Protease Inhibitor Cocktail (Sigma Aldrich, cat. 4693159001) (1 tablet dissolved in 1.5 ml nuclease-free H_2O)
0.1 M	PMSF (Bioshop, cat. PMS123.5)
fill to 5 ml	TBS
	store at 4°C

Western blot 4% stacking gel (5.6 ml)

1.26 ml	0.5 M Tris-HCl pH 6.8
0.48 ml	40% Acrylamide / Bis-Acrylamide (Bioshop, cat. ACR004.500)
50 µl	10% SDS (Bioshop, cat. SDS002.500)
25 µl	10% APS (Bioshop, cat. AMP001.10)
15 µl	TEMED (Bioshop, cat. TEM001.25)

Western blot 10% separating gel (10 ml)

2.5 ml	1.5 M Tris-HCl pH 8.6
2.5 ml	40% Acrylamide / Bis-Acrylamide (Bioshop, cat. ACR004.500)
100 µl	10% SDS (Bioshop, cat. SDS002.500)
50 µl	10% APS (Bioshop, cat. AMP001.10)
15 µl	TEMED (Bioshop, cat. TEM001.25)

Western blot 5x loading buffer (10 ml)	
10%	20% SDS (Bioshop, cat. SDS002.500)
0.3125 M	Tris-HCl pH 6.8
25 mM	DTT (Bioshop, cat. DTT001)
25%	Sucrose (Bioshop, cat. SUC600)
	store at -20°C

Western blot 10x SDS-PAGE running buffer (1 l)	
0.25 M	Tris Base (Bioshop, cat. TRS003)
1.92 M	Glycine (Bioshop, cat. GLN001.1)
1%	20% SDS (Bioshop, cat. SDS002.500)

Western blot transfer buffer (1 l)	
25 mM	Tris Base (Bioshop, cat. TRS003)
192 mM	Glycine (Bioshop, cat. GLN001.1)
20%	Methanol pure (Chempur, cat. 116219904)
	store at 4°C

Nematode lysis buffer (50 ml)	
52 mM	Potassium chloride (Bioshop, cat. POC888.500)
10 mM	Tris pH 8.0 (Bioshop, cat. TRS222.500)
2.5 mM	Magnesium chloride (Bioshop, cat. MAG520)
0.45%	10% NP40 (Bioshop, cat. NON505.500)
0.45%	Tween20 (Bioshop, cat. TWN510.100)
0.05%	2% Gelatin (Bioshop)
	store as aliquots at 4°C

1.8. Media for culture bacteria and *C. elegans*

Table 15. Components of bacterial and nematode plates.

LB plates with Ampicillin (1 l)	
20%	LB Broth Lennox (Bioshop, cat. LBL405)
15%	Agar (Bioshop, cat. AGR001)
	autoclave and cool down to 50°C, then add:
100 µg/ml	Ampicillin (Bioshop, cat. AMP201)

LB plates with Ampicillin and Tetracycline (1 l)

20%	LB Broth Lennox (Bioshop, cat. LBL405)
15%	Agar (Bioshop, cat. AGR001)
	autoclave and cool down to 50°C, then add:
100 µg/ml	Ampicillin (Bioshop, cat. AMP201)
12.5 µg/ml	Tetracycline (Bioshop, cat. TET701)

NGM 2% plates (1 l)

20%	Agar (Bioshop, cat. AGR001)
2.5%	Peptone, Bacteriological (Bioshop, cat. PEP403.1)
0.51 mM	Sodium chloride (Bioshop, cat. SOD001)
	autoclave and cool down to 50°C, then add:
5 µg/ml	sterile Cholesterol (Bioshop, cat. CHL500) (in EtOH from POCH, cat. 396420113)
1 mM	sterile Calcium chloride, dihydrate (Bioshop, cat. CCL302.500)
1 mM	sterile Magnesium sulfate (Bioshop, cat. MAG513)
25 mM	sterile Potassium phosphate, pH 6.0
	(132 mM Potassium phosphate dibasic (Bioshop, cat. PPD303.500)
	868 mM Potassium phosphate monobasic (Bioshop, cat. PPM302))
	adjust pH of 1 M Potassium phosphate to 6.0 with 1 M Potassium hydroxide (POCH, cat. P5958))

RNAi plates (1 l)

20%	Agar (Bioshop, cat. AGR001)
2.5%	Peptone, Bacteriological (Bioshop, cat. PEP403.1)
0.51 mM	Sodium chloride (Bioshop, cat. SOD001)
	autoclave and cool down to 50°C, then add:
5 µg/ml	sterile Cholesterol (Bioshop, cat. CHL500) (in EtOH from POCH, cat. 396420113)
1 mM	sterile Calcium chloride, dihydrate (Bioshop, cat. CCL302.500)
1 mM	sterile Magnesium sulphate (Bioshop, cat. MAG513)
25 mM	sterile Potassium phosphate, pH 6.0
	(132 mM Potassium phosphate dibasic (Bioshop, cat. PPD303.500)
	868 mM Potassium phosphate monobasic (Bioshop, cat. PPM302))
	adjust pH of 1 M Potassium phosphate to 6.0 with 1 M Potassium hydroxide (POCH, cat. P5958))
1 mM	IPTG (Blirt, cat. B35) sterile and fresh, covered with aluminum foil
50 µg/ml	Ampicillin (Bioshop, cat. AMP201)

2. Methods

2.1. General animal handling

Animals were grown at 20°C in Hettich incubator on standard 9 cm normal growth medium 2% (NGM 2%) plates made in Integra Mediajet and Mediaclave 10 and seeded with 1 ml of OP50 *E. coli* bacteria cultured overnight in New Brunswick Scientific Exella E24 Incubator Shaker at 37°C 200 rpm (Brenner, 1974). Gravid adults were synchronized by hypochlorite treatment and incubated in 1x M9 buffer overnight on shaker. Synchronized nematodes in L1 stage were counted and a defined number of larvae were transferred to seeded NGM 2% plates or RNAi plates. For all experiments animals were grown to young adult stage.

2.2. Synchronization of nematodes by hypochlorite treatment

Gravid nematodes with many eggs were harvested with 1x M9 buffer in a 15 ml tube, centrifuged at 1600 g for 1 min and the supernatant was removed. After washing in 1x M9 buffer (1 - 3 times) 8 ml of pre-cooled bleaching solution was added to the pellet and the tube was shaken at room temperature (RT) until destruction of adult animals which was monitored under the microscope. Bleaching reaction was stopped by centrifuging at 1600 g for 1 min, removing the supernatant and adding 1x M9 buffer. Pellet was washed 2 times in 1x M9 buffer. After the last wash, pellet was resuspended in 10 ml of 1x M9 buffer and rotated at 20°C overnight. The next morning, synchronized L1 nematodes were counted and a defined number of larvae were transferred to seeded plates.

2.3. Generating double and triple mutant animals

2.3.1. Crossing of strains

Naturally *C. elegans* are self-fertilizing hermaphrodites. In order to cross different strains of *C. elegans*, males were generated by heat shocking nematodes in L4 / young adult stage for 1 h at 37°C in incubator INCU-Line IL10 and transferring them to 25°C. After 3 - 4 days at 25°C, 2% - 5% of animals in the F1 generation developed into males. 20 males from one strain and 10 hermaphrodites in the L4 stage from the other strain were transferred to 3.5 cm NGM 2% plate and incubated for additional 24 h at 25°C. Next day, single hermaphrodites were transferred to a new plate and incubated at 20°C. Animals from the F1 generation were moved to a new plate and incubated at 20°C. Crossing was considered successful if males were visible in the F1 generation. Nematodes from the F2 generation at the L4 stage were separated to a new plate and incubated at 20°C. For strains with deletions, single worm PCR and agarose gel electrophoresis were performed to select a homozygous strain of a specific genotype. For strains with a point mutation, the genotype was confirmed by Sanger Sequencing at the Laboratory of Molecular Biology Techniques at the University of Adam Mickiewicz in Poznan. Obtained strains were added to the database of Ciosk's laboratory with an indicated RAF number. One day starved animals from two 9 cm NGM 2% plates were rinsed with a nematode freezing solution and snap-frozen in a volume of 0.25 ml in cryotubes. Next, tubes were incubated on ice for 15 min and then transferred to -80°C and liquid nitrogen. After a few days of freezing the strain one tube of nematodes was thawn at RT, then the animals were transferred to NGM 2% plates to check if they were able to recover.

2.3.2. Nematode lysis for genotyping

For genotyping, *C. elegans* were lysed in 9.5 µl of nematode lysis buffer supplemented with 0.01 mg/ml Proteinase K dissolved in ddH_2O. Single animal in a gravid stage was put into this solution and spin down for 10 sec. Lysis was performed in a Thermocycler ProFlex PCR System, according to protocol listed in **Table 16**.

Table 16. Nematode lysis protocol.

Temperature	Time	Cycles
65°C	19 min	1
95°C	11 min	1
4°C	∞	

2.3.3. PCR reaction and agarose gel electrophoresis

Primers for standard PCR reaction were designed based on gene sequences available in the UCSC Genome Browser Gateway database. Primers were designed using Primer 3.0 software, by selecting pairs of primers of approximatively 20 base pairs (bp), for which the melting temperatures did not differ more than 2°C. Primers ordered from Sigma Aldrich are listed in **Table 10**. 0.7 µl of the nematode lysate was added to 5 µl of GoTaq G2 Green Master Mix 2x, mixed with 0.3 µl of 10 µM forward primer, 0.3 µl of 10 µM reverse primer and 3.7 µl of nuclease-free H_2O. PCR reaction was performed in a thermocycler ProFlex PCR System, according to protocol described in **Table 17**. Electrophoresis was performed on a 2% agarose gel for products less than 800 bp and on a 1% agarose gel for products longer than 800 bp supplemented with SimplySafe (5 µl / 100 ml of gel) for band visualization. PCR products of the expected size were identified using a control DNA 1 kb Plus DNA Ladder and run for 35 min at 100 mV in 1x tris-acetate-EDTA (TAE) buffer. The agarose gel was scanned using Azure Biosystems c600.

Table 17. PCR thermocycler cycling protocol.

Temperature	Time	Cycles
94°C	1 min	1
94°C	15 sec	35
xx°C	15 sec	
72°C	yy min	
4°C	∞	

xx – the melting point of the primers
yy - time depends on the length of the product, 1 kb of the product requires 1 min

2.4. RNA interference

2.4.1. Preparation of genomic DNA

Wild-type animals from two completely starved 9 cm NGM 2% plates were collected and washed three times with 1x M9 by centrifugation at 1600 g for 1 min. 600 µl of Cell Lysis Solution was added to 100 µl of the nematode pellet and transferred to a 1.5 ml microcentrifuge tube. 20 µl of 20 mg/ml Proteinase K was added, mixed by inverting and incubated at 55°C for about 4 h under agitation, with periodic inversion. 10 mg/ml RNase A was added with a final concentration 40 µg/ml, mixed by inverting and incubated at 37°C for 1 h, with mixing by inversion every 15 min. Then, the sample was incubated on ice for 1 min. 200 µl of Protein Precipitation Solution was added to the lysate, the sample was vortexed for 20 sec at high speed, incubated on ice for 5 min and centrifuged at 15000 g for 10 min at 4°C. The upper phase was transferred to a new 1.5 ml microcentrifuge tube. 600 µl of 99.7% 2-propanol was added, mixed, centrifuged at 15000 g for 15 min at 4°C and the supernatant was removed. The pellet was washed with 1 ml of 70% ethanol and centrifuged at 7500 g for 5 min at 4°C. The pellet was dissolved in 50 µl of nuclease-free H_2O. The concentration of genomic DNA was measured using Nanodrop One C and adjusted to 100 ng/µl.

2.4.2. Preparation of the RNAi bacterial clone for *pept-1* gene

In order to create RNAi bacterial clone for *pept-1*, primers were designed based on the genomic sequence available on UCSC Genome Browser Gateway database (**Table 7**). The primer sequences are listed in **Table 10** and the schematic design of *pept-1* cloning primers is shown in **Figure 52**. The restriction site for XmaI and two additional nucleotides were added at the 5' ends of oligonucleotides to avoid potential problems during PCR amplification. A PCR reaction was performed using 200 ng of genomic DNA in a 50 µl reaction according to the protocol for the Phusion High-Fidelity PCR Kit. The PCR cycle protocol is shown in **Table 18**. After amplification, the expected size of the PCR product was checked during 2% agarose gel electrophoresis ran at 60 V for 45 min in 1x TAE

buffer using a control 1 kb Plus DNA Ladder. The PCR product band stained with SimplySafe (5 µl / 100 ml of gel) was visualized in Azure Biosystems c600, purified by the QIAqiuck PCR Purification Kit and dissolved in 20 µl of nuclease-free H_2O. The vector L4440 shown in **Figure 53** was used to create the RNAi bacterial clone for *pept-1*. L4440 vector and PCR-amplified insert were digested with XmaI restriction enzyme according to the protocol shown in **Table 19**. During ligation, 2.5 µl of nuclease-free H_2O, 1 µl of vector, 1 µl of T4 DNA ligase buffer 10x and 0.5 µl of T4 DNA ligase were added to 5 µl of insert. The reaction mixture was incubated for 1 h at RT and put on ice for 1 min. For transformation, competent *Escherichia coli* DH5α bacteria strain were briefly centrifuged and thawed on ice. 5 µl of ligation reaction was added to 50 µl of thawed DH5α bacteria and incubated on ice for 15 min. Then, mixture was heat shocked at 42°C for 45 sec and put on ice for 1 min. 800 µl of RT LB buffer was added to the sample and incubated at 37°C for 40 min on Thermomixer F1,5 at 300 rpm. After centrifugation of the sample at 500 g for 1 min, 800 µl of supernatant was discarded and the pellet was resuspended in the remaining LB buffer and poured on 9 cm fresh LB plate with Ampicillin. After overnight incubation at 37°C in an incubator INCU-Line IL10, 3 colonies were taken and colony PCR was performed. To 5 µl of GoTaq G2 Green Master Mix 2x, mixed with 0.3 µl of 10 µM forward primer, 0.3 µl of 10 µM reverse primer for *pept-1* clone and 3.7 µl of nuclease-free H_2O, one bacterial colony was added. PCR reaction was performed according to the cycling protocol provided in **Table 20.** After confirming the presence of the insert in the bacterial colony on a 2% agarose gel electophoresis, the same colonies were suspended in 3 mL of LB buffer with 3 µl of 100 mg/ml Ampicillin and 3 µl of 12.5 mg/ml Tetracycline and incubated overnight in New Brunswick Scientific Exella E24 Incubator Shaker at 37°C 200 rpm. The plasmid DNA was isolated using Plasmid Mini Kit and sent for sequencing analysis with forward primer complementary to L4440 vector listed in **Table 10**. Chosen constructs with correctly oriented protein coding DNA fragments were used for further experiments. Bacterial glycerol stock was prepared by mixing 0.5 ml of overnight bacterial culture with 0.5 ml of 50% glycerol and frozen at -80°C.

Figure 52. Scheme presenting primers used for *pept-1* cloning.

Table 18. PCR thermocycler cycling protocol.

Temperature	Time	Cycle
98°C	30 sek	1
98°C	10 sec	2
56°C	30 sec	
72°C	34 sec	
98°C	10 sec	28
67°C	30 sec	
72°C	35 sec	
72°C	10 min	1
4°C	∞	

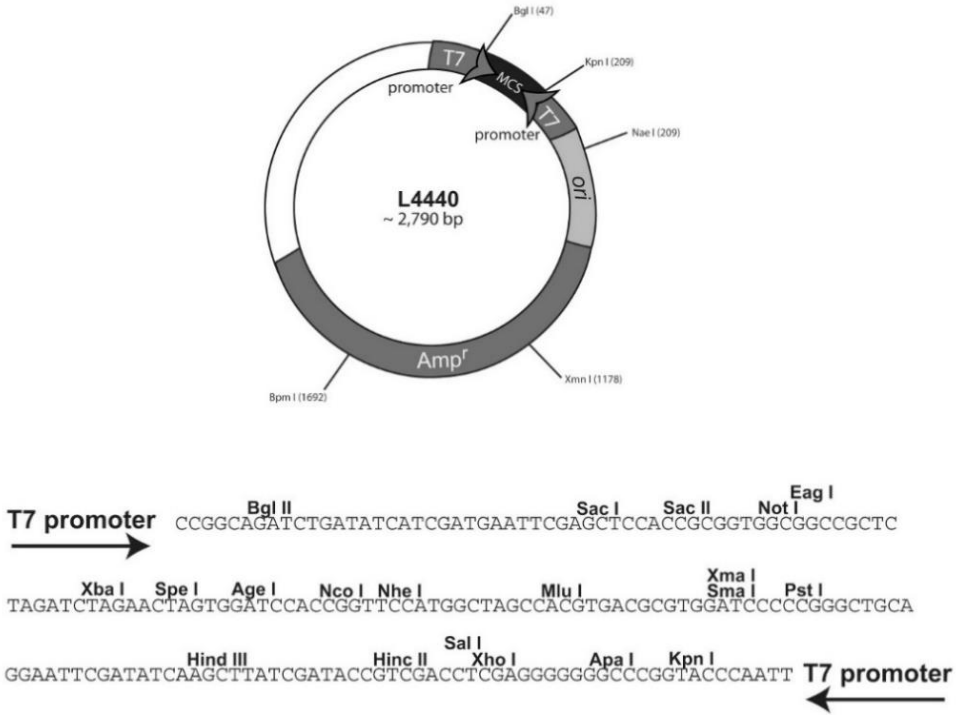

Figure 53. Map of L4440 vector. Image from AddGene.

Table 19. Restriction enzyme digestion protocol**.**

Incubation	Vector L4440	PCR amplified insert
37°C for 1 h	2 µl Cut Smart Buffer	2 µl Cut Smart Buffer
	0.5 µl XmaI	0.5 µl XmaI
	1 µg L4440	17.5 µl insert
50°C for 15 min	1 µl CIP	-
-	Purify with Monarch PCR and DNA Cleanup Kit	Purify with Monarch PCR and DNA Cleanup Kit
-	elute in 20 µl of nuclease-free H_2O	elute in 15 µl of nuclease-free H_2O

Table 20. Colony PCR thermocycler cycling protocol.

Temperature	Time	Cycles
95°C	3 min	1
94°C	1 min	1
94°C	15 sec	35
67°C	15 sec	
72°C	35 sec	
4°C	∞	

2.4.3. Preparation RNAi plates with bacteria from RNAi libraries

RNAi clones from the RNAi libraries (Ahringer or Vidal), listed in **Table 5**, were streaked onto the LB Ampicillin-Tetracycline plates and incubated overnight at 37°C. Next day, a liquid bacterial culture was prepared from 3 bacteria colonies in 3 ml of LB buffer containing 3 µl of 100 mg/ml Ampicillin and 3 µl of 12.5 mg/ml Tetracycline and incubated at 37°C 200 rpm overnight. Plasmid DNA was isolated using Plasmid Mini Kit and sequenced using forward primer for L4440 (**Table 10**). If the sequence of the bacterial clone was correct, mRNA silencing was performed. RNAi bacteria was cultured in 5 ml of LB buffer containing 5 µl of 100 mg/ml Ampicillin and 5 µl of 12.5 mg/ml Tetracycline in New Brunswick Scientific Exella E24 Incubator Shaker at 37°C 200 rpm overnight. Culture was diluted 1:20 in LB buffer containing 100 mg/ml Ampicillin and incubated at 37°C 200 rpm for 4h until an exponential growth phase. 9 cm RNAi plates with 1 mM IPTG

and 50 µg/ml Ampicillin were seeded with 0.5 ml of diluted RNAi bacteria culture. To silence the two mRNAs in animals, both overnight cultures were mixed 1:1 and 0.5 ml of this mixture was applied to RNAi plates. The L4440 (empty) vector was used as a negative RNAi control. *C. elegans* were placed on RNAi plates as L1 larvae and grown until L4 or young adult stage at 20°C protected from light.

2.5. Amino acids sequence alignment

The amino acids sequences of *H. sapiens* Regnase-1 (NM_025079), PEPT1 (NM_005073) and *C. elegans* REGE-1 (NM_059584.7), PEPT-1 (NM_076686.6) were downloaded from UCSC Genome Browser Gateway (**Table 7**). The alignment was performed using the multiple sequence alignment tool ClustalOmega (**Table 7**).

2.6. 3D protein structure

The amino acids sequences of *H. sapiens* Regnase-1 (NM_025079), PEPT1 (NM_005073) and *C. elegans* REGE-1 (NM_059584.7), PEPT-1 (NM_076686.6) were downloaded from UCSC Genome Browser Gateway (**Table 7**). 3D protein structure prediction were made in the program Pyre 2 (**Table 7**) and colored in UCSF Chimera (**Table 7**).

2.7. Oil red O staining

Oil red O staining (ORO) was performed to measure the fat content. 0.5 g of ORO was mixed with 100 ml of 99.7% 2-propanol and stirred for 24 h on Magnetic Stirrer MS11HS Wigo 500 turns / min 20°C, protected from direct light. Solution was filtered through 0.22 µm pore syringe filter, diluted in ddH_2O to 60%, stirred for 12 h and filtered again. Animals were synchronized by hypochlorite treatment and grown on RNAi plates at 20°C to the young adult stage. About 3000 young adult animals were washed off the plates and washed three times with 1x M9 buffer. Animals were fixed with 1 ml of 75% 2-propanol, transferred to 1.5 ml microcentrifuge tube and shaken for 15 min at 1400 g.

After fixation followed by spinning and removal of 2-propanol, animals were suspended in 1 ml of 60% ORO solution and stained for 3 h on a shaker at 1400 g, protected from light. Stained nematodes were washed four times with PBS-T, centrifuged for 1 min at 1600 g, placed on 3% agar pads and imaged on Nikon SMZ25 with DeltaPix color camera and 60x zoom. All image-processing steps were done with the Fiji / imageJ software (Schindelin et al., 2012). The analyzes were performed using photographs containing an image of whole nematode. The calculations were performed in two steps. At first, the signal from the red color was measured. The raw image was converted from RGB to HSB color space, the background was subtracted and then red signal selection was performed through the red pixel threshold for the Hue channel between 0 and 7. The next step was to create a binary mask with the saturation channel and use it for the thresholded image. Image was converted to 32-bit and zero pixel values were replaced by NaN. For further analysis, the integrated density of all remaining pixels was used as the signal coming from the ORO-stained nematode. In the next step, the area of the nematode was calculated. Raw image was converted to 8-bits and background was subtracted. To measure the surface of the nematode, a threshold for 250 was set and the area of the particles larger than 3000 pixels was measured. The signal from red pixels was compared to the animal area. 30 animals were imaged per strain in three biological replicates. Relative fat level was calculated in relation to wild-type animals. Two tailed t-test was used to calculate significance with Graph Pad / Prism 8.

2.8. Triglyceride assay

Total TAG content was determined using Triglyceride Quantification Colorimetric / Fluorometric Kit. Animals were synchronized by hypochlorite treatment and grown on RNAi plates at 20°C to the young adult stage. After collecting 6000 animals and two washes in PBS, the sample was divided into two 15 ml falcons with an equal volume. One part was used to measure the TAG content and the other part was used to measure the amount of protein. The samples were transferred to 1.5 ml protein LoBind tubes using a glass pipet. Samples were centrifuged for 3 min at full speed and 4°C. Sample used for protein quantification was washed with 0.5 ml of PBS and sample used for TAG assay was washed

with 0.5 ml of TAG buffer. After centrifugation for 10 min at full speed at 4°C, buffers were removed using a syringe with a thin needle to have approximately 70 µl of buffer left, frozen in liquid nitrogen and kept at -80°C until lysis. All samples were sonicated using precooled Picoruptor with Minichiller 300 for 30 cycles with 30 sec on and 30 sec off. Samples suspended in PBS were centrifuged for 10 min at full speed at 4°C, diluted 5 times in 0.15 M NaCl and the protein concentration was determined by measuring absorbance at A280 using Nanodrop One C by diluting 2 µl of the sample with 8 µl of 0.15 M NaCl and blank 2 µl PBS with 8 µl of 0.15 M NaCl. For TAG measurement samples were filled to 300 µl with TAG buffer, heated twice to 95°C for 5 min and animal debris was excluded by centrifugation for 10 min at full speed and 4°C. 25 µl of the supernatant were used to assess TAG content according to the manufacturer's protocol. Measurements were performed in biological triplicates and technical duplicates using 96 Well Polystyrene Cell Culture Microplates and Victor Nivo Multiple Plate Reader. Calculations of the TAG level were carried out according to manufacturer's protocol adjusted to the protein content of the sample. Relative TAG level was calculated in relation to wild-type animals fed with bacteria containing an empty vector. Two tailed t-test was used to calculate significance with Graph Pad / Prism 8.

2.9. Visualization of lipid droplets

LDs were visualized through the lipid marker DHS-3 tagged with GFP. The *ldrIs1[dhs-3p::dhs-3::GFP + unc-76(+)]* strain was crossed with the target strain or the mRNA of gene of interest was silenced using RNAi. Animals in the young adult stage were transferred and anesthetized into a drop of 1 M levamisole hydrochloride on 3% agar pads, covered with a cover slip and immediately imaged using Leica confocal microscope with objective 63x and zoom 10x by taking photos from multiple layers and overlaying the images. Pictures were taken next to the vulva, as shown in **Figure 54**, for 5 animals per strain in three biological replicates. The background was removed in LAS X SP8 software. The diameter of the LDs was measured as an average from 30 droplets per strain per one biological replicate in Fiji / imageJ software. Two tailed t-test was used to calculate significance with Graph Pad / Prism 8.

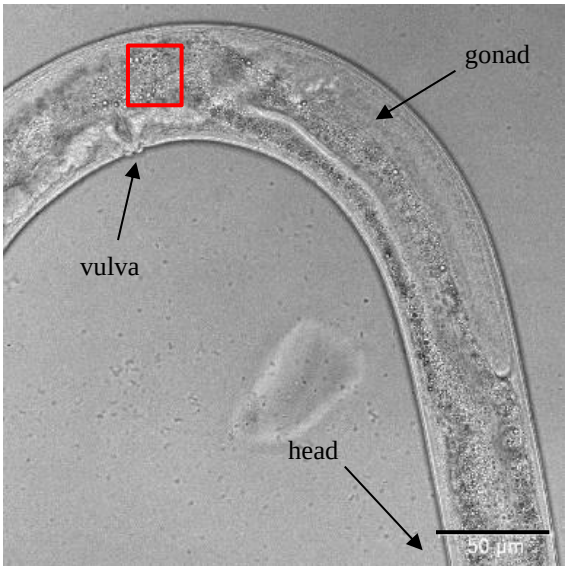

Figure 54. Anatomical localization for imaging of lipid droplets. Picture was taken using 20x with 1x zoom lens. The red frame marks the place where the pictures were taken in order to measure the size of LDs at a magnification of 63x with 10x zoom on Leica confocal microscope. Scale bar represents 50 µm.

2.10. Visualization of PEPT-1::GFP

The localization of PEPT-1 transporter was determined using the *pept-1(syb3497)X* strain where PEPT-1 was tagged with GFP. Animals in young adult stage were transferred and anesthetized into a drop of 1 M levamisole hydrochloride on 3% agar pads, covered with a cover slip and immediately imaged using Leica confocal microscope with objective 63x and zoom 5.8x. 5 animals were imaged per strain in three biological replicates. The background was removed in LAS X SP8 software. The signal location was determined based on information provided in the Worm Atlas.

2.11. Imagining using microscope ZEISS Imager Z2 with Axiocam 506 mono

Animals in the young adult stage were transferred and anesthetized into a drop of 1 M levamisole hydrochloride on 3% agar pads, covered with a cover slip and immediately imaged using microscope ZEISS Imager Z2 with Axiocam 506 mono camera. The localization of MRP-1 transporter was visualized using animals expressing MRP-1 protein tagged with mCherry, *mrp-1b(syb2461)X*, and objective 63x with exposure time 500 ms. The localization of SOD-5 was determined using animals expressing SOD-5 protein

tagged with GFP, *wuIs57[pPD95.77 sod-5::GFP; rol-6(su1006)]*, and objective 63x with exposure time 50 ms. The localization of DAF-16 was determined using animals expressing DAF-16 protein tagged with GFP, *daf-16(syb707)I*, and objective 63x with exposure time 200 ms. The signal location was determined based on information provided in the Worm Atlas (**Table 7**).

2.12. RT-qPCR

2.12.1. Total RNA isolation and cDNA synthesis

Animals were synchronized by hypochlorite treatment, placed on NGM 2% or RNAi plates as L1 larvae and grown to young adult stage at 20°C. After collecting 3000 animals and two washes in 1x M9, samples were re-suspended in 700 µl of Tri Reagent, snap-frozen in liquid nitrogen and kept at -80°C until lysis. Animals were lysed by five freeze-thaw cycles in liquid nitrogen and 42°C. Then, 140 µl of 99.5% chloroform was added to the sample, shaken for 20 sec and left to stand for 2 min at RT. After centrifugation at 12000 g for 10 min at 4°C, 700 µl of upper phase was transferred to a new microcentrifuge tube. RNA purification was performed according to the Direct-zol RNA MicroPrep protocol. 1000 ng (final 50 ng/µl) of RNA was used for reverse transcription according to the manufacturer's protocol using High-Capacity cDNA Reverse Transcription Kit. The protocol for cDNA synthesis performed in ProFlex PCR System thermocycler is shown in the **Table 21.**

Table 21. Protocol used for cDNA synthesis.

Temperature	Time	Cycle
25°C	10 min	1
37°C	120 min	1
85°C	5 min	1
4°C	∞	

2.12.2. RT-qPCR reaction

For RT-qPCR cDNA was diluted 12.5 times (final 4 ng/µl). 4 µl of diluted cDNA, 5 µl of AmplifyMe SG Universal Mix and 0.5 µl of 10 µM forward and reverse primers were mixed and pipetted to a 96 x 0.1 ml Well Plate and sealed with Opti-Seal Optical Sealing Sheet. Primers were designed complementary to the coding sequences available in the UCSC Genome Browser Gateway database (**Table 7**). Primers of approximately 20 bp, with similar annealing temperature (± 2°C), giving a PCR product of approximatively 200 bp, were designed using Primer 3.0 software, and are listed in **Table 11**. Self-dimerization and hairpin formation was checked in the Oligo Calculator software. Primers were ordered from Sigma Aldrich and dissolved in ddH_2O to a final primer concentration of 10 µM. Actin 1 was used as a reference gene. RT-qPCR cycling protocol is shown in **Table 22**. Ct values were calculated using Light Cycler 480 II. Measurements were done in biological and technical triplicates.

Table 22. RT-qPCR thermal protocol.

Temperature	Time	Cycles
95°C	3 min	1
95°C	5 sec	45
60°C	30 sec	
95°C	5 sec	1
70°C	1 min	1
95°C	∞	

2.12.3. Calculations

The ΔΔCt method was used to calculate the relative amount of transcript in tested samples. The difference (Δ) between the Ct of the tested gene and the reference gene, and the difference between the calculated values for the control and research group were determined. The obtained value was substituted into the formula allowing to calculate the fold change (Fc): $Fc = 2^{-\Delta\Delta Ct}$. Two tailed t-test was used to calculate the significance with Graph Pad / Prism 8.

2.13. Western blot

2.13.1. Preparation of the *C. elegans* protein extract

Animals were synchronized by hypochlorite treatment and grown on RNAi plates at 20°C to the young adult stage. 3000 synchronized young adult animals were collected using the 1x M9 buffer, centrifuged at 1600 g for 1 min and pellets were washed three times using the 1x M9 buffer. After the last wash, pellets were centrifuged and washed using cold tris buffered saline (TBS) buffer pH 7.5. Pellets were resuspended in 0.5 ml cold TBS with protease inhibitors and transferred to the 1.5 ml protein LoBind tubes using glass pipets. After centrifugation for 1 min at full speed at 4°C, buffer was removed using a syringe with a thin needle to have approximately 70 µl of buffer, frozen in liquid nitrogen and kept at -80°C until lysis. For lysis, thawed samples were centrifuged for 10 min at full speed at 4°C. Nematodes were sonicated using precooled Picoruptor with Minichiller 300 for 30 cycles, with 30 sec on and 30 sec off, centrifuged for 20 min at full speed at 4°C and the supernatant was transferred to the new tube. The amount of protein was determined using Nanodrop One C by measuring absorbance at A280 (2 µl sample with 8 µl 0.15 M NaCl) with blank (2 µl TBS containing protease inhibitors with 8 µl 0.15 M NaCl).

2.13.2. SDS-polyacrylamide gel electrophoresis (SDS-PAGE)

For protein electrophoresis samples were diluted with cold TBS containing protease inhibitors to obtain 100 µg of proteins in 24 µl mixed with 6 µl of 5x western blot loading buffer. Samples were incubated at 95°C for 5 min, mixed by vortexing, spun down and placed on ice. To separate proteins denaturing 10% polyacrylamide gel with 4% stacking gel on the top was used. Electrophoresis was performed in 1x SDS-PAGE running buffer using 30 µl of sample per well and 6 µl of Page Ruler Plus Prestained Protein Ladder, as a protein size marker, at 90 V for 10 min and 130 V for 1.5 h using Mini Protean Tetra Cell tank.

2.13.3. Semi-dry transfer

After SDS-PAGE gel was washed once with ddH_2O. To activate the 0.2 μm polyvinylidene fluoride membrane (PVDF), it was soaked in methanol for 20 sec. Then, gel, filter papers, PVDF membrane were rinsed with transfer buffer. The gel sandwich was prepared as followed: filter paper, PVDF membrane, gel, filter paper and air bubbles were removed. The transfer was carried out at 1.3 A 25 V for 10 min in Trans – Blot Turbo Transfer System. After transfer, the PVDF membrane was washed 3 times in PBS-T for 5 min on shaker IKA KS 130 Basic with 180 rpm. In the meantime, 5% skim milk was prepared (2.5 g of Skim Milk Powder was dissolved in 50 ml of PBS-T). To prevent the non-specific binding of antibodies, the membrane was incubated with 10 ml of skim milk for 1 h on Mixer MX-T6-S at 45 turns / min. Then, the membrane was incubated with primary antibodies, listed in **Table 23**, diluted in 4 ml of 5% skim milk, overnight at 4°C on a shaker. Next day, the PVDF membrane was washed in PBS-T 3 times for 5 min on a shaker. Then, the membrane was incubated with secondary antibodies, listed in **Table 23,** diluted in 5 ml of 5% skim milk for 1 h on a shaker. The PVDF membrane was washed 3 times in PBS-T for 5 min on a shaker. Femtogram HRP substrate was prepared by mixing 200 μl of Radiance Peroxide with 200 μl of Radiance Plus and applied to the membrane for 2 min. The membrane was scanned in Azure Biosystems c600. Experiments were done in biological triplicates. The relative protein levels were calculated using Image Studio Lite Version 5.2.5. Two tailed t-test were used to calculate significance with Graph Pad / Prism 8. As the PEPT-1 protein size is 94 kDa and the size of the GFP protein is 27 kDa, a band for PEPT-1::GFP of 121 kDa was expected. Antibodies to anti-actin of the size of a protein 42 kDa were used as a control.

Table 23. List of antibodies used in Western blot.

Primary antibodies	Secondary antibodies	Band size
GFP 3:4000	Anti-rabbit 2:5000	27 kDa
Anti-actin, clone C4 2:4000	Anti-mouse 1:5000	42 kDa

2.14. Dipeptide transport activity

Dipeptide transport activity assay was carried out similar as previously reported by *Benner et al. 2011*. Animals were synchronized by hypochlorite treatment, placed on RNAi plates as L1 larvae and grown to L4 stage at 20°C, protected from light. 2000 animals were washed twice in S-basal and divided into two falcons, centrifuged at 2200 g for 3 min and 450 µl of animals' pellet was transferred to new 1.5 ml microcentrifuge tube. 50 µl of 2.5 mM stock solution of the ß – Ala – Lys – AMCA was added to the sample (final concentration 0.25 mM). To the second sample 50 µl of ddH_2O was added as negative control. All samples were incubated for 5 h at 20°C on a rotor, protected from light. Samples were washed four times with S-basal buffer followed by centrifugation at 1600 g for 3 min. 100 µl of the sample was placed per well in a 96 Well Polystyrene Cell Culture Microplates and the fluorescence (Ex: 340 nm, Em: 445 nm) was measured using Victor Nivo Multiple Plate Reader. After measurement, animals were transferred with glass pipet from the 96-well plate to the 1.5 ml protein LoBind tubes and washed two times with PBS followed by centrifugation at full speed for 3 min at 4°C. After the last wash, PBS was removed using a syringe with a thin needle to have approximately 70 µl of buffer, frozen in liquid nitrogen and kept at -80°C until lysis. Thawed samples were sonicated using precooled Picoruptor with Minichiller 300 for 30 cycles, with 30 sec on and 30 sec off, and centrifuged for 20 min at 4°C max speed. The protein concentration was measured by the Bradford method. After subtraction of the autofluorescence, the signal was related to the protein level. Dipeptide uptake was calculated relative to the wild-type fed with bacteria containing an empty vector. The experiment was performed in four biological replicates. Two tailed t-test was used to calculate significance with Graph Pad / Prism 8.

2.15. Determination of protein concentration by the Bradford method

The protein concentration of samples obtained from nematode lysates was determined using colorimetric reaction performed with the Bradford reagent (Bradford, 1976). A standard curve of known concentrations of bovine serum albumin (BSA) was prepared as follows: 0 µg/ml, 125 µg/ml, 250 µg/ml, 500 µg/ml, 750 µg/ml, 1000 µg/ml by mixing 50 µl of diluted BSA with 450 µl of Bradford reagent in 1.5 ml Semi-Micro Disposable

Cuvettes. The samples were prepared accordingly: 35 µl of 0.15 M NaCl, 15 µl of the tested sample and 450 µl of Bradford reagent. The measurements were made using a spectrophotometer Nanodrop One C at a wavelength of λ= 595 nm.

2.16. Oxygen consumption rate (OCR)

2.16.1. Preparation of samples

To determine OCR in *C. elegans,* animals were synchronized by hypochlorite treatment. 3000 animals were placed on RNAi plates as L1 larvae and were grown to the young adult stage at 20°C, protected from light. To test stress conditions like starvation, where there is a reduction in oxygen consumption, wild-type animals fed with bacteria carrying an empty vector were incubated at 20°C until the late L4 stage, then the nematodes were washed three times in 1x M9, centrifuged for 1 min at 1600 g and transferred to RNAi plates without bacteria for a further 4 h in 20°C. Animals were washed three times in 1x M9 followed by centrifugation at 1600 g for 1 min.

2.16.2. Preparation of the chamber and calibration

Cigarette paper and polytetrafluorethylene (PTFE) membrane were cut into 1.5 cm^2 pieces. On top of the dome of the electrode, a drop of KCl, a piece of cigarette paper and PTFE membrane were placed. A small O-ring and a large O-ring were placed around the electrode, and the electrode was connected to both the electrode chamber and to the control unit. The water bath was set to 25°C and connected to the electrode chamber. To calibrate the electrode, the chamber was rinsed twice with sterilized distilled water and 1 ml of 1x M9 at the same temperature (25°C). In the OxyTrace+ program, the temperature was set to 25°C and the stirrer was turned on. In order to establish zero oxygen condition, sodium hydrosulfite (Sigma Aldrich, cat. 71699) was added until the oxygraph reached a plateau. After successful calibration, the chamber was rinsed with 60% ethanol and water, and then a new electrode membrane was prepared in the same manner as described above.

2.16.3. OCR measurement

1 ml of nematodes pellet was transferred to the electrode chamber, stirring was turned on and oxygen consumption was measured for 5 min. After the measurement, nematodes were collected from the chamber into a 15 ml falcon tube with 1x M9 buffer, washed three times in PBS followed by 3 min centrifugation at 2500 g and transferred with a glass pipet into 1.5 ml protein LoBind tubes. After the last centrifugation, at full speed for 10 min at 4°C, PBS was removed using a syringe with a thin needle to have approximately 70 µl of buffer, frozen in liquid nitrogen and kept at -80°C until lysis. Thawed samples were sonicated using precooled Picoruptor with Minichiller 300 for 30 cycles, with 30 sec on and 30 sec off, and centrifuged for 20 min at 4°C max speed. The protein concentration was measured by the Bradford method. The oxygen consumption slope was divided by the amount of protein (nmol / min / ml / mg). OCR was calculated relative to the wild-type animals fed with bacteria carrying an empty vector. The experiment was performed in three biological repeats with three technical replicates per strain. Two tailed t-test was used to calculate the significance with Graph Pad / Prism 8.

REFERENCES

Albertson D. G. and Thomson J. N., (1976). "The pharynx of *Caenorhabditis elegans*". Philosophical Transactions of the Royal Society B: Biological Sciences, 275(938), 299 – 325.

Alghamdi O. A., King N., Jones G. L. and Moens P. D. J., (2017). "A new use of β-Ala-Lys (AMCA) as a transport reporter for PEPT1 and PEPT2 in renal brush border membrane vesicles from the outer cortex and outer medulla". Biochimica et Biophysica Acta (BBA) - Biomembranes, 1860(5), 960 – 964.

Allman E., Johnson D. and Nehrke K., (2009). "Loss of the apical V-ATPase a-subunit VHA-6 prevents acidification of the intestinal lumen during a rhythmic behavior in *C. elegans*". Am J Physiol Cell Physiol, 297, C1071 – C1081.

Ames G. E.-L. and Lecar H., (1992). "ATP-dependent bacterial transporters and cystic fibrosis: analogy between channels and transporters". FASEB J., 6, 2660 - 2666.

An J. H. and Blackwell T. K., (2003). "SKN-1 links *C. elegans* mesendodermal specification to a conserved oxidative stress response". Genes & development, 17(15), 1882 – 1893.

Anantharaman V. and Aravind L., (2006). 'The NYN domains: novel predicted RNAses with a PIN domain-like fold". RNA Biol, 3(1), 18 - 27.

Antebi A., (2015). "Nuclear receptor signal transduction in *C. elegans*". WormBook, 9, 1 - 49.

Apfeld J., O'Connor G., McDonagh T., DiStefano P. S. and Curtis R., (2004). "The AMP-activated protein kinase AAK-2 links energy levels and insulin-like signals to lifespan in *C. elegans*". Genes & development, 18(24), 3004 – 3009.

Aranaz P., Navarro-Herrera D., Zabala M., Romo-Hualde A., López-Yoldi M., Vizmanos J. L., Milagro F. I. and González-Navarro C. J., (2020). "Phenolic compounds reduce the fat content in *Caenorhabditis elegans* by affecting lipogenesis, lipolysis and different stress responses". Pharmaceuticals, 13(11), 355.

Ashrafi K., Chang F. Y., Watts J. L., Fraser A. G., Kamath R. S., Ahringer J., Ruvkun G., (2003). "Genome-wide RNAi analysis of *Caenorhabditis elegans* fat regulatory genes". Nature, 421(6920), 268 – 272.

Ashrafi K., (2007). "Obesity and the regulation of fat metabolism". Wormbook, 1 - 20.

Avery L. and Horvitz H. R., (1990). "Effects of starvation and neuroactive drugs on feeding in *Caenorhabditis elegans*". J. Exp. Zool., 253(3), 263 - 270.

Aye I. L. M. H., Singh A. T. and Keelan J. A., (2009). "Transport of lipids by ABC proteins: interactions and implications for cellular toxicity, viability and function". Chemico-Biological Interactions, 180(3), 327 – 339.

Bahrami A. K. and Zhang Y., (2013). "When females produce sperm: genetics of *C. elegans* hermaphrodite reproductive choice". G3: Genes, Genomes, Genetics, 3(10), 1851 - 1859.

Bar D. Z., Charar C., Dorfman J., Yadid T., Tafforeau L., Lafontaine D. L. J. and Gruenbaum Y., (2016). "Cell size and fat content of dietary-restricted *Caenorhabditis elegans* are regulated by ATX-2, an mTOR repressor". PNAS, 113(32), e4620 – e4629.

Baset H. A., Ford-Hutchinson A. W. and O'Neill G. P., (1998). "Molecular cloning and functional expression of a *Caenorhabditis elegans* aminopeptidase structurally related to mammalian leukotriene A4 hydrolases". The Journal Of Biological Chemistry, 273(43), 27978 – 27987.

Beg A. A., Ernstrom G. G., Nix P., Davis M. W. and Jorgensen E. M., (2008). "Protons act as a transmitter for muscle contraction in *C. elegans*". Cell, 149 – 160.

Bendsen N. T., Hother A. L., Jensen S. K., Lorenzen J. K. and Astrup A., (2008). "Effect of dairy calcium on fecal fat excretion: a randomized crossover trial". Int J Obes (Lond), 32(12), 1816 - 1824.

Benner J., Daniel H. and Spanier B., (2011). "A glutathione peroxidase, intracellular peptidases and the TOR complexes regulate peptide transporter PEPT-1 in *C. elegans*". PLoS ONE, 6(9), e25624.

Benomar S., Lansdon P., Bender A. M., Peterson B. R., Chandler J. R. and Ackley B. D., (2020). "The *C. elegans* CHP1 homolog, *pbo-1*, functions in innate immunity by regulating the pH of the intestinal lumen". PLoS Pathog, 16(1), e1008134.

Blachnio-Zabielska A. U., Koutsari C., Tchkonia T. and Jensen M. D., (2012). "Sphingolipid content of human adipose tissue: relationship to adiponectin and insulin resistance". Obesity (Silver Spring, Md.), 20(12), 2341 – 2347.

Bolla R., (1979). "Developmental nutrition of nematodes: the biochemical role of sterols, heme compounds, and lysosomal enzymes". Journal of Nematology, 11(3), 250 - 259.

Bolm M., Jansen W. T., Schnabel R. and Chhatwal G. S., (2004). "Hydrogen peroxide-mediated killing of *Caenorhabditis elegans*: a common feature of different streptococcal species". Infect. Immun., 72, 1192 – 1194.

Bradford M. M., (1976). "A rapid and sensitive method for the quantitation of microgram quantities of protein utilizing the principle of protein-dye binding". Analytical Biochemistry, 72(1-2), 248 – 254.

Brandsch M., (2013). "Drug transport via the intestinal peptide transporter PepT1". Current Opinion in Pharmacology, 13(6), 881 – 887.

Brenner S., (1974). "The genetics of *Caenorhabditis elegans*". Genetics, 71 – 94.

Brock T. J., Browse J. and Watts J. L., (2006). "Genetic regulation of unsaturated fatty acid composition in *C. elegans*". PLoS Genetics, 2(7), e108.

Brock T. J., Browse J. and Watts J. L., (2007). "Fatty acid desaturation and the regulation of adiposity in *Caenorhabditis elegans*". Genetics, 176(2), 865 – 875.

Broeks A., Gerrard B., Allikmets R., Dean M. and Plasterk R. H., (1996). "Homologues of the human multidrug resistance genes MRP and MDR contribute to heavy metal resistance in the soil nematode *Caenorhabditis elegans*". EMBO J., 15, 6132 – 6143.

Brooks K. K., Liang B. and Watts J. L., (2009). "The influence of bacterial diet on fat storage in *C. elegans*". PLoS ONE, 4(10), e7545.

Bugianesi E., McCullough A. J. and Marchesini G., (2005). "Insulin resistance: a metabolic pathway to chronic liver disease". Hepatology, 42(5), 987 – 1000.

Buis A., Bellemin S., Goudeau J., Monnier L., Loiseau N., Guillou H. and Aguilaniu H., (2019)." Coelomocytes regulate starvation-induced fat catabolism and lifespan extension through the lipase LIPL-5 in *Caenorhabditis elegans*". Cell Reports 28, 1041 – 1049.

Buyse M., Berlioz F., Guilmeau S., Tsocas A., Voisin T., Péranzi G., Merlin D., Laburthe M., Lewin M. J. M., Rozé C. and Bado A., (2001). "PepT1-mediated epithelial transport of dipeptides and cephalexin is enhanced by luminal leptin in the small intestine". J. Clin. Invest., 108(10), 1483 – 1494.

Calder P. C., (2015). "Functional roles of fatty acids and their effects on human health". Journal of Parenteral and Enteral Nutrition, 39(1), 18 – 32.

Calzada E., Onguka O. and Claypool S. M., (2016). "Phosphatidylethanolamine metabolism in health and disease". International Review of Cell and Molecular Biology, 321, 29 – 88.

Cao Z., Hao Y., Fung C. W., Lee Y. Y., Wang P., Li X., Xie K., Lam W. J., Qiu Y., Tang B. Z., et al., (2019). "Dietary fatty acids promote lipid droplet diversity through seipin enrichment in an ER subdomain". Nature Communications, 10(1), 2902.

Cartwright T. A., Campos C. R., Cannon R. E. and Miller D. S., (2013). „Mrp1 is essential for sphingolipid signaling to p-glycoprotein in mouse blood–brain and blood–spinal cord barriers". Journal of Cerebral Blood Flow & Metabolism, 33(3), 381 – 388.

Casares D., Escribá P. V. and Rosselló C. A., (2019). "Membrane lipid composition: effect on membrane and organelle structure, function and compartmentalization and therapeutic avenues". International journal of molecular sciences, 20(9), 2167.

Chan J. P., Brown J., Hark B., Nolan A., Servello D., Hrobuchak H. and Staab T. A., (2017). "Loss of sphingosine kinase alters life history traits and locomotor function in *Caenorhabditis elegans*". Frontiers in Genetics, 8, 132.

Chasnov J. R., (2013). “The evolutionary role of males in *C. elegans*”. Worm, 2(1), e21146.

Chavez V., Mohri-Shiomi A., Maadani A., Vega L. A. and Garsin D. A., (2007). “Oxidative stress enzymes are required for DAF-16-mediated immunity due to generation of reactive oxygen species by *Caenorhabditis elegans*”. Genetics, 176, 1567 - 1577.

Chen G., Korfhagen T. R., Xu Y., Kitzmiller J., Wert S. E., Maeda Y., Gregorieff A., Clevers H. and Whitsett J. A., (2009). “SPDEF is required for mouse pulmonary goblet cell differentiation and regulates a network of genes associated with mucus production”. The Journal of clinical investigation, 119(10), 2914 – 2924.

Chen W.-W., Yi Y.-H., Chien C.-H., Hsiung K.-C., Ma T.-H., Lin Y.-C., Lo S. J., Chang T.-C., (2016). “Specific polyunsaturated fatty acids modulate lipid delivery and oocyte development in *C. elegans* revealed by molecular-selective label-free imaging”. Scientific Reports, 6(1), 32021.

Cheng X., Jiang X., Tam K. Y., Li G., Zheng J. and Zhang H., (2019). “Sphingolipidomic analysis of *C. elegans* reveals development- and environment-dependent metabolic features”. International journal of biological sciences, 15(13), 2897 – 2910.

Chiang S.-H. and MacDougald O. A., (2003). "Will fatty worms help cure human obesity?". Trends Genet, 19(10), 523 - 525.

Choi S. and Snider A. J., (2015). "Sphingolipids in high fat diet and obesity-related diseases". Mediators of Inflammation, 2015(520618), 1 - 12.

Choi M.-K., Son S., Hong M., Choi M. S., Kwon J. Y. and Lee J., (2016). “Maintenance of membrane integrity and permeability depends on a patched-related protein in *Caenorhabditis elegans*”. Genetics, 202(4), 1411 – 1420.

Clifford D. and Repine J., (1982). “Hydrogen peroxide mediated killing of bacteria”. Molecular and Cellular Biochemistry, 49(3), 143 - 149.

Cohen E. and Dillin A., (2008). “The insulin paradox: aging, proteotoxicity and neurodegeneration”. Nature Reviews Neuroscience, 9(10), 759 – 767.

Cole S. P. C., Bhardwaj G., Gerlach J., Mackie J., Grant C., Almquist K., Stewart A. J., Kurz E. U., Duncan A. M. V. and Deeley R., (1992). “Overexpression of a transporter gene in a multidrug-resistant human lung cancer cell line”. Science, 258(5088), 1650 – 1654.

Cole S. P. C., (2014). “Targeting Multidrug Resistance Protein 1 (MRP1, ABCC1): past, present, and future”. Annu. Rev. Pharmacol. Toxicol., 54, 95 – 117.

Corsi A. K., (2006). “A biochemist’s guide to *C. elegans”.* Anal Biochem, 359(1), 1 – 17.

Corsi A. K., Wightman B. and Chalfie M., (2015). "A Transparent window into biology: A primer on *Caenorhabditis elegans*". WormBook, ed. The *C. elegans* Research Community, WormBook.

Coulondre C. and Miller J. H., (1977). "Genetic studies of the lac repressor. III. Additional correlation of mutational sites with specific amino acid residues". Journal of Molecular Biology, 117(3), 525 – 567.

Cyr N. E., Wikelski M. and Romero L. M., (2008). "Increased energy expenditure but decreased stress responsiveness during molt". Physiological And Biochemical Zoology, 81(4), 452 – 462.

Dalfó D., Michaelson D. and Hubbard E. J. A., (2012). "Sensory regulation of the *C. elegans* germline through TGF-β-dependent signaling in the niche". Current Biology, 22(8), 712 – 719.

Dal Santo P., Logan M. A., Chisholm A. D. and Jorgensen E. M., (1999). "The inositol trisphosphate receptor regulates a 50-second behavioral rhythm in *C. elegans*". Cell 98, 757 – 767.

Daniel H., Spanier B., Kottra G. and Weitz D., (2006). "From bacteria to man: archaic proton-dependent peptide transporters at work". Physiology, 21, 93 – 102.

Dean M., (1995). "Evolution of ATP-binding cassette transporter genes". Current Opinion in Genetics & Development, 5(6), 779 – 785.

Deevska G. M., Rozenova K. A., Giltiay N. V., Chambers M. A., White J., Boyanovsky B. B., Wei J., Daugherty A., Smart E. J., Reid M. B., et al., (2009). "Acid sphingomyelinase deficiency prevents diet-induced hepatic triacylglycerol accumulation and hyperglycemia in mice". The Journal of biological chemistry, 284(13), 8359 – 8368.

Deevska G. M. and Nikolova-Karakashian, (2017). "The expanding role of sphingolipids in lipid droplet biogenesis". Biochimica et Biophysica Acta (BBA) - Molecular and Cell Biology of Lipids, 1862(10), 1155 – 1165.

Deevska G. M., Dotson P. P., Karakashian A. A., Isaac G., Wrona M., Kelly S. B., Merrill A. H. Jr. and Nikolova-Karakashian M. N., (2017). "Novel interconnections in lipid metabolism revealed by overexpression of sphingomyelin synthase-1". The Journal of Biological Chemistry, 292(12), 5110 - 5122.

De Pauw A., Demine S., Tejerina S., Dieu M., Delaive E., Kel A., Renard P., Raes M. and Arnould T., (2012). "Mild mitochondrial uncoupling does not affect mitochondrial biogenesis but downregulates pyruvate carboxylase in adipocytes: role for triglyceride content reduction". American Journal of Physiology-Endocrinology and Metabolism, 302(9), e1123 – e1141.

Depeille P., Cuq P., Passagne I., Evrard A. and Vian L., (2005). "Combined effects of GSTP1 and MRP1 in melanoma drug resistance". British journal of cancer, 93(2), 216 – 223.

Dilberger B., Baumanns S., Schmitt F., Schmiedl T., Hardt M., Wenzel U. and Eckert G. P., (2019). "Mitochondrial oxidative stress impairs energy metabolism and reduces stress resistance and longevity of *C. elegans*". Oxidative Medicine and Cellular Longevity, 1 – 14.

Doonan R., McElwee J. J., Matthijssens F., Walker G. A., Houthoofd K., Back P., Matscheski A., Vanfleteren J. R. and Gems D., (2008). "Against the oxidative damage theory of aging: superoxide dismutases protect against oxidative stress but have little or no effect on life span in *Caenorhabditis elegans*". Genes Dev, 22(23), 3236 -3241.

Dowen R. H., Breen P. C., Tullius T., Conery A. L. and Ruvkun G., (2016). "A microRNA program in the *C. elegans* hypodermis couples to intestinal mTORC2/PQM-1 signaling to modulate fat transport". Genes & Development, 30,1515 – 1528.

Dranse H. J., Waise T. M. Z., Hamr S. C., Bauer P. V., Abraham M. A., Rasmussen B. A. and Lam T. K. T., (2018). "Physiological and therapeutic regulation of glucose homeostasis by upper small intestinal PepT1-mediated protein sensing". Nature Communications, 9(1), 1118.

El-Kabbani O., Darmanin C. and Chung R., (2004). "Sorbitol dehydrogenase: structure, function and ligand design". Current Medicinal Chemistry, 11(4), 465 – 476.

Engelmann B., Streich S., Schönthier U. M., Richter W. O. and Duhm J., (1992). "Changes of membrane phospholipid composition of human erythrocytes in hyperlipidemias. Increased phosphatidylcholine and reduced sphingomyelin in patients with elevated levels of triacylglycerol-rich lipoproteins". Biochimica et Biophysica Acta (BBA) - Lipids and Lipid Metabolism, 1165(1), 32 – 37.

Escorcia W., Ruter D. L., Nhan J. and Curran S. P., (2018). "Quantification of lipid abundance and evaluation of lipid distribution in *Caenorhabditis elegans* by Nile Red and Oil Red O staining". Journal of visualized experiments : JoVE, (133), 57352.

Espelt M. V., Estevez A. Y., Yin X. and Strange K., (2005). "Oscillatory Ca^{2+} signaling in the isolated *Caenorhabditis elegans* intestine: role of the inositol-1,4,5-trisphosphate receptor and phospholipases C beta and gamma". The Journal of general physiology, 126(4), 379 – 392.

Ewald C. Y., Castillo-Quan J. I. and Blackwell T. K., (2017). "Untangling longevity, dauer, and healthspan in *Caenorhabditis elegans* Insulin/IGF-1-signalling". Gerontology, 64(1), 96 – 104.

Felix M.-A. and Braendle C., (2010). "The natural history of *Caenorhabditis elegans*". Curr. Biol., 20(22), R965 - R969.

Flens M. J., Izquerido M. A., Scheffer G. L., Fritz J. M., Meijer C. J. L. M., Scheper R. J. and Zaman G. J. R., (1994). "Immunochemical detection of the multidrug resistance-associated protein MRP in human multidrug-resistant tumor cells by monoclonal antibodies". Cancer Res. 54(17), 4557 – 4563.

Gamsjaeger R., Liew C., Loughlin F., Crossley M. and Mackay J., (2007). "Sticky fingers: zinc-fingers as protein-recognition motifs". Trends in Biochemical Sciences, 32(2), 63 – 70.

Ganapathy V. and Leibach F. H., (1983). "Role of pH gradient and membrane potential in dipeptide transport in intestinal and renal brush-border membrane vesicles from the rabbit. Studies with L-carnosine and glycyl-L-proline". J Biol Chem, 258(23), 14189 – 14192.

Ganapathy M. E., Brandsch M., Prasad P. D., Ganapathy V. and Leibach F. H., (1995). „Differential recognition of b-lactam antibiotics by intestinal and renal peptide transporters, PEPT 1 and PEPT 2". The Journal Of Biological Chemistry, 270(43), 25672 – 25677.

Gao M., Cui H. R., Loe D. W., Grant C. E., Almquist K. C., Cole S. P. and Deeley R. G., (2000). "Comparison of the functional characteristics of the nucleotide binding domains of multidrug resistance protein 1". J. Biol. Chem., 275(17), 13098 - 13108.

Garg A., Roske Y., Yamada S., Uehata T., Takeuchi O. and Heinemann U., (2021). "PIN and CCCH Zn-finger domains coordinate RNA targeting in ZC3H12 family endoribonucleases". Nucleic Acids Res, 49(9), 5369 - 5381.

Geillinger K. E., (2012). "Transcriptional regulation of the peptide transporter 1 and its role in development in Caenorhabditis elegans assessed by proteome analysis". Unpublished data from PhD thesis.

Geillinger K. E., Kipp A. P., Schink K., Röder P. V., Spanier B. and Daniel H., (2014). "Nrf2 regulates the expression of the peptide transporter PEPT1 in the human colon carcinoma cell line Caco-2". Biochimica et Biophysica Acta (BBA) - General Subjects, 1840(6), 1747 – 1754.

Gillies P. and Robinson C., (1988). "Decreased plasma membrane fluidity in the development of atherosclerosis in cholesterol-fed rabbits". Atherosclerosis, 70(1 - 2), 161 – 164.

Goberdhan D. C., Ogmundsdóttir M. H., Kazi S., Reynolds B., Visvalingam S. M., Wilson C. and Boyd C. A., (2009). "Amino acid sensing and mTOR regulation: inside or out?" Biochem Soc Trans, 37(1), 248 - 252.

Goncharova E. A., (2013). "mTOR and vascular remodeling in lung diseases: current challenges and therapeutic prospects". The FASEB Journal, 27(5), 1796 – 1807.

Gonzalez A., Hall M. N., Lin S.-C. and Hardie D. G., (2020). "AMPK and TOR: The yin and yang of cellular nutrient sensing and growth control". Cell Metabolism, 31(3), 472 – 492.

Gray J. M., Hill J. J. and Bargmann C. I., (2005). "A circuit for navigation in *Caenorhabditis elegans*". Proc Natl Acad Sci USA, 102(9), 3184 - 3191.

Green R. A., Audhya A., Pozniakovsky A., Dammermann A., Pemble H., Monen J., Portier N., Hyman A., Desai A. and Oegema K., (2008). "Expression and imaging of fluorescent proteins in the *C. elegans* gonad and early embryo". Methods in Cell Biology, 179– 218.

Greer E. L., Dowlatshahi D., Banko M. R., Villen J., Hoang K., Blanchard D., Gygi S. P. and Brunet A., (2007). "An AMPK-FOXO pathway mediates longevity induced by a novel method of dietary restriction in *C. elegans*". Current Biology, 17(19), 1646 – 1656.

Greer E. R., Perez C. L., Van Gilst M. R., Lee B. H. and Ashrafi K., (2008). "Neural and molecular dissection of a *C. elegans* sensory circuit that regulates fat and feeding". Cell Metab, 8(2), 118 – 131.

Gumucio J. P., Qasawa A. H., Ferrara P. J., Malik A. N., Funai K., McDonagh B. and Mendias C. L., (2019). "Reduced mitochondrial lipid oxidation leads to fat accumulation in myosteatosis". FASEB journal : official publication of the Federation of American Societies for Experimental Biology, 33(7), 7863 – 7881.

Gusarov I., Pani B., Gautier L., Smolentseva O., Eremina S., Shamovsky I., Katkova-Zhukotskaya O., Mironov A. and Nudler E., (2017). "Glycogen controls *Caenorhabditis elegans* lifespan and resistance to oxidative stress". Nature communications, 8, 15868.

Habacher C., Yanwu G., Venz R., Kumari P., Neagu A., Gaidatzis D., Harvald E. B., Færgeman N. J., Gut H. and Ciosk R., (2016). "Ribonuclease-mediated control of body fat". Developmental Cell, 39(3), 359 – 369.

Habacher C. and Ciosk R., (2017). "ZC3H12A/MCPIP1/Regnase-1-related endonucleases: An evolutionary perspective on molecular mechanisms and biological functions". Bioessays, 39(9), 1700051.

Habacher C., (2018). „An auto-regulatory module controls fat metabolism in *Caenorhabditis elegans*". PhD thesis, unpublished data.

Hänel V., Pendleton C. and Witting M., (2019). "The sphingolipidome of the model organism *Caenorhabditis elegans*". Chemistry and Physics of Lipids, 222, 15 - 22.

Hansen M., Flatt T. and Aguilaniu H., (2013). "Reproduction, fat metabolism, and life span: what is the connection?". Cell metabolism, 17(1), 10 – 19.

Harrison R. A. and Vickers S. E., (1990). "Use of fluorescent probes to assess membrane integrity in mammalian spermatozoa". J. Reprod. Fertil., 88(1), 343 – 352.

Hashimoto T., Igarashi J. and Kosaka H., (2009). "Sphingosine kinase is induced in mouse 3T3-L1 cells and promotes adipogenesis". Journal of lipid research, 50(4), 602 – 610.

Heimbucher T., Hog J., Gupta P. and Murphy C. T, (2020). "PQM-1 controls hypoxic survival via regulation of lipid metabolism". Nature Communications, 11(1), 4627.

Hellerer T., Axang C., Brackmann C., Hillertz P., Pilon M. and Enejder A., (2007). "Monitoring of lipid storage in *Caenorhabditis elegans* using coherent anti-Stokes Raman scattering (CARS) microscopy". Proc. Natl. Acad. Sci. USA, 104(37), 14658 - 14663.

Hibshman J. D., Leuthner T. C., Shoben C., Mello D. F., Sherwood D. R., Meyer J. N. and Baugh L. R., (2018). "Non-selective autophagy reduces mitochondrial content during starvation in *Caenorhabditis elegans*". American Journal of Physiology-Cell Physiology, 315(6), C781 - C792.

Hindlet P., Bado A., Kamenicky P., Delomenie C., Bourasset F., Nazaret C., Farinotti R. and Buyse M., (2009). "Reduced intestinal absorption of dipeptides via PepT1 in mice with diet-induced obesity is Associated with leptin receptor down-regulation". The Journal of Biological Chemistry, 284(11), 6801 – 6808.

Hodgkin J., Horvitz H. R. and Brenner S., (1979). "Nondisjunction mutants of the nematode *Caenorhabditis elegans*." Genetics, 91(1), 67 - 94.

Hodgkin J., (1983). "Male phenotypes and mating efficiency in *Caenorhabditis elegans*". Genetics, 103(1), 43 - 64.

Horikawa M. and Sakamoto K., (2010). "Polyunsaturated fatty acids are involved in regulatory mechanism of fatty acid homeostasis via daf-2/insulin signaling in *Caenorhabditis elegans*". Molecular and Cellular Endocrinology, 323(2), 183 – 192.

Horst D., Gu X., Bhasin M., Yang Q., Verzi M., Lin D., Joseph M., Zhang X., Chen W., Li Y.-P., et al., (2010). "Requirement of the epithelium-specific Ets transcription factor SPDEF for mucous gland cell function in the gastric antrum". Journal of Biological Chemistry, 285(45), 35047 – 35055.

Huvenne H. and Dubern B., (2014). "Monogenic forms of obesity". Molecular Mechanisms Underpinning the Development of Obesity, 9 – 21.

Hyde S. C., Emsley P., Hartshorn M. J., Mimmack M. M., Gileadi U., Pearce S. R., Mimmack M. M., Gileadi U., Pearce S. R., Gallagher M. P., et al., (1990). "Structural model of ATP-binding proteing associated with cystic fibrosis, multidrug resistance and bacterial transport". Nature, 346(6282), 362 – 365.

Iram S. H. and Cole S. P. C., (2011). "Expression and function of human MRP1 (ABCC1) is dependent on amino acids in cytoplasmic loop 5 and its interface with nucleotide binding domain 2". The Journal Of Biological Chemistry, 286(9), 7202 – 7213.

Iyer J., DeVaul N., Hansen T. and Nebenfuehr B., (2018). "Using microinjection to generate genetically modified *Caenorhabditis elegans* by CRISPR/Cas9 editing". Microinjection, 1874, 431 – 457.

Jedlitschky G., Leier I., Buchholz U., Barnouin K., Kurz G. and Keppler D., (1996). "Transport of glutathione, glucuronate, and sulfate conjugates by the MRP gene-encoded conjugate export pump". Cancer Research, 56, 988 - 994.

Ji L., Li H., Gao P., Shang G., Zhang D. D., Zhang N. and Jiang T., (2013). "NRF2 pathway regulates multidrug-resistance associated protein 1 in small cell lung cancer." PLoS ONE, 8(5), e63404.

Jo H., Shim J., Lee J. H., Lee J. and Kim J. B., (2009). "IRE-1 and HSP-4 contribute to energy homeostasis via fasting-induced lipases in *C. elegans*". Cell Metabolism, 9(5), 440 – 448.

Johansen M. R. and Færgeman N. J., (2018). "A stable isotope labelling approach for analysis of metabolism in metazoans with abnormal lipid storage". Unpublished master thesis.

Johnson D. and Nehrke K., (2010). "Mitochondrial fragmentation leads to intracellular acidification in *Caenorhabditis elegans* and mammalian cells". Mol. Biol. Cell, 21, 2191 - 2201.

Jones P. M. and George A. M., (1999). "Subunit interactions in ABC transporters: towards a functional architecture". FEMS Microbiology Letters, 179(2), 187 – 202.

Jones K. T., Greer E. R., Pearce D. and Ashrafi K., (2009). "Rictor/TORC2 regulates *Caenorhabditis elegans* fat storage, body size and development through *sgk-1*". PLoS Biology, 7(3), e1000060.

Jones S. E., Whitehead K., Saulnier D., Thomas C. M., Versalovic J. and Britton R. A., (2011). "Cyclopropane fatty acid synthase mutants of probiotic human-derived *Lactobacillus reuteri* are defective in TNF inhibition". Gut Microbes, 2(2), 69 - 79.

Kahn-Kirby A. H., Dantzker J. L. M., Apicella A. J., Schafer W. R., Browse J., Bargmann C. I. and Watts J. L., (2004). "Specific polyunsaturated fatty acids drive TRPV-dependent sensory signaling *in vivo*". Cell, 119, 889 – 900.

Kao Y. C., Ho P. C., Tu Y. K., Jou I. M. and Tsai K. J., (2020). "Lipids and Alzheimer's disease". International journal of molecular sciences, 21(4), 1505.

Kaul T. K., Reis Rodrigues P., Ogungbe I. V., Kapahi P. and Gill M.S., (2014). "Bacterial fatty acids enhance recovery from the dauer larva in Caenorhabditis elegans". PLoS ONE, 9(1), e86979.

Kelley D. E. and Goodpaster B. H., (2001). "Skeletal muscle triglyceride. An aspect of regional adiposity and insulin resistance". Diabetes Care, 24(5), 933 - 941.

Killer M., Wald J., Pieprzyk J., Marlovits T. C. and Löw C., (2021). "Structural snapshots of human PepT1 and PepT2 reveal mechanistic insights into substrate and drug transport across epithelial membranes". Science Advances, 7(45), eabk3259.

Kim H. and Colaiácovo M. P., (2019). "CRISPR-Cas9-guided genome engineering in *Caenorhabditis elegans*". Current Protocols in Molecular Biology, 129(1), e106.

Kimura K. D., Tissenbaum H. A., Liu Y. and Ruvkun G., (1997). "*daf-2*, an insulin receptor-like gene that regulates longevity and diapause in *Caenorhabditis elegans*". Science, 277(5328), 942 - 946.

Kitaoka S., Morielli A. D. and Zhao F.-Q., (2016). "FGT-1-mediated glucose uptake is defective in insulin/IGF-like signaling mutants in *Caenorhabditis elegans*". FEBS Open Bio, 6(6), 576 – 585.

Kniazeva M., Sieber M., McCauley S., Zhang K., Watts J. L. and Han M., (2003). "Suppression of the ELO-2 FA elongation activity results in alterations of the fatty acid composition and multiple physiological defects, including abnormal ultradian rhythms, in *Caenorhabditis elegans*". Genetics, 163(1), 159 – 169.

Kolodziejczak D., Spanier B., Pais R., Kraiczy J., Stelzl T., Gedrich K., Scherling C., Zietek T. and Daniel H., (2013). "Mice lacking the intestinal peptide transporter display reduced energy intake and a subtle maldigestion/malabsorption that protects them from diet-induced obesity". Am J Physiol Gastrointest Liver Physiol, 304(10), G897 – G907.

Koopman M., Michels H., Dancy B. M., Kamble R., Mouchiroud L., Auwerx J., Nollen E. A. and Houtkooper R. H., (2016). "A screening-based platform for the assessment of cellular respiration in *Caenorhabditis elegans*". Nat Protoc, 11(10), 1798 - 816.

Kopelman P. G., (2000). "Obesity as a medical problem". Nature, 404(6778), 635 - 643.

Korbecki J. and Bajdak-Rusinek K., (2019). "The effect of palmitic acid on inflammatory response in macrophages: an overview of molecular mechanisms". Inflamm Res, 68(11), 915 - 932.

Korfhagen T. R., Kitzmiller J., Chen G., Sridharan A., Haitchi H.-M., Hegde R. S., Divanovic S., Karp C. L. and Whitsett J. A., (2012). "SAM-pointed domain ETS factor mediates epithelial cell-intrinsic innate immune signaling during airway mucous metaplasia". Proceedings of the National Academy of Sciences, 109(41), 16630 – 16635.

Kowalski G. M., Kloehn J., Burch M. L., Selathurai A., Hamley S., Bayol S. A. M., Lamon S., Watt M. J., Lee-Young R. S., McConville M. J., et al., (2015). "Overexpression of sphingosine kinase 1 in liver reduces triglyceride content in mice fed a low but not high-fat diet". Biochimica et Biophysica Acta (BBA) - Molecular and Cell Biology of Lipids, 1851(2), 210 – 219.

Kwong E. K., Li X., Hylemon P. B. and Zhou H., (2017). "Sphingosine kinases/sphingosine 1-phosphate signaling in hepatic lipid metabolism". Current Pharmacology Reports, 3(4), 176 – 183.

Lai C.-H., Chou C.-Y., Ch'ang L.-Y., Liu C.-S. and Lin W., (2000). "Identification of novel human genes evolutionarily conserved in *Caenorhabditis elegans* by comparative proteomics". Genome Res., 10(5), 703 – 713.

Lant B. and Storey K. B., (2010). "An overview of stress response and hypometabolic strategies in *Caenorhabditis elegans*: conserved and contrasting signals with the mammalian system". Int. J. Biol. Sci., 6(1), 9 - 50.

Larance M., Bailly A. P., Pourkarimi E., Hay R. T., Buchanan G., Coulthurst S., Xirodimas D. P., Gartner, A. and Lamond A. I., (2011). "Stable-isotope labeling with amino acids in nematodes". Nature methods, 8(10), 849 – 851.

Lee S. S., Kennedy S., Tolonen A. C. and Ruvkun G., (2003). "DAF-16 target genes that control *C. elegans* life-span and metabolism". Science, 300(5619), 644 – 647.

Lee K., Escobar I., Jang Y., Kim W., Ausubel F. M. and Mylonakis E., (2020). "In the model host *Caenorhabditis elegans*, sphingosine-1-phosphate-mediated signaling increases immunity toward human opportunistic bacteria". Int. J. Mol. Sci., 21, 7813.

Leier I., Jedlitschky G., Buchholz U., Center M., Cole S. P. C., Deeley R. G. and Keppler D., (1996). "ATP-dependent glutathione disulfide transport mediated by the MRP gene-encoded conjugate export pump". Biochem. J., 314, 433 – 437.

Leverve X., Batandier C. and Fontaine E., (2007). "Choosing the right substrate". Novartis Found Symp, 280, 108 - 121.

Li F., Yin Y., Tan B., Kong X. and Wu G., (2011). "Leucine nutrition in animals and humans: mTOR signaling and beyond". Amino Acids, 41(5), 1185 – 1193.

Li Z. and Graham B. H., (2012). "Measurement of mitochondrial oxygen consumption using a Clark electrode". Methods in molecular biology (Clifton, N.J.), 837, 63 – 72.

Li H., Liu X., Wang D., Su L., Zhao T., Li Z., Lin C., Zhang Y., Huang B., Lu J. and Li X., (2017). "O-GlcNAcylation of SKN-1 modulates the lifespan and oxidative stress resistance in *Caenorhabditis elegans*". Scientific reports, 7, 43601.

Li Y., Ding W., Li C. and Liu Y., (2020). "HLH-11 modulates lipid metabolism in response to nutrient availability". Nature communications, 11(1), 5959.

Li W., Li S., Wang X., Chen H.-Y., Hao H. and Wang K.-J., (2022). "Internal carbohydrates and lipids as reserved energy supply in the pubertal molt of Scylla paramamosain". Aquaculture, 549, 0044 - 8486.

Lipert B., Wegrzyn P., Sell H., Eckel J., Winiarski M., Budzynski A., Matlok M., Kotlinowski J., Ramage L., Malecki M., et al., (2014). "Monocyte chemoattractant protein-induced protein 1 impairs adipogenesis in 3T3-L1 cells". Biochim Biophys Acta, 1843(4), 780 - 788.

Liu Z., Li X., Ge Q., Ding M. and Huang X., (2014). "A lipid droplet-associated GFP reporter-based screen identifies new fat storage regulators in *C. elegans*". Journal of Genetics and Genomics, 41(5), 305 - 313.

Loe D. W., Almquist K. C., Cole S. P. C. and Deeley R. G., (1996a). ATP-dependent 17b-estradiol 17-(b-D-glucuronide) transport by multidrug resistance protein: inhibition by cholestatic steroids". J. Biol. Chem. 271, 9675 – 9682.

Loe D. W., Almquist K. C., Deeley R. G. and Cole S. P. C., (1996b). "Multidrug resistance protein (MRP)-mediated transport of leukotriene C4 and chemotherapeutic agents in membrane vesicles: demonstration of glutathione-dependent vincristine transport". J. Biol. Chem. 271, 9683 – 9689.

Losko M., Dolicka D., Pydyn N., Jankowska U., Kedracka-Krok S., Kulecka M., Paziewska A., Mikula M., Major P., Winiarski M., et al., (2020). "Integrative genomics reveal a role for MCPIP1 in adipogenesis and adipocyte metabolism". Cellular and Molecular Life Sciences, 77, 4899 – 4919.

Lu S. C., (2009). "Regulation of glutathione synthesis". Molecular aspects of medicine, 30(1-2), 42 – 59.

Lucia M. B., Savarino A., Straface E., Golotta C., Rastrelli E., Matarrese P., Rutella S., Malorni W., and Cauda R., (2005). "Role of lymphocyte Multidrug Resistance Protein 1 in HIV infection". JAIDS Journal of Acquired Immune Deficiency Syndromes, 40(3), 257 – 266.

Luz A. L., Rooney J. P., Kubik L. L., Gonzalez C. P., Song D. H. and Meyer J. N., (2015). "Mitochondrial morphology and fundamental parameters of the mitochondrial respiratory chain are altered in *Caenorhabditis elegans* strains deficient in mitochondrial dynamics and homeostasis processes". PLoS ONE, 10(6), e0130940.

Luz A. L., Godebo T. R., Bhatt D. P., Ilkayeva O. R., Maurer L. L., Hirschey M. D. and Meyer J. N., (2016). "Arsenite uncouples mitochondrial respiration and induces a Warburg-like effect in *Caenorhabditis elegans*". Toxicological Sciences, *152*(2), 349 - 362.

Ma M. M., Chen J. L., Wang G. G., Wang H., Lu Y., Li J. F., Yi J., Yuan Y. J., Zhang Q. W., Mi J., et al. (2007). "Sphingosine kinase 1 participates in insulin signalling and regulates glucose metabolism and homeostasis in KK/Ay diabetic mice". Diabetologia, 50(4), 891 – 900.

Maceyka M., Harikumar K. B., Milstien S. and Spiegel S., (2012). "Sphingosine-1-phosphate signaling and its role in disease". Trends in cell biology, 22(1), 50 – 60.

Manohar C. F., Bray J. A., Salwen H. R., Madafiglio J., Cheng A., Flemming C., Marshall G. M., Norris M. D., Haber M. and Cohn S. L., (2004). "MYCN-mediated regulation of the MRP1 promoter in human neuroblastoma". Oncogene 23, 753 – 762.

Mao R., Yang R., Chen X., Harhaj E. W., Wang X. and Fan Y., (2017). "Regnase-1, a rapid response ribonuclease regulating inflammation and stress responses". Cellular & Molecular Immunology, 14(5), 412 – 422.

Massey P. R., Fojo T. and Bates S. E., (2013). "ABC transporters: involvement in multidrug resistance and drug disposition". Handbook of anticancer pharmacokinetics and pharmacodynamics, 373 – 400.

Matsushita K., Takeuchi O., Standley D. M., Kumagai Y., Kawagoe T., Miyake T., Satoh T., Kato H., Tsujimura T., Nakamura H. and Akira S., (2009). "Zc3h12a is an RNase essential for controlling immune responses by regulating mRNA decay". Nature, 458(7242), 1185 – 1190.

McCallum K. C. and Garsin D. A., (2016). "The role of reactive oxygen species in modulating the *Caenorhabditis elegans* immune response". PLoS Pathog, 12(11), e1005923.

McClanahan P. D., McCloskey R. J., Ng Tung Hing M., Raizen D. M. and Fang-Yen C., (2020). "Dehydrated *Caenorhabditis elegans* stocks are resistant to multiple freeze-thaw cycles". G3: Genes, Genomes, Genetics, 10(12), 4505 - 4512.

McDonald M. K., Fritz J.-A., Jia D., Scheuchner D., Snyder F. F., Stanislaus A., Curle J., Li L., Stabler S. P. and Allen R. H., (2017). "Identification of ABC transporters acting in vitamin B12 metabolism in *Caenorhabditis elegans*. Molecular Genetics and Metabolism, 122(4), 160 – 171.

McElwee J. J., Schuster E., Blanc E., Thornton J. and Gems D., (2006). "Diapause-associated metabolic traits reiterated in long-lived *daf-2* mutants in the nematode *Caenorhabditis elegans*". Mechanisms of Ageing and Development, 127(5), 458 – 472.

McGhee J. D., (2007). "The *C. elegans* intestine". WormBook, ed. The *C. elegans* Research Community, WormBook.

McKay R. M., McKay J. P., Avery L. and Graff J.M., (2003). "*C. elegans*: a model for exploring the genetics of fat storage". Dev Cell, 4(1), 131 – 142.

Meikle P. J. and Summers S. A., (2016). "Sphingolipids and phospholipids in insulin resistance and related metabolic disorders". Nature Reviews Endocrinology, 13(2), 79 – 91.

Meissner B., Boll M., Daniel H. and Baumeister R., (2004). "Deletion of the intestinal peptide transporter affects insulin and TOR signaling in *Caenorhabditis elegans*". J. Biol. Chem., 279, 36739 – 36745.

Meister P., Schott S., Bedet C., Xiao Y., Rohner S., Bodennec S., Hudry B., Molin L., Solari F., Gasser S. M. and Palladino F., (2011). "*Caenorhabditis elegans* heterochromatin protein 1 (HPL-2) links developmental plasticity, longevity and lipid metabolism". Genome Biology, 12, R123.

Mejia-Martinez F., Franco-Juarez B., Moreno-Arriola E., Hernández-Vázquez A., Martinez-Avila M., Gómez-Manzo S., Marcial-Quino J., Carvajal K., Velazquez-Arellano A. and Ortega-Cuellar D., (2017). "The MXL-3/SBP-1 axis is responsible for glucose-dependent fat accumulation in *C. elegans*". Genes, 8, 307.

Mihaylova M. M. and Shaw R. J., (2012). "The AMP-activated protein kinase (AMPK) signaling pathway coordinates cell growth, autophagy, & metabolism". Nat Cell Biol., 13(9), 1016 – 1023.

Mitra P., Oskeritzian C. A., Payne S. G., Beaven M. A., Milstien S. and Spiegel S., (2006). "Role of ABCC1 in export of sphingosine-1-phosphate from mast cells". PNAS, 103(44), 16394 – 16399.

Mitsutake S. and Igarashi Y., (2013). "Sphingolipids in lipid microdomains and obesity". Obesity, 91, 271 – 284.

More V. R. and Slitt A. L., (2011). "Alteration of hepatic but not renal transporter expression in diet-induced obese mice". Drug Metab Dispos, 39(6), 992 - 999.

Moreno-Arriola E., EL Hafidi M., Ortega-Cuéllar D. and Carvajal K., (2016). "AMP-activated protein kinase regulates oxidative metabolism in *Caenorhabditis elegans* through the NHR-49 and MDT-15 transcriptional regulators". PLoS ONE, 11(1), e0148089.

Morrow C. S., Smitherman P. K., Diah S. K., Schneider E. and Townsend A. J., (1998). "Coordinated action of glutathione S-transferases (GSTs) and multidrug resistance protein 1 (MRP1) in antineoplastic drug detoxification. Mechanism of GST A1-1- and MRP1-associated resistance to chlorambucil in MCF7 breast carcinoma cells" J. Biol. Chem. 273(32), 20114 – 20120.

Moussa O., Turner D. P., Feldman R. J., Sementchenko V. I., McCarragher B. D., Desouki M. M., Fraig M. and Watson D. K., (2009). "PDEF is a negative regulator of colon cancer cell growth and migration". Journal of Cellular Biochemistry, 108(6), 1389 – 1398.

Mullaney B. C. and Ashrafi K., (2009). "*C. elegans* fat storage and metabolic regulation". Biochimica et Biophysica Acta (BBA) - Molecular and Cell Biology of Lipids, 1791(6), 474 – 478.

Mullaney B. C., Blind R. D., Lemieux G. A., Perez C. L., Elle I. C., Faergeman N. J., Van Gilst M. R., Ingraham H. A and Ashrafi K., (2010). "Regulation of *C. elegans* fat uptake and storage by acyl-CoA synthase-3 is dependent on NR5A family nuclear hormone receptor *nhr-25*". Cell Metab, 12(4), 398 - 410.

Muller S., Ziegler O., Donner M., Drouin P. and Stoltz J. F., (1990). "Rheological properties and membrane fluidity of red blood cells and platelets in primary hyperlipoproteinemia". Atherosclerosis, 83(2-3), 231 – 237.

Murphy C. T., McCarroll S. A., Bargmann C. I., Fraser A., Kamath R. S., Ahringer J., Li H. and Kenyon C., (2003). "Genes that act downstream of DAF-16 to influence the lifespan of *Caenorhabditis elegans*". Nature, 424(6946), 277 – 283.

Nehrke K., (2003). "A reduction in intestinal cell pHi due to loss of the *Caenorhabditis elegans* Na+/H+ exchanger NHX-2 increases life span". The journal of biological chemistry, 278(45), 44657 – 44666.

Nehrke K., (2014). "Membrane ion transport in non-excitable tissues". WormBook, 2014, 1–22.

Ng L. F. and Gruber J., (2019). "Measurement of respiration rate in live *Caenorhabditis elegans*". Bio-protocol, 9(10), e3243.

Nguyen C. Q., Hall D. H., Yang Y. and Fitch D. H. A., (1999). "Morphogenesis of the *Caenorhabditis elegans* male tail tip". Developmental Biology, 207, 86 – 106.

Nikaido H., (2002). "How are the ABC transporters energized?". PNAS, 99(15), 9609 - 9610.

Nikolova-Karakashian M. N. and Rozenova K. A., (2010). "Ceramide in stress response". Advances in experimental medicine and biology, 688, 86 – 108.

Niswender K. D. and Schwartz M. W., (2003). "Insulin and leptin revisited: adiposity signals with overlapping physiological and intracellular signaling capabilities". Frontiers in Neuroendocrinology, 24(1), 1 – 10.

Nixon M., Mackenzie S. D., Taylor A. I., Homer N. Z. M., Livingstone D. E., Mouras R., Morgan R. A., Mole D. J., Stimson R. H., Reynolds R. M., et al., (2016). "ABCC1 confers tissue-specific sensitivity to cortisol versus corticosterone: A rationale for safer glucocorticoid replacement therapy". Science Translational Medicine, 8(352), 352ra109 – 352ra109.

Noble T., Stieglitz J. and Srinivasan S., (2013). "An integrated serotonin and octopamine neuronal circuit directs the release of an endocrine signal to control *C. elegans* body fat". Cell Metab, 18(5), 672 – 684.

Noy N., (2007). "ligand specificity of nuclear hormone receptors: sifting through promiscuity". Biochemistry, 46(47), 13461 – 13467.

Ntambi J. M., (1999). "Regulation of stearoyl-CoA desaturase by polyunsaturated fatty acids and cholesterol". J Lipid Res., 40(9), 1549 - 1558.

Ogg S. and Ruvkun G., (1998). "The *C. elegans* PTEN Homolog, DAF-18, acts in the insulin receptor-like metabolic signaling pathway". Molecular Cell, 2(6), 887 – 893.

O'Rourke E. J., Soukas A. A., Carr C. E. and Ruvkun G., (2009). "*C. elegans* major fats are stored in vesicles distinct from lysosome-related organelles". Cell Metabolism, 10(5), 430 – 435.

O'Rourke E. J. and Ruvkun G., (2013). "MXL-3 and HLH-30 transcriptionally link lipolysis and autophagy to nutrient availability". Nat. Cell Biol., 15(6), 668 - 676.

Paek J., Lo J. Y., Narasimhan S. D., Nguyen T. N., Glover-Cutter K., Robida-Stubbs S., Suzuki T., Yamamoto M., Blackwell T. K. and Curran S. P., (2012). "Mitochondrial SKN-1/Nrf mediates a conserved starvation response". Cell metabolism, 16(4), 526 – 537.

Palamiuc L., Noble T., Witham E., Ratanpal H., Vaughan M. and Srinivasan S., (2017). "A tachykinin-like neuroendocrine signalling axis couples central serotonin action and nutrient sensing with peripheral lipid metabolism". Nat Commun, 8, 14237.

Palikaras K., Lionaki E. and Tavernarakis N., (2015). „Coordination of mitophagy and mitochondrial biogenesis during ageing in *C. elegans*". Nature, 521(7553), 525 – 528.

Pang G., Xie J., Chen Q. and Hu Z., (2014a). "Energy intake, metabolic homeostasis, and human health". Food Science and Human Wellness, 3(3-4), 89 – 103.

Pang S., Lynn D. A., Lo J. Y., Paek J. and Curran S. P., (2014b). "SKN-1 and Nrf2 couples proline catabolism with lipid metabolism during nutrient deprivation". Nature communications, 5, 5048.

Park K. S., Korfhagen T. R., Bruno M. D., Kitzmiller J. A., Wan H., Wert S. E., Khurana Hershey G. K., Chen G. and Whitsett J. A., (2007). "SPDEF regulates goblet cell hyperplasia in the airway epithelium". The Journal of clinical investigation, 117(4), 978 – 988.

Perez C. L. and Van Gilst M. R., (2008) ."A 13C isotope labeling strategy reveals the influence of insulin signaling on lipogenesis in *C. elegans*". Cell Metabolism, 8, 266 – 274.

Pfeiffer J., Johnson D. and Nehrke K., (2008). "Oscillatory transepithelial H^+ flux regulates a rhythmic behavior in *C. elegans*". Curr Biol, 18. 297 – 302.

Pierce S. B., Costa M., Wisotzkey R., Devadhar S., Homburger S. A., Buchman A. R., Ferguson K. C., Heller J., Platt D. M., Pasquinelli A. A., et al., (2001). "Regulation of DAF-2 receptor signaling by human insulin and *ins-1*, a member of the unusually large and diverse *C. elegans* insulin gene family". Genes & Development, 15(6), 672 – 686.

Porta-de-la-Riva M., Fontrodona L., Villanueva A. and Cerón J., (2012). "Basic *Caenorhabditis elegans* methods: synchronization and observation". Journal of Visualized Experiments, 10(64), e4019.

Possik E., Ajisebutu A., Manteghi S., Gingras M. C., Vijayaraghavan T., Flamand M., Coull B., Schmeisser K., Duchaine T., van Steensel M., Hall D. H. and Pause A., (2015). "FLCN and AMPK confer resistance to hyperosmotic stress via remodeling of glycogen stores". PLoS genetics, 11(10), e1005520.

Poveda A., Koivula R. W., Ahmad S., Barroso I., Hallmans G., Johansson I., Renström F. and Franks P. W., (2016). "Innate biology versus lifestyle behaviour in the aetiology of obesity and type 2 diabetes: the GLACIER Study". Diabetologia, 59, 462 – 471.

Prasad N., Singh H., Jaiswal A., Chaturvedi S. and Agarwal V., (2021). "Overexpression of P-glycoprotein and MRP-1 are pharmacogenomic biomarkers to determine steroid resistant phenotype in childhood idiopathic nephrotic syndrome". The Pharmacogenomics Journal, 21, 566 – 573.

Pyne N. J., El Buri A., Adams D. R. and Pyne S., (2018). "Sphingosine 1-phosphate and cancer". Advances in Biological Regulation, 68, 97 – 106.

Qi Y., Chen J., Lay A., Don A., Vadas M., Xia P., (2013). "Loss of sphingosine kinase 1 predisposes to the onset of diabetes via promoting pancreatic -cell death in diet-induced obese mice". FASEB J., 27, 4294 – 4304.

Rankin C. H., (2002). "From gene to identified neuron to behaviour in *Caenorhabditis elegans*". Nature Reviews Genetics, 3(8), 622 – 630.

Rankinen T., Zuberi A., Chagnon Y. C., Weisnagel S. J., Argyropoulos G., Walts B., Perusse L. and Bouchard C., (2006). "The human obesity gene map: the 2005 update". Obesity, 14(4), 529 - 644.

Ray K., (2021). "Intercrypt goblet cells — the key to colonic mucus barrier function". Nature Reviews Gastroenterology & Hepatology, 18(7), 455 – 455.

Rinia H. A., Burger K. N. J., Bonn M. and Muller M., (2008). "Quantitative label-free imaging of lipid composition and packing of individual cellular lipid droplets using multiplex CARS microscopy". Biophys. J., 95(10), 4908 – 4914.

Robbiani D. F., Finch R. A., Jäger D., Muller W. A., Sartorelli A. C. and Randolph G. J., (2000). "The leukotriene C4 transporter MRP1 regulates CCL19 (MIP-3β, ELC)–dependent mobilization of dendritic cells to lymph nodes". Cell, 103(5), 757 – 768.

Rustan A. C. and Drevon C. A., (2005). "Fatty acids: structures and properties". Encyclopedia of Life Sciences.

Saurin W., Hofnung M. and Dassa E., (1999). "Getting in or out: early segregation between importers and exporters in the evolution of ATP-binding cassette (ABC) transporters". Journal of Molecular Evolution, 48(1), 22 – 41.

Scerbak C., Vayndorf E. M., Parker J. A., Neri C., Driscoll M. and Taylor B. E., (2014). "Insulin signaling in the aging of healthy and proteotoxically stressed mechanosensory neurons". Frontiers in Genetics, 5(212), 1 - 14.

Schindelin J., Arganda-Carreras I., Frise E., Kaynig V., Longair M., Pietzsch T., Preibisch S., Rueden, C. Saalfeld S., Schmid B., et al., (2012). "Fiji: an open-source platform for biological-image analysis". Nat Methods 9, 676 - 682.

Schmokel V., Memar N., Wiekenberg A., Trotzmuller M., Schnabel R. and Doring F., (2016). "Genetics of lipid-storage management in *Caenorhabditis elegans* embryos". Genetics, 202, 1071 - 1083.

Schneider E., Wilken S. and Schmid R., (1994) "Nucleotide induced conformational changes of MalK, a bacterial ATP binding cassette transporter protein". J. Biol. Chem., 269, 20456 - 20461.

Schneider E., (1998). "ATP-binding-cassette (ABC) transport systems: Functional and structural aspects of the ATP-hydrolyzing subunits/domains". FEMS Microbiology Reviews, 22(1), 1 – 20.

Senchuk M. M., Dues D. J., Schaar C. E., Johnson B. K., Madaj Z. B., Bowman M. J., et al., (2018). "Activation of DAF-16/FOXO by reactive oxygen species contributes to longevity in long-lived mitochondrial mutants in *Caenorhabditis elegans*". PLOS Genetics, 14(3), e1007268.

Shen H., Smith D. E., Keep R. F., Xiang J. and Brosius III F. C., (2003). "Targeted disruption of the PEPT2 gene markedly reduces dipeptide uptake in choroid plexus". The Journal Of Biological Chemistry, 279(35), 36739 – 36745.

Sheng M., Hosseinzadeh A., Muralidharan S. V., Gaur R., Selstam E. and Tuck S., (2015). "Aberrant fat metabolism in *Caenorhabditis elegans* mutants with defects in the defecation motor program". PLOS ONE, 10(4), e0124515.

Sheps J. A., Ralph S., Zhao Z., Baillie D. L. and Ling V., (2004). "The ABC transporter gene family of *Caenorhabditis elegans* has implications for the evolutionary dynamics of multidrug resistance in eukaryotes". Genome Biol., 5(3), R15.

Shi X., Li J., Zou X., Greggain J., Rødkær S. V., Færgeman N. J., Liang B. and Watts J. L., (2013). "Regulation of lipid droplet size and phospholipid composition by stearoyl-CoA desaturase". Journal of lipid research, 54(9), 2504 – 2514.

Shimokawa T., (2005). "C/EBP functionally and physically interacts with GABP to activate the human myeloid IgA Fc receptor (Fc R, CD89) gene promoter". Blood, 106(7), 2534 – 2542.

Sobańska D., Komur A. A., Chabowska-Kita A., Gumna J., Kumari P., Pachulska-Wieczorek K. and Ciosk R., (2021). „An mRNA silencing mechanism reliant on the cooperation between REGE-1/Regnase-1 and RLE-1/Roquin-1". bioRxiv preprint

Solmi M., Veronese N., Manzato E., Sergi G., Favaro A., Santonastaso P. and Correll C. U., (2015). "Oxidative stress and antioxidant levels in patients with anorexia nervosa: A systematic review and exploratory meta-analysis". International Journal of Eating Disorders, 48(7), 826 – 841.

Son J. M., Sarsour E. H., Balaraju A. K., Fussell J., Kalen A. L., Wagner B. A., Buettner G. R. and Goswami P. C., (2017). "Mitofusin 1 and optic atrophy 1 shift metabolism to mitochondrial respiration during aging". Aging Cell, 16(5), 1136 - 1145.

Sonnhammer E. L. L. and Durbin R., (1997). "Analysis of protein domain families in *Caenorhabditis elegans*". Genomics, 46(2), 200 – 216.

Soukas A. A., Kane E. A., Carr C. E., Melo J. A. and Ruvkun G., (2009). "Rictor/TORC2 regulates fat metabolism, feeding, growth, and life span in *Caenorhabditis elegans*". Genes Dev, 23(4), 496 - 511.

Spanier B., Lasch K., Marsch S., Benner J., Liao W., Hu H., Kienberger H., Eisenreich W. and Daniel H., (2009). "How the intestinal peptide transporter PEPT-1 contributes to an obesity phenotype in *Caenorhabditis elegans*". PLoS One, 4(7), 6279.

Spanier B., Wallwitz J., Zapoglou D., Idrissou B., Fischer C., Troll M., Petzold K. and Daniel H., (2018). "The reproduction rate of peptide transporter PEPT-1 deficient *C. elegans* is dependent on dietary glutamate supply". Frontiers in molecular biosciences, 5, 109.

Srinivasan S., Sadegh L., Elle I. C., Christensen A. G. L., Faergeman N. J. and Ashrafi K., (2008). "Serotonin regulates *C. elegans* fat and feeding through independent molecular mechanisms". Cell Metab, 7(6), 533 – 544.

Srinivasan S., (2015). "Regulation of body fat in *Caenorhabditis elegans*". Annu. Rev. Physiol., 77(1), 161 – 178.

Stanley W. C., Khairallah R. J. and Dabkowski E. R., (2012). "Update on lipids and mitochondrial function: impact of dietary n-3 polyunsaturated fatty acids". Current opinion in clinical nutrition and metabolic care, 15(2), 122 – 126.

Steinbaugh M. J., Narasimhan S. D., Robida-Stubbs S., Moronetti Mazzeo L. E., Dreyfuss J. N., Hourihan J. M., Raghavan P., Operan T. N., Esmaillie R. and Blackwell T. K., (2015). "Lipid-mediated regulation of SKN-1/Nrf in response to germ cell absence". eLife, 4, e07836.

Su L. J., Zhang J. H., Gomez H., Murugan R., Hong X., Xu D., Jiang F. and Peng Z. Y., (2019). "Reactive oxygen species-induced lipid peroxidation in apoptosis, autophagy, and ferroptosis". Oxidative medicine and cellular longevity, 5080843.

Sulston J. E. and Horvitz H. R., (1977). "Post-embryonic cell lineages of the nematode, *Caenorhabditis elegans*". Developmental Biology, 56(1), 110 – 156.

Sulston J. E., Schierenberg E., White J. G. and Thomson J. N., (1983). "The embryonic cell lineage of the nematode *Caenorhabditis elegans*". Developmental Biology, 100(1), 64 – 119.

Sun X., Chen W.-D. and Wang Y.-D., (2017). "DAF-16/FOXO transcription factor in aging and longevity". Frontiers in Pharmacology, 8, 548.

Sze J. Y., Victor M., Loer C., Shi Y. and Ruvkun G., (2000). "Food and metabolic signaling defects in a *Caenorhabditis elegans* serotonin-synthesis mutant". Nature, 403(6769), 560 – 564.

Tanaka T., Ikita K., Ashida T., Motoyama Y., Yamaguchi Y. and Satouchi K., (1996). "Effects of growth temperature on the fatty acid composition of the free-living nematode *Caenorhabditis elegans*". Lipids, 31(11), 1173 – 1178.

Tauchi-Sato K., Ozeki S., Houjou T., Taguchi R. and Fujimoto T., (2002). "The surface of lipid droplets is a phospholipid monolayer with a unique fatty acid composition". J. Biol. Chem., 277(46), 44507 – 44512.

Tedesco L., Corsetti G., Ruocco C., Ragni M., Rossi F., Carruba M. O., Valerio A. and Nisoli E., (2018). "A specific amino acid formula prevents alcoholic liver disease in rodents". Am J Physiol Gastrointest Liver Physiol, 314(5), G566 - G582.

Tejerina S., De Pauw A., Vankoningsloo S., Houbion A., Renard P., De Longueville F., Raes M. and Arnould T., (2009). "Mild mitochondrial uncoupling induces 3T3-L1 adipocyte de-differentiation by a PPARγ-independent mechanism, whereas TNFα-induced de-differentiation is PPARγ dependent". J Cell Sci, 122 (1), 145 – 155.

Tepper R. G., Ashraf J., Kaletsky R., Kleemann G., Murphy C. T. and Bussemaker H. J., (2013). "PQM-1 complements DAF-16 as a key transcriptional regulator of DAF-2-mediated development and longevity". Cell, 154(3), 676 – 690.

Thamotharan M., Bawani S. Z., Zhou X. and Adibi S. A., (1999). "Hormonal regulation of oligopeptide transporter pept-1 in a human intestinal cell line". Am. J. Physiol., 276(4), C821 – C826.

The *C. elegans* Sequencing Consortium, (1998). "Genome sequence of the nematode *C. elegans*: a platform for investigating biology." Science, 282(5396), 2012 - 2018.

Thiebaut F., Tsuruo T., Hamada H., Gottesman M. M., Pastan I. and Willingham M. C., (1987). "Cellular localization of the multidrug-resistance gene product P-glycoprotein in normal human tissues". Proc. Nat. Acad. Sci. U.S.A., 84, 7735 - 7738.

Thyagarajan B., Blaszczak A. G., Chandler K. J., Watts J. L., Johnson W. E., Graves B. J., (2010). "ETS-4 is a transcriptional regulator of life span in *Caenorhabditis elegans*". PLoS Genet, 6(9), e1001125.

Timmons L. and Fire A., (1998). "Specific interference by ingested dsRNA". Nature, 395(6705), 854 – 854.

Trayhurn P., (2007). "Adipocyte biology". Obes. Rev., 8(s1), 41 – 44.

Tullet J. M. A., Hertweck M., An J. H., Baker J., Hwang J. Y., Liu S., Oliveira R. P., Baumeister R. and Blackwell T. K., (2008). "Direct inhibition of the longevity-promoting factor SKN-1 by insulin-like signaling in *C. elegans*". Cell, 132(6), 1025 – 1038.

Turek M. and Bringmann H., (2014). "Gene expression changes of *Caenorhabditis elegans* larvae during molting and sleep-like lethargus. PLoS ONE, 9(11), e113269.

Udasin R. G., Wen X., Bircsak K. M., Aleksunes L. M., Shakarjian M. P., Kong A. N., Heck D. E., Laskin D. L. and Laskin J. D., (2016). "Nrf2 regulates the sensitivity of mouse keratinocytes to nitrogen mustard via Multidrug Resistance-Associated Protein 1 (Mrp1)". Toxicological sciences : an official journal of the Society of Toxicology, 149(1), 202 – 212.

Urbatsch I. L., Beaudet L., Carrier I. and Gros P., (1998). "Mutations in either nucleotide-binding site of P-glycoprotein (Mdr3) prevent vanadate trapping of nucleotide at both sites". Biochemistry, 37(13), 4592 – 4602.

Van Gilst M. R., Hadjivassiliou H. and Yamamoto K. R., (2005). "A *Caenorhabditis elegans* nutrient response system partially dependent on nuclear receptor NHR-49". Proc. Natl Acad. Sci. USA, 102(38), 13496 – 13501.

Van Helvoort A., Smith A. J., Sprong H., Fritzsche I., Schinkel A. H., Borst P. and van Meer G., (1996). "MDR1 P-glycoprotein is a lipid translocase of broad specificity, while MDR3 P-glycoprotein specifically translocates phosphatidylcholine". Cell, 87(3), 507 – 517.

von Reuss S. H. and Schroeder F. C., (2015). "Combinatorial chemistry in nematodes: modular assembly of primary metabolism-derived building blocks". Nat Prod Rep, 32(7), 994 - 1006.

Vowels J. J. and Thomas J. H., (1992). "Genetic analysis of chemosensory control of dauer formation in *Caenorhabditis elegans*". Genetics, 130, 105 – 123.

Vrablik T. L., Petyuk V. A., Larson E. M., Smith R. D. and Watts J. L., (2015). "Lipidomic and proteomic analysis of *Caenorhabditis elegans* lipid droplets and identification of ACS-4 as a lipid droplet-associated protein". Biochim Biophys Acta.- Molecular and Cell Biology of Lipids, 1851(10), 1337 – 1345.

Walker J. E., Saraste M., Runswick M. J. and Gay N. J., (1982). "Distantly related sequences in the K- and L-subunits of ATP synthase, myosin, kinases and other ATP requiring enzymes and a common nucleotide binding fold". EMBO J. 1(8), 945 - 951.

Wallis J. G., Watts J. L. and Browse J., (2002). "Polyunsaturated fatty acid synthesis: what will they think of next?". Trends in Biochemical Sciences, 27(9), 467 – 473.

Wang J., Badeanlou L., Bielawski J., Ciaraldi T. P. and Samad F., (2014). "Sphingosine kinase 1 regulates adipose proinflammatory responses and insulin resistance". American journal of physiology. Endocrinology and metabolism, 306(7), E756 – E768.

Watts J. L. and Browse J., (2002). "Genetic dissection of polyunsaturated fatty acid synthesis in *Caenorhabditis elegans*". Proc. Natl. Acad. Sci. U. S. A, 99(9), 5854 – 5859.

Watts J. L., (2009). "Fat synthesis and adiposity regulation in *Caenorhabditis elegans*". Trends in Endocrinology and Metabolism, 20(2), 58 – 65.

Watts J. L. and Ristow M., (2017). "Lipid and carbohydrate metabolism in *Caenorhabditis elegans*". Genetics, 207(2), 413 – 446.

Westlake C. J., Cole S. P. and Deeley R. G., (2005). "Role of the NH2-terminal membrane spanning domain of multidrug resistance protein 1/ABCC1 in protein processing and trafficking". Molecular biology of the cell, 16(5), 2483 – 2492.

White A. M., Varney M. A., Watson S. P., Rigby S., Liu C. S., Ward J. G., Reese C. B., Graham H. C. and Williams R. J., (1991). "Influence of Mg^{2+} and pH on n.m.r. spectra and radioligand binding of inositol 1,4,5- trisphosphate". Biochem J, 278, 759 – 764.

White B., (2009). "Dietary fatty acids". Am Fam Physician., 80(4), 345 - 350.

Willett W. C., Dietz W. H. and Colditz G. A., (1999). "Guidelines for healthy weight". New England Journal of Medicine, 341(6), 427 – 434.

Wilson D. F., (2017). "Oxidative phosphorylation: regulation and role in cellular and tissue metabolism". The Journal of physiology, 595(23), 7023 – 7038.

Witting M. and Schmitt-Kopplin P., (2016). "The *Caenorhabditis elegans* lipidome". Archives of Biochemistry and Biophysics, 589, 27 – 37.

Wolf K. K., Paine M. F. and Watkins P. B., (2010). "Metabolic barrier of the gastrointestinal tract". Comprehensive Toxicology, 53 – 75.

Wong C. and Roy R., (2020). "AMPK regulates developmental plasticity through an endogenous small RNA pathway in *Caenorhabditis elegans*". Int. J. Mol. Sci., 21, 2238.

World Health Organization, (1998). "Obesity: preventing and managing the global epidemic: report of a WHO Consultation on Obesity". World Health Organization, Geneva, 276.

Wu Q., Zhi L., Qu Y. and Wang D., (2016). "Quantum dots increased fat storage in intestine of *Caenorhabditis elegans* by influencing molecular basis for fatty acid metabolism". Nanomedicine: Nanotechnology, Biology and Medicine, 12(5), 1175 – 1184.

Xie M. and Roy R., (2015). "AMP-activated kinase regulates lipid droplet localization and stability of adipose triglyceride lipase in *C. elegans* dauer larvae". PLoS ONE, 10(6), e0130480.

Xu C., Wensing T. and Beynen A. C., (1998). "Effects of high calcium intake on fat digestion and bile acid excretion in feces of veal calves". J Dairy Sci, 81, 2173 – 2177.

Xu J., Peng W., Sun Y., Wang X., Xu Y., Li X., Gao G. and Rao Z., (2012a). "Structural study of MCPIP1 N-terminal conserved domain reveals a PIN-like RNase". Nucleic Acids Research, 40(14), 6957 – 6965.

Xu N., Zhang S. O., Cole R. A., McKinney S. A., Guo F., Haas J. T., Bobba S., Farese R. V. Jr and Mak H. Y., (2012b). "The FATP1-DGAT2 complex facilitates lipid droplet expansion at the ER-lipid droplet interface". J Cell Biol., 198(5), 895 –911.

Yabe T., Suzuki N., Furukawa T., Ishihara T. and Katsura I., (2005). „Multidrug resistance-associated protein MRP-1 regulates dauer diapause by its export activity in *Caenorhabditis elegans*". Development, 132, 3197 - 3207.

Yamada A., Nagahashi M., Aoyagi T., Huang W. C., Lima S., Hait N. C., Maiti A., Kida K., Terracina K. P., Miyazaki H., et al., (2018). "ABCC1-exported sphingosine-1-phosphate, produced by sphingosine kinase 1, shortens survival of mice and patients with breast cancer". Molecular cancer research : MCR, 16(6), 1059 – 1070.

Yang F., Vought B. W., Satterlee J. S., Walker A. K., Sun Z.-Y. J., Watts J. L. , DeBeaumont R., Saito R. M., Hyberts S. G., Yang S., et al., (2006). "An ARC/Mediator subunit required for SREBP control of cholesterol and lipid homeostasis". Nature, 442(7103), 700 – 704.

Yang J. J., Ann D. K., Kannan R. and Lee V. H. L., (2007). "Multidrug Resistance Protein 1 (MRP1) in rabbit conjunctival epithelial cells: its effect on drug efflux and its regulation by adenoviral infection". Pharmaceutical Research, 24(8), 1490 – 1500.

Yang Y., Mo W. and Zhang J.-T., (2010). "Role of transmembrane segment 5 and extracellular loop 3 in the homodimerization of human ABCC1". Biochemistry, 49(51), 10854 – 10861.

Yano M., Watanabe K., Yamamoto T., Ikeda K., Senokuchi T., Lu M., Kadomatsu T., Tsukano H., Ikawa M., Okabe M., et al., (2011). "Mitochondrial dysfunction and increased reactive oxygen species impair insulin secretion in sphingomyelin synthase 1-null mice". The Journal of biological chemistry, 286(5), 3992 – 4002.

Yen K., Le T. T., Bansal A., Narasimhan S. D., Cheng J.-X., et al., (2010). "A comparative study of fat storage quantitation in nematode *Caenorhabditis elegans* using label and label-free methods". PLoS ONE, 5(9), e12810.

Yokogawa M., Tsushima T., Noda N. N., Kumeta H., Enokizono Y., Yamashita K., Standley D. M., Takeuchi O., Akira S. and Inagaki F., (2016). "Structural basis for the

regulation of enzymatic activity of Regnase-1 by domain-domain interactions". Sci Rep, 6, 22324.

Younce C. W., Azfer A. and Kolattukudy P. E., (2009). "MCP-1 (monocyte chemotactic protein-1)-induced protein, a recently identified zinc finger protein, induces adipogenesis in 3T3-L1 pre-adipocytes without peroxisome proliferator-activated receptor gamma". J Biol Chem, 284(40), 27620 – 27628.

Younce C. and Kolattukudy P. E., (2012). "MCP-1 induced protein promotes adipogenesis via oxidative stress, endoplasmic reticulum stress and autophagy". Cell Physiol Biochem, 30(2), 307 – 320.

Yu L., Fan J. and Xu C., (2019). "Peroxisomal fatty acid β-oxidation negatively impacts plant survival under salt stress". Plant Signal Behav, 14(2), 1561121.

Yun E. J., Lee S. H., Kim S., Kim S. H. and Kim K. H., (2017). "Global profiling of metabolic response of *Caenorhabditis elegans* against *Escherichia coli* O157:H7". Process Biochemistry, 53, 36 – 43.

Zaarur N., Desevin K., Mackenzie J., Lord A., Grishok A. and Kandror K. V. (2019). "ATGL-1 mediates the effect of dietary restriction and the insulin/IGF-1 signaling pathway on longevity in *C. elegans*". Mol Metab, 27, 75 - 82.

Zalcberg J., Hu X. F., Slater A., Parisot J., El-Osta S., Kantharidis P., Chou S. T. and Parkin J. D., (2000). "MRP1 not MDR1 gene expression is the predominant mechanism of acquired multidrug resistance in two prostate carcinoma cell lines". Prostate Cancer Prostatic Dis. 3, 66 – 75.

Zecić A., Dhondt I. and Braeckman B. P., (2019). "The nutritional requirements of *Caenorhabditis elegans*". Genes & Nutrition, 14(1).

Zhang P., Na H., Liu Z., Zhang S., Xue P., Chen Y., Pu J., Peng G., Huang X., Yang F., et al., (2012). "Proteomic study and marker protein identification of *Caenorhabditis elegans* lipid droplets". Molecular & Cellular Proteomics, 11(8), 317 – 328.

Zhang Y., Viennois E., Zhang M., Xiao B., Han M. K., Walter L., Garg P. and Merlin D., (2016). "PepT1 expression helps maintain intestinal homeostasis by mediating the differential expression of miRNAs along the crypt-villus axis". Scientific Reports, 6, 27119.

Zhao Z., Sheps J. A., Ling V., Fang L. L. and Baillie D. L., (2004). "Expression analysis of ABC transporters reveals differential functions of tandemly duplicated genes in *Caenorhabditis elegans*". Journal of Molecular Biology, 344(2), 409 – 417.

Zou C.-G., Tu Q., Niu J., Ji X.-L. and Zhang K.-Q., (2013) "The DAF-16/FOXO transcription factor functions as a regulator of epidermal innate immunity". PLoS Pathog, 9(10), e1003660.